Acid Catalysed Alkylation of Diphenyl Ether with Methanol over Shape-Selective Zeolites

by

John Phenyo Pheko Ntshabele

Submitted in partial fulfilment of the requirements for the degree of

Master of Science in Engineering

September 2005

Catalysis Research Unit

Department of Chemical Engineering

UNIVERSITY OF CAPE TOWN

ACKNOWLEDGEMENTS

The author would like to thank A/Prof JCQ Fletcher for his dedication to giving guidance throughout this work. It was really an honour to be under the supervision of someone with such great leadership and his insight in the content of this work.

A big thank you also goes to Mr W Böhringer, who was my immediate supervisor, for his willingness to share his knowledge and provide guidance in conjunction with the above-mentioned supervisor, throughout the duration of this work.

I would like to acknowledge my colleagues, Dr N Phala and Dr G Klatt who helped me establish the right path with the application of molecular modelling in this work and for interpretation of experimental results. I would also like to acknowledge Dr Klatt for the molecular dynamics results included in this work and Dr K Möller for his input in the interpretation of molecular dynamics results.

Mr T Tobler, for your immense effort in the design and assembly of the equipment for experimentation in this work, I also thank you.

An acknowledgement also goes to Mr V Smith who assisted with TGA analysis of the catalysts used in this work.

Prof E van Steen, for your input in the thermodynamic analysis part of this work, I thank you also.
I extend my thanks also to Dr H Manstein for assistance with the layout of the graphs.

The workshop personnel, the staff and fellow postgraduate students of the Department of Chemical Engineering who contributed in many different ways to make this work a success, I also thank you.

I am also grateful to Merisol, NRF, THRIP and UCT for their financial support, without which this work would not have succeeded.

SYNOPSIS

Phenolic by-product streams from coal coking operations, crude oil refineries and in particular, coal gasification processes are processed to recover phenol and individual cresol and xylenol isomers. The cresol fraction from these streams accounts for 40% of the industrial demand in USA, Western Europe and Japan.

The cresol fraction from high temperature coking and that from crude oil refineries are rich in *m*-cresol, whereas the fractions from low temperature coking and coal gasification are rich in *o*-cresol.

Direct alkylation of phenol with methanol over basic catalysts, such as MgO or Fe-based catalysts yield almost exclusively *o*-cresol. Processes have been commercialised to produce *o*-cresol this way.

Selectivity in methylation of phenol over acidic catalysts depends primarily on temperature and the acidity of the catalyst. It is reported that direct methylation of phenol with methanol over weakly acidic catalysts yields predominantly *o*-cresol, whilst catalysts with medium acidity yield primarily *o*- and *p*-cresol, with significant anisole formation at lower temperatures (≈ 200°C). *m*-Cresol is, however, formed with significant selectivity only over strongly acidic catalysts or at higher temperatures (typically 300°C and more).

To date, only one industrial process is known which is selective to *p*-cresol but has the disadvantage of co-formation of inorganic salt, which is costly to dispose of. *p*-Selective methylation of phenol over shape selective zeolites has not shown much success yet, giving poor selectivity, with *p*-/*o*-cresol ratios of up to 1.5 and the major product being anisole at lower temperature.

It was the aim of this work to therefore investigate an alternative route for selective production of *p*-cresol from methanol and phenol, via a three-stage process. In this process route, phenol is first condensed to diphenyl ether, followed by methylation of the ether to *p*-phenoxy toluene and *p*-tolyl ether (i.e. the mono- and the di-*para*-methylated diphenyl ether, respectively), and finally

the cleavage of the methylated products to *p*-cresol. The focus of this work was on the methylation step of this process route only, and was studied over shape selective and non-shape selective acid zeolites.

It was established through screening of different zeolites and optimisation of reaction conditions that Zeolyst mordenite (CBV90A) was the most suitable one for methylation due to its high selectivity to *para*-alkylation, with *p*/*m*-ratios of up to 4.5 for the phenoxy toluenes (mono-methylated product). At low temperature (250°C), the fraction of the mono-methylated products was almost free of the *meta*-isomer, with *p*/*m*-ratios of more than 50. However, by-product selectivities of about 40%, based on diphenyl ether converted, were obtained as heavy products.

Molecular modelling was attempted to quantify the experimental results to indicate whether product selectivity (by mass transfer control inside the zeolite pores) or transition state selectivity is responsible for the high *p*/*o*-ratios obtained. Even though molecular dynamics calculations suggest the relative diffusivities inside mordenite channels to be in the order $p \rangle o \gg m$, the results were disqualified on the basis of the errors associated with the force fields applied for the simulations, because they result in an error of the calculated diffusion coefficients that is larger than the differences between these coefficients.

The observation that 1,2-shift isomerisation does not take place and that isomerisation by transalkylation is likely to be hindered in the mono-dimensional non-interconnected pore system of zeolite mordenite, led to the conclusion that intra-zeolite isomerisation which is a prerequisite for product shape selectivity, may not take place. Therefore the high *p*-selectivities obtained would be due to denying access of the alkylating agent to the *o*-position on the diphenyl ether molecule in the restricted spatial environment of the mordenite pores, hence transition state selectivity.

Due to absence of literature data for the thermodynamic properties of the intermediate products in the process route from phenol to *p*-cresol, various estimate methods were used to predict thermodynamic feasibility of each process stage. The process stages are phenol condensation to diphenyl ether, first and second methylation of diphenyl ether to *p*-phenoxy toluene and *p*-tolyl

ether, respectively, as well as cleavage of the methylated products to *p*-cresol. Water is also present in all the process stages. The prediction of thermodynamic equilibria from these estimate methods was only partially successful, suggesting very high equilibrium conversion for the methylation steps, as expected, but producing inconsistent and contradictory results for phenol condensation and *p*-tolyl ether cleavage steps.

TABLE OF CONTENTS

APPENDICES

LIST OF FIGURES

LIST OF TABLES

NOMENCLATURE

BHT : 2,6-di-tert-butyl-p-cresol (Butyl Hydroxy Toluene)

HT : high temperature

MD : molecular dynamics

LT : low temperature

DPE : diphenyl ether

OPT : *o*-phenoxy toluene

PPT : *p*-phenoxy toluene

MPT : *m*-phenoxy toluene

PTE : *p*-tolyl ether

OMN : octamethyl naphthalene

HMN : heptamethyl naphthalene

MFC : mass flow controller

For acronyms of compounds and compound families identified in the DPE methylation product, see the fold out page at the end of the book.

LIST OF SYMBOLS

η = effectiveness factor

η = number of possible optical isomers

σ = maximum number of internal and external permutations allowed, on a molecule

σ_m = molecular length constant

ϕ = Thiele modulus

β = designation for the reciprocal of the product of Boltzmann constant and temperature

σ_{ext} = maximum number of external permutations allowed, on a molecule

ν_i = stoichiometric coefficient of species i

ξ = shape factor of catalyst particles and zeolite crystallites

μ = chemical potential

$\Re$ = radius of zeolite crystallites

Λ = ratio of molecular diameter to zeolite channel diameter

a = slope of a Mean Square Displacement versus time plot

A = Helmoltz energy

A = van Krevelen and Chermin constant

A_i = area percentage of species i as recorded on the chromatogram table

B = van Krevelen and Chermin constant

c = proportionality constant in the probability function

C_P = heat capacity at constant pressure

$C_{P,i}$ = heat capacity of species i at constant pressure

C_V = heat capacity at constant volume

d_c = zeolite channel diameter

d_m = molecular diameter

D_i = diffusion coefficient of species i inside the zeolite pore

dw = non-expansion work done on a particle

E_i = energy of quantum state i

E = enthalpy

F = Newton's force

F_{Newton} = resultant force acting upon a particle or atom

G = Gibbs free energy

k_B = Boltzmann's constant

K_{eq} = equilibrium constant

k_i = intrinsic rate constant of species i

$k_{i,\,obs}$ = observed rate constant of species i

L = characteristic length of a catalyst particle, indicative of the diffusion path length

L = reactor bed depth

MFR = molar feed ratio

m = mass of an atom

m_j = mass of molecule j

N = number of particles or atoms in the system

N_A = Avogadro's number

N_{Atoms} = number of atoms per molecule

n_{ci} = number of carbons detected per molecule of species i

$n_{i,DPE}$ = number of moles of DPE converted to species i

N_i = number of moles of species i

n_j = the frequency of the j^{th} group in a molecule

P = system pressure

P_i = probability of finding a system in the i^{th} quantum state

Q = partition function

R = gas constant, with the value of 8.314 J/mol.K

r = position of a molecule

$\langle r(t) \rangle$ = mean square displacement

S_i = selectivity of species i (percentage of species i in the total product)

S_{obs} = observed selectivity

S_f^o = absolute entropy of formation at normal conditions

s = drift speed of a molecule in the zeolite pore

S = entropy

T = temperature in Kelvin

T^o = normal temperature (298 K)

T(t) = temperature of the system as a function of time

Ta, Tb, Tc, Td, Te: sets of reactor bed temperature as a function of bed depth

t = time travelled by a molecule in a zeolite pore

U = internal energy

$U_{Potential}$ = potential energy

$U_{Kinetic}$ = kinetic energy of the system

V = system volume

v_j = linear velocity of a particle or atom in the zeolite pore

$v(t)$ = velocity of an atom as a function of time

WHSV= weight hourly space velocity

x = length of a path travelled by a particle in x-direction

X_{DPE} = conversion

X_{eq} = equilibrium conversion

Y_i = yield of species i

ΔG = change in Gibb's free energy

ΔG_f = change in Gibb's free energy of formation

$\Delta G°$ = change in Gibb's free energy at normal conditions

ΔG_i = change in Gibb's free energy of species i

ΔG_{rxn} = change in Gibb's free energy of the reaction

ΔG_{vKv} = change in Gibb's free energy of reaction, based on van Krevelen and Chermin method

ΔG_{Benson} = change in Gibb's free energy of reaction, based on Benson method

ΔG_{Joback} = change in Gibb's free energy of reaction, based on Joback method

ΔH = change in enthalpy

ΔH_f = change in enthalpy of formation

$\Delta H°$ = change in enthalpy at normal conditions

ΔH_i = change in enthalpy of species i

ΔH_{rxn} = change in enthalpy of the reaction

ΔS = change in entropy

ΔS_{rxn} = change in entropy of the reaction

$\Delta_a, \Delta_b, \Delta_c, \Delta_d, \Delta_H, \Delta_S, \Delta_G$ = tabulated constants for the group contributions

Δt = change in time

DEFINITIONS

Phenolics	A pool of aromatic alcohols comprising of phenol, cresols and xylenols
Stoichiometry	Number of moles of methanol required to convert diphenyl ether to di-para-methylated product, in a balanced chemical equation

1. INTRODUCTION

South Africa is a leading world producer of methylated phenols, that is cresols and xylenols. The source of the raw materials is the coal gasification operations of Sasol.

In October 1997, Merisol was formed as a joint venture between Sasol Limited (South Africa) and Merichem (USA) with the objective to merge their respective phenolics manufacturing and marketing operations (Sasol, 2001). Consequently, phenolic raw materials obtained from Sasol's coal gasification are worked up and marketed by Merisol.

By-product streams from coal coking operations, gaseous and liquid fuel production (from both crude oil and coal) are the primary feedstock in the production of phenols by Merisol (Merisol, 2001). In USA, Merisol acquires coal gasification liquors and coal tars extracts from Dakota Gasification Co. as well as spent refinery caustic solutions and processes them into high purity phenol, cresols and their derivatives (Merisol, 2001). In South Africa, Sasol's coal gasification liquors are the source of phenolics, from which phenolics are extracted using the Phenosolvan process (Sasol, 2001 and Fiege, 2000), see Figure 1-1.

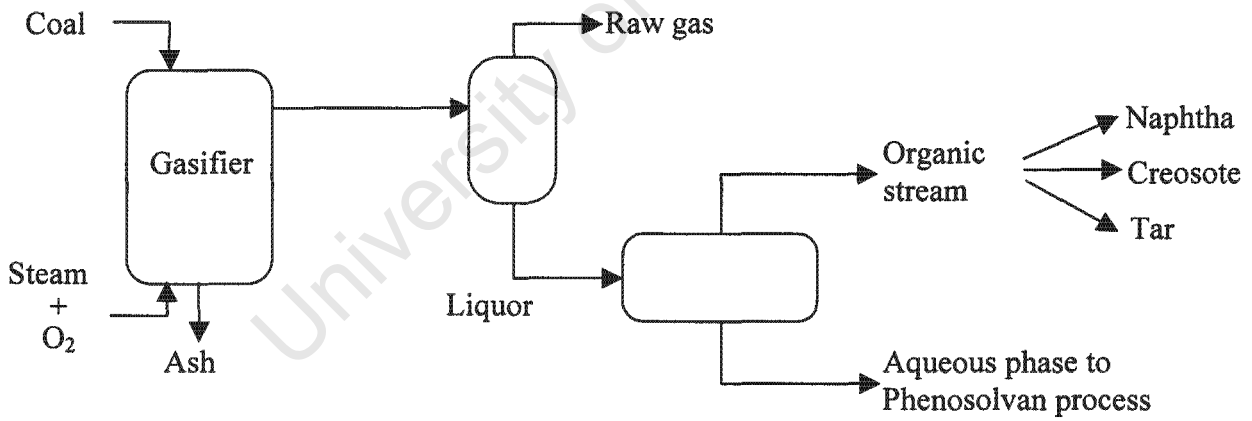

Figure 1-1: Coal gasification process as a source of phenolics (Venter, 1997)

The phenols containing aqueous phase is sent to the Phenosolvan process for recovery of the phenols. The naphtha stream is reported to be 50% by weight in phenolics (Venter, 1997). Venter and Niewoudt (2001) developed a process for the extraction of the phenolics from the naphtha, with the use of a water-glycol solution.

Phenols and their derivatives have a wide range of applications ranging from use as antiseptics, disinfectants, perfume additives, preserving agents, herbicides or monomers for resins, to use as cleaning agents in textile industries (EPA, 1997).

Phenolic resins used as engineering plastics (e.g. novolaks, resols) are gaining industrial importance and application due to their mechanical strength and durability, properties which make them competitive with metals. Phenols are monomers, as well as precursors to monomers for these engineering plastics (Bhattacharya, 1997; Kopf and Little, 1993).

Phenols are aromatic alcohols. Of particular importance, within the family of phenols, are phenol, cresols and xylenols. Phenol is the parent compound in this family, and it is an aromatic ring substituted with a hydroxyl group. Cresols are mono-methyl-phenols, whereas xylenols are di-methyl-phenols, see Figure 1-2.

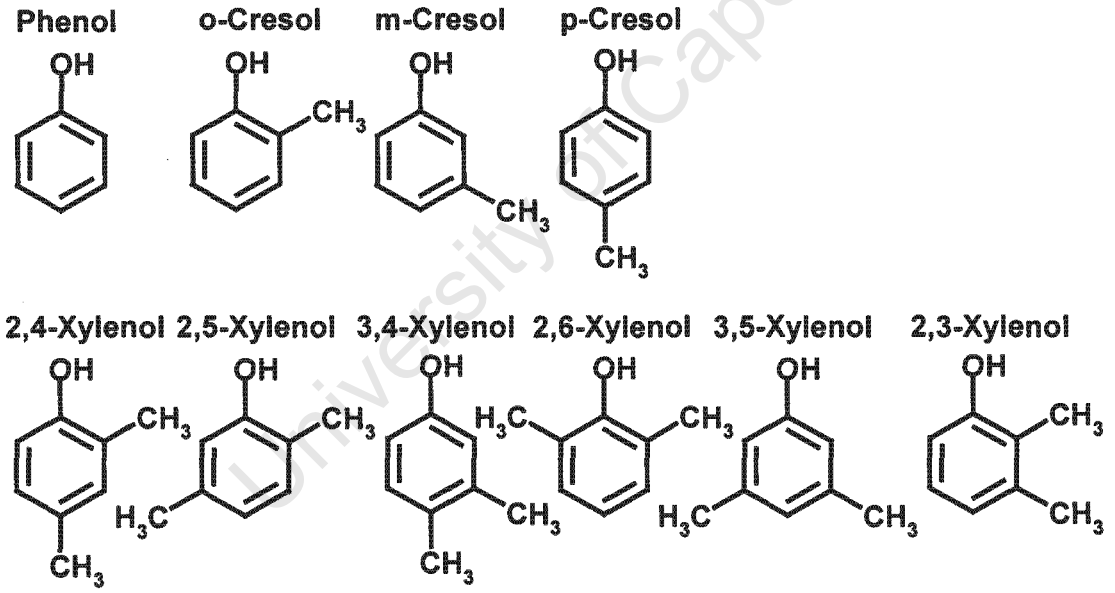

Figure 1-2: Different types of phenols

Coal tar was the first source of phenols and was the only source until the early 20th century. The increasing demand of phenols led to the development of other sources, which include spent refinery caustics as well as liquors from coal gasification (McMurry, 1992). Phenols from coking processes, coal gasification and spent refinery caustics are called "natural phenols", probably

because they are obtained from thermal decomposition of natural organic materials (Collin and Höke, 1995). Today, synthetic phenols are produced because the natural sources were unable to meet the continuous increase in the market demand.

Cresol fractions from spent refinery caustics and high temperature coking tars are rich in the *m*-cresol, whereas those from coal gasification liquors and low temperature coking tars are rich in *o*-cresol (Fiege, 2000).

Merisol's phenolics are derived mainly from "natural" sources (Merisol, 2001), and since the yield of individual phenols in these phenolic streams is almost invariant, the total output of the cresols will always be low in p-cresol (Fiege, 2000).

The demand of individual phenols in the market fluctuates and thus, Merisol's source of phenols (particularly cresols and xylenols) is not well suited to follow the market because it is invariant. Synthetic processes are therefore becoming increasingly important to meet the demand and/or shortages of specific cresol and xylenol isomers in the market.

One of the ways to get higher phenols synthetically is by alkylation of phenol. Methylation of phenols is one of the important industrial processes to produce cresols, continually growing due to new applications of industrial plastics, of which cresols are precursors (Kopf and Little, 1993).

Alkylation can be generally defined as the reaction or process in which an alkyl group is added to another organic molecule. When a methyl group is added, the reaction can be referred to as methylation.

Methylation of phenol with methanol preferentially yields *o*-cresol (Lorence et al., 1993). This reaction forms significant amounts of anisole (phenyl methyl ether) as a by-product at lower temperature (typically around 200 to 250 °C).

Very high selectivity to *o*-cresol is obtained with amphoteric and particularly basic catalysts. Processes have been commercialised to produce *o*-cresol and 2,6-xylenol by phenol methylation, over amphoteric γ-alumina, basic magnesium oxide and silica-supported basic iron-vanadium

oxide catalysts. These processes run at temperatures above 300 °C (Hammershaimb et al., 1993; Fiege, 2000). The high process temperature, in the latter, is probably due to the low activity of the catalysts and favourable to avoid anisole formation.

Selectivity of methylation of phenol to cresols over acid catalysts depends primarily on temperature and the acidity of the catalyst (Sinitsyna and Romanovskii, 1992; Landau et al., 1997). It is reported that alkylation of phenol with methanol over weakly acidic catalysts yields predominantly *o*-cresol, whilst catalysts of medium acidity yield primarily *o*- and *p*-cresol, both with significant anisole formation at lower temperature (typically 200 to 250 °C). *m*-Cresol on the other hand, only gets formed with significant selectivity over strongly acidic catalysts and also at higher temperatures (Sinitsyna and Romanovskii, 1992). In thermodynamic equilibrium, at 380°C, *m*-cresol predominates and the isomer distribution is *o* : *m* : *p* = 36 : 48 : 16 (Imbert et al., 2000).

p-Selective methylation of phenol over shape selective zeolites such as H-beta, ZSM-5, etc. has not shown much success yet, giving poor selectivity, the major product being anisole at low temperature and giving mainly *o*- and *m*-cresol at high temperature (Landau et al., 1997; Fiege, 2000). Anisole however undergoes intramolecular rearrangement to cresols, but mostly to *o*-cresol (Moon et al., 2001; Xu et al., 1997).

However, recent work has revealed that phenol methylation over large crystals (1 μm diameter) of zeolite H-MCM-22 produces enhanced *p*-selectivity with *p/m*-ratios of up to unity. These results were obtained at medium temperature and pressure, i.e. 300°C, 1 bar, in gas phase and result in no *m*-cresol formation when the methylation is carried out at low temperatures (200°C) and high pressures (>20 bar) in liquid phase (O'Connor et al., 2003; Moon et al., 2004 and Moon et al., 2002)

It can be summarised that over acid zeolites:

- *o*-Cresol can be produced with rather high selectivity by methylation of phenol,
- *m*-Cresol can be obtained with about 50% selectivity under conditions that force the methylation reaction towards the isomer equilibrium,
- *p*-Cresol is not yet attainable with high selectivity, via phenol methylation.

Only a single industrial process is known, to this day, which is selective to *p*-cresol (via toluene sulphonation, see Section 2.1.11.1) but it has the disadvantage of formation of inorganic salts as co-products, which are costly to dispose of (Fiege, 2000).

Preliminary studies for a three-stage process were carried out at the University of Cape Town (Ndlovu and Gxavu, 2000), which indicated that *p*-cresol can be produced from phenol and methanol, with high selectivity, in a three-stage process as follows :

1. condensation of phenol to diphenyl ether (DPE)
2. highly selective alkylation of diphenyl ether with methanol, to *p*-phenoxy toluene (PPT) and/or *p*-tolyl ether (PTE) over shape selective acid zeolites
3. cleavage of *p*-tolyl ether to *p*-cresol and of *p*-phenoxy toluene to *p*-cresol and phenol

The reaction stages are represented in Figure 1-3. The second stage is the subject of this study.

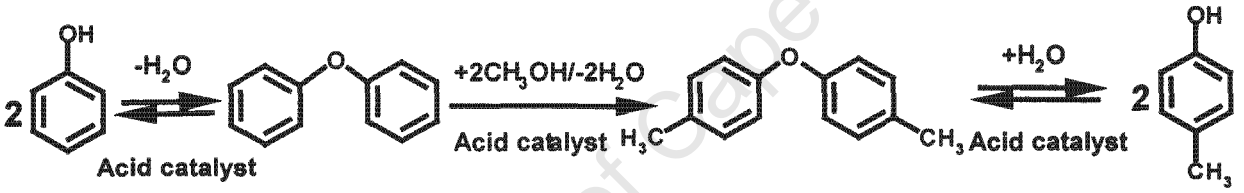

Figure 1-3: Three stage process route from phenol to p-cresol

1.1 REACTION UNDER STUDY

The reaction to be studied is methylation of diphenyl ether with methanol over shape selective zeolites, as shown in Figure 1-4.

Diphenyl ether is formed as by-product during the acid catalysed methylation of phenol and in the alkaline chlorobenzene hydrolysis process. Both of these processes are commercialised (Fiege, 2000). However, the idea here is to purposely get diphenyl ether directly from condensation of phenol.

The idea of methylating an ether form of phenol over shape selective catalysts is to :

- Introduce steric constraints on the *o*-positions due to their close positioning in the ether molecule. These constraints are expected to reduce *o*-selectivity and increase *p/o*-ratio.
- Reinforce the spatial constraints in the interacting zeolite pore-DPE system, in comparison to the zeolite pore-phenol system. These constraints are expected to increase *p*-selectivity and the *p/o*- ratio, either by transition state selectivity or product shape selectivity.
- Avoid the formation of anisole (the methyl-phenyl ether), which gets formed significantly in phenol methylation at temperatures below 250°C (Fiege, 2000 and Moon et al., 2001).
- Avoid methylation in the *m*-position. Low temperature methylation is of specific interest also because it would hinder methylation of the ether in the *m*-position, the reason being that *m*-methylation is only favoured at high temperatures (typically above 350°C, for acid catalysts, Fiege, 2000 and Moon et al., 2001).

A product mixture that is free from *m*-cresol or *m*-substituted products is attractive because separation and purification of *p*-/*m*-cresol mixtures is a costly process due to the close boiling points of the two isomers (201.9 and 202.2°C, respectively). Separation of this binary mixture cannot be carried out economically by distillation (Fiege, 2000; Moon et al., 2001).

Consequently, the reaction would ideally be run kinetically controlled such that methylation will not occur in the *m*-position. *o-M*ethylation would further be suppressed with the use of shape selective catalysts, and the result would be selective methylation in *p*-position only or at least with high preference.

Methylation of diphenyl ether is expected to occur sequentially as shown in Figure 1-4. This was concluded from the results obtained by Fujita et al. (1992), in which both mono-methylated and di-alkylated forms of diphenyl ether were obtained as well as from the results of Ndlovu and Gxavu (2000).

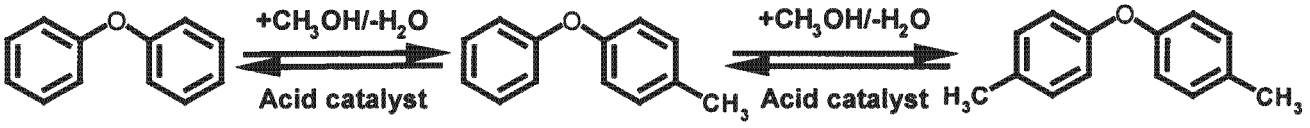

Figure 1-4: Reaction under study

The ether bridge in phenol ethers is very stable. When the ether bridge is between two aromatic rings, the carbon-oxygen bond is even more stable and only gets cleaved under drastic conditions (Fiege et al., 2000). Diphenyl ether was therefore expected to remain stable throughout the alkylation reaction.

The resulting mono- or di-alkylated products of Figure 1-4 would finally be cleaved to form *p*-cresol or phenol and *p*-cresol, respectively. According to Fiege (2000), *p*-tolyl ether is more hydrolysable than diphenyl ether. This was found when ethers formed as by-products in the alkaline chlorotoluene hydrolysis were recycled into the process for hydrolysis (Fiege, 2000).

Phenol is also used in the production of the following chemicals (Wallace, 1993; Jordan et al., 2002):

- Aniline – Halcon process, in which the hydroxy group is replaced via ammonolysis.
- Adipic acid – obtained by oxidatively cleaving the phenol ring.
- Alkylphenols (e.g. cresols, xylenols, 4-tert-butylphenol, octylphenols, etc.) – phenol is alkylated with methanol or the corresponding olefin.
- Salicylic acid – obtained by addition of CO_2 to phenol.
- Chlorophenols – by chlorination of phenol

These chemicals are used in the production of diverse consumer goods as well as process materials (e.g. insulating foams, adhesives, plasticisers, herbicides, insecticides, dyes, flavourants, etc.) and thus are of industrial as well as economic importance (Jordan et al., 2002).

In pure form, phenol is used as a disinfectant, an additive in germicidal paints, as well as for medicinal purposes (EPA, 1997).

Six synthetic processes have been developed for production of phenol, and they are summarised as follows (Jordan et al., 2002) :

- Benzene sulphonation – hydrolysis of the sulfonate in molten alkali hydroxide.
- Chlorination of benzene – alkaline hydrolysis of chlorobenzene
- Chlorination of benzene – steam hydrolysis of chlorobenzene (Raschig process)
- Dehydrogenation of cyclohexanol
- Toluene oxidation to benzoic acid – oxidative decarboxylation of benzoic acid
- Benzene alkylation to cumene – oxidation of cumene to cumene hydroxyperoxide – cleavage of the hydroperoxide to phenol and acetone (Hock process)

Among these processes only the Hock process and toluene oxidation are of current industrial importance. Toluene oxidation is economically viable when the price of toluene is lower than that of benzene. Benzene sulphonate and chlorobenzene hydrolysis processes were abandoned due to sodium sulphate and sodium chloride co-product formation. The Raschig process has been discontinued due to its high running costs. Similarly, the other processes were also abondoned for economic reasons (Jordan et al., 2002).

In phenol production, the Hock process dominates, particularly among the newly built plants and is reported to account for more than 95 % of the world's phenol production (Wallace, 1996). Acetone is formed as a co-product in the Hock process but the expansion of this process has not been hindered by this coupled production because there is still a market for acetone (Jordan et al., 2002).

Total phenol production capacity for USA, Canada, France, Italy, Japan, Spain, Finland, Korea, India, Mexico, Brazil, Eastern Europe and Germany was reported to amount to 5 million tons in 2000 (Jordan et al., 2002).

2.1.2 Cresols

Cresols were originally obtained from coal tar and, after World War II, from spent refinery caustics too. Cresols from coal tars (gasification and coking) and from spent refinery caustics are called "natural cresols", probably because they are obtained from thermal decomposition of natural organic materials (Collin and Höke, 1995). Natural cresols are produced from coal gasification, coal coking and spent refinery caustics in the ratio 50:35:15 (Fiege, 2000).

Combined quantities of cresols and xylenols produced worldwide are small (less than 10%) in comparison to the world's production of phenol. They are given in Table 2-1.

Table 2-1: Cresol and xylenol output by major producers[a] in 1984 and 1998 (Fiege, 1987 and Fiege, 2000).

	Quantity [tons] in 1984	Quantity [tons] in 1998
Phenol	[b]3 400 000	[c]5 000 000
Cresols	[b]220 000	175 000
Xylenols	[b]145 000	165 000

[a]Major cresol producers in 1998 were US, Europe, Japan and South Africa
[b]Excludes South Africa
[c]Phenol quantity in 2000

Approximately 60% of these cresols were produced synthetically and the rest were recovered from gasification liquors, coal tars and spent caustics (Fiege, 2000).

Contribution by major cresol producers in 1998 is given in Table 2-2.

Table 2-2: Cresol output by the major producers in 1998 (Fiege, 2000)

Country	Quantity [tons] in 1998
US	42 000
Europe	50 000
Japan	58 000
South Africa	25 000

The total output of natural cresols by the major producers diminished, over the last ten years, due to, among other reasons, declining availability of coal tars from coking processes and spent refinery caustics. Increasing environmental costs have, particularly in the US and Europe, led to major industrial changes like restructuring, capacity reductions and plant closures (Fiege, 2000).

2.1.2.1 Uses of cresols

Cresols are used primarily as chemical intermediates to many industrial products varying from herbicides, pesticides, flavour and fragrance compounds, antioxidants, explosives, resins, etc.

In pure form, *o*-cresol is used primarily as a solvent, a disinfectant, for phenol-formaldehyde resin production, as well as a precursor to epoxy-cresol-novolac, *p*-chloro-ortho-cresol, etc. Epoxy cresol novolac is used as a sealing material in integrated circuits/chips and *p*-chloro-ortho-cresol is a precursor to herbicides (Fiege, 2000).

m-Cresol is used in the manufacture of an explosive, 2,4,6-trinitro *m*-cresol, as well as a synthetic intermediate to flavour and fragrance compounds like musk, ambrette and insecticides like pyrethroid (Fiege, 2000).

p-Cresol is mainly used in the production of 2,6-di-*tert*-butyl-*p*-cresol (BHT), which is a non-staining, light-resistant antioxidant. Pure *p*-cresol also finds application as (Fiege, 2000):

- A precursor to other antioxidants (e.g. 2,6-dicyclopentyl-*p*-cresol)
- An additive in the process to Tinuvin 326, a UV absorber
- A precursor to 2,6-dinitro-*p*-cresol, a polymerisation inhibitor of styrene

- A precursor to dye intermediates like 2-nitro-p-cresol
- In the fragrance industry, where *p*-cresol is used in the production of anisaldehyde.

Mixtures of *m*- and *p*-cresol are used as disinfectants, preservatives, additives to soaps and they also find application in ore flotation.

2.1.2.2 Cresols from coal tars and coal gasification liquors

A typical product yield from a coking process is shown in Figure 2-1. Tar containing about 8% by volume of phenolics is produced as a by-product of coking. This is where, in coking operations, phenolics are recovered for processing into individual phenols (Collin and Höke, 1995).

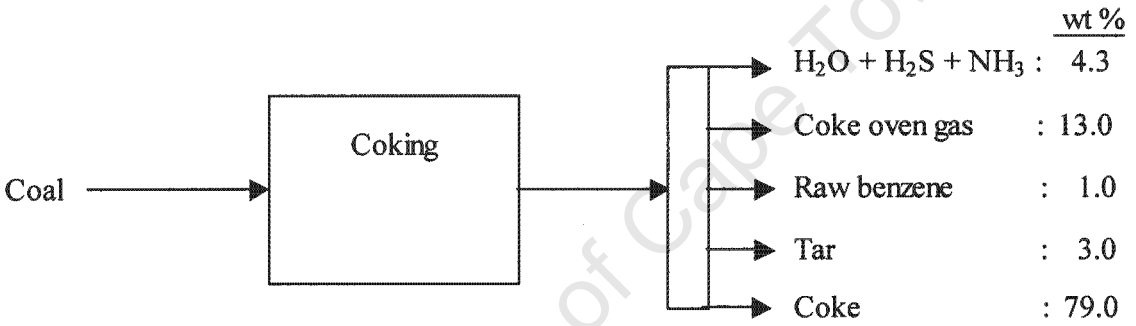

Figure 2-1: Coal coking as a source of phenolics (Collin and Höke, 1995)

Yields of the individual phenols from coal tars depend largely on the starting material, operating conditions (mainly temperature and residence time), reactor type and the mode of operation (Fiege, 2000).

Typical yields of phenols obtained from coal tars of different processes are given in Table 2-3 (Fiege, 2000).

Table 2-3: Phenols yields on weight percent basis. The last row gives the total mass (kilogram) of the phenolics obtained per ton of water-free bituminous coal (Fiege, 2000).

	Hydrogenation	LT coking	Lurgi gasifier tar	HT coking			Lignite tar
	ca. 470°C	600-650 °C	850 °C, 20 bar	1200-1300 °C			
				USA	UK	FRG	
Phenol	18.8	6.1	4.3	22.2	19.5	25.5	43.3
o-Cresol	7.1	6.1	5.0	8.9	10.6	12.8	11.3
m-Cresol	16.5	3.9	8.1	15.6	15.0	25.5	12.1
p-Cresol	7.1	3.5	6.5	10.0	8.8	12.8	12.1
Xylenols	24.7	26.5	24.2	13.3	15.9	12.8	21.3
$C_{9+}OH$	25.9	53.9	51.9	30.0	30.1	10.6	
Total	100	100	100	100	100	100	100
Total mass of phenols[1]	85	23	3.22	0.9	1.13	0.47	14.1

[1]Kilogram phenolics per ton of water-free bituminous coal.

Bituminous coal as the feed to the processes listed in Table 2-3 gives highest yields of phenolics for the sump-phase hydrogenation, the lowest temperature process. However, this is not a commercially applied process. In low temperature (LT) carbonisation, bituminous coal gives intermediate amounts of phenolics whereas high temperature (HT) coking yields the least amount of phenolics. Gasification of lignite (in a Lurgi gasifier) on the other hand yields higher amounts of phenolics than gasification of bituminous coal (Fiege, 2000).

High temperature (HT) coking has, as a traditional source for cresols and xylenols, given annual quantities of about 35 000 tons of these worldwide. This was the yield from bituminous coal as a starting material, and it has declined over the last 40 years (probably due to more efficient coking operations that yielded less by-products such as tar and the decline in town gas manufacturing).

In the United Kingdom, low temperature coal tars generated during the production of smokeless solid fuels (Coalite process) yield ten times more phenols than the tars from HT coking. The yields from this process have also declined in the 1990s (Fiege, 2000).

Sasol's coal gasification liquors are presently the world's largest source of natural cresols and xylenols, with an annual output averaging at about 45 000 tons. According to Fiege (2000), these liquors have a phenolics distribution similar to that obtained from low temperature coking.

The product stream from the Lurgi coal gasifier is separated into three phases, a gas phase and two immiscible liquid phases (Figure 1-1). The two liquid phases are the aqueous phase originating from the steam fed to the gasifier and the organic phase composed largely of the volatile matter liberated from coal by thermal decomposition (Collin and Höke, 1995).

The aqueous stream traps a fraction of the phenolics generated in the gasifier. These phenolics are recovered by means of the Phenosolvan process, as shown in Figure 2-2 (Venter and Nieuwoudt, 2001).

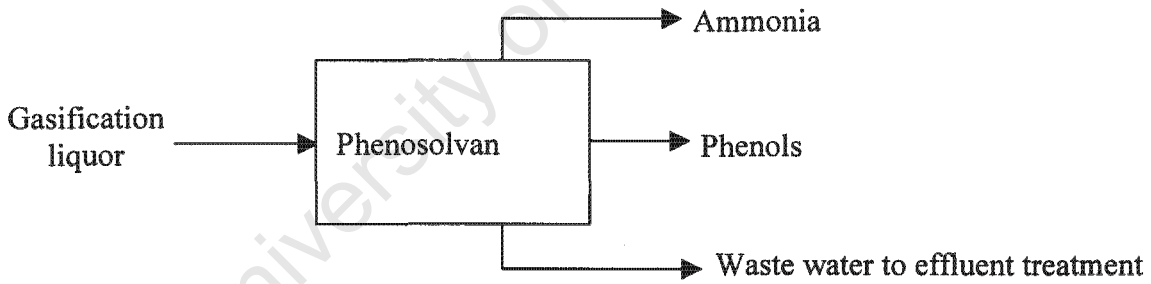

Figure 2-2: Phenosolvan process for recovery of phenols (Venter and Nieuwoudt, 2001)

According to Venter and Nieuwoudt (2001), the organic stream from the gasifier shown in Figure 1-1 is mainly made up of neutral oils (aromatics and naphthalenes), phenolics and neutral bases (pyridines and aromatic amines). The naphtha stream taken from this organic stream is reported to be 50 % phenolics by weight (Venter, 1997; Nieuwoudt, 1997). Nieuwoudt (1998) proposed recovery of the phenolics from the naphtha stream by means of liquid-liquid extraction, using a water-glycol solution as a solvent for retaining the phenolics and using paraffins as antisolvents to retain the neutral bases.

Dakota Gasification Co., in the United States, produces about 25 000 tons per annum of natural cresols and xylenols from gasification of lignite in Lurgi gasifiers (Fiege, 2000), for manufacturing synthetic natural gas (Smoot, 1995). As with Sasol's facilities, phenolics are recovered from the liquors of the gasification stage.

In the case of HT tar from the coke oven process, phenolics are recovered by extraction with sodium hydroxide solution (Fiege, 2000).

Companies that isolate phenols from coal tar are Merisol (United States and South Africa), Dakota Gasification Co. of the United States, Coalite Chemicals in the United Kingdom, Rütgers-VfT in Germany, DEZA Corporation of Czech Republic and four Japanese companies. Dakota Gasification Co. only isolates phenol from their gasification liquors and sells the crude cresylic fraction to others like Merisol, for further processing (Fiege, 2000).

2.1.2.3 Cresols from spent caustics

Naphtha fractions from catalytic and thermal cracking in the petroleum industry contain about 0.1 % phenols, by weight. In the sweetening process (i.e. scrubbing off of acid sulphur compounds with concentrated alkaline solutions), phenol, cresols and xylenols are also extracted due to their acid properties.

The spent caustics contain, on average, 20 – 25 % C_6 – C_8 phenols and 10 – 15 % sulphur compounds by weight (Fiege, 2000).

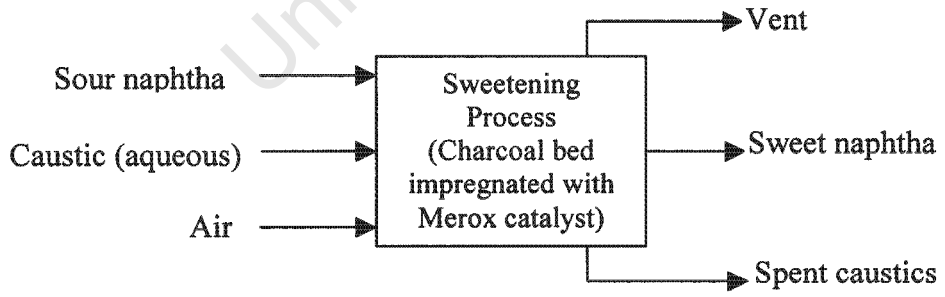

Figure 2-3: Sweetening of naphtha by Merox process (Marx, 1995)

In the Merox sweetening process, shown in Figure 2-3, the reactor is packed with charcoal impregnated with a Merox catalyst. The catalyst is composed of iron-group metals to promote oxidation of mercaptans in the naphtha to disulphides, using air as the source of oxygen (Marx, 1995). The Merox process is however reported to be low in the yield to phenols (Fiege, 2000).

Phenolate caustics from HT tar and LT tar, spent refinery caustics and caustics obtained from gasification naphthas, are treated with carbon dioxide or hydrogen sulphide to release the crude phenols from their sodium salts. Scrubbing with water lowers the alkali content of the crude phenol. This is then followed by azeotropic dehydration of the crude phenol (Marx, 1995).

In the United States, the firms that processed spent refinery caustics were Merichem, Northwest Petrochemical and PMC Specialties, until around 1990. However, Northwest Petrochemical and PMC Specialties closed down their operations mainly due to competition, particularly from synthetic o-cresol producers. Other reasons for closure were increased environmental restrictions and an overall lack of raw materials. Merichem, which was already the biggest producer among the three, became the only processor of spent refinery caustics in the United States. Merichem's capacity for phenolics was estimated to be about 55 000 tons in 1996 and this number includes phenolics from other sources such as gasification liquors of Dakota Gasification (Fiege, 2000).

Typical composition of the phenolic fraction from spent refinery caustics is given in Table 2-4. The phenolics mixture is separated by distillation into phenol, *o*-cresol, *m*-/*p*-cresol mixture and xylenols (Fiege, 2000).

Table 2-4: Compositions (% weight) of the phenolics from refinery spent caustics (i.e. crude oil derived phenols)

Phenol	*o*-Cresol	*m*-Cresol	*p*-Cresol	Xylenols	$C_{9+}OH$
20 %	18 %	22 %	9 %	28 %[a]	3 %

[a] Includes ethyl phenols

Recovery of cresylics from refinery caustics has been largely confined to the United States. German refiners, for example, use different techniques and production of spent caustics would be

insufficient for economical processing. The reason being that desulphurisation is carried out by a process which is low in the yield to phenols (Fiege, 2000).

Recovery of cresols from spent refinery caustics is also declining in the US because refineries are changing over to either hydrotreating or UOP's Merox process, partly because the price of caustic soda went up in recent years. Also, the Merox process produces considerably smaller quantities of spent caustics and leaves substantial amounts of cresols in the gasoline (Fiege, 2000).

2.1.2.4 Recovery of the individual cresols

The crude phenol fraction undergoes rectification under vacuum (Fiege, 2000).

Whereas phenol and *o*-cresol can be distilled off individually, *m*-cresol and *p*-cresol have close boiling points (202.23°C for *m*-cresol and 201.94°C for *p*-cresol), which makes it difficult for them to be separated by means of simple distillation techniques (Fiege, 2000; Intille, 2001)

The present industrial technique for separation of *m*-/*p*-cresol mixture is by first alkylating the mixture with isobutene and then separating by distillation. The alkylation product is mainly 2,6-di-*tert*-butyl-*p*-cresol (BHT), an antioxidant, which is an industrially desired product responsible for the highest consumption of *p*-cresol.

Other techniques have been developed, for separation of *m*-/*p*-cresol, and they are summarised as follows:

Crystallisation: The two isomers have melting points which are 22°C apart. This makes high purity separation of these isomers possible by means of fractionated crystallisation. Sumitomo Chemicals runs a plant which utilises this technique and has been in operation since 1986 (Fiege, 2000).

Adsorption: Molecules, when forced through microporous solids such as a zeolites, diffuse at different rates due to their different molecular diameters. *p*-Cresol is the fastest diffusing one among the cresol isomers due to its smaller molecular diameter. As a result, when a mixture of *m*- and *p*-cresol is passed through a zeolite bed, *p*-cresol diffuses faster and occupies the void

volume of the zeolite, whereas *m*-cresol is either excluded from entering the pores or if it does diffuse through, very little diffuses through. Merichem has industrialised a process based on this separation technique (Fiege, 2000).
Other separation processes have been commercialised which involve selective conversion of one of these isomers into another product which is easily removed from the mixture (Fiege, 2000).

It is estimated that the manufacturers themselves consumed about 25 % of the total cresol produced in 1998. About 45 % were processed in the form of pure *p*-cresol and pure *o*-cresol and the rest as isomer mixtures. It is also estimated that 40 000 tons per annum of *m*-/*p*-cresol mixture is separated into pure *m*-cresol with co-production of BHT (Fiege, 2000).

2.1.3 Synthetic cresols

Cresol recovery from coal tars and spent refinery caustics became insufficient to meet the market demand, from 1965. Cresols have been produced synthetically on an increasingly large scale since and today, synthetic cresols account for 60 % of the total demand in Japan, Europe and the United States. The remaining 40 % is met by natural cresols, i.e. those obtained from coal tars and spent refinery caustics (Fiege, 2000).

See Section 2.1.11 for synthetic processes.

2.1.4 Xylenols

Xylenols are dimethylated phenols and exist in six isomeric forms (see Figure 1-2). Natural phenolics streams contain all six isomers, the distribution of which is dependent on the raw materials and the conditions of formation. The xylenol fraction from spent refinery caustics is generally rich in 2,4-xylenol and has a low content of 3,5-xylenol. Xylenols from bituminous coal tar are however rich in 3,5-xylenol (Fiege, 2000).

Table 2-5: Xylenol distribution from bituminous coal tar (Fiege, 2000)

Isomer	3,5-X	2,4-X	2,3-X	2,5-X	2,6-X	3,4-X
Percentage	31.9	28.1	14.1	13.6	6.9	6.5

The total quantities of xylenols produced in 1984 and 1998 were 145 000 and 165 000 ton, respectively, as given in Table 2-1. According to Fiege (2000), among the six isomers, 2,6-xylenol is the most important one for economic reasons. It is reported that 2,6-xylenol accounted for 125 000 tons of the 165 000 tons of xylenols produced in 1998, most of which was produced synthetically by means of phenol methylation (Fiege, 2000).

Other individually produced isomers, 2,4-xylenol, 2,5-xylenol and 3,5-xylenol, accounted for ca. 10 000 tons altogether, by synthesis as well as by isolation from mixtures. Xylenol mixtures accounted for 30 000 to 40 000 tons, in 1998 (Fiege, 2000).

Synthetic xylenol is produced in the US, Europe and Japan in the ratio 54:24:22 (Fiege, 2000).

2.1.5 Production and uses of diphenyl ether

The idea for the process route of Figure 1-3 is to use phenol as the source of diphenyl ether. Therefore, for the scope of this work, not much in terms of the alternative sources of diphenyl ether will be discussed.

Most phenol ethers can be synthesised by reaction of phenols with alkyl or aryl halides in weakly basic aqueous media. Diphenyl ether is formed as a by-product during the methylation of phenol over acid catalysts and in the high-pressure base-catalysed hydrolysis of chlorobenzene (Fiege et al., 2000). Etherification, by phenol condensation, is a preceding step to the reaction under study, as shown in Figure 1-3.

Due to its thermal stability, the eutectic mixture of diphenyl ether with biphenyl is used as a heat transfer medium for high temperature applications. Diphenyl ether is also used as a fragrance component and as a starting material for various organic intermediates. In the production of polyesters, it is used as a processing aid and its polybromine derivatives are used as fire retardants (Fiege et al., 2000).

2.1.6 General properties of phenols

Phenol and cresols are hygroscopic. Phenol has limited solubility in water between 0 and 65°C, but is totally miscible with water above 65°C (Jordan et al., 2002). Cresols are however less soluble in water than phenol. Water-soluble organic compounds, such as methanol increase phenol and cresol solubility in water (Fiege, 2000).

Phenols are weak acids, due to resonance stabilisation of the phenoxide ion when the proton of the hydroxyl group is removed. The phenoxide ion is stabilised by delocalisation of the negative charge from the oxygen into the aromatic nucleus. Acidity of phenols decreases with increasing molecular weight (Fiege, 2000).

2.1.7 Properties of phenol ethers

Ethers can be regarded as organic derivatives of water in which the hydrogen atoms have been replaced by organic substrates. Consequently, they have a geometry close to that of water. They have a tetrahedral structure, with oxygen sp^3 hybridised. Two axes of the oxygen tetrahedron are occupied by the organic substituents and the other two by the free electron pairs of the oxygen atom. Thus ethers are not linear but angular. This makes them slightly polar but less polar than the corresponding alcohols (McMurry, 1992).

The ether linkage in phenol ethers is very stable. The C-O bond in completely aromatic ethers such as DPE is cleaved only under drastic conditions such as in the presence of alkali and at high temperature. In contrast, the aliphatic C-O bond in semi-aromatic ethers, like anisole or ethyl phenyl ether, is split by treatment with strong acids to form phenol and the corresponding alkyl compound, i.e. an olefin, and in the presence of water, an alcohol (Fiege et al., 2000).

Cleavage of aromatic ethers over strong acids (H-zeolites) in the presence of water was also observed (Ndlovu and Gxavu, 2000).

2.1.8 Reactivity of phenols

The aromatic nucleus of the phenol can undergo electrophilic substitution. Electron density from the OH group is discharged onto the ring, and in this way activates it, also controlling the orientation of the incoming electrophile (Lorence et al., 1993).

The phenol ring can be alkylated, acylated, hydroxylated, nitrated, halogenated or sulphonated (Fiege et al., 2000).

Substituents on an aromatic ring change its electronic properties. The effects of the substituents relevant to the reaction under study are summarised as follows:

- An oxygen atom bonded to an aromatic ring imposes inductive and mesomeric effects onto the ring (Sykes, 1986). Oxygen inductively withdraws the electron density from the ring, but mesomerically discharges electron density onto the ring. However, the mesomeric effect is much more pronounced than the inductive effect (McMurry, 1992).
- A methyl group on an aromatic ring discharges electron density onto it by both, hyperconjugation and inductive effects (Sykes, 1986). The methyl group on an aromatic ring also activates the ring by inductive effects increasing the electron density in the ortho- and para-positions of the ring (McMurry, 1992). The effect of a methyl group is however, much weaker than the effect of a hydroxyl group.

Due to its strong resonance effect, the hydroxyl group of the phenol activates the ring for electrophilic attack, increasing the electron density on the ring (McMurry, 1992). Electron density discharged from the oxygen onto the ring is high in the ortho- and para-positions (see Figure 2-4) and, as a result, a hydroxyl substituent is kinetically ortho- and para-directing (Sykes, 1986). This means that an electron deficient reactant (electrophile), such as a carbenium ion, is most favoured to bond to the ring in the para- and the ortho-positions.

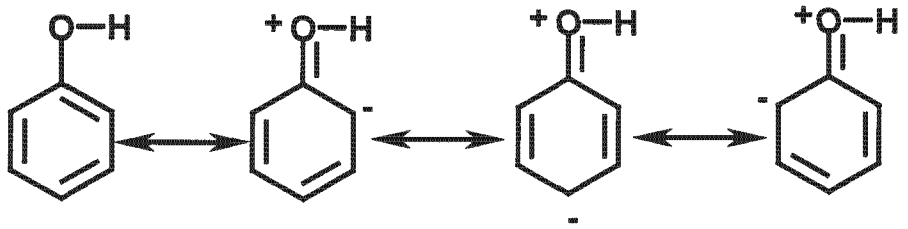

Figure 2-4: Resonance states of a phenol molecule

The combined electron density reinforcement effect by the hydroxyl and the methyl group is additive when the methyl group is in the meta-position with respect to the hydroxyl group.

2.1.9 Reactivity of aromatic ethers

The presence of the electronegative oxygen atom in the angular molecule causes ethers to be slightly polar (McMurry, 1992).

Aromatic ethers (e.g. diphenyl ether), like phenols, can undergo electrophilic substitution at any of the three positions on the ring. The phenyl ring in aromatic ethers can be alkylated, acylated, hydroxylated, nitrated, halogenated or sulphonated. Figure 2-5 shows the different resonance structures for substitution at these positions.

In acid catalysed electrophilic substitution, the transition states for ortho- and para-substitutions have one more resonance structure (canonical form) than for meta-substitution. Stability of a transition state increases with increasing number of canonical forms, hence ortho- and para-structures are the more stable transition states of the alkylation reactions (McMurry, 1992), as illustrated in Figure 2-5. The additional canonical form, in which the positive charge is located on the oxygen, is inherently more stable than the other three complementary ones (Sykes, 1986).

Consequently, under kinetically controlled reaction conditions, ortho- and para-methylation is favoured over meta-methylation (Sykes, 1986). Analogous to phenol (Moon, 2001), no meta-substitution is expected to occur under mild conditions, ≤ 200°C.

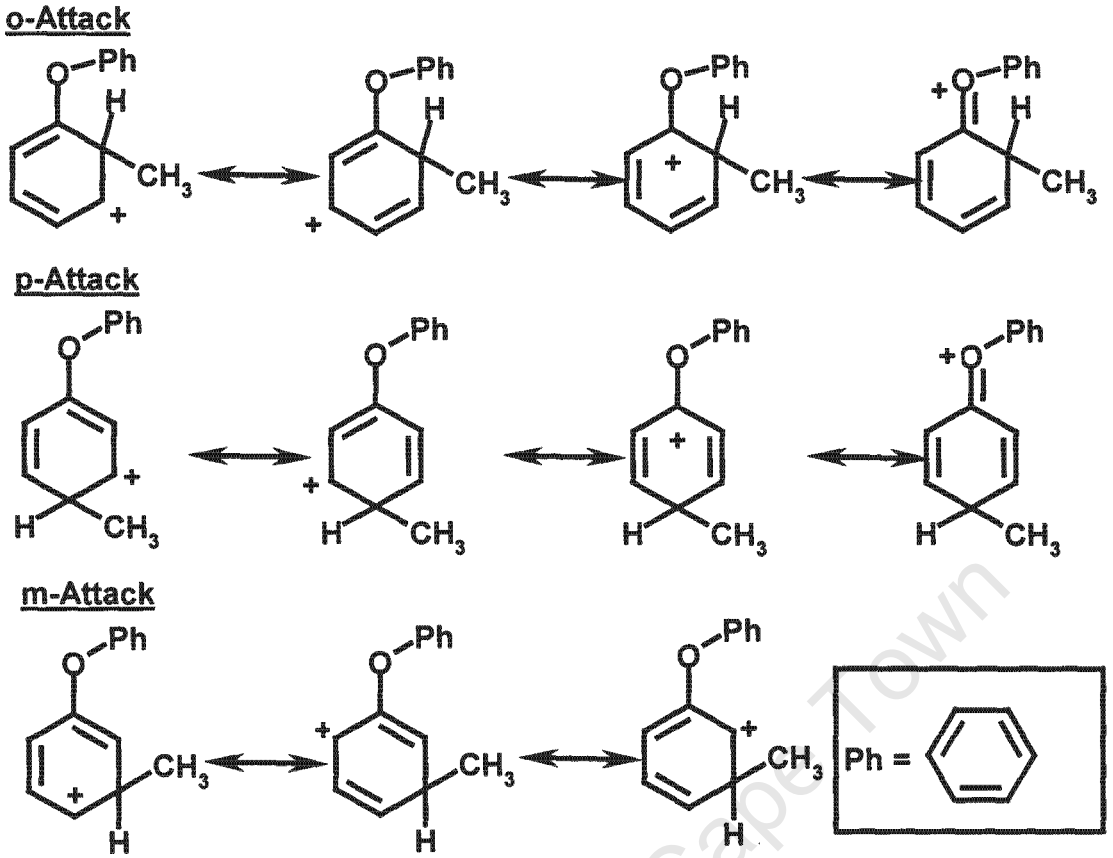

Figure 2-5: Canonical forms for electrophilic methylation of diphenyl ether (adopted from Sykes, 1986). Ph stands for phenyl, as shown at the bottom right of this figure.

Analogous to phenols, attachment of a methyl group onto a ring of aromatic ether alters the ring properties by inductive effects, which are pronounced in the para- and the ortho-positions with respect to the methyl group. The position of the methyl group relative to the oxygen atom determines whether its *o*- and *p*-directing effects are slightly reinforced (*m*-position) or weakened (*o*- and *p*-position). However, the inductive effect of the methyl group is minor in comparison to the resonance effects of the oxygen atom, hence a mono-methylated aromatic ether like phenoxy toluene will essentially maintain its aromatic reactivity on both rings as before methylation.

The ether group in ethers is generally inert to many reagents (McMurry, 1992).

2.1.10 Thermodynamic equilibrium of cresol isomers

Selectivities of cresols in thermodynamic equilibrium is of the order: $m > o > p$

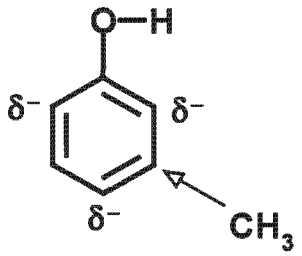

Figure 2-6: Electron density distribution responsible for the different thermodynamic stabilities of cresol isomers

Stability of *m*-cresol is the highest, thermodynamically, because the methyl group at the *m*-position of the phenol can still discharge its electron density into ring the because the electron density on the m-position is not enhanced by the electron discharge from the oxygen.

According to Imbert et al. (2000), the distribution of cresol isomers in an equilibrium mixture is as shown in Table 2-6. Note the discrepancy of Imbert's equilibrium distributions obtained over various catalysts.

Table 2-6: Gas phase equilibrium distribution of cresol isomers at 380°C (Imbert et al., 2000)

Cresol isomer	Calculated from data in Stull et al. (1969)	Experimental - USHY (Imbert et al., 2000)	Experimental – HZSM5 (Imbert et al., 2000)
ortho	37 %	44 %	36 %
meta	58 %	42 %	48 %
para	5 %	14 %	16 %

Fritsch et al. (2003) studied liquid phase isomerisation of the three cresol isomers over H-ZSM5, at 380°C and confirmed Imbert's results of the last column of Table 2-6.

2.1.11 Commercial p-Cresol manufacture

Toluene sulphonation is the only commercial process selective to *p*-cresol. *p*-Cresol is however also produced as a by-product in the production of the other isomers. Outputs from toluene sulphonation and other commercial processes in which *p*-cresol is also obtained are summarised in Table 2-7.

Table 2-7: Yields of *p*-cresol from various commercial processes (Fiege, 2000)

Process	Cresol distribution
Alkali fusion of toluenesulphonates	10% *o*-cresol, 10% *m*-cresol, 80% *p*-cresol
Alkaline chlorotoluene hydrolysis	10% *o*-cresol, 50% *m*-cresol, 25% *p*-cresol, 15% by-products
Cymene hydroperoxide cleavage	0% *o*-cresol, 60% *m*-cresol, 40% *p*-cresol
Phenol methylation over γ-alumina	99% o-cresol, 1% *m*-/*p*-cresol
Biller process – homogeneously catalysed phenol methylation (phased out in 1990)	58% *o*-cresol, 42% *p*-cresol, almost free of *m*-cresol

The first three processes of Table 2-7 use toluene as a starting material. *o*-Cresol can be recovered easily from a cresol mixture by distillation, but the meta- and para- isomers have very close boiling points and need complex cost intensive procedures for separation (Fiege, 2000; Intille, 2001).

2.1.11.1 Toluene sulphonation

This process is aimed mainly at *p*-cresol manufacture. It is the only commercial process that is highly selective to *p*-cresol (80%). Several companies produce p-cresol through this process and their production capacities are summarised in Table 2-8.

Table 2-8: *p*-Cresol producers (by toluene sulphonation) and production capacities world-wide as at 2000 (Fiege, 2000)

Company, country	Capacity [t/a]
PMC, US	18 000
Inspec Fine Chemicals, UK	12 000
Beraton, Russia	3 000
Konan Chemicals, Japan	4 000
Honshu Chemical Industry Co., Japan	2 500
Gujarat Aromatics, India	4 000

The process consists of four reaction stages as shown in Figure 2-7.

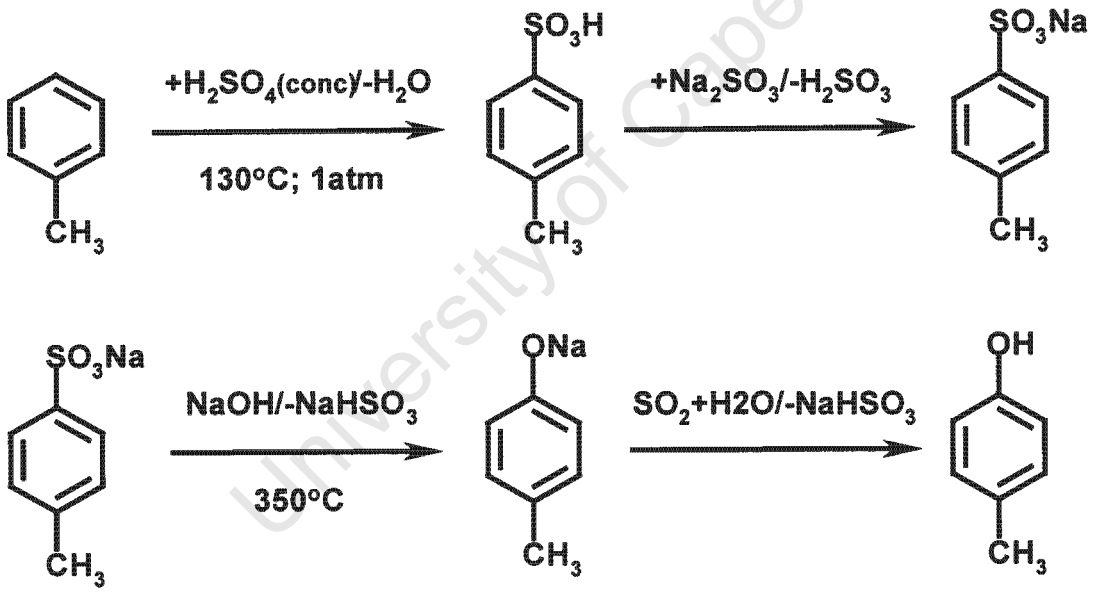

Figure 2-7: Reaction steps in *p*-cresol manufacture by toluene sulphonation (Fiege, 2000)

The sulphonation reaction is reversible and favoured in strong acid. An arene-sulphonic acid or salt, when heated at 300°C or higher in the presence of NaOH, yields the corresponding sodium phenolate. That is, a hydroxyl group replaces the sulphonate group. Hydrolysis eventually releases the corresponding phenol (McMurry, 1993).

Handling of the inorganic salt co-products (particularly sodium sulphite) unavoidably formed from this process is a problem to the industry. Inspec Fine Chemicals upgrades sodium sulphite into a product suitable for paper industry and PMC oxidise their sodium sulphite with air to form sodium sulphate (Fiege, 2000).

Toluenesulphonic acid made by sulphonation of toluene is a mixture of mainly para toluene sulphonic acid and some meta and ortho isomers. All isomers are converted to the corresponding cresol isomers, in the subsequent process steps (Intille, 2001).

Isomers of *p*-cresol are produced as by-products and their distribution depends mainly on sulphonation conditions. Composition of the crude cresol from this process is typically 6 – 12 % *o*-cresol, 6 – 12 % *m*-cresol and 80 – 85 % *p*-cresol (see Table 2-7) (Fiege, 2000).

The yield of *p*-cresol, based on toluene, can be as high as 80 %. Low *m*-cresol content is obtained under kinetically controlled conditions (mild sulphonation and mild alkali fusion), whereas sulphonation at high temperature and long residence time eventually yields an isomer mixture (of toluenesulphonic acids) at thermodynamic equilibrium. Alkali fusion of this mixture yields a cresol isomer mixture of composition: 5% ortho, 56% meta and 39% para (Fiege, 2000).

2.1.11.2 *Alkaline chloro-toluene hydrolysis*

This process produces a mixture of the cresol isomers and is used primarily when a high *m*-cresol content is required. The process stages are summarised as follows (Fiege, 2000):

- Chlorination of toluene with chlorine in the presence of $FeCl_3$ and disulphur dichloride, yielding primarily *o*- and *p*-chlorotoluene.
- Hydrolysis of chlorotoluene isomers with excess sodium hydroxide at 375°C and 290 bar.
- Sodium phenolate mixture from hydrolysis is neutralised to recover the corresponding cresols.

The product composition is given in Table 2-7.

2.1.11.3 Cymene hydroperoxide cleavage

This process allows production of mainly *m*- and *p*-cresol and very little *o*-cresol and is analogous to the Hock process for phenol synthesis from benzene. Process stages are summarised as follows (Fiege, 2000):

- Toluene alkylation with propylene over $AlCl_3$ and HCl, at 70°C, to form cymene isomers.
- Oxidation of cymenes to cymene hydroperoxides with air, at 105°C, in the presence of an alkali. (*o*-Cymene does not oxidise readily and also inhibits oxidation of its isomers and this results in a low overall yield for cresols).
- Cleavage of the peroxides to cresols and acetone, with an acid catalyst.

The product selectivities are given in Table 2-7.

2.1.11.4 Phenol methylation over γ-alumina

γ-Alumina is one of the industrially applied catalysts for phenol methylation, to yield cresols. The process is carried out either in gas or liquid phase. Cresol distribution is given in Table 2-7. At reaction temperature of 300 – 320°C, methanol to phenol molar ratio of 2 and at a liquid space velocity of unity per hour, *o*-cresol, 2,6-xylenol and *m*-/*p*-cresol mixture are formed in the ratio 82:17:1, respectively. Product distribution is highly dependent on the process conditions, favouring *m*-cresol at high temperature (Fiege, 2000).

2.1.11.5 Biller process

In the Biller process, aqueous zinc-halide/hydrogen-halide solutions are used as homogeneous catalysts in phenol methylation at 230°C and 25 bar. This process yields an almost *m*-cresol free product, which is expected because of low temperature operation (Fiege, 2000). This process, however, suffers a problem of requiring highly corrosion resistant tantalum lined equipment. The Biller process was phased out in 1990. Product selectivities of this process are given in Table 2-7.

2.1.12 *p*-Cresol via methylation of aromatic ethers

Methylated aromatic ethers, when they undergo hydrolysis, yield cresols corresponding to the methylation position in the former ether. Since this is the subject of this work, selective methylation of aromatic ethers will be discussed separately in this sub-chapter.

None of the routes discussed below has been commercialised.

2.1.12.1 Methylation of aromatic ethers by bulky methylating agents

Fujita et al. (1992) patented a process for methylation of diphenyl ether with polymethylated naphthalenes as the alkylating agents. The polymethylated naphthalenes used had a minimum of five methyl substituents. $AlCl_3$ was used as a catalyst.

The reaction was performed in the liquid phase, at 50 °C. A mixture of diphenyl ether and $AlCl_3$ was reacted with the methylating agent, octamethylnaphthalene (OMN), dissolved in *o*-dichlorobenzene, to give both the mono-methylated 4-methyldiphenyl ether (i.e. *p*-phenoxy toluene (PPT)) and the di-methylated 4,4'-dimethyldiphenyl ether (i.e. *p*-tolyl ether (PTE)) (Fujita et al., 1992).

Selectivities of 52 % and 30 % were obtained for PPT and PTE, respectively, with diphenyl ether (DPE) conversion of 81 % (Fujita et al., 1992). Nothing was mentioned about the by-products of the reaction, which account for the remaining 18% of the product mixture.

No explanation was obtained from the authors for the high *p*-selectivity observed. The high selectivity could be due to steric constraints imposed by the bulky alkylating agent, denying access to the *o*-position of the ether. If the catalyst, $AlCl_3$, forms a complex with the oxygen in the ether, access by such bulky methylating agents to the *o*-position of DPE would be denied. The *m*-position, for the given reaction conditions, is less reactive and this would leave the *p*-position as the only favoured methylation position.

The reaction studied by Fujita et al. (1992) is shown in Figure 2-8.

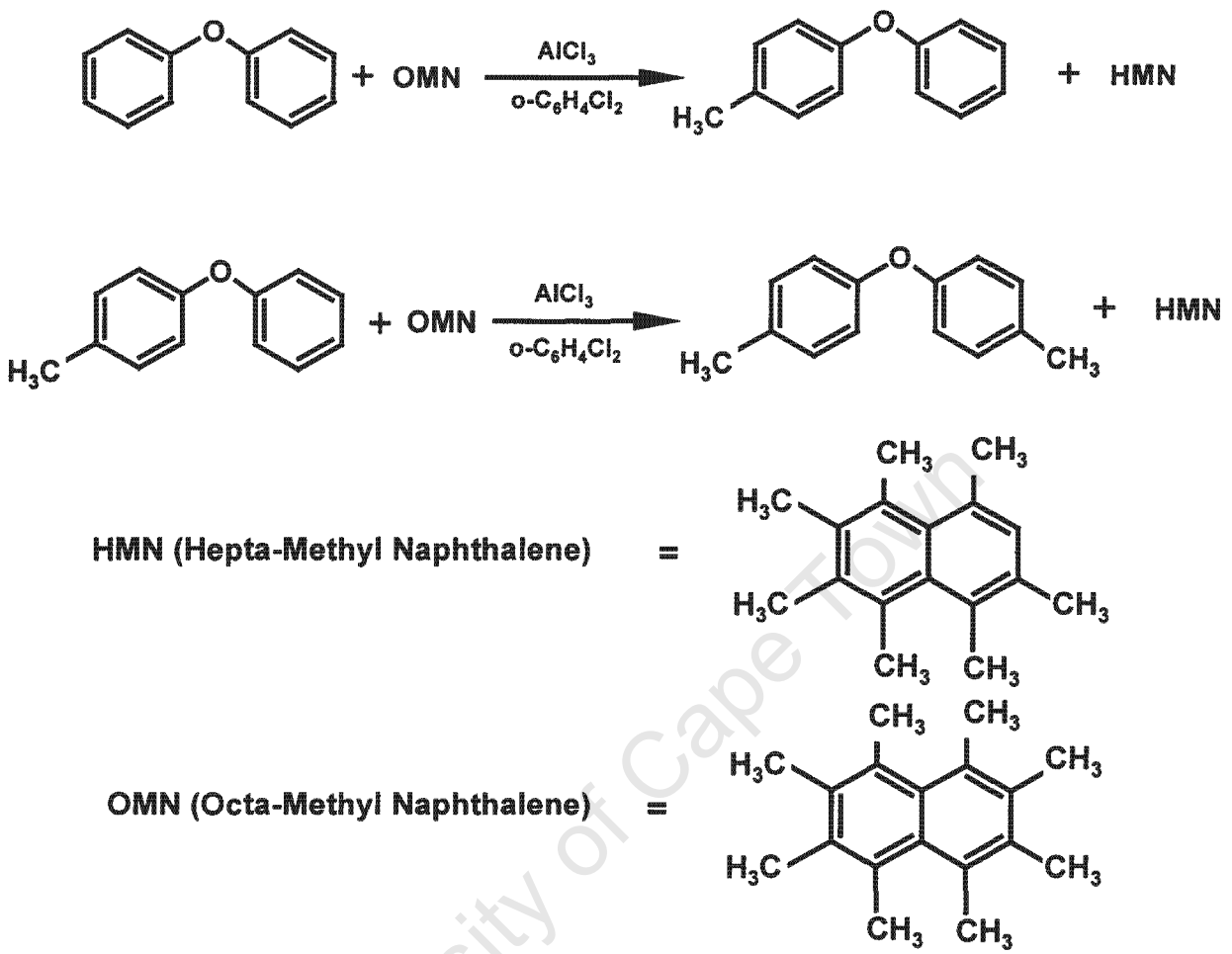

Figure 2-8: Methylation of diphenyl ether with bulky methylating agent (adopted from Fujita et al., 1992)

During transalkylation (i.e. transfer of a methyl group from octamethyl naphthalene to diphenyl ether), any methyl group can be removed to give heptamethyl naphthalene.

The apparent disadvantages of this process are the use of harmful halo-aromatics as solvents, which need to be handled with care and the use of a highly corrosive non-recoverable catalyst. The methylating agent is also a non-common industrial material.

The reaction was studied on a laboratory scale and not commercialised. The concept of this process is however interesting because it is directly related to the reaction under study.

2.1.12.2 Alkylation of diphenyl ether with methanol over H-ZSM5

Chantal et al. (1985) carried out methylation of diphenyl ether with methanol over H-ZSM5 catalyst, in a fixed bed reactor. The reactants were fed as a mixture of 10% by weight methanol (molar ratio DPE:Methanol = 5:3).

At a space velocity of 1.2 h^{-1} (based on total mass fed), and at temperatures of 350, 400 and 450°C, the conversions of diphenyl ether were 7.5, 12.8 and 2.4 %, respectively. The pressure for this reaction was not reported. Helium was used as a carrier, giving an indication of sub-atmospheric feed partial pressure, hence a gas phase reaction.

The decline of conversion of diphenyl ether at reaction temperature of 450°C could be due to consumption of methanol by the competing side reactions such as formation of hydrocarbons (i.e. methanol-to-gasoline reaction).

Alkylation of phenol with methanol was also carried out in the same study under the same conditions as for diphenyl ether – methanol mixture. Conversions for phenol were found to be 52.2, 67.2 and 78.3 %, increasing with reaction temperatures of 350, 400 and 450°C, respectively.

The authors attributed the low conversion of diphenyl ether, in comparison to phenol, to its low effective diffusivity in the pores of H-ZSM5 zeolite.

This reaction was only carried out on a laboratory scale, and no further information was provided about its commercialisation.

2.1.12.3 Alkylation of diphenyl ether with methanol over H-beta

A study was conducted by Ndlovu and Gxhavu (2000) in which diphenyl ether was alkylated with methanol in an autoclave reactor, operated in batch mode at 250°C and autogeneous pressure, over H-beta crystal powder of SiO_2/Al_2O_3 ratio of 25. Methanol/DPE molar feed ratio was 2.

The major products of the reaction were *o*-phenoxy toluene and *p*-phenoxy toluene but no preference for *p*-alkylation.

It was also established, corresponding to observations by Fujita et al (1992), that diphenyl ether methylation with methanol is a consecutive reaction.

2.1.13 Other synthetic routes to *p*-cresol.

Ever since the recovery of cresols from coal tar and spent refinery caustics became insufficient to meet the rising market demands, synthetic methods have been developing for these compounds (Fiege, 2000). However, synthetic routes are still under-developed for selective *p*-cresol synthesis. Efforts to develop new process routes specific to *p*-cresol are addressed in this section.

2.1.13.1 p-Cresol by isomerisation of its isomers

Different catalysts such as $AlCl_3$, AlF_3, BF_3, amorphous alumino-silicates, phosphoric acid, etc., have been used for isomerisation of cresols and were proved unsatisfactory. The main disadvantages of these catalysts include the disproportionation of the cresols to phenol and xylenols, as well as environmental constraints (Fiege, 2000).

In the case of *p*-cresol, either *o*-cresol or *m*-cresol (or a mixture of *o*- and *m*-cresol) would be introduced as the feed. Favourable isomerisation temperatures are reported to be above 300°C. However, *p*-cresol manufacture by isomerisation of other cresol isomers will lead to high separation costs due to the mixture of all the three cresol isomers (Fiege, 2000).

2.1.13.2 p-Cresol by oxidative catalysis

Rodkin et al. (2000) carried out a study in which aromatics were catalytically oxidised by nitrous oxide (N_2O), over Fe-ZSM-5. In their experiments, oxygen was loaded on Fe-ZSM-5, at 250 °C through the decomposition of N_2O with evolution of N_2 into the gas phase. The organic vapour of the aromatic to be oxidised then replaced the gas in the reaction volume.

Oxidation occurred by O-atom insertion in a C-H bond. The product from toluene oxidation comprised 30 % benzyl alcohol and 70 % cresols. The cresols were in the ratio *o*:*m*:*p* = 1:1:2.5, thus a *p*-cresol content of more than 50% was obtained in the cresol fraction.

Bearing in mind that a shape selective catalyst (Fe-ZSM-5) was used, Rodkin et al. (2000) concluded that regioselective hydroxylation was strongly influenced by the constraints imposed

by the micropores of the zeolite matrix. This conclusion was however not substantiated by further tests on wide pore or amorphous materials.

The reaction was pilot-tested by Solutia Inc. in co-operation with the Boreskov Institute of Catalysis. According to Rodkin et al. (2000), these pilot tests were successfully carried out at Solutia's facilities in Pensacola, USA. This process route, however, suffers from the need for a cheap source of N_2O and a market for the benzylalcohol by-product, which could be the reasons why it was not commercialised.

2.1.13.3 Diels-Alder route to p-cresol

This is a three-stage process, deemed to be highly selective to *p*-cresol (Fiege, 2000). However, the patent for this process claims 30% and 50% selectivities for the first and the last stages, respectively (Koennecke et al., 1968). The reaction steps are summarised in Figure 2-9 and Figure 2-10.

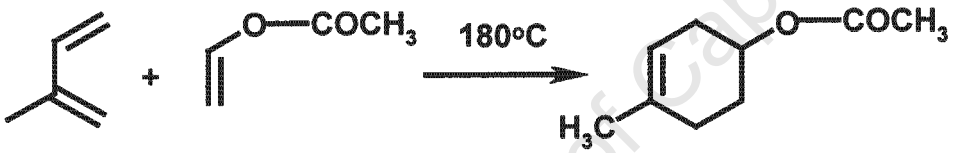

Figure 2-9: Cyclisation, the first stage of Diels-Alder route to *p*-cresol (Fiege, 2000)

The first step is a ring closure of isoprene and vinyl acetate (Figure 2-9). This step is carried out in an autoclave with 1 % hydroquinone, at 180°C and elevated pressure, to yield a cycloolefinic ester (Fiege, 2000). Different orientations of the reactants of Figure 2-9 would lead to *m*-cresol. This could be the reason why selectivity of the first step is only 30%.

The ester is saponified with methanol to yield a cyloolefinic alcohol, which is eventually dehydrogenated over platinum to yield *p*-cresol, as shown in Figure 2-10 (Fiege, 2000):

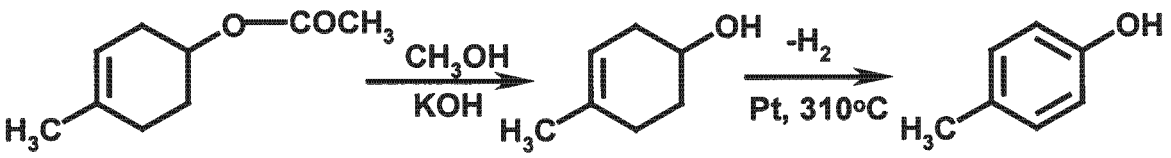

Figure 2-10: Second and third reaction stages of Diels-Alder route to p-cresol (Fiege, 2000)

It is claimed that the process has high yields, when the unconverted starting materials are recycled (Fiege, 2000). According to Fiege (2000), the disadvantage of this process is its expensive recycle rates. Again considering the process economics, the starting materials in this process are relatively expensive. This could mean that the conversion per pass in the cyclisation step is very low. No details were provided about whether this process is commercialised.

2.1.13.4 p-Cresol synthesis by Gulf oxychlorination

This synthetic route is analogous to the Raschig process for phenol synthesis. In this process, toluene is chlorinated with HCl in the presence of oxygen, giving chlorotoluene and water, with chlorotoluene being subsequently hydrolysed with steam (Fiege, 2000).

Gulf Research Development Co. achieved a para to ortho cresol ratio of 0.5 with 32% selectivity to the para-isomer, at a conversion of 80%, based on toluene fed. The product is reported to contain small quantities of *m*-cresol (Fiege, 2000).

Exploitation of this process for commercial purposes reveals a necessity for recycling HCl released in the hydrolysis step and also imposes severe demands for the plant to be corrosion resistant.

2.1.13.5 Baeyer-Villiger oxidation of p- or o-methylbenzaldehyde

In this process performic acid is prepared by reacting hydrogen peroxide with excess formic acid. *p*-Methylbenzaldehyde is then oxidised with perfomic acid to form *p*-tolyl formate. Hydrolysis of the latter leads to *p*-cresol and formic acid. It is reported that a *p*-cresol yield of 85 % is obtained at 100 % conversion of *p*-methylbenzaldehyde (Fiege, 2000).

According to Fiege (2000), the starting material (*p*-methylbenzaldehyde) can be produced from toluene and carbon monoxide in a process developed by Mitsubishi, called MGC PTAL process.

2.1.14 Phenol methylation over acid zeolites

Whereas phenol methylation with methanol over γ-alumina is the state of the art, phenol methylation over acid zeolites is not yet commercialised (Fiege, 2000).

Methylation of phenol over acid zeolites has been studied and reported in the literature. A few of these results are discussed here.

Sinitsyna and Romanovski (1992) carried out a vapour phase methylation of phenol over pentasils of SiO_2/Al_2O_3 ratios ranging from 69 to 84, in the temperature range of 350 – 450°C, at a space velocity of 2.2 h^{-1} (total feed) and a molar feed ratio of unity. Results are summarised in Table 2-9.

Table 2-9: Average rates [mmol·g^{-1}·h^{-1}] of formation of products in the alkylation of phenol with methanol, over pentasils (Sinitsyna and Romanovski , 1992)

	SiO_2/Al_2O_3	T [°C]	Anisole	*o*-Cresol	*p*-Cresol	*m*-Cresol	Xylenols
Zeolite I	69	350	0.7	2.6	1.1	1.6	1.1
		400	0.5	2.5	1.0	2.0	1.4
		450	0.4	1.9	0.8	2.6	2.2
Zeolite II	78	350	1.6	1.4	0.5	0.4	0.4
		400	0.9	1.6	0.7	0.6	0.7
		450	0.7	2.5	1.1	1.0	1.1
Zeolite III	86	350	0.8	3.2	1.2	0.5	0.7
		400	0.6	3.0	1.1	1.2	1.1
		450	0.4	2.1	1.0	2.0	1.8
Zeolite IV	84	350	0.8	1.7	0.7	0.4	0.6
		400	0.7	2.6	1.0	0.4	1.0
		450	0.5	2.9	1.2	0.9	1.5

With the use of ammonia desorption, three regions of acidic centres were characterised by means of temperature ranges as follows:

- weak acid centres: 100 – 200°C
- medium acid centres: 200 – 250°C
- strong acid centres: 250 – 550°C

The concentrations of acidic centres were determined for each zeolite, and based on the average rates of Table 2-9, "regional rates" were determined for each product formed. The "regional rates" are shown in Table 2-10.

Table 2-10: "Regional rates" [mmol·mmol-(desorbed)NH_3^{-1}·h^{-1}] of the formation of products in the alkylation of phenol with methanol over various zeolites at different temperatures (Sinitsyna and Romanovski , 1992)

Acidic centre	T [°C]	Anisole	*o*-Cresol	*p*-Cresol	*m*-Cresol	Xylenols
Weak	350	3.9	0.2	0	0	0.1
	400	3.1	0.1	0.5	0.3	0.2
	450	2.5	5.9	2.5	0.3	0.4
Medium	350	0.5	14.3	5.7	0	3.2
	400	0.4	20.4	6.7	1.3	6.0
	450	0.2	12.4	5.3	5.2	9.4
Strong	350	0.3	8.2	3.5	7.3	3.9
	400	0.1	4.4	1.8	9.2	4.1
	450	0	0	0	10.8	6.7

It was concluded that anisole formation was favoured on weakly acidic centres and *m*-cresol on strongly acidic centres. *p*-Cresol and *o*-cresol were said to be favoured on medium acidity sites.

In another work by the same research group (Sinitsyna and Romania, 1993), anisole yield was found to be high at low temperatures, and low at high temperatures, whereas *m*-cresol yield was favoured at high temperatures. In the latter study, pentasils were also modified with P_2O_5 and MgO. The authors concluded that modifications increased the selectivity to *p*-cresol by a factor close to 2. Some of the results upon which this was concluded are given in Table 2-11. Nonetheless, the predominant isomer was still *o*-cresol.

Table 2-11: Cresol distribution from phenol methylation over modified pentasils at 400°C, 1 h^{-1} space velocity and methanol/phenol molar ratio of 2 (Sinitsyna and Romania, 1993)

Modifier	Conversion of phenol	*o*-Cresol	*p*-Cresol	*m*-Cresol
None	48	51.5	22.8	25.7
5 wt% P_2O_5	41	54.6	31.8	13.6
6 wt% MgO	29	47.1	35.3	17.6
Equilibrium mixture[a)]	—	35.8	8.7	55.5

[a)]According to Sinitsyna and Romania (1993).

Xu et al. (1997) also studied methylation of phenol with methanol over zeolite H-beta of SiO_2/Al_2O_3 ratio of 28.2. The reaction was carried out in gas phase in a flow system at 200 and 300 °C, and at atmospheric pressure. Methanol to phenol molar ratio of 5:1 was used, diluted with nitrogen at a molar ratio of 1:6. In the total product pool, anisole was the predominant product at 200 °C, with the cresol fraction rich in the ortho isomer. Neither the breakdown of the cresol fraction nor that of the xylenol fraction was reported. At 300 °C, conversion of phenol increased such that the xylenol fraction was more than the cresol fraction in the total product pool. Anisole selectivity was decreased by a factor of about 6, and *o*-cresol was still the predominant isomer, in the cresol fraction. The ratio of *p*-/*o*-cresol was less than 0.5 in all experiments.

Several zeolites were screened by Landau et al. (1997), for phenol methylation. The reactions were carried out in gas phase in a fixed bed reactor at atmospheric pressure with methanol:phenol molar feed ratio of 0.5, phenol weight-hourly space velocity of 1.8 h^{-1} and nitrogen mole fraction of 0.87. The reactor temperature was 300 °C. Several catalysts were screened, as shown in Table 2-12.

Table 2-12: Product composition from phenol methylation over various acid zeolites (SiO_2/Al_2O_3 ratios in brackets). T=300°C; P=1atm; molar ratio methanol/phenol=0.5; phenol WHSV=1.8h^{-1} and P_{feed}=0.13 atm (Landau et al., 1997)

Zeolite (SiO_2/Al_2O_3 ratio)	H-Beta (25)	H-Mordenite (17)	H-Y (60)	H-ZSM-5 (30)
X_{Phenol} (%)	29	11	22	31
$S_{Anisole}$ (%)	28	41	32	35
$S_{o\text{-}Cresol}$ (%)	37	23	32	36
$S_{m\text{-}Cresol}$ (%)	11	10	10	11
$S_{p\text{-}Cresol}$ (%)	18	18	21	14
$S_{Methyl\ anisole}$ (%)	5	5	5	3
$S_{Xylenols}$ (%)	0.1	0	0	1
p-/o-Cresol	0.49	0.78	0.65	0.39

H-mordenite showed the highest *p*-cresol to *o*-cresol ratio of about 0.8, but at the same time, showed the highest selectivity to anisole. H-mordenite gave a conversion of 11 %. *m*-Cresol selectivity was the same for all the catalysts, even though the conversions were different. H-beta zeolite was reported as the most stable catalyst, in terms of deactivation (Landau et al., 1997).

According to Landau et al (1997), methanol side reaction to dimethyl ether was negligible.

2.1.14.1 Enhanced p-selectivity over zeolite H-MCM-22

The highest *p-/o*-cresol ratio from phenol methylation to date was reported by Moon (Moon et al., 2001; Moon et al., 2002; Moon, 2003; Moon et al., 2004 and O'Connor et al., 2003) in which phenol methylation was carried out over several acid zeolites including H-MCM-22, in an autoclave reactor. At the reaction temperature of 200°C and autogeneous pressure of more than 20 bar in the liquid phase, H-MCM-22 gave a *p-/o*-cresol ratio of 1.3, at a phenol conversion of 2.4%, with only traces of *m*-cresol formed. Anisole was still the predominant product with selectivity in excess of 90%.

Product compositions obtained by Moon at low temperature and high pressure in liquid phase are given in Table 2-13.

Table 2-13: *p-/o*-Cresol ratio and phenol conversion from liquid phase, batch phenol methylation over different catalysts (200°C, 21 - 23 bar, 1:1 molar feed ratio, modified weight hourly space velocity = 8 h^{-1}) (Moon et al., 2002)

	Phenol conversion (%)	*p-/o*-Cresol ratio
H-ZSM-5	9.5	0.4
H-MCM-22	2.4	1.3
SiO_2 - Al_2O_3	0.4	0.4
H/Na-ZSM-5	1.2	0.6
H/Na-MCM-22	2.0	0.3

The results also showed that selectivities did not change with residence time or conversion (Moon et al., 2002)

It was found that *p*-selective phenol methylation over zeolite H-MCM-22 was introduced by internal mass transport limitations, hence product selectivity (O'Connor et al., 2003). The reason could be the unique pore system of zeolite MCM-22, with independent two-dimensional interconnected medium pore channels (Leonowicz et al., 1994; Lawton et al., 1998; Baerlocher et al., 2001). It was also shown that the *p-/o*-cresol ratio increased with increasing Thiele modulus. A *p-/o*-cresol ratio of unity was achieved at 300°C in gas phase, over large (1 μm) crystals (see Figure 2-11).

In Figure 2-11, the *p-/o*-cresol ratio is plotted vs. a modified Thiele modulus:

$$\phi_{mod} / (1/D_i)^{0.5} = \xi \, r \, X^{0.5}$$

with:

- assumption of first order kinetics
- assumption of rate constant k being proportional to, approximately, conversion X for differential operation; i.e. low conversion

- assumption of characteristic length = radius of crystallites, $\Re$, with spheres of $\Re$ = 0.2 μm for H-ZSM-5 and platelets of 0.2 - 1 μm for H-MCM-22 samples
- D_i = diffusion coefficient of species i, in the zeolite pores
- ξ = shape factor of zeolite crystallites

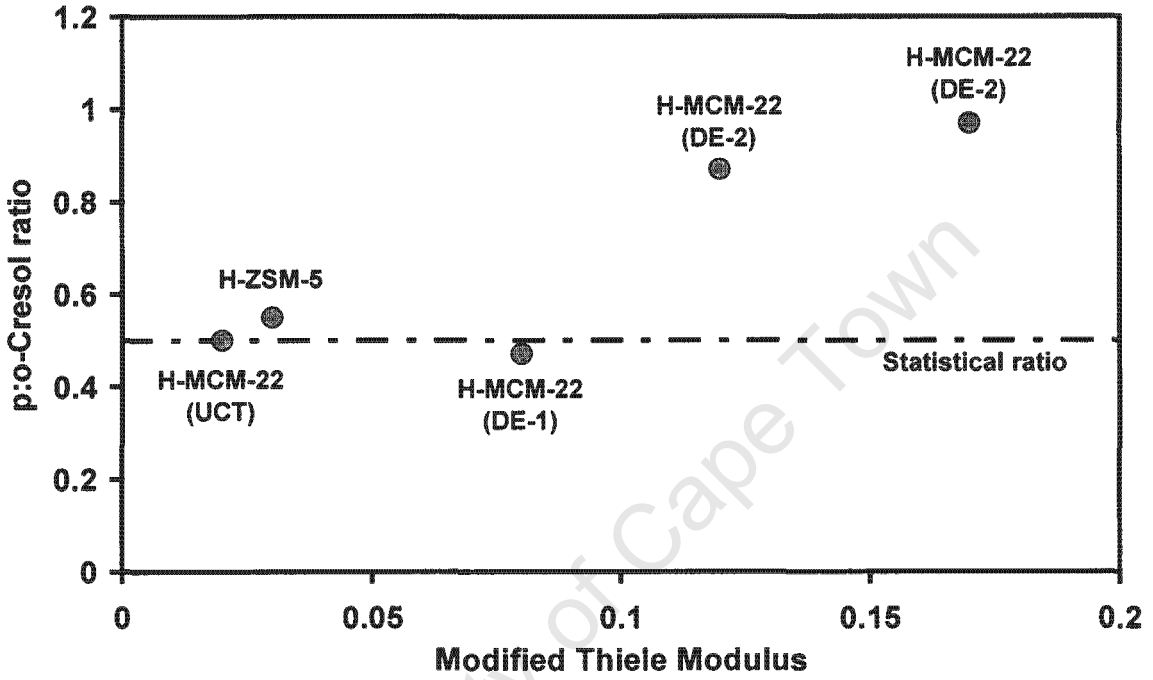

Figure 2-11: Relationship between *p*-/*o*-cresol ratio over zeolite H-MCM-22 crystals of different size and activity vs. a modified Thiele modulus (gas phase alkylation, methanol to phenol ratio = 1 mol/mol, 300°C, 0.2 bar feed partial pressure, W/F=0.07 $g_{cat}.h/g_{feed}$).

The results of Figure 2-11 were also supported by Moon et al. (2004), where it was shown that high pressure, low temperature liquid phase operation enhanced *p*-selective phenol methylation. It was also concluded that this was due to high occupation of the zeolite pore system by phenol under these conditions, hence increased diffusion constraints for desorbing products.

Commercialisation of this process would of course require maintaining such high *p*-/*o*-cresol ratios at significantly higher conversions to avoid high recycle rates, which would necessitate high capital, and operating costs. It was found by Moon et al. (2002) that the low reaction temperature selectivities did not change with conversion.

2.2 CATALYSIS

Catalysis is a process whereby chemical reactions take place over materials which speed up reactions and are themselves not consumed during the reactions. Such materials are called catalysts. These materials may selectively speed up one or more of a range of possible reactions, for a particular feed, at specific conditions. It is usually preferred that the catalysts should affect only one or more specific reaction(s), and catalysts that possess this property are referred to as selective (Fogler, 1999 and Shriver et al., 1994).

Catalysis and the development thereof are important because this is one of the major ways in which rates, yields and selectivity are increased in industrial processes (Fogler, 1999). Catalysts are used in the production of major organic chemicals and petroleum products such as petrochemicals, fuels and poly-alkene plastics. Nowadays, catalysts are also gaining industrial importance because they are a means of achieving a cleaner environment, in some processes, by destruction of pollutants as well as through cleaner industrial processes with fewer by-products (Shriver et al., 1994).

2.2.1 Energetics of catalysis

Catalysts only increase the rate of approach to thermodynamic equilibrium, in a chemical reaction, but do not alter the equilibrium (Gates, 1993). This means that reactions that are not thermodynamically favoured cannot be made favourable by catalysts (Shriver et al., 1994). In a system of parallel reactions, however, the proportion of one or more product compounds may exceed their simultaneous equilibrium proportion due to a selective catalyst.

Every chemical reaction has an energy barrier called activation energy. This is the energy that has to be taken up by the reactants to reach a transition state, before being converted into products (Fogler, 1999). A catalyst accelerates the reaction by lowering this energy barrier, as illustrated in Figure 2-12.

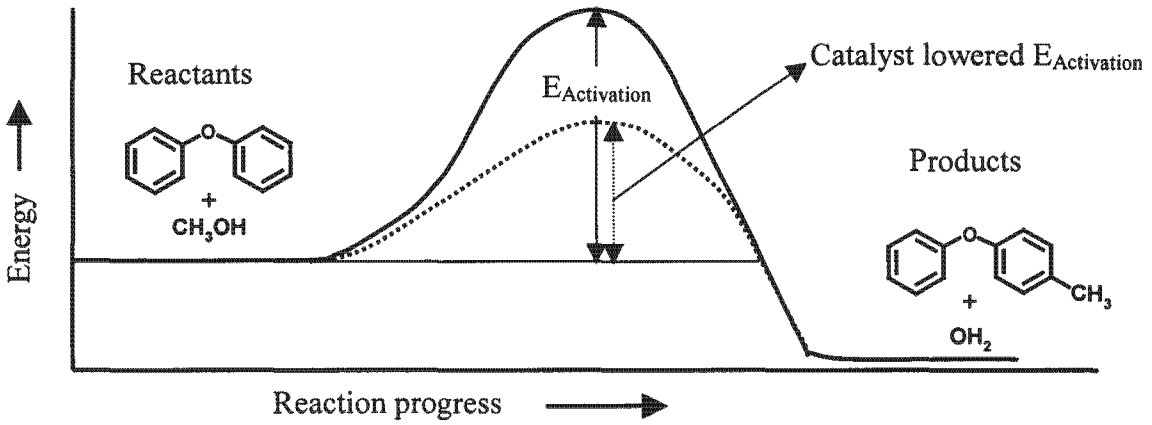

Figure 2-12: Catalyst effect on activation energy in a chemical reaction. ***(adopted from Fogler (1999) and drawn for diphenyl ether methylation)***

Catalysts increase the rates of reactions by giving the reactants alternative pathways or mechanisms, which have lower activation energy (Shriver et al., 1994). They form bonds with one or more reactants and in that way open up alternative pathways to the conversion of the reactants into products (Gates, 1993).

2.2.2 Heterogeneous catalysis

Catalytic processes can be homogeneous or heterogeneous. Heterogeneous catalysis occurs when a solid catalyst is used in a reaction where the reactant(s) and/or product(s) are liquids or gases or a combination of these, whereas homogeneous catalysis occurs when the catalyst is in solution with at least one of the reagents (Fogler, 1999).

Most of the catalysed industrial processes are heterogeneous, with the catalyst in the solid phase and the reactants and products in the liquid or gaseous phase, just like in the reaction under study. Heterogeneous catalysis is often more economically attractive than homogeneous catalysis because of simple and complete separation of the resulting product mixture from the catalyst (Fogler, 1999).

In heterogeneous catalysis, the reaction occurs at the fluid-solid interface or at the active site and thus a large interfacial area is desired for high reaction rates per unit mass of a catalyst. Solid catalysts provide a high surface area by porosity in their structure (Fogler, 1999).

2.2.3 Molecular sieves and zeolites

In some porous crystalline materials, the pores are so small that they allow only specific molecules of a certain shape and a certain maximum size to diffuse through them and prevent the larger ones from entering or leaving the pores. Materials of this type are called molecular sieves (Fogler, 1999).

Molecular sieves form the basis for very selective catalysts because the pores can control the residence time of different molecules inside the pores, via mass transport control, i.e. diffusion constraints. Some of them have spacious pore crossing sections or large spaces called cages, which can accommodate bulky transition states. Of particular technological importance among the different classes of molecular sieves are the zeolites. They are crystalline aluminosilicates with channels of less than 12 Å in diameter (Kühl and Kresge, 1993).

Zeolites are inorganic polymers with AlO_4 and SiO_4 tetrahedra interconnected "infinitely", in a three-dimensional structure/pattern (McCusker and Baerlocher, 2001). The tetrahedra are linked to each other by the sharing of oxygen atoms. Each AlO_4 tetrahedron bears an overall negative charge which has to be balanced by an extra framework cation. In the case of both natural and synthetic zeolites, the cations are usually elements from groups IA and IIA, of the periodic table (Flanigen, 2001).

The zeolite framework structure has voids or channels (two or three dimensionally interconnected in some zeolites), which are occupied by water molecules and the charge balancing cations. These cations are mobile and readily undergo ion exchange. The water molecules in the voids can also be removed, reversibly, by application of heat. Removal of water simply leaves voids and micropores, with the crystalline host structure still intact (Flanigen 2001).

The zeolite pores are characterised by the size of the ring defining the pore. The pore size is classified according to the number of T-atoms (Si or Al) in the ring. A zeolite with pores made of 8-membered rings is considered to be a small pore zeolite, the one with 10-membered rings as a medium pore zeolite and the one with 12-membered rings as a large pore one, with average pore diameters of 4.1, 5.5 and 7.4 Å, respectively (McCusker and Baerlocher, 2001).

According to Flanigen (2001), the zeolite framework has to be viewed as somewhat flexible, and the framework size, shape and pore diameters respond to changes in temperature and guest species.

There are two basic types of zeolite structures. The first is comprised of cage-like voids interconnected by windows. The second has uniform channel systems. The preferred structure in adsorption and many catalytic applications is that which has two- or three-dimensionally interconnected void or channel systems, to provide rapid intra-crystalline diffusion (Flanigen, 2001).

There are more than 70 novel, distinct zeolite structures known today, and they have pore sizes in the range of 3 to 10 Å, with pore volumes of 0.1 to 0.35 m^3/kg (Flanigen, 2001).

2.2.4 Adsorption and catalysis

In heterogeneous catalysis one or all of the reactants is/are usually considered to adsorb (usually by chemisorption) onto the solid surface and then get transformed into a form which allows it to undergo further transformation readily (Atkins, 1994).

Zeolites adsorb molecules into their channels or reject them based on differences in size, shape and other properties such as polarity. When the aperture of a molecular sieve or zeolite is small in comparison to the approaching molecule, the repulsive interaction becomes dominant and the diffusing molecule requires a specific activation energy to be able to pass through the aperture. During adsorption of various molecules, the micropores can be filled and emptied reversibly. Adsorption in zeolites is said to be a simple pore filling and not the usual surface area adsorption phenomenon (Kühl and Kresge, 1993).

2.2.4.1 Acidity of zeolites

The charge balancing cations, in zeolites, are usually ion exchanged for ammonium ions to introduce acid function. Calcination of the zeolite in its ammonium form results in expulsion of ammonia gas, which leaves a proton behind. The latter, associated with the bridging oxygen between an aluminium and a silicon atom, is a strong Brönsted acid site (Kühl and Kresge, 1993).

Silanol groups are hydroxyl groups terminating the zeolite framework on the outer surface of the zeolite crystals. According to Martens and Jacobs (2001), these silanol groups, together with the bridging oxygen atoms on the exterior zeolite crystal surface, are much weaker Brönsted acid sites than the hydroxyl groups formed by the charge balancing protons associated with the aluminium atoms inside the micropores.

The number of strong acid sites in the zeolite increases proportionally with the aluminium content, because aluminium is directly related to the number of Brønsted acid sites present in the zeolite. The strengths of the individual acid sites however, decrease with increasing aluminium content (Gates, 1993).

2.2.5 Selectivity

In many chemical processes, side reactions are a problem because they usually produce unwanted, i.e. non-economic and non-environmentally friendly products. Selective catalysts must therefore yield high proportions of the desired product and minimum amounts of by-products (Shriver et al., 1994).

Selectivity can therefore be defined as a measure of a property of a catalyst to direct a reaction into a specific path, with specific products (Gates, 1993). It is often defined as the ratio of the rate of the desired reaction to the sum of all other reactions occurring (Gates, 1993).

2.2.5.1 Shape selectivity in zeolites

Martens and Jacobs (2001) define shape selectivity as reaction specificity resulting from the presence of a sterically confined environment wherein the molecules are converted. Shape selective catalysis occurs in the bulk of the zeolite crystals (Martens and Jacobs, 2001).

Catalytic behaviour of acid zeolites depends on pore openings, dimensions of the channel system, acid sites and the internal space available for transition states and reaction intermediates (McCusker and Baerlocher, 2001). Similarly, shape selectivity in zeolites usually coincides with the matching of size and shape of the reactants, transition states and products, with the size and shape of the micropores (Martens and Jacobs, 2001).

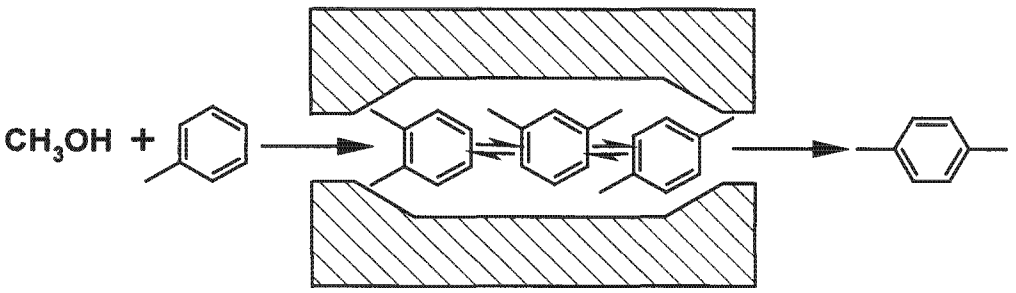

Figure 2-14: Product selectivity (Csicsery, 1984)

2.2.5.2.3 Transition state shape selectivity

Spatial constraints can occur around a reaction intermediate or a transition state located inside a cage, channel or channel crossing of the zeolite crystallite, such that only certain configurations are possible. This is termed transition state shape selectivity (Martens and Jacobs, 2001).

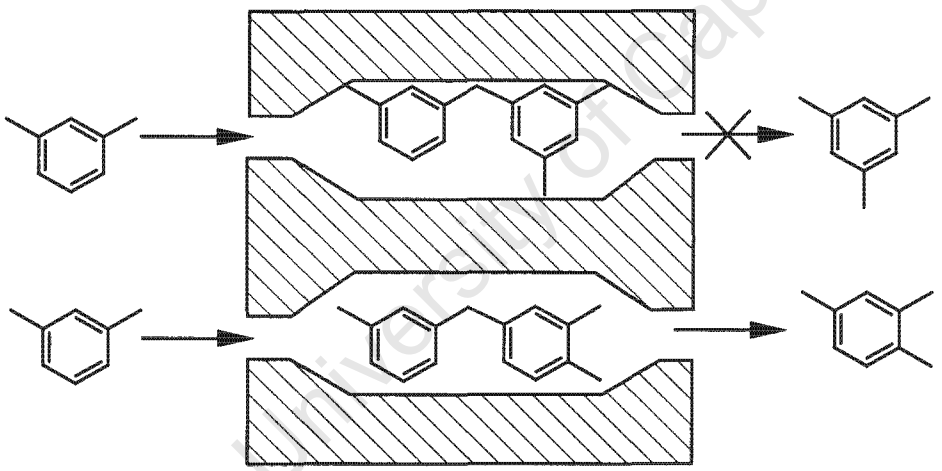

Figure 2-15: Transition state shape selectivity (Csicsery, 1984)

In some cases, product and transition state shape selectivity are not readily distinguishable. A distinction between the two can be established by changing the zeolite crystal size, because product selectivity is dependent on the length of the diffusion path whereas transition state shape selectivity is not (Martens and Jacobs, 2001).

2.2.5.3 Modelling intracrystallite diffusion and shape selectivity

When there is a large diffusivity difference between molecules inside the zeolite channels, and the diffusion rate of the slowest diffusing species (product or reactant) cannot keep up with their rate of conversion or formation, a special kind of selectivity occurs and this selectivity is termed configurational diffusion selectivity. In molecular sieves, both reactant and product selectivity are forms of configurational diffusion selectivity (Chen et al., 1994).

Reactant and product selectivity in zeolites can be explained and quantified by using the Thiele modulus. Any species taking part in a reaction occurring inside a zeolite pore can be modelled with this modulus. If the species is a reactant, the concentration drops progressively from the external surface of a zeolite particle, to the centre of the particle. However, if the species is a product, the concentration will be highest at the centre of the particle and lowest at the external surface, assuming that the external surface concentration is the same as the bulk concentration (Levenspiel, 1972).

Thiele modulus, ϕ, is defined as the ratio of an internal surface reaction rate, i.e. intrinsic rate, to that of a diffusion rate inside a catalyst particle. In a simple case of a first order reaction, the modulus is given by Equation 2-1 (Fogler, 1999).

$$\phi = L\sqrt{\frac{k_i}{D_i}} \qquad \textbf{Equation 2-1}$$

where: k_i = intrinsic rate constant of species i

L = characteristic length of a particle, indicative of the diffusion path length

D_i = diffusion coefficient of species i

When a reaction is diffusion limited, the observed or apparent rate constant, $k_{i,\,obs}$, is lower than the intrinsic rate constant, k_i. A mathematical relation of the latter is as shown in Equation 2-2.

$$k_{i,obs} = \eta \cdot k_i \qquad \textbf{Equation 2-2}$$

where: η = effectiveness factor

Effectiveness factor is defined as the ratio of the observed rate to that of the intrinsic rate (Fogler, 1999).

The relationship between η and ϕ is dependent on the crystallite geometry and the reaction order. For a first order reaction, the effectiveness factor is related to the Thiele modulus according to Equation 2-3 (Fogler, 1999; Chen et al., 1994).

$$\eta = \frac{\xi}{\phi}\left(\frac{1}{\tanh\phi} - \frac{1}{\phi}\right) \qquad \textbf{Equation 2-3}$$

where: ξ = shape factor of zeolite crystallites

At large values of Thiele modulus, Equation 2-3 reduces to Equation 2-4.

$$\eta = \frac{\xi}{\phi} \qquad \textbf{Equation 2-4}$$

Combining Equation 2-1 and Equation 2-4 gives Equation 2-5.

$$\eta = \frac{\xi}{L}\sqrt{\frac{D_i}{k_i}} \qquad \textbf{Equation 2-5}$$

For two parallel reactions wherein reactants diffuse through the zeolites, observed selectivity is determined by Equation 2-6 (Chen et al., 1994).

$$S_{obs} = \frac{k_{i,obs}}{k_{j,obs}} = \frac{\eta_i k_i}{\eta_j k_j} = \frac{\phi_j k_i}{\phi_i k_j} = \sqrt{\frac{\eta_i \cdot D_i}{\eta_j \cdot D_j}} \qquad \textbf{Equation 2-6}$$

When isomers are formed from the same reactants, as in the case of the reaction under study, wherein diphenyl ether is methylated to *o*-phenoxy toluene, *p*-phenoxy toluene or *m*-phenoxy toluene, selectivity can be modelled according to Equation 2-7.

$$\left(\frac{k_{DPE\rightarrow PPT}}{k_{DPE\rightarrow OPT}}\right)_{obs} = \left(\frac{D_{PPT}}{D_{OPT}}\left(\frac{k_{DPE\rightarrow PPT}}{k_{DPE\rightarrow OPT}}\right)_{intrinsic}\right)^{1/2} \qquad \textbf{Equation 2-7}$$

2.2.6 Pore systems of zeolites of interest

Channel geometry primarily governs selectivity over zeolites during reactions, whereas acidity primarily governs activity of these catalysts (Kühl and Kresge, 1993). Catalyst performance is largely measured by reaction kinetics because the catalyst influences the rate of reaction (Gates, 1993).

A list of candidates tested for the reaction under study is given in Table 2-14, together with their pore geometries.

Table 2-14: Pore systems (Meier et al., 1996) of the zeolites tested for the reaction under study

Catalyst (ring size)	Pore dimensions [Å]	Channel system	Cages and voids
Beta (BEA) (12-membered)	6.4 x 7.6 (2 systems) 5.5 x 5.5	3-dimensionally interconnected	pore intersections
ZSM-5 (MFI) (10-membered)	5.4 x 5.6 5.1 x 5.5	2-dimensional; 3-dimensionally interconnected	off-set pore intersections
Mordenite (MOR) (12-membered)	6.7 x 7.0 2.6 x 5.7	1-dimensional	small side pockets in wide channels
Faujasite (FAU) (12-membered)	7.4 x 7.4 (windows between cages)	3-dimensional interconnected	spherical cages of 13Å diameter

2.2.6.1 Zeolite Beta

In zeolite beta (BEA), two types of well-defined layers of the building units (pentasils – 5-ring units), mirrored against each other, are stacked in more or less random fashion. Zeolite beta has a 3-dimensional interconnected channel system, with 12-ring pore openings, so that it is a large pore zeolite (McCusker and Baerlocher, 2001).

Zeolite beta has two perpendicular straight channel systems, each with a cross section of 6.4 x 7.6 Å. The third channel is sinusoidal with a cross section of 5.5 x 5.5 Å, and is also perpendicular to the straight channels interconnecting in 3-dimensional pore crossings (Jansen et al., 1997).

2.2.6.2 Zeolite ZSM-5

The framework of zeolite ZSM-5 (MFI) is of pentasil units (i.e. five T-atom rings). It has 10-membered ring pore openings, which means that it is a medium pore zeolite, with 2-dimensional channel system (McCusker and Baerlocher, 2001).

ZSM-5 has a 2-dimensional pore system consisting of straight channels of 5.3 x 5.6 Å, which are interconnected with sinusoidal channels of 5.1 x 5.5 Å running perpendicular to them. Interconnections are staggered, resulting in a 3-dimensionally-interconnected pore system of spacious channel cross-section (Jansen et al., 1997).

The channel structure of medium pore zeolites like ZSM-5 does not have supercages at the intersections of the channel system (Chen at al., 1994).

Coking in zeolites is believed to be due to formation of large polycyclics inside wide cavities such as supercages, which are ascribed to be an environment for coke precursor formation. Slow deactivation in medium pore zeolites such as ZSM-5 has been attributed to this very reason that they do not have supercages (Chen et al, 1994).

ZSM-5 is used widely in refinery and petrochemical processes (McCusker and Baerlocher, 2001), probably largely due to the fact that it deactivates much more slowly in comparison with other zeolites that have supercages.

2.2.6.3 Zeolite Mordenite

The framework of zeolite mordenite (MOR) is built of pentasil units, joined to each other to form chains. It has 12- and 8-ring pore openings. The channel system with 8-ring pore openings extends in the same direction as the 12-ring ones (McCusker and Baerlocher, 2001).

Mordenite has a semi-two-dimensional channel system. The straight parallel channels of 6.5 x 7.0 Å diameter intersect perpendicularly with a third small channel of 2.6 x 5.7 Å. The latter are, however, extremely staggered, effectively forming side pockets with no connection to the adjacent wide channel (Jansen et al., 1997).

Major industrial applications of zeolite mordenite are as follows (Roland and Kleinschmit, 2003):

- Xylene isomerisation
- Xylene production by tolune disproportionation
- Production of *m*-chlorobenzene and *m*-dichlorobenzene
- Dimethylamine synthesis from methanol and ammonia

Zeolite mordenite has been reported to be suitable for para selective alkylation reactions with bulky reactants (see Section 2.2.8).

2.2.6.4 Zeolite Y

Zeolite Y consists of spherical sodalite units connected via 6-membered ring prisms resulting in large cavities referred to as supercages. The supercages have 12-ring pore openings forming windows connecting these supercages. Consequently, zeolite Y has a 3-dimensional channel system (McCusker and Baerlocher, 2001).

The large cages have a diameter of 12 Å and they are connected via apertures (windows) of 7.4 Å, in diameter (Jansen et al., 1997).

2.2.6.5 Ultrastable zeolite Y

This zeolite is produced by carefully controlled dealumination process, which results in enhanced hydrothermal stability, reduced ion-exchange capacity and a smaller unit cell than the parent material from which it is prepared (Szostak, 2001). In the conventional zeolite Y, the minimum silicon to aluminium ratio is about 2.5, whereas ultrastable Y (USY) has a minimum of about 4 (Engelhard, 2004). This means that USY is relatively poorer in aluminium atoms and enriched in silicon, and thus the acid site density is decreased. It is this aluminium deficiency that is responsible for additional stability in USY (Szostak, 2001).

2.2.7 Catalyst lifetime

One of the important characteristics of a catalyst is its longevity, that is, a good catalyst must have a long life. In a catalytic cycle, the catalyst must for an ideal case be fully restored to its former state. However, catalysts are often coked, fouled or partially lost during the reaction (Fogler, 1999).

Reasonable amounts of the catalyst must emerge unchanged from a large number of catalytic cycles, for it to be economically viable (Shriver, 1994).

Stability of a catalyst in terms of activity is thus an important criterion for their comparison and it is defined as a measure of rate of loss of activity and/or selectivity (Gates, 1993).

2.2.8 Shape selective reactions over zeolite mordenite

Zeolite mordenite has, probably due to its mono-dimensional straight pore system (see Section 2.2.6.3), despite its large pore diameter of 6.5 x 7.0 Å, found interest and application in shape-selective catalysis, predominantly with multi-cyclic compounds such as naphthalene and biphenyl or with long chain alkylating agents. Biphenyl and naphthalene are the starting materials to the precursors of high performance heat resistant fibres and thermotropic liquid crystals (Mera and Takata, 2003; Sage, 2003).

Examples of shape selective catalysis with mordenite are as follows:

- In the alkylation of biphenyl with propene. Selectivity to para di-isopropylation was reported to be 84 % at a conversion level of 69 % (as reviewed by Hölderich and van Bekkum, 2001). This reaction was also studied by Matsuda et al. (1995) over mordenite zeolites of various SiO_2/Al_2O_3 ratios. The alkylation products were exclusively mono- and di-para propylated biphenyl. No significant amounts of ortho- or meta-propylated product were reported.
- In another study reviewed by Hölderich and van Bekkum (2001), phenol was alkylated with 1-octanol over RE-Y, mordenite and ZSM-12. Among the three zeolites, mordenite gave the highest selectivity to para-substituted product.
- Isopropylation of naphthalene with propylene was studied by Brzozowski and Tecza (1998), over H-mordenite, HY and amorphous alumino-silicate. The ratio of 2,6-di-isopropyl naphthalene to that of 2,7-di-isopropyl naphthalene was found to be the highest for H-mordenite, indicating shape selectivity.
- Horniakova et al. (2002) carried out molecular and quantum mechanical studies, computationally determining and analysing molecular dimensions and diffusion parameters of mono- and di-isopropyl biphenyl as well as mono-*tert*-butylbiphenyl isomers in H-MOR and

H-BEA zeolite frameworks. In both zeolite frameworks, 4- and 4,4'-substituted isomers were found to have the highest diffusivities.

Enhanced *p*-selectivity for reactions over mordenite is usually ascribed to transport control effects, i.e. product selectivity.

2.3 THERMODYNAMICS

The route to synthetic p-cresol from phenol, via DPE, is a three-stage process according to the following sequence of reactions (shown in Figure 1-3 and Figure 1-4) :

1. Phenol condensation to diphenyl ether (DPE)
2.a Methylation of DPE to p-phenoxy toluene (PPT)
2.b Methylation of PPT to p-tolyl ether (PTE)
3. Cleavage of p-tolyl ether to p-cresol

Methylation of DPE to PTE seems to occur sequentially (Fujita et al., 1992; Ndlovu and Gxavu, 2000), with addition of one methyl group at a time (see Section 2.1.12.1 and Section 2.1.12.3). This means that the middle reaction stage of Figure 1-3 actually comprises of two distinct consecutive reaction steps as shown in Figure 1-4. Results for thermodynamic calculations will therefore be presented for sequential methylation only.

Thermodynamic analysis of the above reaction steps was carried out to determine their equilibrium conversion at different temperatures. Knowledge of equilibrium conversion is important because it determines the limits for the kinetic regime, giving the maximum theoretical yield for a particular product in a chemical reaction. Knowledge of the equilibrium also provides information about possible measures to shift the limits.

Literature data for the Gibbs free energy of formation could only be partially used for reaction step one (because there is no experimental Gibbs free energy value for diphenyl ether). The Gibbs free energy of formation of DPE given in the literature (Daubert et al., 1990) is not an experimentally determined value but an estimate from Benson's method (discussed in Section

2.3.1.3). The other reaction steps involve compounds for which no data is available from the literature

Different estimation methods are available in the literature for calculating thermodynamic properties of the species involved in these reactions. The results obtained from these methods are compared. Reid et al. (1987) describe several methods of differing accuracy with deviations of up to 5 kcal/mol (20 kJ/mol), for estimation of thermodynamic properties of pure ideal gases. The methods are as follows:

a. Van Krevelen and Chermin's method – estimates Gibbs free energy of formation for pure substances
b. Joback's method – estimates enthalpy of formation and Gibbs free energy of formation and heat capacities
c. Benson's method – estimates enthalpy of formation, absolute entropy and specific heat capacities
d. Yoneda's method – estimates enthalpy of formation, absolute entropy and specific heat capacities

All the methods involve group estimation schemes related to the molecular structure. The group contribution data for these methods was taken from Reid et al. (1987). The property methods presented by Reid et al. (1987) assume that intermolecular forces play no role, hence an ideal gas assumption.

Gibbs free energy change for a chemical reaction, at any temperature T, is given by Equation 2-8:

$$\Delta G_{rxn}(T) = \Delta H_{rxn}(T) - T\Delta S_{rxn} \qquad \textbf{Equation 2-8}$$

The change in Gibbs free energy of the reaction is also related to the chemical equilibrium constant, K_{eq}, according to the expression:

$$\ln(K_{eq}(T)) = \frac{-\Delta G_{rxn}(T)}{RT} \qquad \textbf{Equation 2-9}$$

Small errors in the estimation of ΔG_{Rxn} are amplified in the calculation of K_{eq} because of the exponential character of Equation 2-9. According to Reid et al. (1987), the estimation errors are more serious when $\left|\frac{\Delta G_{rxn}(T)}{RT}\right| >> 0$.

The thermodynamic equilibrium constants predicted from the estimation methods are thus only indicative of the feasibility of the reactions and the trend with temperature but cannot accurately predict equilibrium constants and hence equilibrium concentrations.

Temperature dependency of the Gibb's free energy of formation of a species i is given by Equation 2-10. $\Delta H_i(T)$ is the enthalpy of formation of species i, at temperature T.

$$\Delta G_i(T) = T\left(\frac{\Delta G_i^o}{T^o} + \int_{T^o}^{T} -\frac{\Delta H_i(T)}{T^2} dT\right) \qquad \textbf{Equation 2-10}$$

$$\Delta H_i(T) = \Delta H_i^o + \int_{T^o}^{T} C_{P,i}(T) dT \qquad \textbf{Equation 2-11}$$

The Gibb's free energy of the reaction, ΔG_{Rxn}, is also given by the difference between the Gibb's free energies of the products and the reactants according to Equation 2-12.

$$\Delta G_{rxn}(T) = \sum \nu_i \Delta G_i(T) \qquad \textbf{Equation 2-12}$$

The symbol ν_i is the stoichiometric coefficient, in a chemical equation. It is positive for the products and negative for the reactants.

2.3.1 Estimation methods

Equilibrium conversions at normal conditions were estimated with the methods described in Section 2.3.1.1 to Section 2.3.1.3.

Summaries of the estimations of the thermodynamic properties of the compounds, used for Figure 5-45 to Figure 5-48 are shown in Appendix I. Using properties estimated from the same

method, equilibrium curves were generated for the different reaction steps, for all reactants and products.

2.3.1.1 Van Krevelen and Chermin's method

This method estimates the Gibbs free energy of formation directly as a function of temperature according to the equation:

$$\Delta G_{vKv} = A + (B + R \ln(\sigma_{ext}))T \qquad \textbf{Equation 2-13}$$

where : A, B : van Krevelen and Chermin constants

σ_{ext} : the maximum number of possible external permutations of the molecule

R : gas constant

T : temperature in K

The constants A and B have no physical meaning. They are neither the heat of formation nor the entropy of formation. Correction for symmetry ($+R \cdot \ln(\sigma_{ext})$) has to be applied to the parameter B in Equation 2-13. According to Reid et al. (1987), this method is accurate to within 5 kcal/mol (21 kJ/mol), hence only the feasibility of the reaction and the trend with temperature can be estimated but not the accurate equilibrium concentrations.

Group increments are given for the constants A and B for particular temperature ranges (see Appendix I). The constants A and B are added up for each group contribution. In the case of repeating groups, the constant is simply multiplied by the frequency of that group per molecule (Reid et al., 1987).

2.3.1.2 Joback's method

Joback used the data from Stull et al. (1969) to obtain atomic and molecular group contributions (Δ_H and Δ_G) for ΔH_f°(298 K), ΔG_f°(298 K) and polynomial coefficients (Δ_a, Δ_b and Δ_c) relating C_p to temperature. The properties for each compound are then estimated according to the following equations :

$$\Delta H_f^\circ(298K) = 68.29 + \sum_j n_j \Delta_H$$ **Equation 2-14**

$$\Delta G_f^\circ(298K) = 53.88 + \sum_j n_j \Delta_G$$ **Equation 2-15**

$$C_p(T) = \left(\sum_j n_j \Delta_a - 37.93\right) + \left(\sum_j n_j \Delta_b + 0.210\right)T + \left(\sum_j n_j \Delta_c - 3.91x10^{-4}\right)T^2 + \left(\sum_j n_j \Delta_d + 2.06x10^{-7}\right)T^3$$ **Equation 2-16**

where : Δ_a, Δ_b, Δ_c, Δ_d, Δ_H, Δ_G : tabulated constants for the group contributions

n_j : the frequency of the j^{th} group in a molecule

ΔH_f° and ΔG_f° are given in kJ/mol

T is given in K

$C_p(T)$ is given in J/(mol.K)

2.3.1.3 Benson's method

In this method, contributions are given only for atoms with valences greater than unity. The method estimates $\Delta H_f^\circ(298K)$, $S_f^\circ(298K)$ and $C_p(T)$ for each compound. These are estimated according to the equations :

$$\Delta H_f^\circ(298K) = \sum_j n_j \Delta_H$$ **Equation 2-17**

$$S_f^\circ(298K) = \sum_j n_j \Delta_S - R \ln \sigma + R \ln \eta$$ **Equation 2-18**

$$C_p(T) = \sum_j n_j C_{pj}(T)$$ **Equation 2-19**

where : Δ_H, Δ_S : tabulated constants for the group contributions

n_j : the frequency of the j^{th} group in a molecule

R : gas constant

σ : number of possible internal and external permutations of the molecule

η : number of possible optical isomers

$C_{pj}(T)$: heat capacity of j^{th} group in a molecule, given for different temperatures

ΔH_f^o and ΔG_f^o are given in kJ/mol

$C_p(T)$ is given in J/(mol.K)

The group contributions of Benson's method estimate absolute entropy, S^o_f (Equation 2-18), from which the change in entropy of formation is calculated. It is called absolute entropy because it is relative to a zero value at absolute zero temperature. However, the use of abolute entropy in chemical reactions results in cancellation of the standard state entropies of elements, making it possible to apply the values of abolute entropy directly (Reid et al, 1987).

Knowing the entropy absolute entropy of compounds participating in a chemical reaction, the change in entropy of the reaction can be calculated according to Equation 2-20.

$$\Delta S^o_{rxn}(298K) = \sum_j \nu_j S^o_{f,j}(298K) \qquad \textbf{Equation 2-20}$$

Similarly, the change in the enthalpy of the reaction can be calculated according to Equation 2-21.

$$\Delta H^o_{rxn}(298K) = \sum_j \nu_j H^o_{f,j}(298K) \qquad \textbf{Equation 2-21}$$

The change in Gibbs free energy is calculated from Equation 2-22, which is analogous to Equation 2-18.

$$\Delta G^o_{rxn}(298K) = \Delta H^o_{rxn}(298K) - T\Delta S^o_{rxn}(298K) \qquad \textbf{Equation 2-22}$$

The correction for temperature in the Gibbs free energy of the reaction is calculated according to Equation2-8 to Equation 2-10 and Equation 2-9.

2.3.1.4 Yoneda's method

Application of each estimation method was on the basis of being able to find estimate values for each species participating in a given reaction. Yoneda's method was not applied due to unsuccess

in estimates for aromatic ethers. It was still used for the other compounds to compare the values that could be obtained for other compounds with the other methods (see Appendix I.5).

In the case of Yoneda's method, the estimation starts with a base molecule and thereafter continues with sequential modification of the structure by substituting with other groups to obtain the final structure. A group contribution value is associated with each substitution and when the final structure is obtained, the group contribution values are summed up to get the value of the thermodynamic property.

The method of Yoneda, similar to the Benson method, estimates $\Delta H_f^o(298K)$, $S_f^o(298K)$ and $C_p(T)$, for each compound. The equations for the change in enthalpy and entropy are exactly the same as in the method of Benson, i.e. Equation 2-21 and Equation 2-20, respectively, except that the entropy term does not, int the case of the method of Yoneda, correct for the number of permutations and the number of optical isomers. The heat capacity of each compound as a function of temperature is estimated for each species according to Equation 2-23.

$$C_p(T) = \sum_j n_j \Delta_a + \left(\sum_j n_j \Delta_b \right) \frac{T}{1000} + \left(\sum_j n_j \Delta_c \right) \left(\frac{T}{1000} \right)^2 \qquad \textbf{Equation 2-23}$$

where : Δ_a, Δ_b, Δ_c : tabulated constants for the group contributions

n_j : the frequency of the j^{th} group in a molecule

T in K

$C_p(T)$ has units of J/(mol.K)

2.3.1.5 Ideal gas

Ideal gas data (see Section 5.11.1) refers to literature data (Sinnot, 1999) which does not take into account the non-idealities of species in a mixture.

2.3.1.6 Data from ASPEN

ASPEN is a simulation package and has a database of thermodynamic properties of most compounds available in the literature. Its accuracy is thus dependent on the accuracy of the literature data. The data used in ASPEN is thus the ideal gas data with corrections for non-idealities.

This simulation tool has unique advantage of being able to account for non-ideality of real compounds thermodynamic properties at conditions different from standard or normal conditions, by accounting for fugacity deviations as well temperature related non-idealities. Fugacity coefficients are calculated in the package subroutines by using compound properties at the critical point. The binary interaction parameters of the species in a chemical reaction are also accounted for in ASPEN, with the use of built-in subroutines.

2.3.2 Water

All these methods, with the exception of van Krevelen and Chermin's method, have no group contributions to estimate the properties of water. Water appears as a product or reactant in each of the process steps of Figure 1-3. Literature data was therefore used for water, in such cases (Sinnot, 1999), see Section 5.11. The method of van Krevelen and Chermin estimates the Gibb's free energy of water within 1 kJ/mol accuracy.

2.4 MOLECULAR MODELLING

2.4.1 Thermodynamics from quantum chemistry

In search for yet a better estimate method for thermodynamic properties, quantum chemistry was used to estimate thermodynamic properties of the reactants and products of the process route shown in Figure 1-3 and Figure 1-4.

Electronic structure calculations were used to analyse the energetics of the individual species. Quantum chemical calculations allow prediction of the interatomic energies and to find the stationery points on the potential energy surface. According to van Santen et al. (2001), quantum chemical calculations agreed with experimental data only when the geometry of the molecule was allowed to relax. This implies that there is a need to optimise the geometry of the molecule to find the stationery points on the potential energy surface and to identify transition states with fully relaxed structures, which is only possible when quantum chemical computer routines are available (van Santen et al., 2001).

The time independent static properties of molecules can be obtained from the time independent Schrödinger equation (Springborg, 1997).

The participant molecules of the reaction investigated were studied using "DMol" program, interfaced with "Materials Studio". "Materials Studio" is a molecular modelling package whereas "DMol" is an ab initio quantum chemistry software package for performing theoretical calculations within a reasonable level of accuracy (Accelrys Inc., 2001).

The idea of expressing the total energy of the system as a functional of electron density was introduced shortly after the formulation of quantum mechanics, in the mid-1920s. However, the accuracy of these early attempts was far from satisfactory due to the crude treatment of the kinetic energy term, in the absence of molecular orbitals (Accelrys Inc, 2001).

It was in the 1960s that an exact theoretical framework called the Density Functional Theory (DFT) was introduced, providing a foundation for calculations of better accuracy. In Density Functional Theory, the total energy of the system is made up of three terms, which are the kinetic energy, the Coulomb energy and the exchange-correlation energy. This three-term energy formulation is said to be exact, but has the disadvantage that the actual expression for the exchange-correlation energy is unknown (Accelrys Inc., 2002).

In quantum mechanics, all the properties of the system are expressed in terms of the wavefunction which is obtained by solving the Schrödinger equation. A wavefunction is simply a mathematical function, analogous to a concept of trajectory in classical mechanics, and is said to have all the information necessary to know about the location and the motion of the particle that it describes (Atkins, 1994).

"DMol" program allows for prediction of optimised geometry of the individual molecules studied as well as estimates of their thermodynamic properties. The program uses the partition functions from statistical thermodynamics to estimate the properties (Accelrys Inc, 2001).

Statistical thermodynamics relates the microscopic properties of individual molecules to those of their macroscopic (bulk) properties because the properties of bulk matter depend on the

properties of individual particles of which it is composed. Microscopic and macroscopic studies are the two major broad classes of phenomena in chemistry. The main theoretical framework for studying bulk properties of matter is thermodynamics (or kinetics, for non-equilibrium phenomena). The fundamental equations for studying macroscopic systems are the first, the second and the third laws of thermodynamics. In microscopic systems, the theoretical framework is quantum mechanics with the Schrödinger equation as the fundamental equation (Atkins, 1994).

Statistical thermodynamics is typically a model building process, starting off with a theoretical model of the particles, atoms, molecules, etc., making up a sample and then statistically averaging the properties of these individual particles to the bulk sample. If the model is a collection of molecules which do not interact with each other, the bulk properties become those of an ideal gas. Properties of a non-ideal gas would be obtained by including in the model, the potential energy of interactions between the molecules.
The use of statistical thermodynamics is necessary because detailed application of either quantum mechanics or classical mechanics to real macroscopic systems is made impossible by the fact that one would have to solve the Schrödinger equation for a system of the order of 10^{24} equations. This is a system of equations for the nuclei and the electrons in a mole of a substance like hydrogen gas (Atkins, 1994).

Experimentally measured values of mechanical variables like P, V and H are long time averages on the time scale of molecular events. Therefore, instead of following the time development of a particular macroscopic system, one focuses attention on an imaginary ensemble (collection) of a very large number of macroscopic systems, each macroscopically identical to the system of interest. However, an ensemble will, on a molecular level, contain systems in very large number of different quantum states (Salzman, 2000).

Statistical thermodynamics hinges upon the basic function called a partition function. A brief overview of its derivation is discussed in this section. To start the derivation, assume that the probability, P_i, of finding a system in the i^{th} quantum state with energy E_i is proportional to a Boltzmann factor (Salzman, 2000).

$$\Rightarrow P_i \propto e^{-\frac{E_i}{k_B \cdot T}}$$

$$k_B = \frac{R}{N_A}$$ **Equation 2-24**

where : T = temperature of the system in Kelvin

k_B = Boltzmann's constant

N_A = Avogadro's number

Using notation $\beta = \frac{1}{k_B \cdot T}$

$$P_i \propto e^{-\beta \cdot E_i}$$

The sum of all probabilities must be unity, i.e., $\sum_i P_i = 1$

If the proportionality constant is c, $P_i = c \cdot e^{-\beta \cdot E_i}$

Therefore : $\sum_i c \cdot e^{-\beta \cdot E_i} = 1$

$$\Rightarrow c = \frac{1}{\sum_i e^{-\beta \cdot E_i}}$$ **Equation 2-25**

$$\text{Let } Q = \sum_i e^{-\beta \cdot E_i}$$ **Equation 2-26**

The quantity Q is termed a partition function. This is an important quantity because it connects the mechanical properties of the system with thermodynamics through quantised energies E_i. Q is a function of T (through β) and also a function of the mechanical variables in the model (through the energies E_i) (Salzman, 2002).

The internal energy, U, is the ensemble average of the sum of all the potential and kinetic energies of all the particles in the system. In other words, U is the total average mechanical energy of the ensemble.

$$U = \sum_i E_i P_i$$

$$U = \sum_i E_i \frac{e^{-\beta E_i}}{Q} \qquad \textbf{Equation 2-27}$$

$$U = \frac{1}{Q}\sum_i E_i e^{-\beta E_i}$$

Noting that $E_i e^{-\beta \cdot E_i} = -\frac{\partial}{\partial \beta} e^{-\beta \cdot E_i}$

$$\Rightarrow \frac{1}{Q} E_i e^{-\beta \cdot E_i} = -\frac{1}{Q}\frac{\partial}{\partial \beta} e^{-\beta \cdot E_i}$$

$$\therefore U = \frac{1}{Q}\sum_i -\frac{\partial}{\partial \beta} e^{-\beta \cdot E_i} = -\frac{1}{Q}\frac{\partial}{\partial \beta}\sum_i e^{-\beta \cdot E_i} = -\frac{1}{Q}\frac{\partial Q}{\partial \beta} = -\frac{\partial \ln Q}{\partial \beta} \qquad \textbf{Equation 2-28}$$

The above equation for U is the main one from which all other statistical thermodynamic properties are derived. Other properties are obtained as follows:

$$C_V = \frac{\partial U}{\partial T}\cdot\Big|_V \qquad \textbf{Equation 2-29}$$

$$S = \int_{T_o}^{T} \frac{C_V}{T} \cdot dT \qquad \textbf{Equation 2-30}$$

$$A = U - TS$$

$$P = -\frac{\partial A}{\partial V}\cdot\Big|_{T,N}$$

$$H = U + PV \qquad \textbf{Equation 2-31}$$

$$G = H - TS \qquad \textbf{Equation 2-32}$$

The assumptions underlying these derivations are summarised as follows:

1. Molecules are free to move amongst each other (ideal gas).

2. The energy of each molecule is independent of the composition of the system. This means that the energy of the system is equal to the sum of the molecular energies and there are no pair-wise interaction energies between the molecules.
3. Thermal equilibrium is established.
4. Molecules are indistinguishable, i.e. of the same kind.
5. Temperatures considered are well above the absolute zero temperature.

2.4.2 Diffusion in Zeolites

Diffusion of molecules within zeolite pores is important in relation to the application of zeolites as shape selective catalysts. Intracrystalline diffusion is referred to as configurational diffusion when the molecules are large enough that they barely fit through the pores (Gates, 1993). Configurational diffusion can be modelled as a series of molecular jumps and is thus an activated process in which the activation energy barrier arises mainly from steric hindrance. As a result, the diffusional activation energy of the modelled molecule is directly related to the pore size of the zeolite (Ruthven and Post, 2001).

Intracrystalline diffusivity can be predicted in three different ways, summarised as follows :

- Transition state theory : In this theory, a molecule hops from one adsorption site to another. The molecule is conceptualised as passing over an energy barrier as it migrates from one position to the next (van Santen et al., 2001). This approach requires a correct physical picture of the transition state as well as an accurate calculation of the system force field (i.e. the second derivative of the potential energy) to estimate the entropy and the activation energy (Ruthven and Post, 2001).

- Monte Carlo calculation : This approach is more widely used. It is based on the statistical representation of a diffusion process as a random walk with a factor like an Arrhenius factor ($e^{-Ea/RT}$) assigned to represent the probability of a successful molecular jump (Ruthven and Post, 2001).

- Molecular dynamics (MD) calculation : In this approach, equations of motion from classical mechanics are solved for a molecule whose movement is constrained by the zeolite pore wall (Ruthven and Post, 2001).

In MD, classical mechanics is used to follow the trajectory of the system over a finite time period. The calculations are comprised of two major steps. In the first step, the trajectory of the system is generated with the use of the Verlet algorithm. The algorithm uses the third degree Taylor expansion of the positions, r (a vector), of each atom around time, t, according to Equation 2-33 and Equation 2-34 (van Santen et al., 2001).

$$r(t+\Delta t) = r(t) + \frac{dr(t)}{dt} + \frac{1}{2}\frac{d^2r(t)}{dt^2}\Delta t^2 + \frac{1}{6}\frac{d^3r(t)}{dt^3}\Delta t^3 \qquad \textbf{Equation 2-33}$$

$$r(t-\Delta t) = r(t) - \frac{dr(t)}{dt} + \frac{1}{2}\frac{d^2r(t)}{dt^2}\Delta t^2 - \frac{1}{6}\frac{d^3r(t)}{dt^3}\Delta t^3 \qquad \textbf{Equation 2-34}$$

A combination of Equation 2-33 and Equation 2-34 gives Equation 2-35.

$$r(t+\Delta t) = 2r(t) - r(t-\Delta t) + \frac{d^2r(t)}{dt^2}\Delta t^2 \qquad \textbf{Equation 2-35}$$

The latter is solved simultaneously with Newton's equation of motion given in Equation 2-36. In Equation 2-36 F_{Newton} is the resultant force acting upon the particle (van Santen et al., 2001).

$$m\frac{d^2r(t)}{dt^2} = F_{Newton} = -\frac{dU_{potential}}{dr} \qquad \textbf{Equation 2-36}$$

In Equation 2-36, m is the particle mass and $U_{Potential}$ is the potential energy. The velocity of the particle or atom is averaged according to Equation 2-33 and Equation 2-34, as given in Equation 2-37 (van Santen et al., 2001).

$$v(t) = \frac{dr(t)}{dt} = \frac{r(t+\Delta t) + r(t-\Delta t)}{2\Delta t} \qquad \textbf{Equation 2-37}$$

The kinetic energy of the system is then calculated from the velocities according to

$$U_{Kinetic} = \frac{1}{2}\sum_{j=1}^{N} m_j v_j^2(t) \qquad \textbf{Equation 2-38}$$

In Equation 2-38, N refers to the number of particles or atoms in the system. The system temperature is given by Equation 2-39.

$$T(t) = \frac{2}{3}\frac{U_{Kinetic}}{N \cdot k_B} \qquad \textbf{Equation 2-39}$$

where k_B is the Boltzmann constant.

MD calculations are generally executed on small systems of typically 10^4 particles or less. The implementation of periodic boundary conditions is usually a way to preserve a link with real systems, as well as avoid wall and surface effects. The idea behind this concept is to replicate the simulation box to form an infinite lattice in space so that if the molecule leaves the box during the simulation, its image enters the box again at the opposite side (van Santen et al., 2001).

There are different types of MD simulations, which are classified by their thermodynamic ensemble names, e.g. NVE (maximises the entropy of the system), NVT (minimises the Helmholtz energy of the system), NPT (minimises the Gibbs free energy of the system), and NPH (minimises the internal energy of the system).
The letters refer to :

N = constant number of moles
V = constant volume
E = constant energy
T = constant temperature
P = constant pressure
H = constant enthalpy

According to van Santen et al. (2001), the NVE ensemble is the recommended one for the calculation of diffusion constants, because it does not interfere with the velocities of the system during the simulation. The diffusion coefficient is then estimated from the generated trajectories by using an Einstein relationship given in Equation 2-40 (van Santen et al., 2001).

$$D = \lim_{t\to\infty} \frac{a}{6 \cdot N_{Atoms}}$$ **Equation 2-40**

where: a = the slope of the plot of total Mean Square Displacement vs time (see Appendix VIII)

N_{Atoms} = the total number of atoms per molecule

The MD approach requires an accurate calculation of the system potential and hence the force on each atom. Consequently, the set of equations to be solved is very bulky and computationally expensive (Ruthven and Post, 2001).

In this work, the intracrystalline diffusion of the different methylation products of diphenyl ether in zeolite mordenite, was studied using MD. Self diffusion MD calculations for the aromatic ether/zeolite system studied proved to be cumbersome and this was observed from lengthy simulation periods, which still gave non-repeatable results from one simulation to the next (see Appendix VIII).

This problem led to a slightly different approach namely a concept of application of a constant force on a molecule, i.e. a forced diffusion approach. In this approach, relative diffusion coefficients, and not absolute coefficients are obtained.

The maximum non-expansion work that can be done per molecule, when it moves from a chemical potential of μ, at constant temperature and pressure, to another potential of $\mu+d\mu$ is $dw = d\mu$ (Atkins, 1994). When the chemical potential of a system depends on a position x, the non-expansion work is given by:

$$dw = d\mu = -\left.\frac{d\mu}{dx}\right|_{T,P} dx$$ **Equation 2-41**

The force, F, applying the work is related to the work as follows:

$$dw = -F \cdot dx$$ **Equation 2-42**

This implies that the slope of the chemical potential of a system wherein a molecule is displaced from one position to the next, in a zeolite, can be interpreted as an effective force per mole of that substance (Atkins, 1994).

The effective diffusion force per mole is thus:

$$F = -\left.\frac{d\mu}{dx}\right|_{T,P} \qquad \textbf{Equation 2-43}$$

In this case, the flux of diffusing particles is considered to be due to the force acting upon them. This force may be the concentration gradient or external resultant force such as differential pressure. When a constant force is applied, the particle velocity increases until it eventually reaches a steady drift speed, s, and at this point, the applied force is equal to the retarding force. The drift speed (analogous to terminal velocity for a free falling object in a non-vacuum environment) is proportional to the applied force.

The mean square displacement, $\langle r(t) \rangle$, is the average distance that a molecule travels over time, t. When the diffusion is induced by a force such as in Equation 2-43, the drift speed, s, is related to mean square displacement by Equation 2-44:

$$\langle r(t) \rangle = (s \cdot t)^2 \qquad \textbf{Equation 2-44}$$

The drift speed in Equation 2-44 is obtained from the velocity of a particle (atom) according to Equation 2-45, analogous to Equation 2-37.

$$s = v(t) = \frac{dr(t)}{dt} = \frac{r(t+\Delta t) + r(t-\Delta t)}{2\Delta t} \qquad \textbf{Equation 2-45}$$

In Equation 2-40 the relation between mean square displacement and diffusivity is given, for infinite diffusion time. Considering the diffusion in finite time, Einstein relation is given by Equation 2-46 (Chen et al., 1994).

$$D = \frac{\langle r(t) \rangle}{6 \cdot t}$$ **Equation 2-46**

where:

D = diffusivity

$\langle r(t) \rangle$ = mean square displacement

t = time travelled by a molecule

Diffusivity plots for various species in ZSM-5, at room temperature, are given in Figure 2-16, plotted as function of the ratio of molecular diameter (d_m) to zeolite channel diameter (d_c). Mathematically, this is represented as $\Lambda = d_m / d_c$.

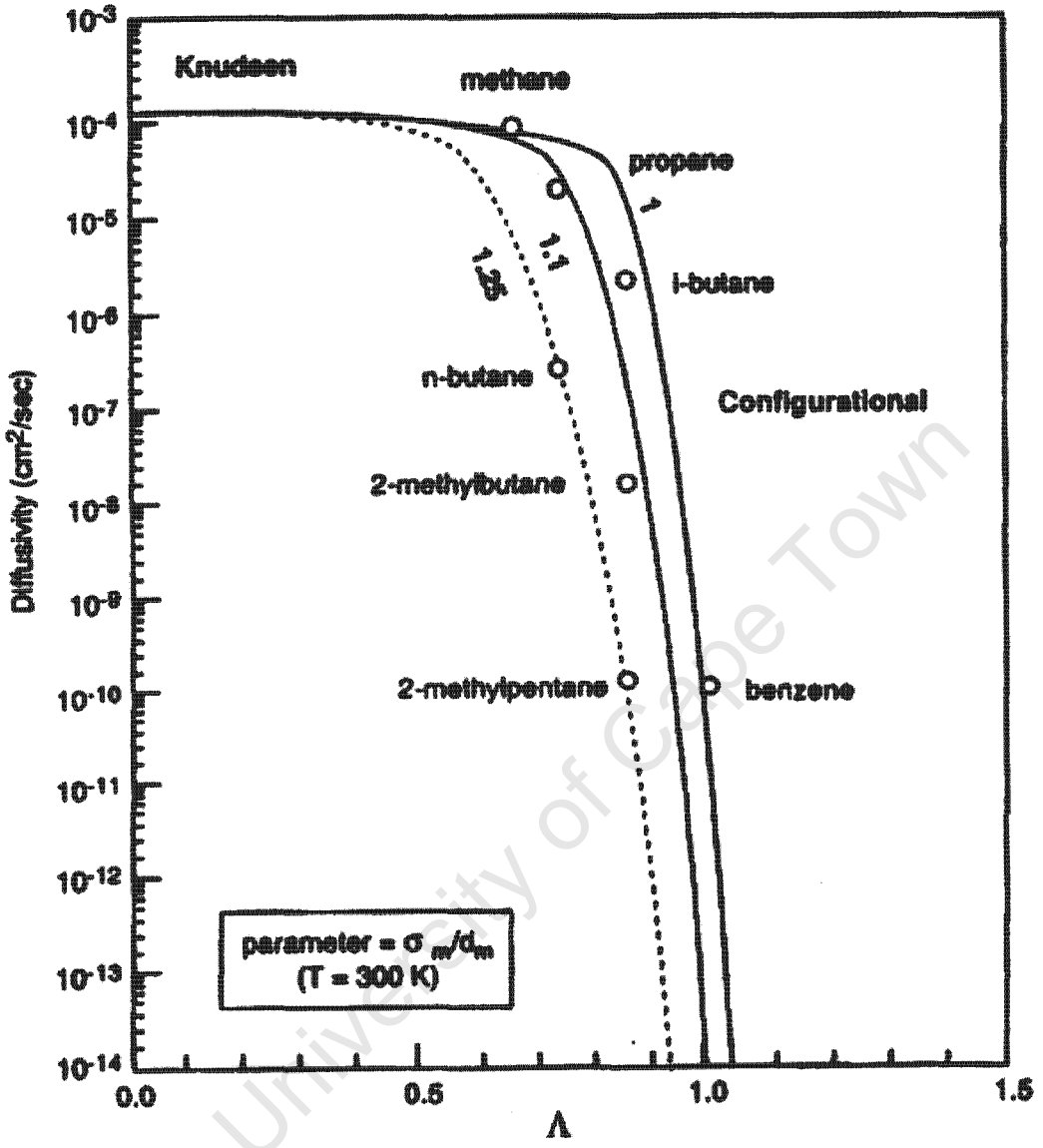

Figure 2-16: Diffusivity of various species in ZSM-5 at 300K, plotted as a function of the ratio of molecular to zeolite pore diameters, Λ (Chen et al., 1995)

Parameter σ_m/d_m, in Figure 2-16 and Figure 2-17 is the ratio of molecular length constant (σ_m) to kinetic diameter, for a molecule.

In Figure 2-16, diffusivities of various species in H-ZSM-5 are plotted as a function of the ratio of the molecular diameter (d_m) to the channel diameter (d_c), at 300 K. Figure 2-17 shows the plot of this relationship for n-butane at various temperatures.

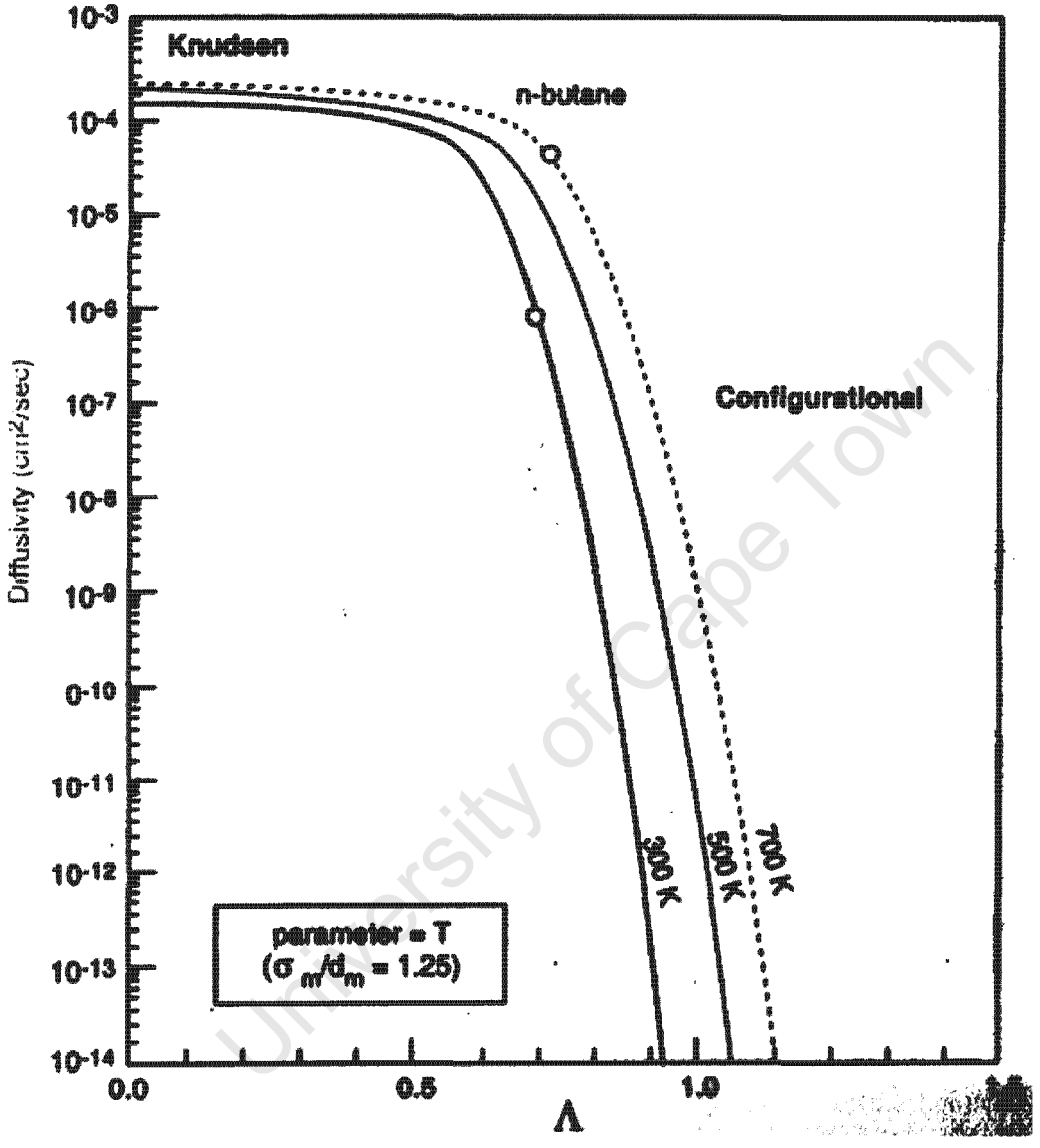

Figure 2-17: Diffussivity of n-butane over ZSM-5 at various temperatures, plotted as a function of the ratio of molecular to pore diameters, Λ (Chen et al., 1995)

The diffusion constants predicted from the simulations may therefore be expected to be in the range of configurational diffusivity as shown in Figure 2-16 and Figure 2-17.

3. RESEARCH OBJECTIVES

This study came into being as a result of a proposed novel process route, highly selective to *p*-cresol, which involves condensation of phenol to diphenyl ether, methylation of diphenyl ether to *p*-phenoxy toluene and *p*-tolyl ether with high selectivity, and cleavage of the methylated ethers to *p*-cresol (and phenol) in three process stages.

The major object of this study was the second stage of Figure 1-3, which is synthesis of a para-methylated derivative of diphenyl ether over shape selective acid zeolite catalysts, with high selectivity. The influence of zeolite pore geometry and acidity, together with process conditions, on this reaction were also to be determined.

It is vital that the proposed novel process route to *p*-cresol via para-methylated diphenyl ether derivatives must produce no *m*-cresol so as to eliminate a need for separation of these two isomers. *o*-Cresol has a boiling point well below that of *p*-cresol such that separation or purification of *p*-cresol from *o*-cresol can be accomplished by common distillation, whereas separation of *p*-cresol from *m*-cresol cannot be attained by common distillation.

Theoretical predictive methods were to be used to estimate, quantify and confirm some thermodynamic, electronic and physical properties of the species participating in the process route and the reaction under study. These were to be quantified and matched against the experimental results.

4. EXPERIMENTAL

4.1 EXPERIMENTAL SETUP

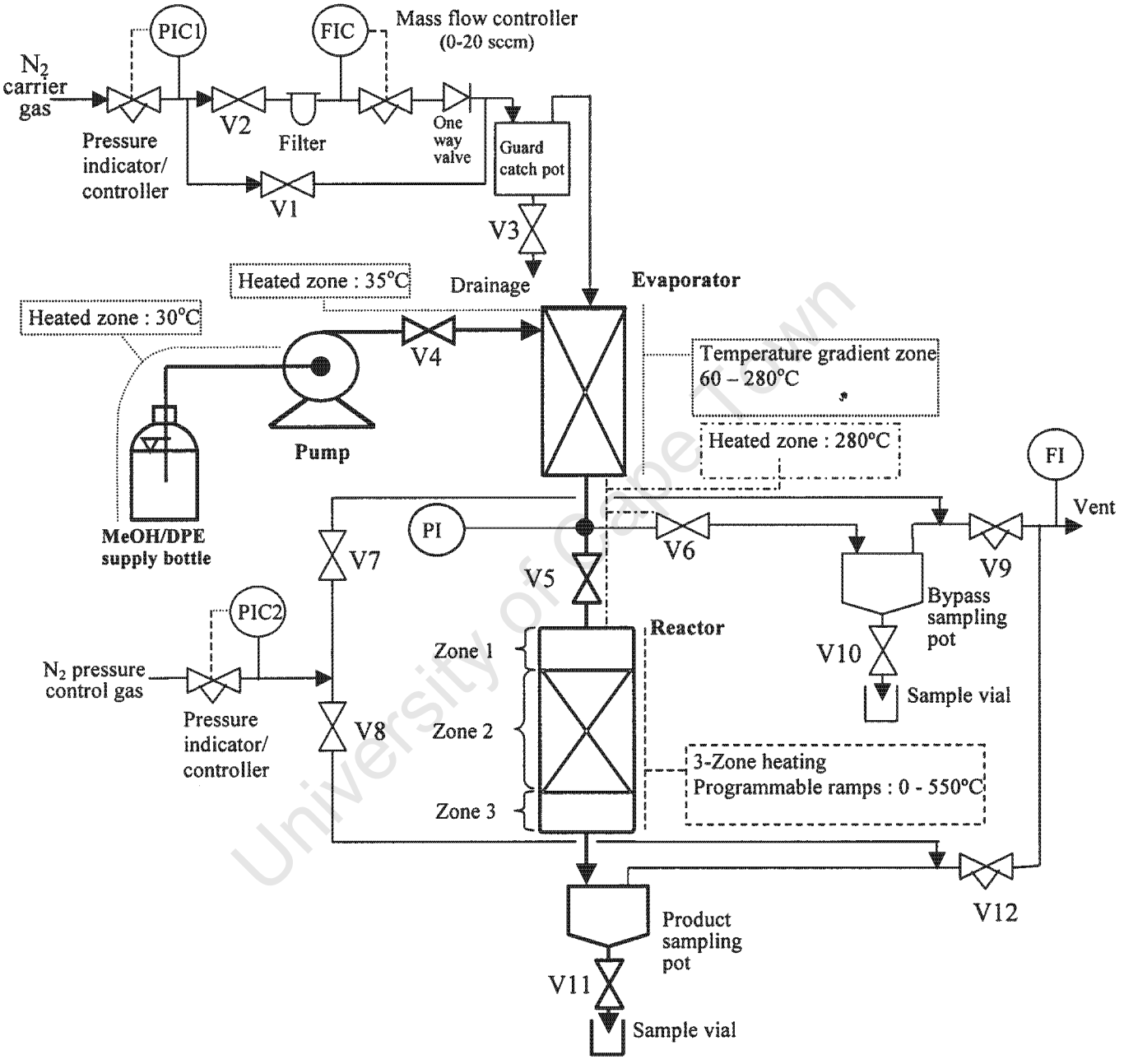

Figure 4-1: Experimental apparatus

The experimental apparatus is shown in Figure 4-1. It consisted of a thermal mass flow controller (MFC) for the carrier gas (N_2), an upstream micro-filter to protect the MFC from dust, a one-way valve in combination with a catch-pot to protect the mass flow controller from accidental back flow of liquid feed, a metering pump, an evaporator/preheater, a reactor packed with dilute catalyst, sampling pots, throttle valves and supply lines for pressure control gas. Bold lines are indicative of the main flow paths of the feed and the product streams.

The liquid feed mixture was pumped to the evaporator/preheater, where it was partially vaporised and taken to the reactor by the carrier gas. Liquid products were collected at room temperature under reaction pressure in a sampling pot, which was emptied regularly for sampling.

4.1.1 Mass flow controller

The experimental setup was equipped with a thermal mass flow controller (MFC), by Unit manufacturer, of a flow range of 0 – 20 sccm (nitrogen) (see Appendix III).

4.1.2 Guard catch-pot

A 450 ml steel, closed, cylindrical container fitted with a drain valve was set in place between the MFC and the liquid feed line, to act as a buffer to protect the MFC in case of a blockage downstream, which could result in the liquid feed being pumped back to the MFC.

The catch-pot had a cone shape inside to ensure complete drainage when emptied.

4.1.3 Dosing of feed

The feed was introduced as a mixture of the two reactants, methanol and diphenyl ether (DPE), in liquid phase and was driven into the evaporator by means of an HPLC pump (Spectrachem Series II).

At slightly elevated temperature, the two compounds were fully miscible throughout the feed ratios applied. Therefore, the feed mixture in the storage bottle and in the pump head was kept at slightly elevated temperatures by means of a light bulb, which ensured that the mixture remained a liquid.

The liquid feed line was wrapped with a heating tape and heated to about 35°C, because DPE has a melting temperature of 26.6°C. This temperature was also kept as far as possible, below the normal boiling point of methanol (60°C), to avoid early evaporation.

4.1.4 Evaporator

The evaporator's purpose was to preheat the feed to the reaction temperature and evaporate the methanol. It was mounted above the reactor and was packed with inert silicon carbide (SiC) particles of an average size of 0.4 mm. A heating tape wound around the line between the evaporator and the reactor was the means of maintaining the temperature of the feed.

The evaporator was encapsulated in an insulated heating tape which was coiled in such a way that the temperature profile down its length increased steadily from 40°C to the reaction temperature, but never beyond 280°C, which was the maximum operating temperature of the packing of the valves in the lines downstream of the evaporator (V5 and V6 of the flowsheet in Figure 4-1).

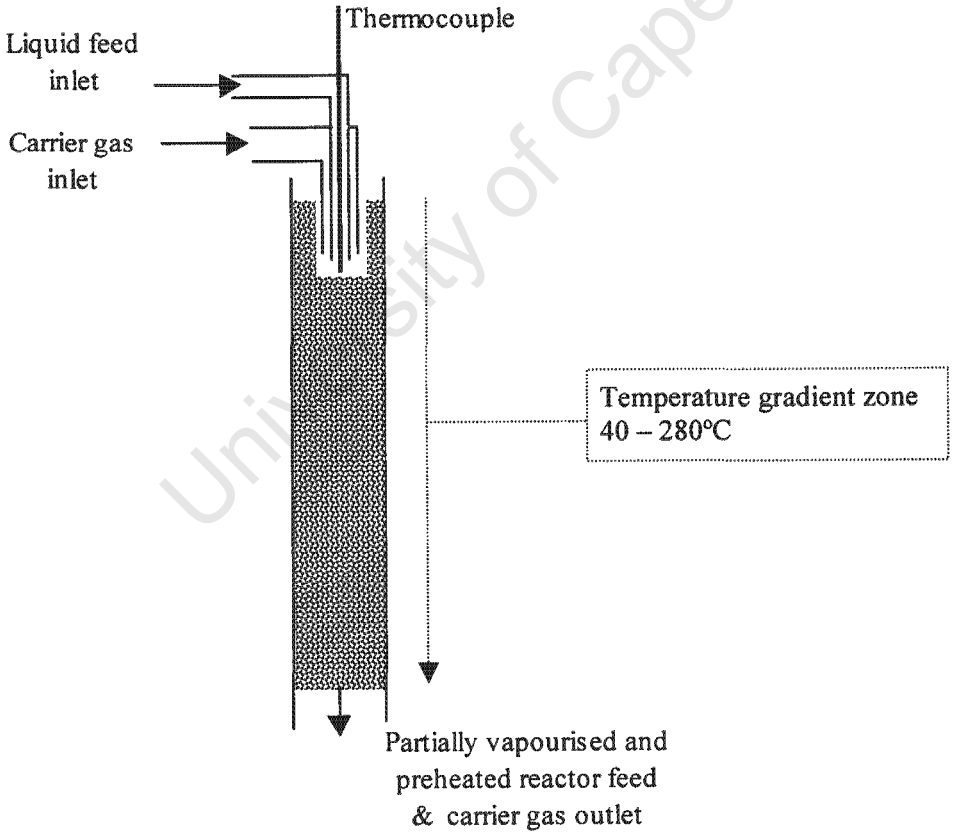

Figure 4-2: Diagram showing a simplified sectional view of the evaporator/preheater

In the evaporator/preheater, the liquid feed line was placed at the inlet inside the carrier gas line and immersed into the packing by about 5 mm, deeper than the gas one. A steel-jacketed thermocouple was inserted inside the liquid line and into the packing, to the same depth as the liquid feed line. The purpose of this thermocouple was to monitor the temperature at the top of the evaporator so as not to exceed the bubble point of the feed mixture at the given pressure and avoid delayed boiling effects in the feed line which could result in variable WHSV and variable partial pressures.

During operation, the liquid feed trickled down through the packing constantly evaporating and the vapour was carried along by N_2 carrier gas. This design allowed for steady vaporisation of the low liquid flows applied.

4.1.5 Reactor

The reactor comprised a cylindrical stainless steel tube with an internal diameter of 19 mm, equipped with a thermo-well (external diameter of 2.8 mm) running through the centre of a tube (see Figure 4-3). The reactor was jacketed by an external tube, which had three distinct zones of steel-jacketed heating coils. A cross-sectional view of the empty reactor is shown schematically in Figure 4-3.

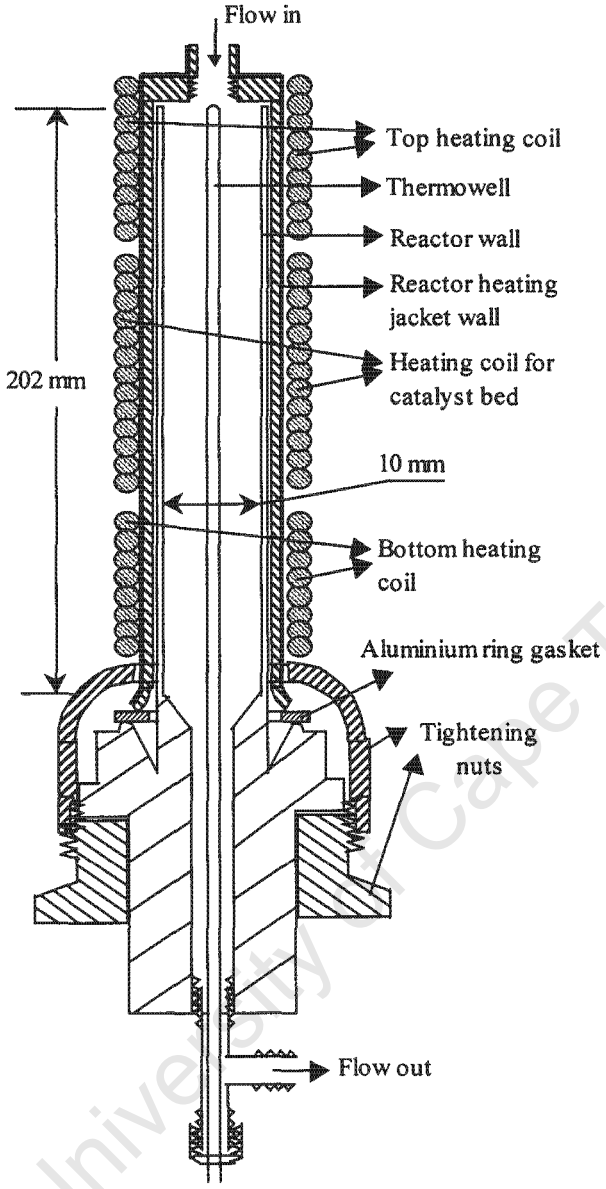

Figure 4-3: Diagram showing the detailed mechanical design of the reactor

The reactor was designed such that the tube holding the catalyst bed ("reactor wall" in Figure 4-3) could be easily assembled or disassembled for loading or unloading, by simply disconnecting the outlet flow line and opening the bottom tightening nut.

There was a clearance of about 1 mm between the external surface of the reactor tube and the internal surface of the heating jacket. Each of the three heating coils had a separate dedicated controller. The middle temperature zone was programmable whereas the other two were not.

Details on the reactor packing are given in Section 4.3.1.

Figure 4-4 shows the isothermal temperature profiles in the reactor recorded during different experiments. Three sets of measurements (Ta to Tc) were taken at 300°C, during three different experiments for a repeatability check (see Appendix VI.1 for numerical data).

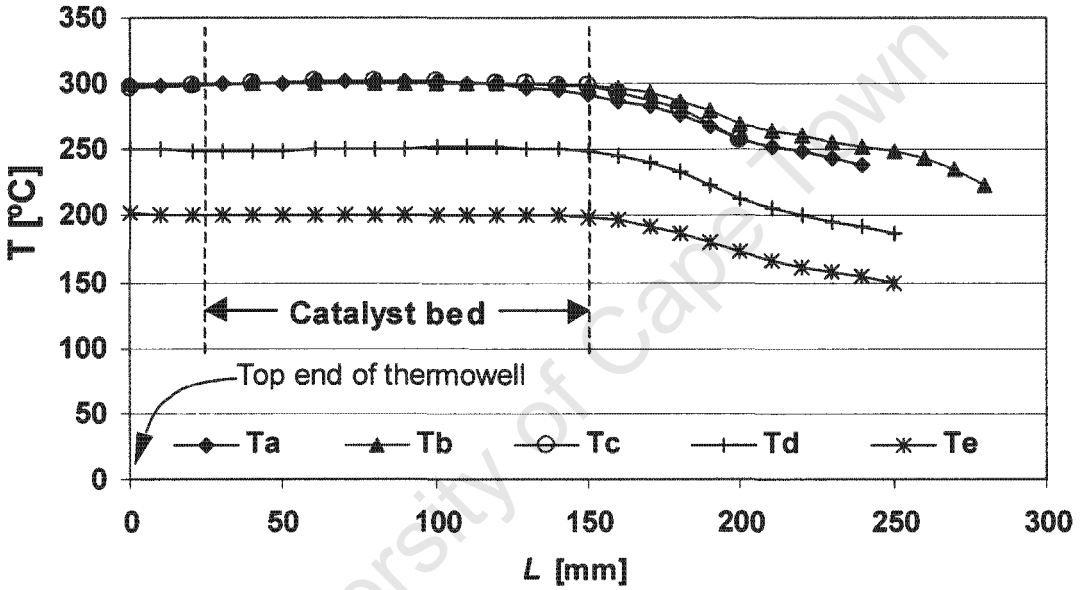

Figure 4-4: Temperature profile down the reactor bed (L=0 refers to the top end of the thermowell)

4.1.6 Pressure regulation

Maintaining constant pressure in the experimental set-up could be achieved by adjusting the outlet needle valve as a throttle or using a backpressure regulator. However, such settings have setbacks, particularly with the operational reliability when handling streams containing condensable materials and tar-like substances.

Constant pressure in this experimental set-up was therefore regulated and maintained by means of a special technique. This was accomplished by connecting a line of nitrogen gas, kept at the desired reaction pressure, to the gas effluent line between the sample pot and the throttle valve (see Figure 4-1, lines connecting next to the throttle valves V9 and V12). The throttle valve was kept more open than required for the gaseous effluent stream from the reactor. Application of this technique prevents condensation of effluent components in the needle valve due to dilution introduced by the pressure control gas.

4.1.7 Sample pot

The sample pot was a simple cylindrical metal container (Figure 4-5) which acted as a collector of the liquid and condensed product from the reactor.

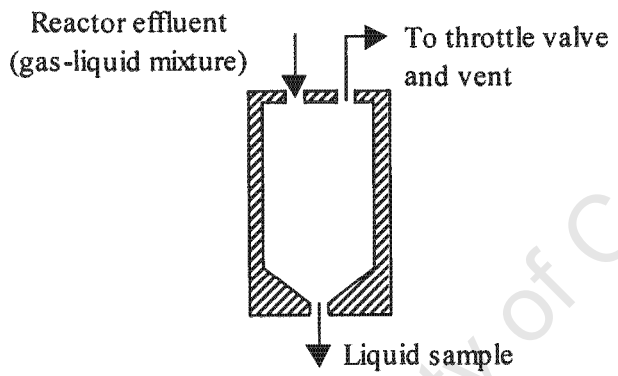

Figure 4-5: Cross-sectional view of the sample pot

The sample pot had a cone-shaped base inside, to ensure complete recovery of the sample with a total volume of 100 ml, based on the volume of the sample collected over a maximum time-on-stream interval of 24 hours at a liquid feed rate of 0.07 ml/min.
The line between the reactor and the sample pot also functioned as a heat exchanger to cool down the reactor effluent, capturing condensable components into the liquid phase. This line was kept at ambient temperature, together with the sample pot.

The reactor product flowed into the sample pot as a gas-liquid mixture, such that the sample pot also played a role of a separator. The gas phase left the pot through the vent line, whereas the liquid phase accumulated in the pot and was drawn into sampling vials from time to time.

4.2 OPERATING CONDITIONS

4.2.1 Standard screening conditions

Zeolite H-beta with a SiO_2/Al_2O_3 ratio of 25 was the candidate catalyst for establishment of the standard conditions, under which the different candidate catalysts were to be screened. It was chosen on the basis of its apparent success from the preliminary studies (Ndlovu and Gxavu, 2000).

A temperature range of 200 to 300°C was considered, in search for the standard screening conditions, based primarily on the previous work for phenol methylation (Moon et al., 2001), which produced comparatively high p-/o-cresol ratios and low selectivity to m-cresol. The reaction pressure was increased stepwise from 1 bar to a maximum of 20 bar.

The molar feed ratio, methanol to DPE, ranged from 0.5 to 4 and the molar carrier gas to feed ratio ranged from 0.5 to 3. Increments were made until a suitable standard screening condition was established (see the steady state summary of experimental results in Appendix IX).

4.2.2 Optimum conditions

Optimum conditions were determined only for the most promising catalyst.

4.2.3 Candidate catalysts for screening

The reaction under study was performed over acidic zeolites, i.e. of the H-form. All the catalysts used were commercial materials (Table 4-1) and they were obtained from the suppliers in H-form, except for CBV21A mordenite, which was in NH_4-form. Catalysts were in the form of crystal powder or extrudates (1.5 mm diameter and 2 – 15 mm in length). All the catalysts were applied as obtained except for the NH_4-mordenite, which was first deammoniated (see Section 4.3.2).

Table 4-1: Candidate catalysts for screening

Catalyst name	Zeolite	SiO_2/Al_2O_3	Form	Supplier
H-beta-25	H-beta (BEA)	25	powder	Süd-Chemie
H-MFI-50	H-ZSM-5 (MFI)	50	powder	Süd-Chemie
H-USY	Ultrastable HY (FAU)	10	powder	Akzo Nobel
H-Mor-40	H-mordenite (MOR)	40	powder	Süd-Chemie
CBV21A	NH_4-mordenite (MOR)	20	extrudates[a]	Zeolyst
CBV90A	H-mordenite (MOR)	90	extrudates[a]	Zeolyst

[a] 1.5 mm in diameter

4.2.4 Chemicals used for the reaction

The chemicals used for the reaction are listed in Table 4-2.

Table 4-2: Chemicals and other materials used for the reaction under study

Compound	Supplier	% Purity
Diphenyl ether	Aldrich	99
Methanol	Aldrich	99
Silicon carbide, 0.4 mm	Norton Abrasives	
Nitrogen	Fedgas	99.99

4.3 EXPERIMENTAL PROCEDURE

4.3.1 Catalyst loading

Experiments were conducted with the catalysts in the same physical form in which it was obtained (crystal powder or extrudates, see Table 4-1). In all the cases, 3 g of the dry mass of catalyst was used and it was diluted with ca. 10 ml of inert silicon carbide (see Appendix V). The dilute catalyst bed was in turn packed between packings of inert silicon carbide. The reactor was packed as shown in Figure 4-6.

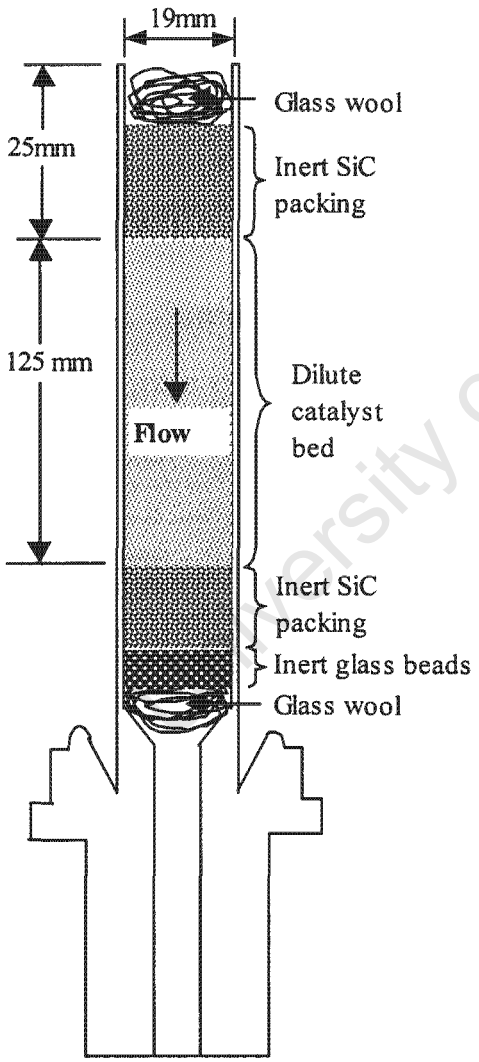

Figure 4-6: Cross-sectional view of the packed reactor (internal tube)

The layer of glass wool at the reactor inlet (on top) was to prevent SiC particles being forced up the reactor, in case of any abrupt, accidental, flow backwards. The top inert layer of SiC was simply to establish uniform flow, per cross-sectional area, for the feed before it got in contact with the catalyst bed and also to serve as a pre-heater, in case the feed required further heating above the outlet temperature of the evaporator.

It was important to grease the thread of the bottom-tightening nut (see Figure 4-3) with a high temperature lubricating grease (copper slip) before closing the reactor for easier un-tightening when the reactor had to be reloaded.

4.3.2 Catalyst pre-treatment and activation

All acidic zeolites have affinity for moisture and other components from ambient air, dependent on their acidity and their free pore space. The catalysts in H-form were dehydrated by flushing them with nitrogen at the reaction temperature. Pretreatment conditions are given in Table 4-3. Zeolyst mordenite (CBV21A) was supplied in ammonium form and was therefore calcined *in situ* at higher temperature. Calcination of CBV21A was carried out at two different temperatures, 400 and 500°C.

Table 4-3: Catalyst pre-treatment (nitrogen flow at 20 ml/min, reaction pressure[a], 3 g of dry catalyst)

Catalyst form	$T_{Calcination}$ [°C]	Temperature program
H-zeolite	250[b]	10°C/min to 250; isothermal 250°C, 2 hours
H-zeolite	300[b]	10°C/min to 300; isothermal 300°C, 2 hours
NH^4-zeolite	400	10°C/min to 400; isothermal 400°C, 2 hours
NH^4-zeolite	500	10°C/min to 500; isothermal 500°C, 2 hours

[a] 20 bar, except introductory and screening conditions search experiments, over H-beta-25 (L1) and H-beta-25 (L4), see Table 5-1.

[b] Temperature of the first experiment in the series

The heating rate in Table 4-3 was established from data as shown in Appendix VI.2.

pre-treatment was completed, the liquid feed was pumped from the feed supply bottle and introduced into the evaporator/pre-heater via valve V4. In the evaporator, the feed was heated, vaporised or partially vaporised and taken up by the carrier gas to the reactor.

The first product sample of a freshly loaded reactor could only be taken more than ten hours after starting the pump because the volume of the experimental set-up had to fill up with liquid first. Samples were drawn into glass vials with sealed screw caps (McCarthy bottles). Samples were collected over different intervals of 2 to 15 hours, depending on the space velocity. Thus, the samples represented the average composition over a time interval.

4.3.5 Shut down

The shut down procedure started by switching off the pump and closing the feed line at valve V4, thereafter flushing the experimental set-up with the carrier gas for about 5 hours at reaction pressure. After all the volatile residues have been flushed out, the temperatures of the reactor, the evaporator/pre-heater and the heating tapes was brought down to room temperature.

Depressurising followed after both flushing and cooling of the reactor were completed. This was accomplished by closing nitrogen supply lines at V2 and V8 and opening V12 slightly more. In this way, nitrogen remaining in the apparatus was vented at V12 until the apparatus was at ambient pressure.

4.4 PRODUCT ANALYSIS : GAS CHROMATOGRAPHY

The reaction under study has water as a co-product of the methylated ether and thus the product collected and drawn from the sample pot was a two-phase liquid made up of an aqueous and an organic phase. Of these phases, only the organic phase was taken for analysis in a gas chromatograph.

Phenyl ethers are insoluble in water and the low solubility of cresols (potential by-products of the reaction under study) in water (Fiege, 1987) is also advantageous making it unnecessary to analyse the aqueous phase.

Phenol, a potential product from cleavage of diphenyl ether, was also considered to be recovered completely by the organic phase, with only trace loss in the aqueous phase. A simple model to check the affinity of phenol to water is given in Appendix X.2.

Injection of the aqueous phase samples in the gas chromatograph proved that there were negligible traces of organic compounds dissolved in the aqueous phase. The exception was methanol which was however, not considered in the product analysis.

4.4.1 Liquid organic phase analysis

The liquid organic phase was analysed in a gas chromatograph equipped with a non-polar GC column and a Flame Ionisation Detector (see Table 4-4, for GC conditions).

Table 4-4: Specifications of the gas chromatograph for analysis of organic liquid product

Gas chromatograph	HP 5890
Column type	Wall coated fused silica capillary
Column length	50 m
Column internal diameter	0.25 mm
Film thickness	0.2 μm
Stationery phase	"PONA"
Carrier gas	Hydrogen
Head pressure	175 kPa gauge
Split ratio	1:200
Volume injected	2 μL
Injector temperature	250°C
Detector	FID
Temperature program	Isothermal 100°C, 5 min; Ramp at 4°C/min to 250°C; Isothermal 250°C, 20 min

Gas chromatograms are shown in Figure 4-7 and Figure 4-8 as well as in Appendix X.

Model compounds used for major peak identification are listed in Table 4-5. Cresols and xylenols were used to determine the range of phenol compounds in the chromatogram, lumped as Ps in

Figure 4-7. Peak identification was carried out by spiking the product samples with mixtures of model compounds (see Appendix X).

Table 4-5: Model compounds used and their normal boiling temperatures for identification (from GC chromatogram) of the reactants and major products obtained from methylation of diphenyl ether (Sinnot, 1999 and Cadogan et al., 1996)

Compound	Normal boiling point [°C]
Methanol	64.6
Phenol	181.8
Diphenyl ether	258
o-Phenoxy-toluene	267
m-Phenoxy-toluene	274
p-Phenoxy-toluene	277.5
p-Tolyl ether	285

The non-polar column separates and elutes the components of a sample essentially according to the order of their boiling points. This holds particularly for members of the same family of compounds, e.g. phenyl ethers. It was therefore expected that the compounds listed in Table 4-5 would elute in exactly the same order as given in the table. This was later confirmed by the chromatogram as shown in Figure 4-7 and Figure 4-8.

4.4.2 Flame ionisation detector

The Gas Chromatograph (GC) was equipped with a Flame Ionisation Detector (FID). The sample effluent from the column of the gas chromatograph is mixed with air and hydrogen and thereafter combusted at the exit of a flame jet in the detector (Sandra, 2003).

The presence of oxygen in a compound reduces the response of the compound in the FID. Peak areas for oxygen compounds must be therefore corrected.

According to Kaiser (1960), the responses of carbon atoms in an FID are as follows:

- Carbon bonded to any element other than oxygen: 100% response
- Carbon bonded with a single bond to an oxygen atom: 55 % response
- Carbon bonded to an oxygen by a double bond: 0 % response

- Carbon bonded to two oxygen atoms by single bonds: 0% response

Responses of the feed and major product constituents calculated on this basis are given in Table 4-6.

Table 4-6: Actual number of carbon atoms and responses in FID per molecule – feed and major product compounds from DPE methylation

Compound	Actual number of carbon atoms, N_{Ci}	Number of carbon atoms detected, n_{ci} [a]
Methanol (MeOH)	1	0.55
Phenol (PhOH)	6	5.55
Phenols (Ps)	9	8.55
Diphenyl ether (DPE)	12	11.1
o-Phenoxy-toluene (OPT)	13	12.1
m-Phenoxy-toluene (MPT)	13	12.1
p-Phenoxy-toluene (PPT)	13	12.1
p-Tolyl ether (PTE)	14	13.1
OADPEs	15	14.1
Heavy phenols (HPs)	20	19.1

[a] Note that for hydrocarbons and other non-oxygen compounds, $N_{ci} = n_{ci}$

Conversion of peak areas to data that is proportional to the amount of carbon eluted from the GC column, necessitated that corrections be made for oxygen containing species. The corrected area was obtained by multiplying the area obtained from the chromatogram by the ratio of the actual number of carbon atoms to that of the number of carbon atoms detected, per molecule (see Equation 4-1).

$$A_{i,corrected} = A_i \cdot \frac{N_{ci}}{n_{ci}} \qquad \textbf{Equation 4-1}$$

with:

A_i = peak area of species i obtained from the table of the chromatogram printout

$A_{i,corrected}$ = corrected peak area of oxygen containing compound

N_{ci} = actual number of carbon atoms per molecule of species i

n_{ci} = number of carbon atoms detected by FID per molecule of species i

Data proportional to the number of moles of species i was obtained by dividing the peak area by the number of carbon atoms detected (see Equation 4-2).

$$N_i = \frac{A_{i,corrected}}{N_{ci}} = \frac{A_i \cdot N_{ci}}{n_{ci} \cdot N_{ci}} = \frac{A_i}{n_{ci}}$$ **Equation 4-2**

with N_i = data proportional to moles of species i

4.4.3 Chromatogram of DPE methylation product

Figure 4-7 and Figure 4-8 show a typical product chromatogram obtained from DPE methylation over mordenite catalysts.

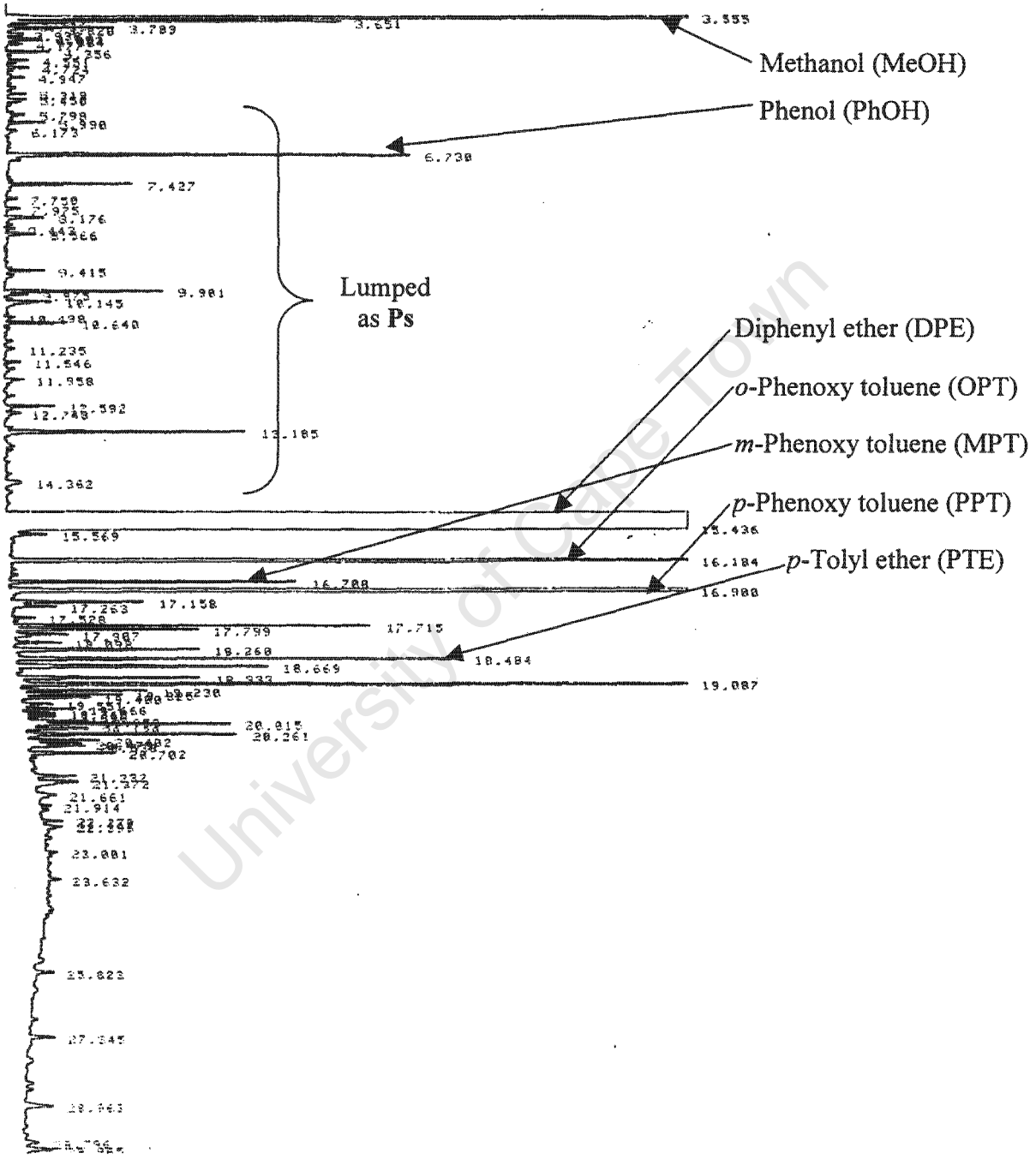

Figure 4-7: First part of the chromatogram from the liquid organic phase (Ps=lumped phenols)

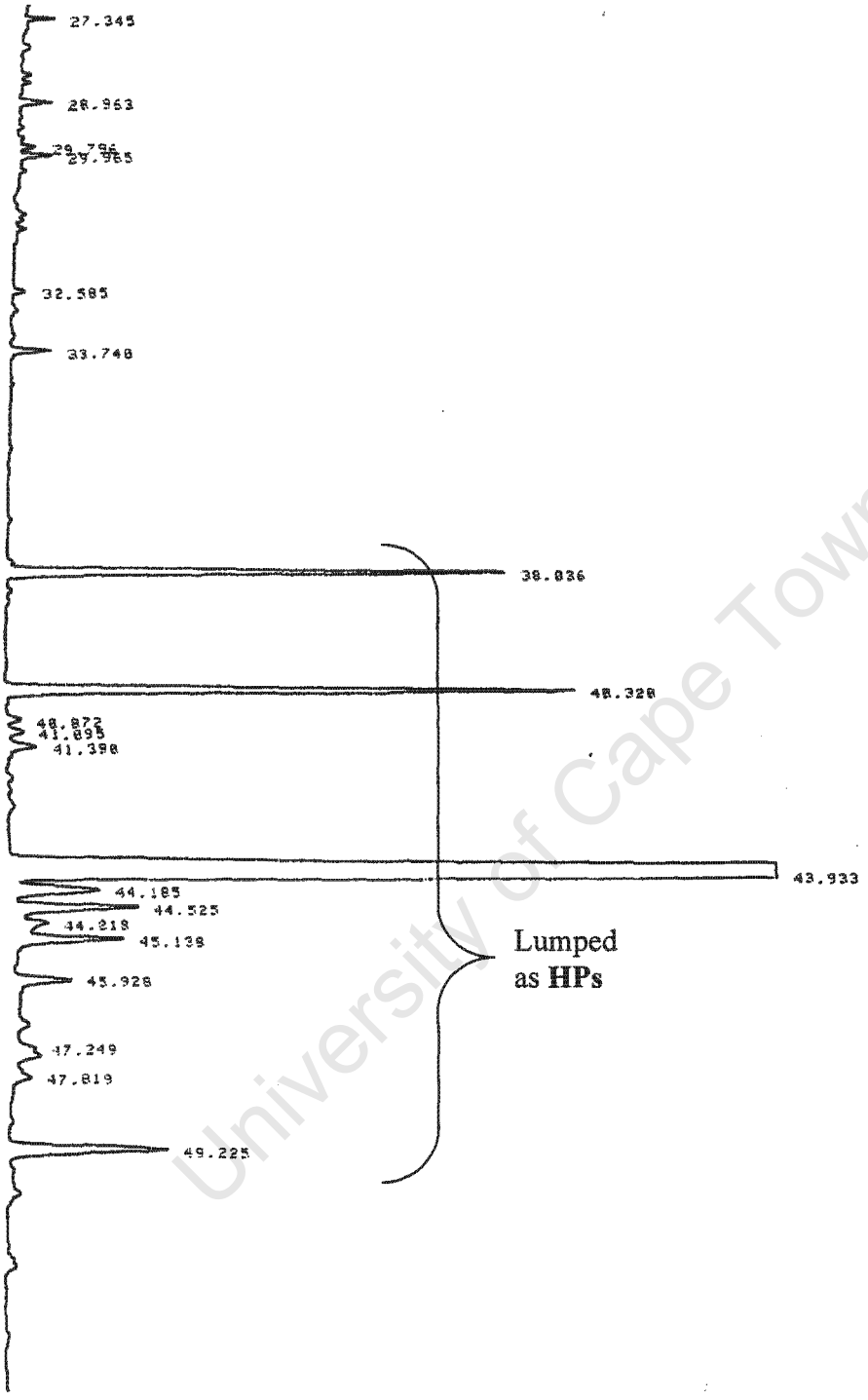

Figure 4-8: Second part of the chromatogram from the liquid organic phase (HPs=heavy products lumped together)

4.4.4 Data work-up

In the experimental results (Chapter 5 and Appendix IX) data was processed as follows:

a. Raw GC data was converted into mole proportional quantities, N_i, for all the species detected on the chromatogram, inclusive of the reactants and the products, according to Equation 4-2, Section 4.4.2

b. Data proportional to moles of products from DPE cleavage or apparent condensation were converted to moles of DPE converted by dividing by 2 or multiplying by 1.5, respectively, i.e. introducing an aromatic ring balance.

c. Conversion was calculated on this basis.

d. Molar product selectivities (also based on ring balance) were calculated by simply changing the product basis to 100%.

e. Product yields were calculated from conversion and selectivities.

f. Molar ratios were calculated based on proportional data (b).

Equations used are as follows:

$$n_{PhOH,DPE} = \frac{N_{PhOH}}{2} \qquad \textbf{Equation 4-3}$$

$$n_{Phenols,DPE} = \frac{N_{Phenols}}{2} \qquad \textbf{Equation 4-4}$$

$$n_{OPT,DPE} = N_{OPT} \qquad \textbf{Equation 4-5}$$

$$n_{MPT,DPE} = N_{MPT} \qquad \textbf{Equation 4-6}$$

$$n_{PPT,DPE} = N_{PPT} \qquad \textbf{Equation 4-7}$$

$$n_{PTE,DPE} = N_{PTE} \qquad \textbf{Equation 4-8}$$

$$n_{OADPEs,DPE} = N_{OADPEs}$$ **Equation 4-9**

$$n_{DPE} = N_{DPE}$$ **Equation 4-10**

$$n_{HPs,DPE} = \frac{3}{2} N_{HPs}$$ **Equation 4-11**

$$X_{DPE} = \frac{\sum n_{i,DPE}}{n_{DPE,unreacted} + \sum n_{i,DPE}}$$ **Equation 4-12**

$$S_j = \frac{n_{j,DPE}}{\sum n_{i,DPE}}$$ **Equation 4-13**

$$Y_j = X_{DPE} * S_j$$ **Equation 4-14**

$$Isomer\_Molar\_Ratio = \frac{n_{i,DPE}}{n_{j,DPE}}$$ **Equation 4-15**

where:

$n_{i,DPE}$	=	number of moles of DPE converted to species i
N_i	=	number of moles of species i
X_{DPE}	=	conversion of DPE
Y_j	=	yield of species j
S_j	=	selectivity of species j

Acronyms of species addressed

PhOH:phenol

Ps :phenols, lumped as carbon number 8 species

DPE :diphenyl ether

OPT :*o*-phenoxy toluene

MPT :*m*-phenoxy toluene

PPT :*p*-phenoxy toluene

HPs :heavy aromatics

In order to understand and interprete the above equations and the data in the appendices, it is important to note the following:

1. Conversion and selectivity are based on the aromatic ring balance.
2. It is assumed that all the rings that entered the reactor also flowed out and are recorded quantitatively in the chromatogram. That is, no accumulation by coking, fouling, etc., in the reactor took place and all the compounds are detectable
3. Mass balance on methanol and its by-products such as dimethyl ether was not done. Most of these are in the gas/vapour phase and leave the apparatus via the vent and are not considered in the GC data evaluation. Some other methanol loss occurs via the aqueous phase.
4. The aromatics compounds are only in trace quantities, for the aqueous phase and the ring balance focuses only on the organic phase.

5. EXPERIMENTAL RESULTS

5.1 EXPERIMENTS CARRIED OUT

In Table 5-1, a summary is given, of the experiments that were carried out. A total of 50 experimental settings were applied with 11 catalyst loads, repeat experiments included. A detailed listing of all individual experiments is appended as a foldout page at the end of the book. The molar ratio of methanol (MeOH) to diphenyl ether (DPE) in the feed was kept at 2 in most experiments, corresponding to stoichiometric amount for the most desired product, p-tolyl ether (PTE). Results are shown in the following graphs (Figure 5-1 to Figure 5-41) with time-on-stream (TOS) as the independent variable. For acronyms, see foldout page at the end of the dissertation.

A summary of results from all experiments is appended as Appendix IX.

The total number of moles in the reaction mixture remains unchanged due to the stoichiometry of the major reactions. The major types of reactions of interest are:

Methanol etherification: $2 \cdot MeOH \rightarrow DME + H_2O$

First methylation: $DPE + MeOH \rightarrow PTI + H_2O$

Second methylation: $PTI + MeOH \rightarrow PTE + H_2O$

Multi-methylation $PTI + MeOH \rightarrow OADPE + H_2O$

Cleavage: $DPE + H_2O \rightarrow 2 \cdot PhOH$

Consequently, the sum of the moles of feed at the reactor inlet and the sum of moles of unconverted feed and products at the reactor outlet is the same. Therefore, the partial pressures of the feed and the products in the reaction mixture are constant and the presence of inert diluent gas has little effects.

At 250°C, the vapour pressures of MeOH and DPE are 93 and 0.8 atmospheres, respectively. The vapour pressure of DPE therefore becomes insignificant in comparison to that of MeOH, and the feed contribution to the gas phase was taken to be solely due to MeOH. This holds even after methanol is converted by the side reaction to dimethyl ether and water.

5.2 PRODUCTS OF THE REACTION

Generally, all the catalysts produced different alkylation products of DPE, lighter products and heavier products.

No conversion was observed for the feed mixture (i.e. methanol and DPE), at 250 and 300°C, in the absence of a catalyst. Even with SiC packing under these conditions, no conversion was observed.

The light products observed include among others, phenol, cresols and xylenols.

Other peaks were observed in the chromatograms around the targeted DPE methylation products. The targeted methylation products were p-Phenoxy Toluene (PPT) and p-Tolyl Ether (PTE). PPT and its other two isomers are lumped as PTI's in the selectivity plots. All other peaks around the methylation products are lumped to be "Other Alkylated Di-Phenyl Ethers" (OADPE's).

The heavy products were usually at most two components for beta, USY and MFI. In the case of mordenites, the heavy fraction was usually dominated by a single peak contributing more than 90% to the heavy fraction (see chromatogram of Figure 4-8).

Superiority of this process route over other widely studied attempts for p-cresol syntheses is the absence of anisole by-product, which always appears as the predominant product in acid catalysed methylation at low to medium temperature, i.e. under the reaction conditions considered in this work.

A foldout page is appended at the end of the dissertation with a list of acronyms used.

5.3 INTRODUCTORY EXPERIMENTS

In Figure 5-1 to Figure 5-4, the results from the introductory experiments carried out over H-beta-25 are shown.

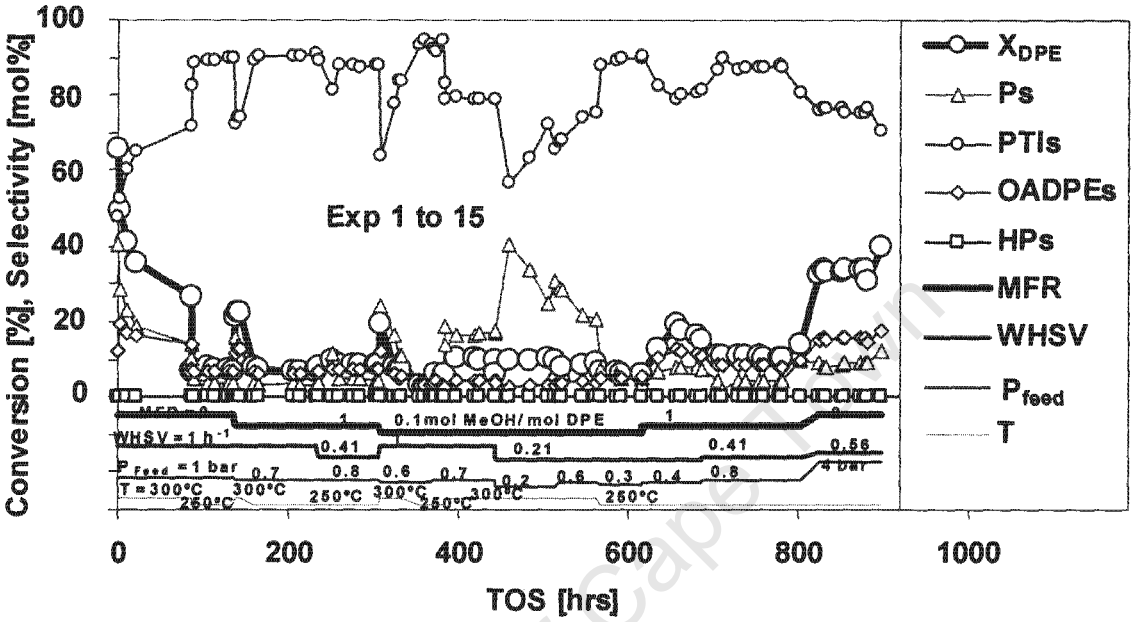

Figure 5-1: DPE conversion and selectivity of the product families from DPE methylation over H-beta-25 (L1) – introductory experiments

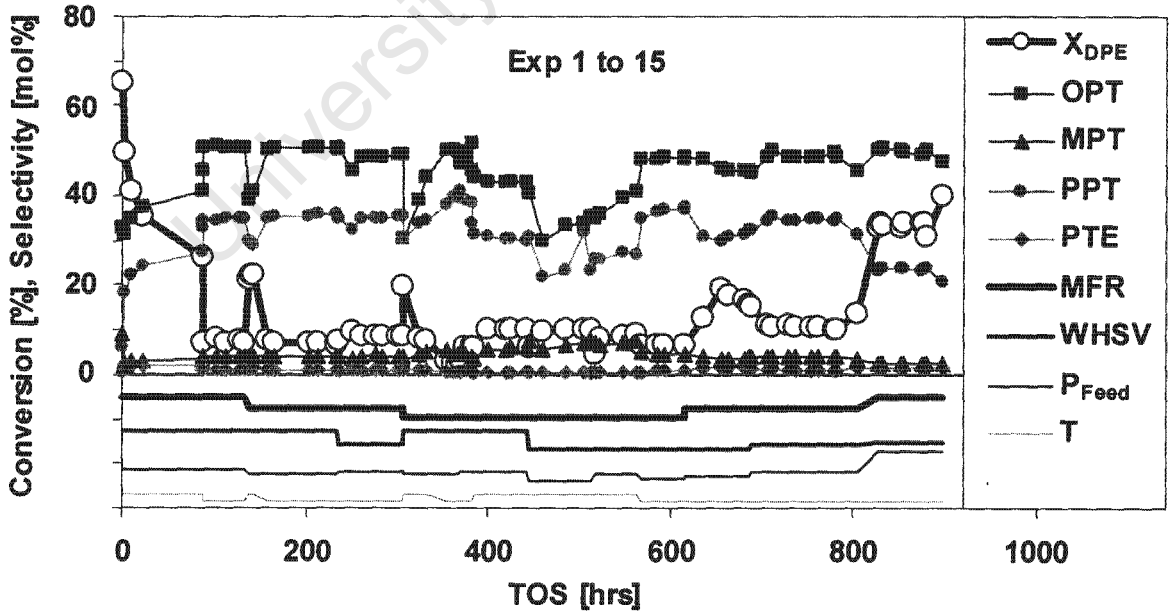

Figure 5-2: DPE conversion and selectivity of important products from DPE methylation over H-beta-25 (L1) – introductory experiments

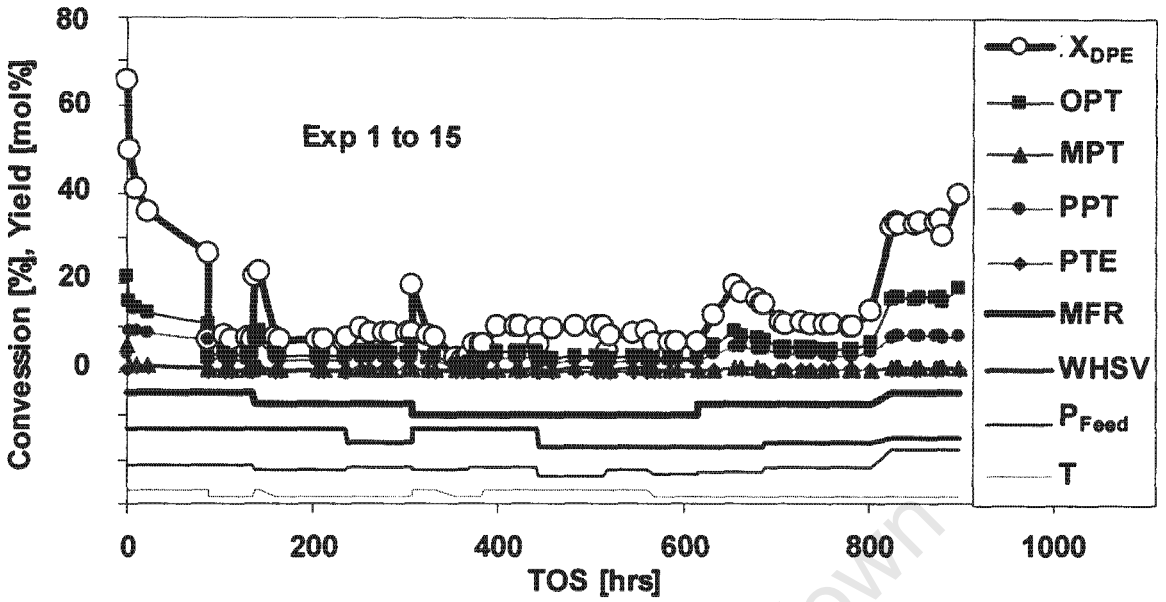

Figure 5-3: DPE conversion and yield of important products from DPE methylation over H-beta-25 (L1) - introductory experiments

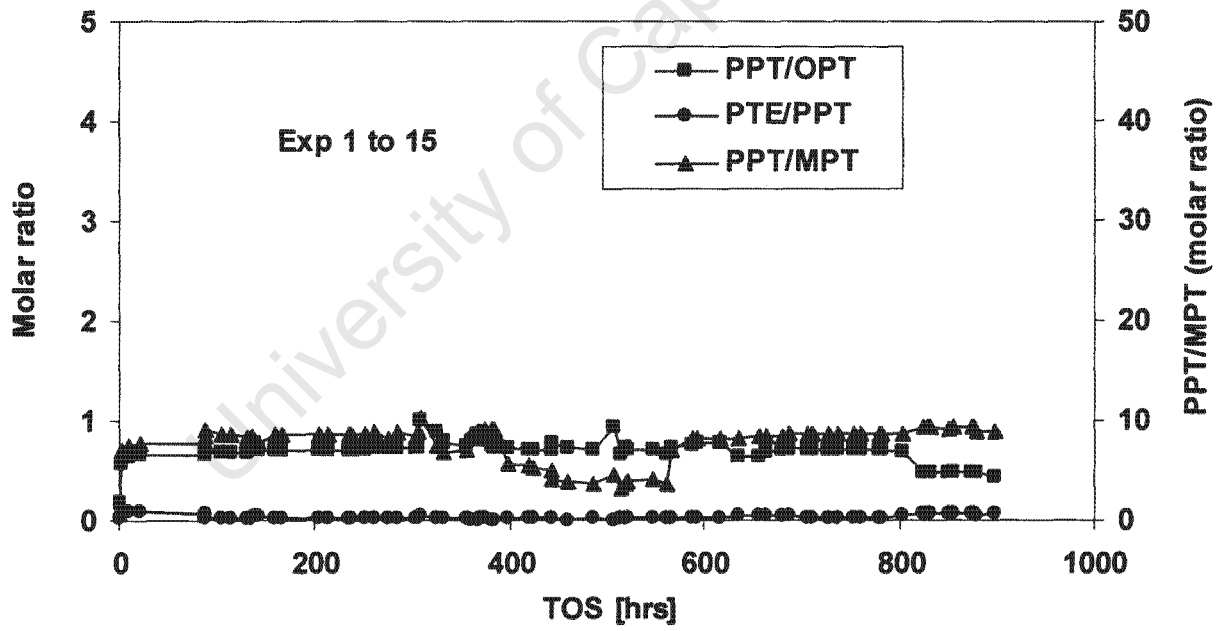

Figure 5-4: Ratios of mono-methylated isomers and ratio of *p*-di- and *p*-mono-methylated products from DPE methylation over H-beta-25 (L1) - introductory experiments

In Figure 5-1, high but steeply declining initial activity during the first 100 hours on stream was observed and this was due to the settling in of the activity of the catalyst.

Change of conditions always resulted in a step change, upwards or downwards. Conversion, selectivity and yield at a particular set of conditions were therefore based on steady state values, after the system has settled.

Overall, high diphenyl ether (DPE) conversion was obtained by a combination of high feed partial pressure (4 bar) and high Molar Feed Ratio (MFR=2) (experiment 15, 800-900 hours on stream period, the last experiment on H-beta-25 (L1)). The second highest conversion was obtained at an MFR of 1 and at either very low WHSV of 0.2 h^{-1} or high reaction temperature (experiments 3 and 13).

At high conversion of 40% over H-beta-25 (L1), selectivity to Phenoxy Toluene Isomers (PTIs) was higher than 70%. PTI selectivities in excess of 90% were only obtained with conversion below 10%.

High conversion and high temperature increased selectivity to Para-Tolyl-Ether (PTE), the desired dimethylated product (Figure 5-2). High temperature also gave rise to a slight increase in PTE selectivity, but at a decrease in selectivity to mono-paramethylated DPE (PPT). At low MFR (0.1), higher temperature proved to increase conversion slightly, but at the expense of selectivity to PTIs.

In the case of equimolar and higher MFR of 2, at low to medium temperature and conversion (<300°C, <20%), selectivity to the individual PTIs remained rather constant for different temperature and conversion levels (Figure 5-2). At conversion of 10% and below, selectivities were 35% and 50% for the *para-* and the *ortho*-isomers, respectively.

Conversion of 10% and below resulted in a slight increase in PPT selectivity with OPT selectivity either remaining constant or decreasing slightly, and this was the case only when temperature was low and DPE was in excess (MFR=0.1). At conversion level of 34%, these selectivities were 20% and 50%, respectively.

Selectivity to heavy aromatic products (HPs) was negligible as long as the feed partial pressure was below 4 bar.

High temperature (300°C), particularly in combination with low space velocity and low feed partial pressure resulted in increased selectivity to the light products lumped as Ps (see Figure 5-1).

In Figure 5-2, as the catalyst activity declines from a high initial value, selectivity of the *meta*-monomethylated isomer (MPT) also declines from a high initial value, whereas the *ortho* (OPT) and the *para* (PPT) isomers rise from initial values of 30% and <1%, respectively.

The yields of the individual isomers followed the conversion trend, i.e. increased when the conversion increased and dropped when the conversion dropped. The yield to the *meta* mono-methylated (MPT) isomer rose slightly at high temperature and low space velocity (see Figure 5-3).

The ratios of the individual PTIs are more or less unaffected by the change in reaction conditions and conversion (see Figure 5-4), except at high temperature (300°C) and high conversion (>20%). When the *para/meta* (PPT/MPT) and *para/ortho* (PPT/OPT) ratios dropped, the ratio of di-to-mono-*para*-methylated products increased, though on a low level.

It therefore seemed reasonable to conduct further experiments at high feed partial pressure, intermediate temperature and molar feed ratio (MFR) of greater than 1.

5.4 SEARCH FOR CATALYST SCREENING CONDITIONS – H-BETA-25

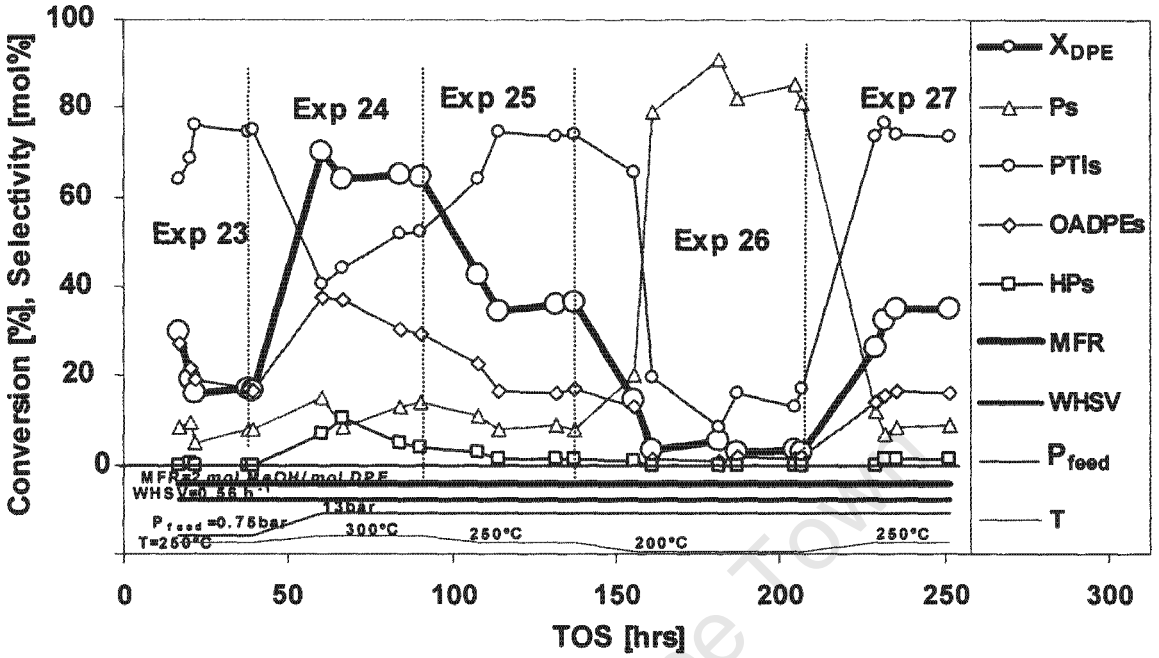

Figure 5-5: DPE conversion and selectivity of the product families from DPE methylation over H-beta-25 (L4)

Results from the search for catalyst standard screening conditions are shown in Figure 5-5 to Figure 5-7 and Figure 5-23. Following on from the introductory experiments, the molar feed ratio was high (MFR=2) and the feed partial pressure was raised to 10 bar, and the catalyst was H-beta-25.

Experiment 27 was a repeat of Experiment 25, with the aim to check the repeatability of this experiment and to establish the deactivation behaviour of the catalyst. No significant difference was observed.

Conversion of up to 65% was obtained at high temperature (see Experiment 24), but this also resulted in low selectivity to the Phenoxy Toluene Isomers (PTIs) and high selectivity to Other Alkylated Di-Phenyl Ethers (OADPE's).

At high temperature and high conversion (Experiment 24), the heavy products (HPs) were significant with selectivity of up to 10%.

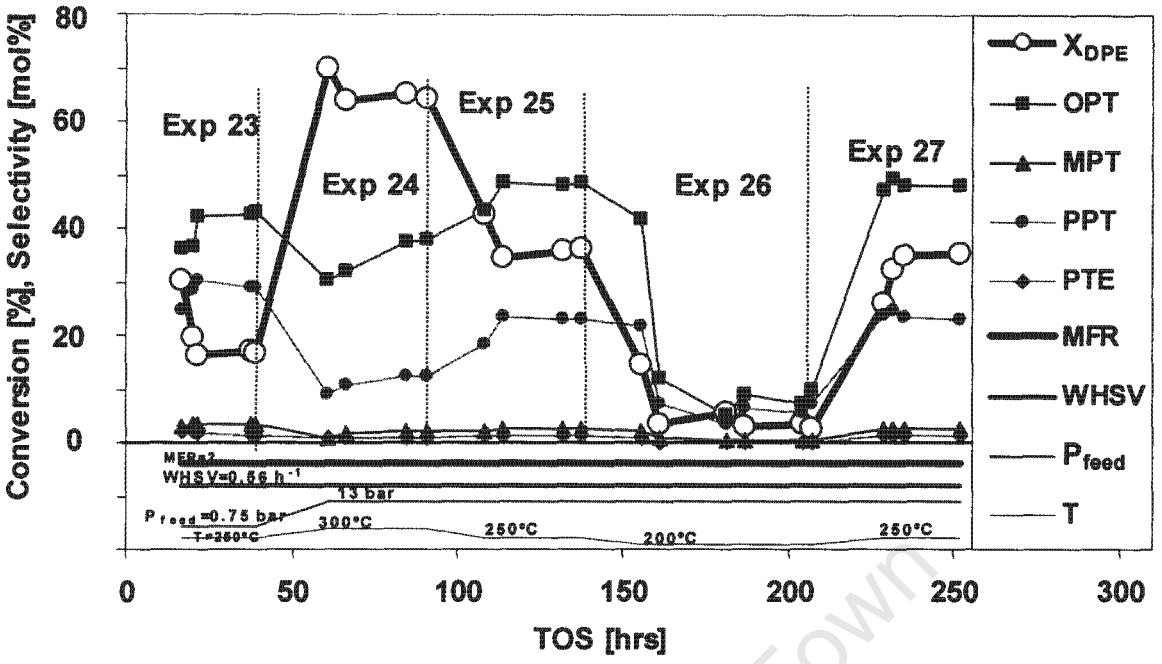

Figure 5-6: DPE conversion and selectivity of important products from DPE methylation over H-beta-25 (L4)

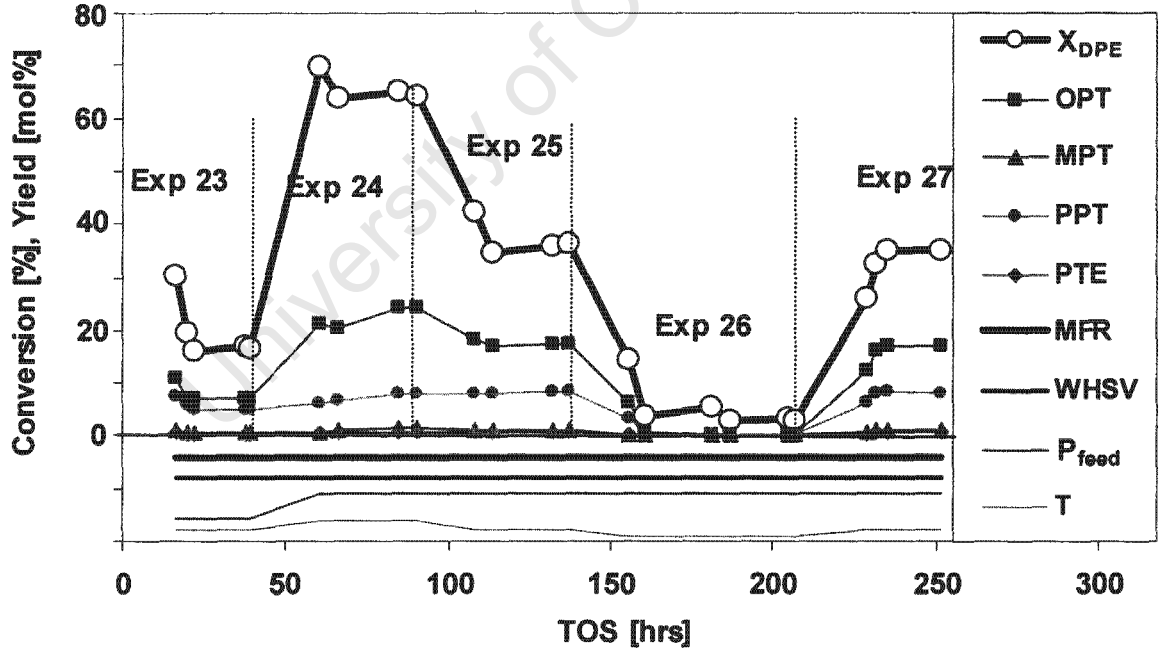

Figure 5-7: DPE conversion and yield of important products from DPE methylation over H-beta-25 (L4)

Low temperature (200°) resulted in a non-favourable product of mostly phenols (Ps) and very low selectivity to PTIs (see Figure 5-5).

From intermediate (250°C) to high temperature (300°C) the yield of OPT increased slightly whereas that of PPT was unaffected by the aforementioned temperature changes (see Figure 5-7). Even though the conversion was low in Experiment 23, selectivity of MPT was slightly higher during this experiment (see Figure 5-6), but this occurred over a fresh catalyst. However, for intermediate to high temperatures, the yield for this isomer (MPT), remained low and unaffected by temperature changes.

The ratios PPT/OPT and PPT/MPT, in Figure 5-23, were high in Experiment 25 and Experiment 27, but highest in Experiment 26, however, the yield of both PPT and PTIs was poor in the latter (i.e. Experiment 26).

Conversion from Experiment 25 and Experiment 27 (see Figure 5-5) at medium temperature of 250°C, seemed reasonable because it was fairly high, with little light and heavy by-product formation. Selectivity to the PTIs was in excess of 70% and selectivity to the *p*-methylated diphenyl ether, PPT, was reasonable as well (20%, see Figure 5-6)

Reaction conditions for Experiment 25 and Experiment 27 were selected as standard conditions to screen the different zeolites for the reaction under study (see Table 5-2).

5.5 CATALYST SCREENING

5.5.1 Conversion, selectivity and yield

In Table 5-2, standard test conditions for catalyst screening are shown and these were derived from introductory and screening experiments of Section 5.3 and Section 5.4. The results obtained over H-beta-25 at the standard conditions are given in Figure 5-5 to Figure 5-7, Experiment 25 and Experiment 27.

Table 5-2: Standard catalyst screening conditions for DPE methylation

T	Temperature	250°C
P_{total}	Total system pressure	20 bar
P_{feed}	Feed partial pressure	13 bar[b]
P_{N2}	Nitrogen partial pressure	7 bar
$m_{dry\ zeolite}$	Mass of dry zeolite	3 g
MFR	Molar feed ratio	2 (mol MeOH)/(mol DPE)[a]
$WHSV_{DPE}$	Weight hourly space velocity, based on DPE	0.56 $g_{DPE}/(g_{dry\ zeolite} \cdot h)$

[a] Zeolites H-MFI-50 and H-Mor-40 were screened at MFR=3.2, with no significant change in WHSV. The different MFR was due to an error which was noticed upfront but could not be corrected due to logistical problems.

[b] Feed partial pressure taken to be solely due to methanol due to very low volatility of DPE

In Table 4-1, the various zeolites screened at the conditions of Table 5-2 are listed. All the catalysts were in powder form, with the exception of the CBV-types, which were extrudates (see Table 4-1).

5.5.1.1 H-MFI-50

Figure 5-8 to Figure 5-10 show DPE conversion, selectivities and yields obtained from DPE methylation over H-MFI-50 zeolite.

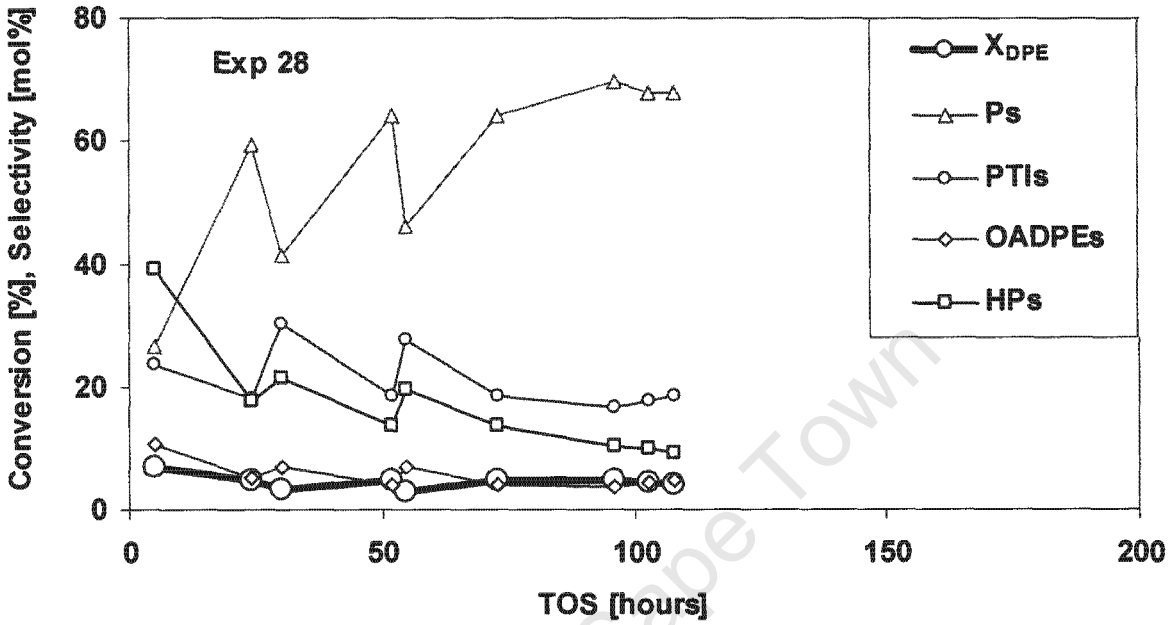

Figure 5-8: DPE conversion and selectivities of the product families from DPE methylation over H-MFI-50 (L1), at standard conditions of Table 5-2, except that MFR=3.2

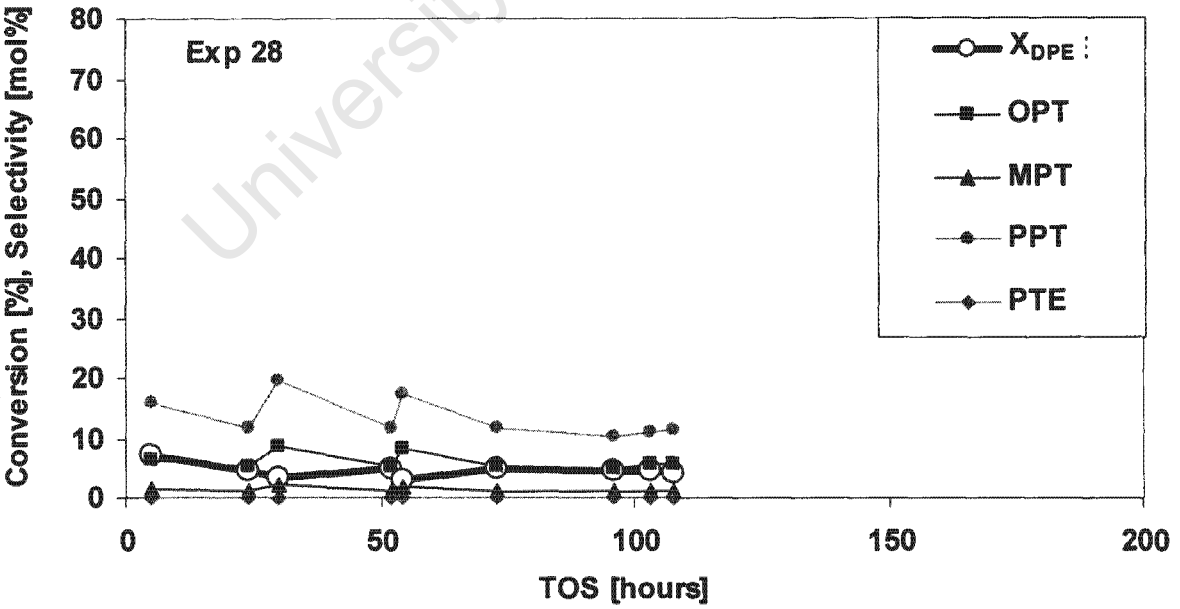

Figure 5-9: DPE conversion and selectivity of important products from DPE methylation over H-MFI-50 (L1)

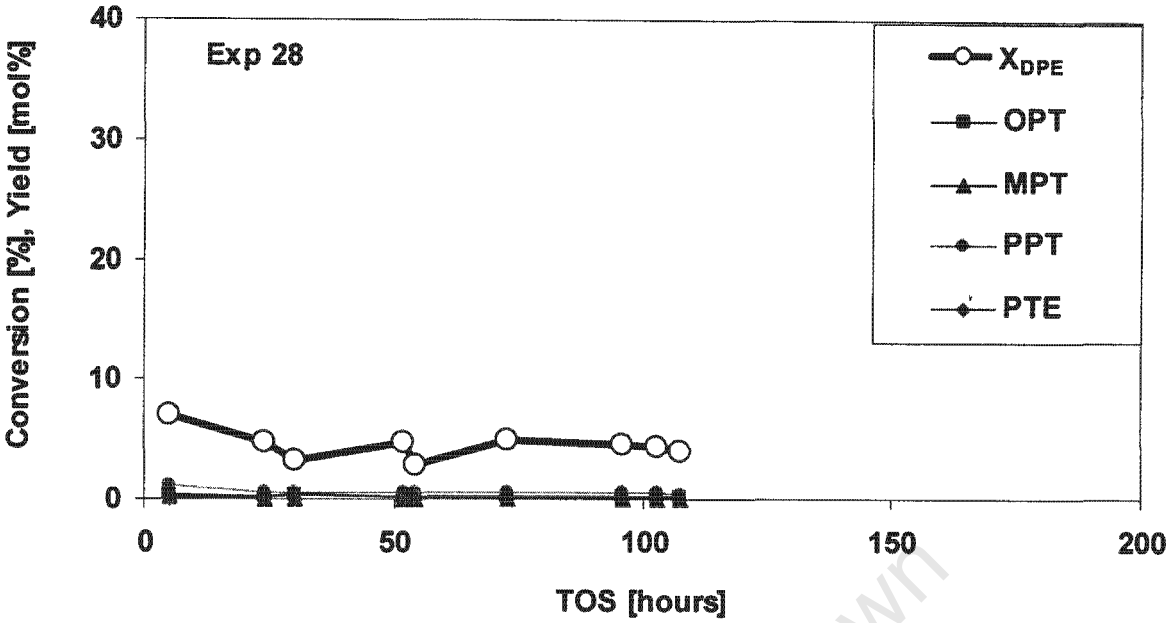

Figure 5-10: DPE conversion and yields of important products from DPE methylation, over H-MFI-50 (L1)

As Figure 5-8 shows, DPE conversion over H-MFI-50 was very low, <10%, and appeared to stabilise after initial deactivation. Selectivity to PTIs was low, around 20%, with high selectivity to light by-product (Ps), ca. 70%. In the PTI fraction, selectivity to the *para*-methylated isomer (PPT) was fairly high, twice as high as selectivity due to OPT (see Figure 5-9). However, yields were minor (see Figure 5-10)

Selectivity of the PTIs was low and its curve almost flat after the higher initial activity of the catalyst settled to steady state conversion (see Figure 5-9). Yields were minor (see Figure 5-10). The light product (Ps) on the other hand increased from an initially low value towards a very high value of ca. 70%, at steady state conversion, whereas the heavy products (HPs) decreased from a high initial value to a low value of ca. 10%, at steady state conversion (see Figure 5-8).

Selectivity of the Other Alkylated Di-phenyl Ethers (OADPEs), just like the PTIs, remained almost flat throughout the screening of H-MFI-50.

5.5.1.2 H-USY

Figure 5-11 to Figure 5-13 show the conversion of DPE, product selectivities and yields obtained from DPE methylation over H-USY.

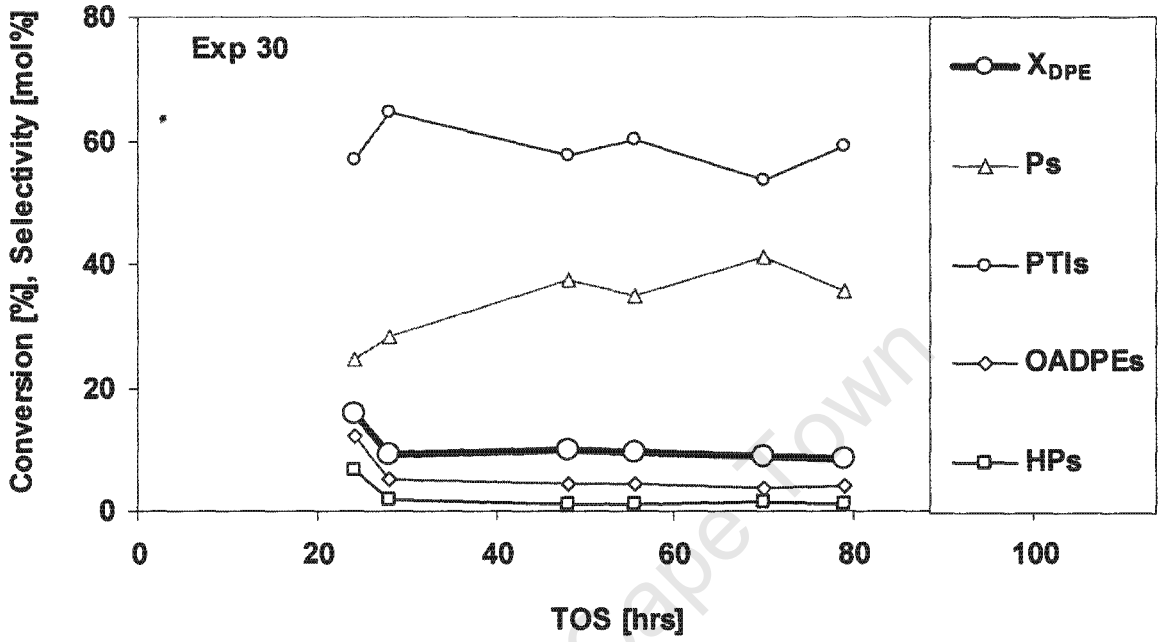

Figure 5-11: DPE conversion and selectivity of the product families from DPE methylation over H-USY (L1), at standard screening conditions of Table 5-2

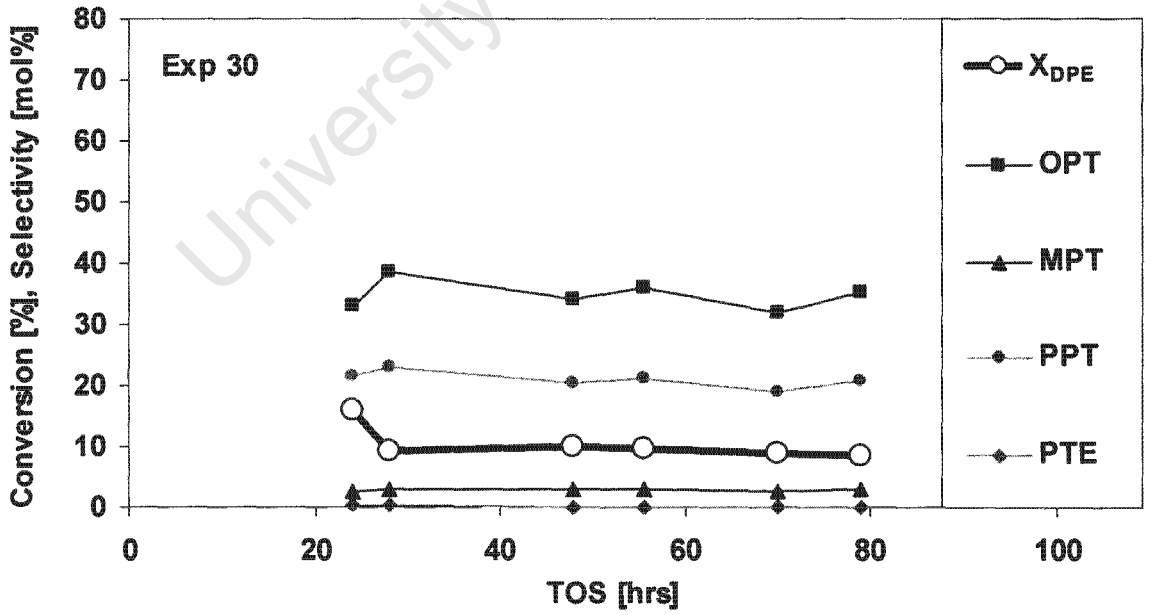

Figure 5-12: DPE conversion and selectivity of important products from DPE methylation over H-USY (L1)

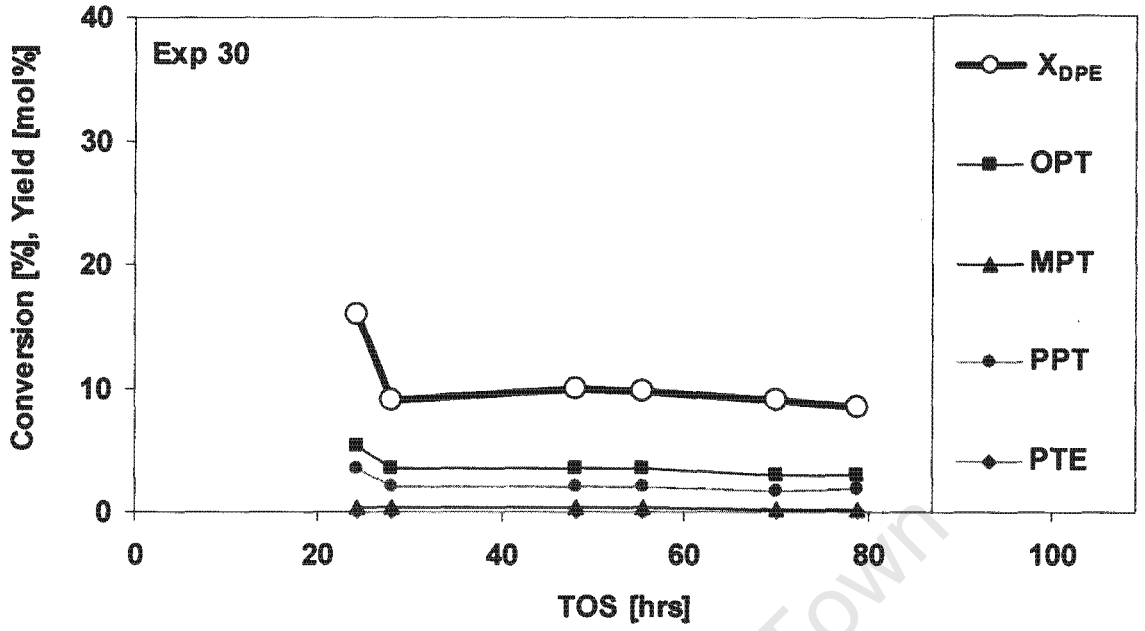

Figure 5-13: DPE conversion and yield of important products from DPE methylation over H-USY (L1)

Zeolite H-USY gave fairly low conversion of 10%, but steady with no significant deactivation. Selectivity to PTIs (phenoxy toluene isomers) was high, with medium selectivity to Ps (light products). Selectivity to OADPEs was low and almost no HPs were formed (see Figure 5-11).

In the PTI fraction, OPT had the highest selectivity, followed by PPT (targeted product) and lastly MPT, with no significant change with time-on-stream (see Figure 5-12).

5.5.1.3 H-Mor-40

Figure 5-14 to Figure 5-16 show DPE conversion, selectivities and yields obtained from DPE methylation over H-Mor-40.

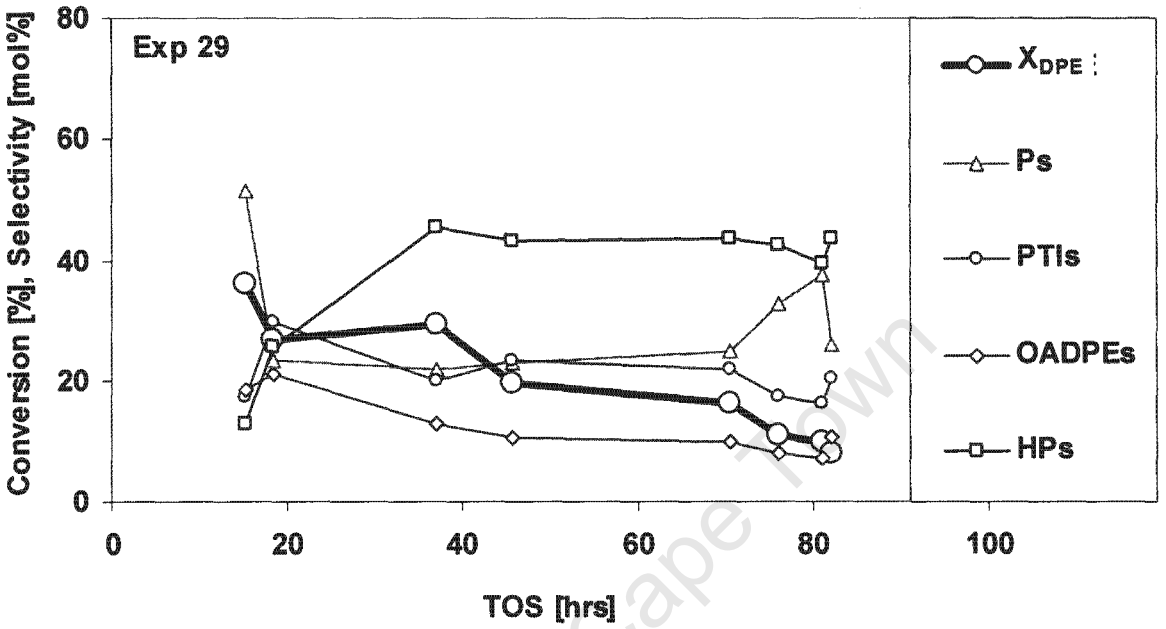

Figure 5-14: DPE conversion and selectivity of the product families from DPE methylation over H-Mor-40 (L1), at standard conditions of Table 5-2, except that MFR=3.2

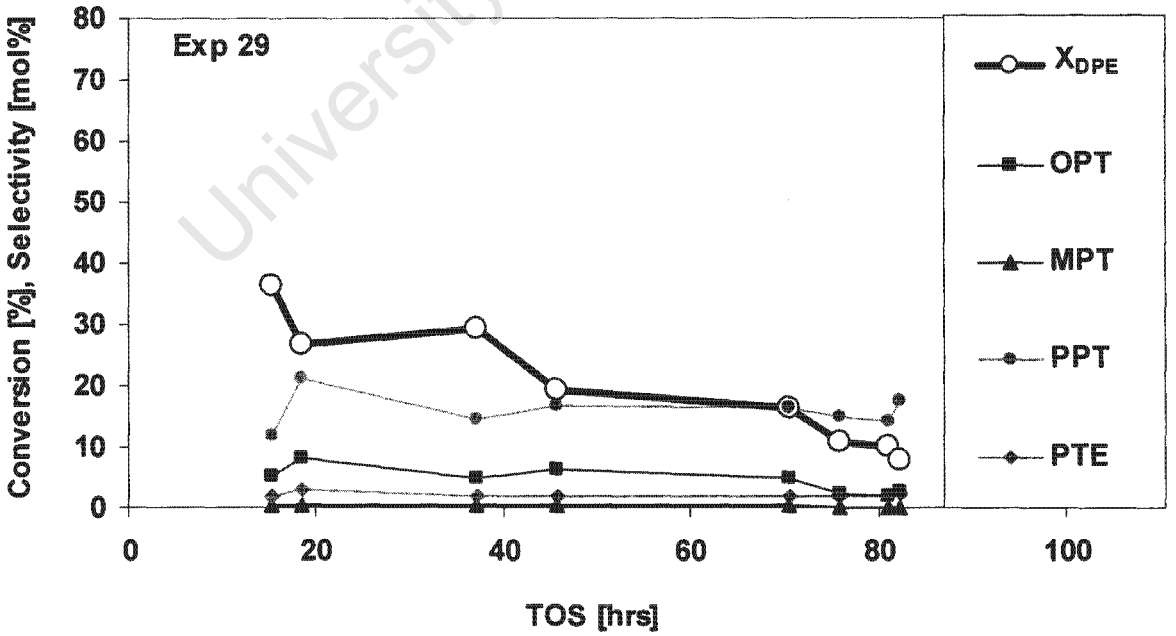

Figure 5-15: DPE conversion and selectivity of important products from DPE methylation over H-Mor-40 (L1)

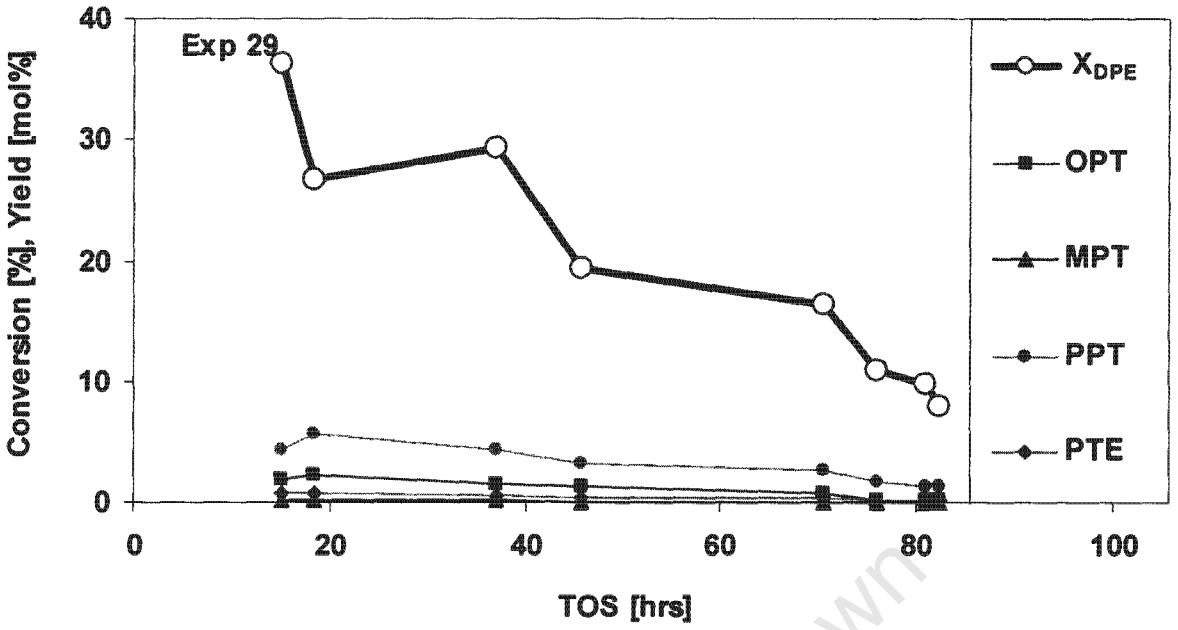

Figure 5-16: DPE conversion and yields of important products from DPE methylation over H-Mor-40 (L1)

H-Mor-40 gave high initial DPE conversion but deactivated quickly without achieving steady state, also giving a high selectivity to the heavy products (HPs), even at low conversion. Selectivity of the PTIs, OADPEs and HPs rose from an initial low value at high initial conversion whereas that of the Ps dropped from initial high value. Overall, selectivity to the PTIs was moderate, together with the Ps, whereas that of the OADPEs was fairly low (see Figure 5-14).

On the other hand, selectivity to and yield of the desired *p*-methylated product, *p*-phenoxy toluene (PPT), was relatively high, higher than those for the *o*-isomer (OPT). MPT was only formed in very small quantities (see Figure 5-15 and Figure 5-16).

5.5.1.4 Mordenite based catalyst CBV21A – calcined at 400°C

Figure 5-17 to Figure 5-19 show DPE conversion, selectivities and yields obtained from DPE methylation over mordenite based catalyst CBV21A, calcined at 400°C.

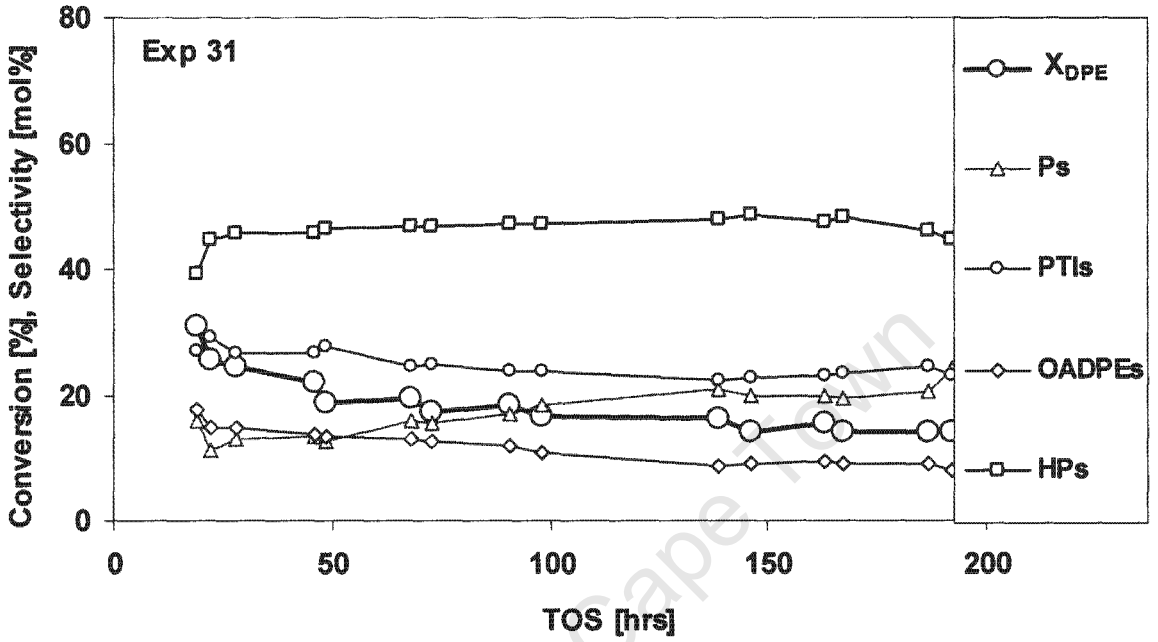

Figure 5-17: DPE conversion and selectivity of the product families from DPE methylation over CBV21A (L1), calcined at 400°C, tested at standard conditions of Table 5-2

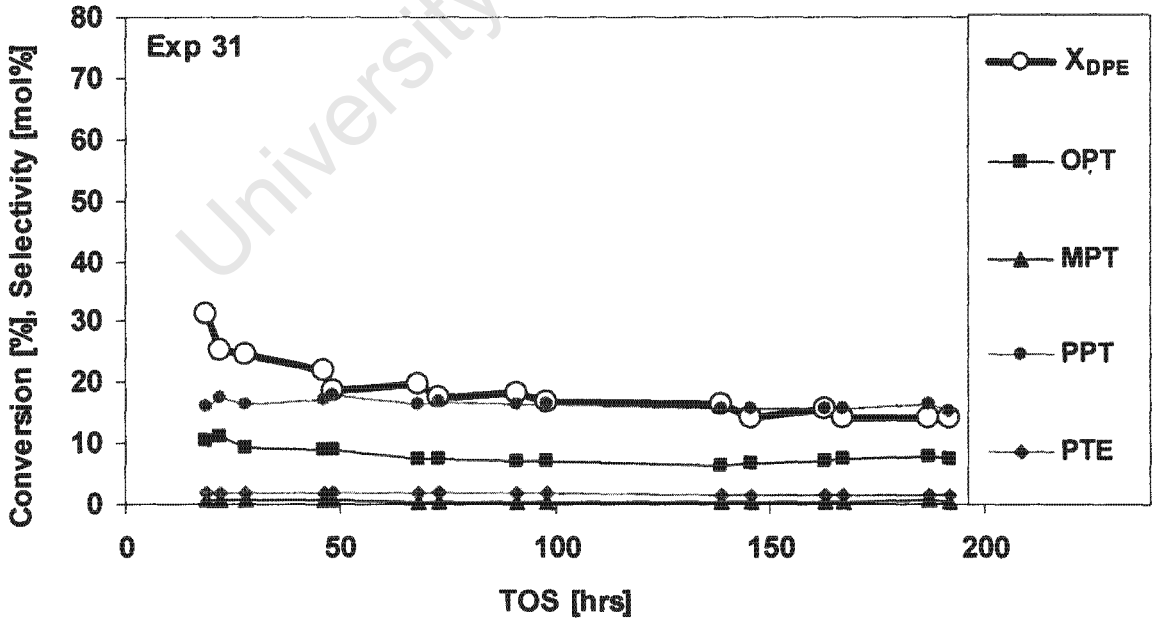

Figure 5-18: DPE conversion and selectivity of important products from DPE methylation over CBV21A (L1), calcined at 400°C

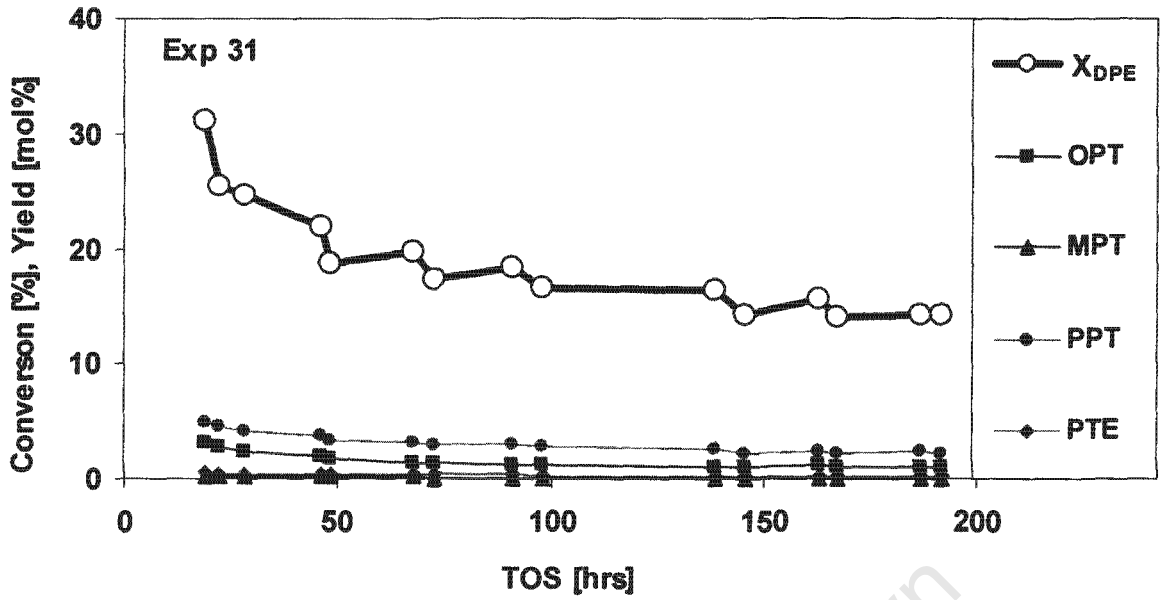

Figure 5-19: DPE conversion and yields of important products from DPE methylation over CBV21A (L1), calcined at 400°C.

DPE conversion over catalyst CBV21A was reasonable, settling at around 15% after 200 hours on stream, but the catalyst still appears to show continuing slow deactivation (see Figure 5-12). Despite the slow deactivation observed, selectivities remain unchanged. However, the yields of individual products declined uniformly with time-on-stream (see Figure 5-19). Selectivity to PTIs was medium (25%), as well as selectivity to Ps, but a fairly high proportion of HPs was formed (see Figure 5-17).

In the PTI fraction (see Figure 5-18), PPT (targeted product) remained high at about 15%, followed by OPT at half that level and lastly MPT with about zero selectivity. Selectivity to the di-*para*-methylated product was even higher than that of MPT throughout the duration of Experiment 31.

Results from DPE methylation over catalyst CBV21A calcined at 500°C are given in Section 5.7.

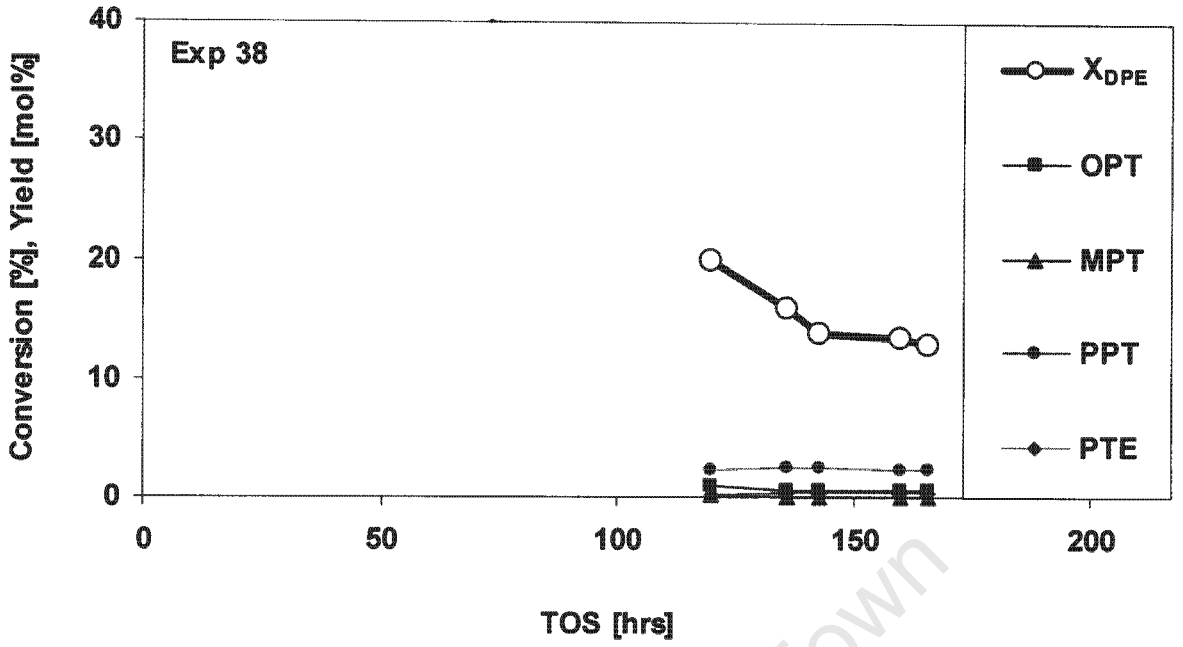

Figure 5-22: DPE conversion and yields of important products from DPE methylation over CBV90A (L1)

Note that the screening experiment at the standard test conditions was preceded by other experiments and only started after 120 hours on stream.

A high initial DPE conversion was obtained over CBV90A, which declined constantly with time-on-stream (see Figure 5-20).

Selectivity to the PTIs continually increased to about 20 mol% after 160 hours on stream, with a simultaneous decrease in OADPE's. However, selectivity to HPs increased even more, with HPs becoming the dominant product with 40% selectivity after 160 hours on stream (see Figure 5-20).

In the PTI fraction, yields were low (see Figure 5-22). Selectivity to the *ortho*-isomer (OPT) remained constant on a low level of ca. 5%, whereas selectivity to the *para*-isomer (PPT) increased to a far higher value of about 20 mol% with time-on-stream.

5.5.2 Isomer ratios

Methylation of diphenyl ether in the *para* position was the aim of the study. Other possible products of methylation are the *ortho* and the *meta* methylated isomers. It therefore became necessary to look at the isomer ratios in the fraction of mono-methylated phenoxy toluenes, PTIs, (PPT/OPT and PPT/MPT), as well as the ratio of di-*para* to mono*para* methylated product (PTE/PPT). Results obtained at the standard screening conditions are shown in Figure 5-23 to Figure 5-28.

While para/meta, i.e. PPT/OPT, ratios obtained over H-beta-25 and H-USY were around 0.5 (see Figure 5-23 and Figure 5-25), ratios obtained over the mordenite based catalysts were significantly higher, around 2 for CBV21A, up to 4.5 for CBV90A and around 8 for H-Mor-40. These were the values towards the end of each of the runs, with initial values still >1 throughout (see Figure 5-27, Figure 5-28 and Figure 5-26). H-MFI-50 also produced a rather high PPT/OPT ratio of around 2 (see Figure 5-24).

Ratios of para/meta phenoxy toluenes, i.e. PPT/MPT, were far higher than the para/ortho ones, varying from ca. 7 (H-USY, see Figure 5-25) to almost 100 (H-Mor-40 at the end of the Experiment 29, see Figure 5-26).

The ratio of di- to mono-methylated products (PTE/PPT) is generally very low, <0.2, changes mainly reflecting conversion (see Figure 5-29).

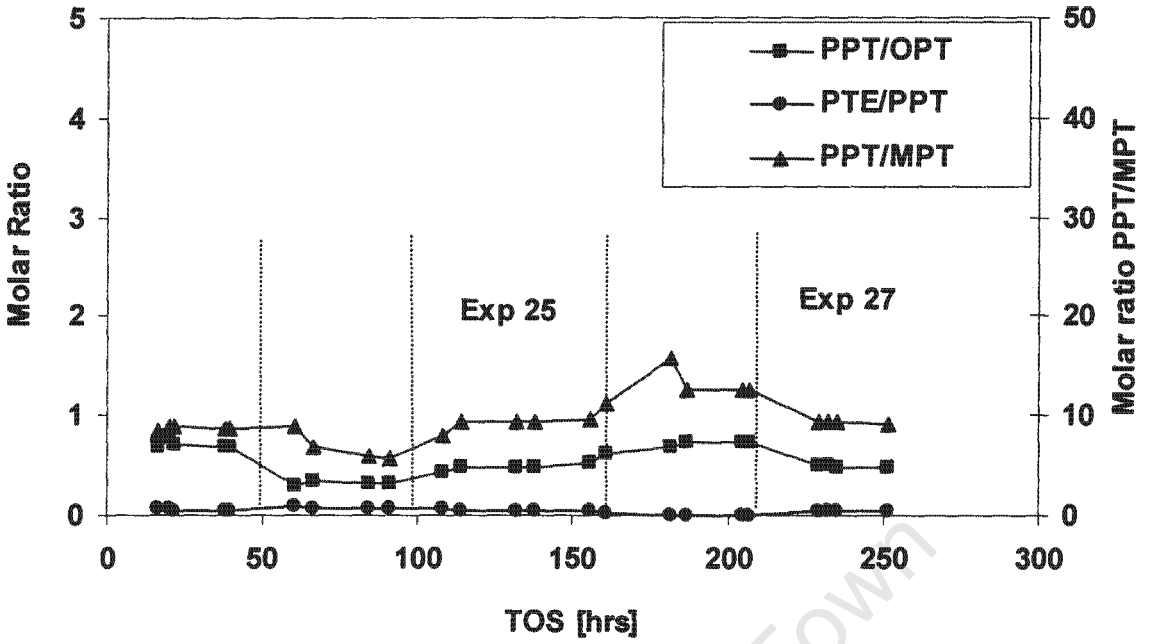

Figure 5-23: Ratios of the mono-methylated and the ratio of di- to the mono-*para* methylated products from DPE methylation over H-beta-25 (L4), at standard screening conditions of Table 5-2 (Exp 25 and Exp 27)

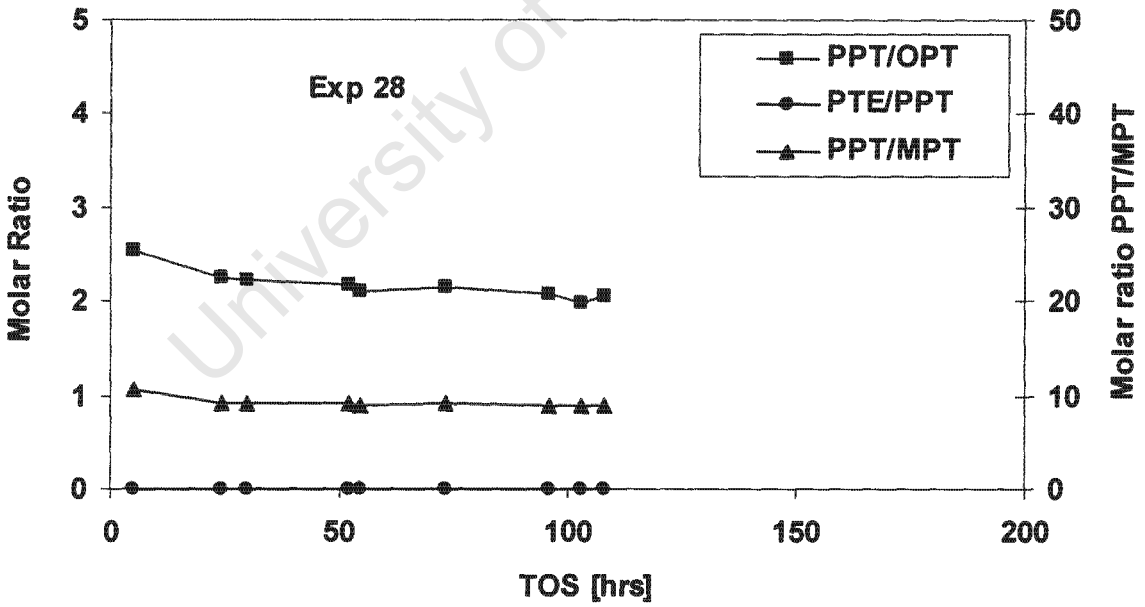

Figure 5-24: Ratios of the mono-methylated and the ratio of the di- to the mono-*para* methylated products from DPE methylation over H-MFI-50 (L1), at standard screening conditions of Table 5-2, except MFR=3.2

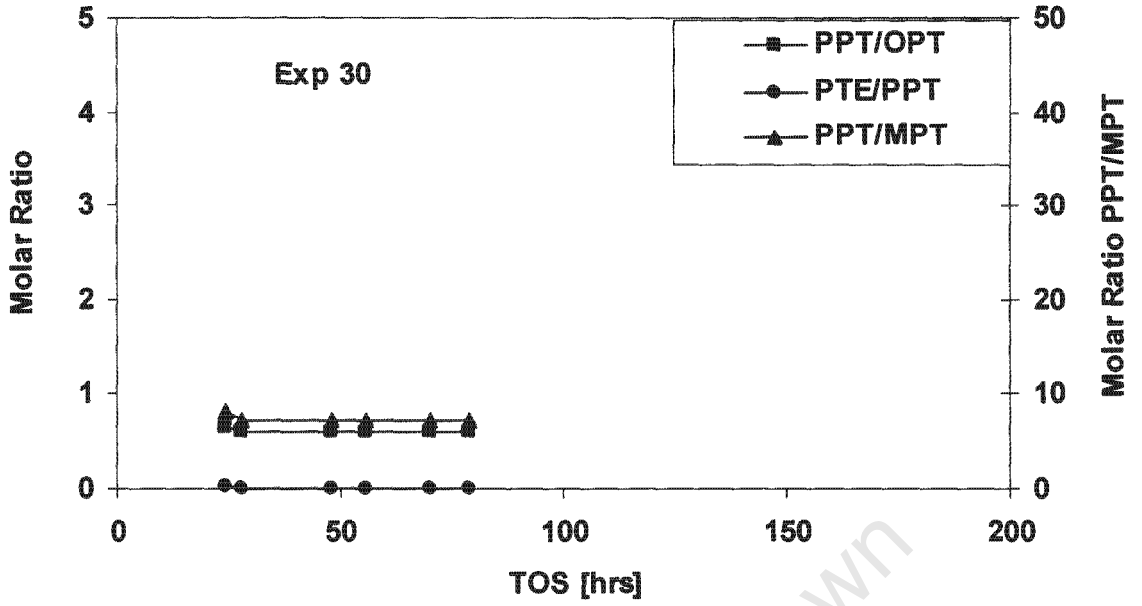

Figure 5-25: Ratios of the mono-methylated and the ratio of the di- to the mono-*para* methylated products from DPE methylation over H-USY (L1), at standard screening conditions of Table 5-2

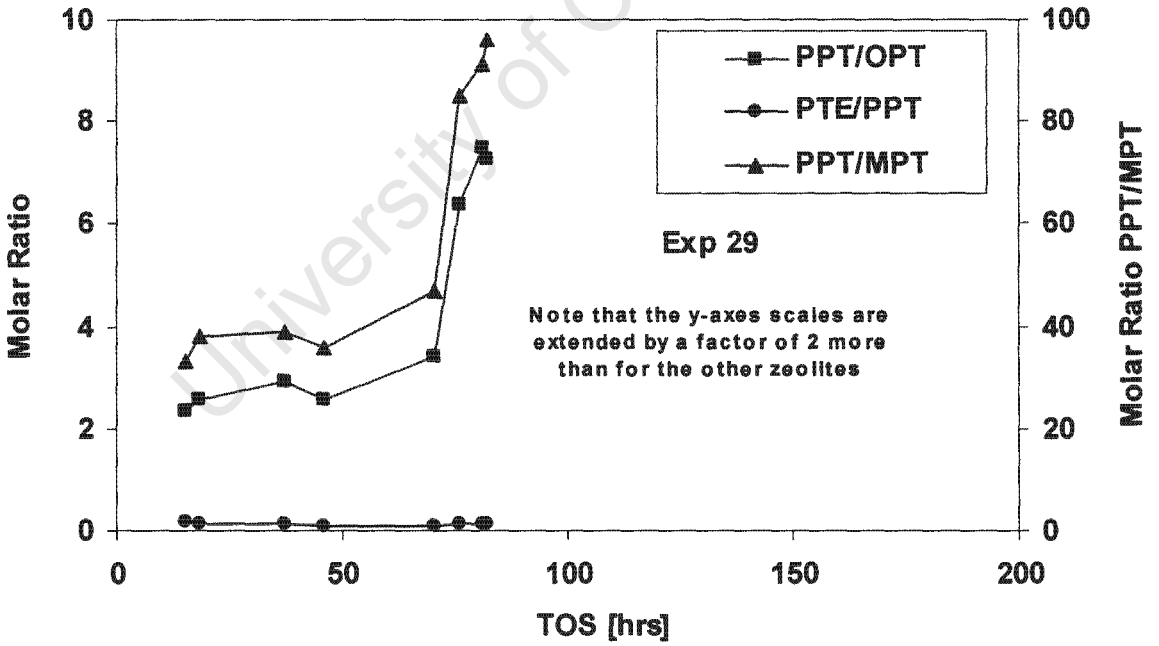

Figure 5-26: Ratios of the mono-methylated and the ratio of the di- to the mono-*para* methylated products from DPE methylation over H-Mor-40 (L1), at standard screening conditions of Table 5-2, except MFR=3.2

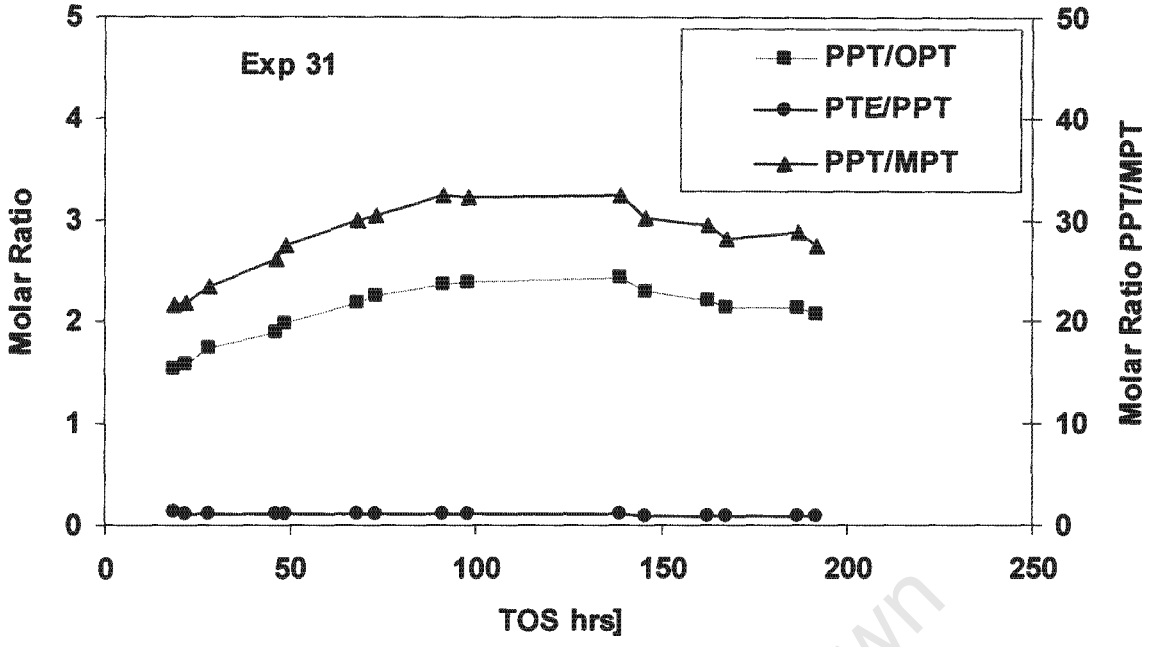

Figure 5-27: **Ratios of the mono-methylated and the ratio of the di- to the mono-*para* methylated products from DPE methylation over CBV21A (L1), calcined at 400°C, tested at standard screening conditions of Table 5-2**

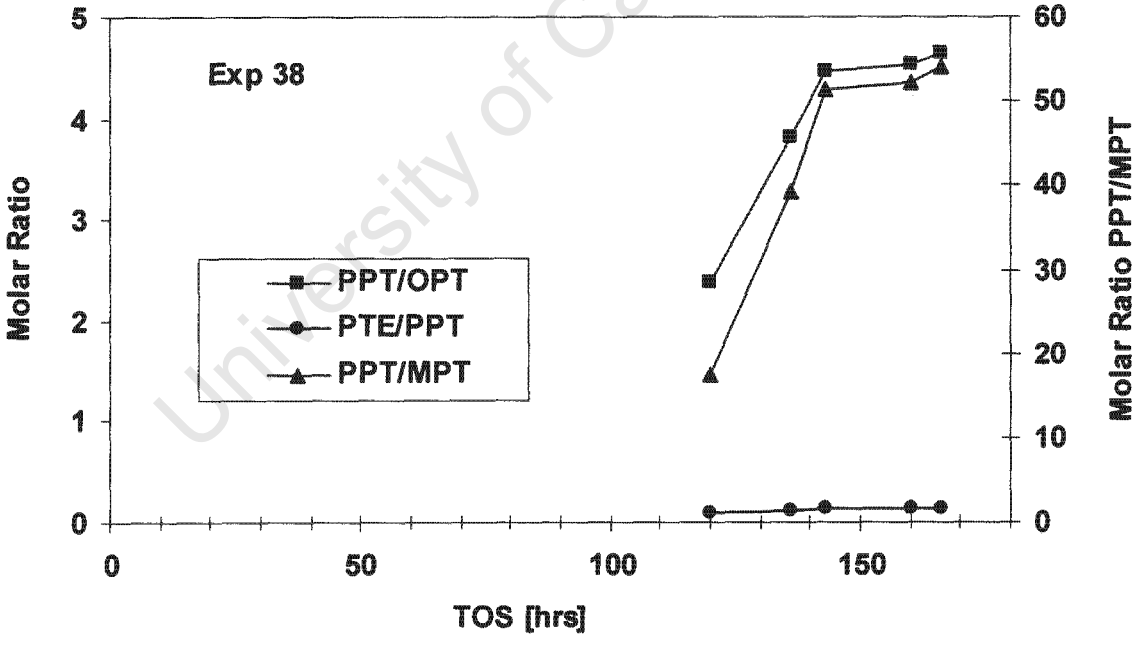

Figure 5-28: **Ratios of the mono-methylated and the ratio of the di- to the mono-*para* methylated products from DPE methylation over CBV90A (L1), at standard screening conditions of Table 5-2**

5.5.3 Conversion

Though the focus of the study was high para-selectivity, conversion was also an important criterion. Figure 5-29 shows the conversion of diphenyl ether over the screened zeolites, with time-on-stream, tested at the standard screening conditions of Table 5-2.

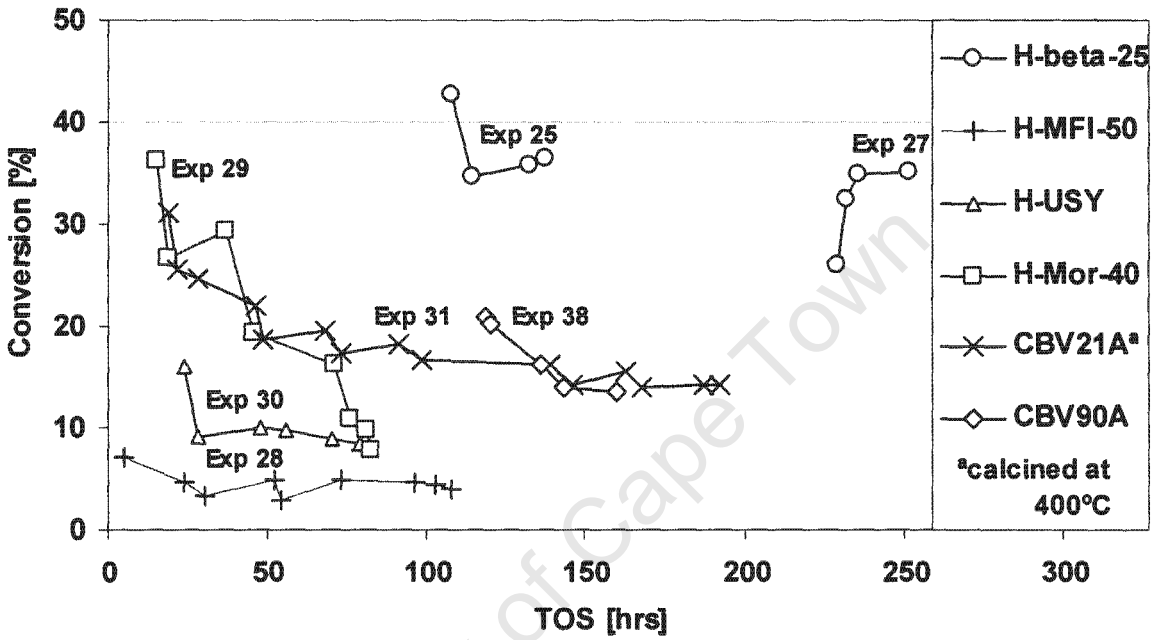

Figure 5-29: DPE conversion from DPE methylation over zeolites tested at the screening conditions of Table 5-2 (except MFR=3.2 for H-MFI-50 and H-Mor-40)

In the case of H-beta-25 and CBV90A zeolites, screening experiments at standard conditions were preceded and interrupted by other experiments over the same load of catalysts and that is why the data for these two zeolites does not start within the first 24 hours of time-on-stream. For all other zeolites, screening experiments commenced on a fresh load of catalyst.

Most catalysts started at high initial activity and reached a form of steady activity level, except for H-MFI-50, which seemed to maintain more or less the same level of activity.

5.5.4 Catalyst lifetime

All the catalysts, except H-Mor-40, reached a form of steady state activity within 50 to 100 hours on stream (see conversion plots from screening tests in Figure 5-29). H-Mor-40 seemed to deactivate rapidly with time-on-stream, not approaching a steady state level. Therefore a very short lifetime can be expected, for H-Mor-40, in comparison to the other catalysts.

Zeolites H-beta-25 and CBV90A proved to have long lifetimes in introductory and optimisation experiments, respectively. H-beta-25 exhibited no significant deactivation over a period of 900 hours on stream (see Figure 5-1). Note the stable operation for repeat experiments in Figure 5-1 (the experiment between 230 and 300 hours on stream and its repeat between 700 and 800 hours on stream) and in Figure 5-5 (Experiment 25 and Experiment 27). CBV90A lost activity by about 3% points of conversion from 12% to 9% (steady state averages) between 250 and 600 hours on stream (see Figure 5-38), i.e. over a period of 350 hours. CBV90A on the other hand takes long to reach a steady state conversion.

5.6 EFFECT OF REACTION TEMPERATURE (CBV21A)

Catalyst CBV21A was also tested at a temperature of 300°C, with all other variables at the standard screening conditions of Table 5-2. Results are shown in Figure 5-30 to Figure 5-33.

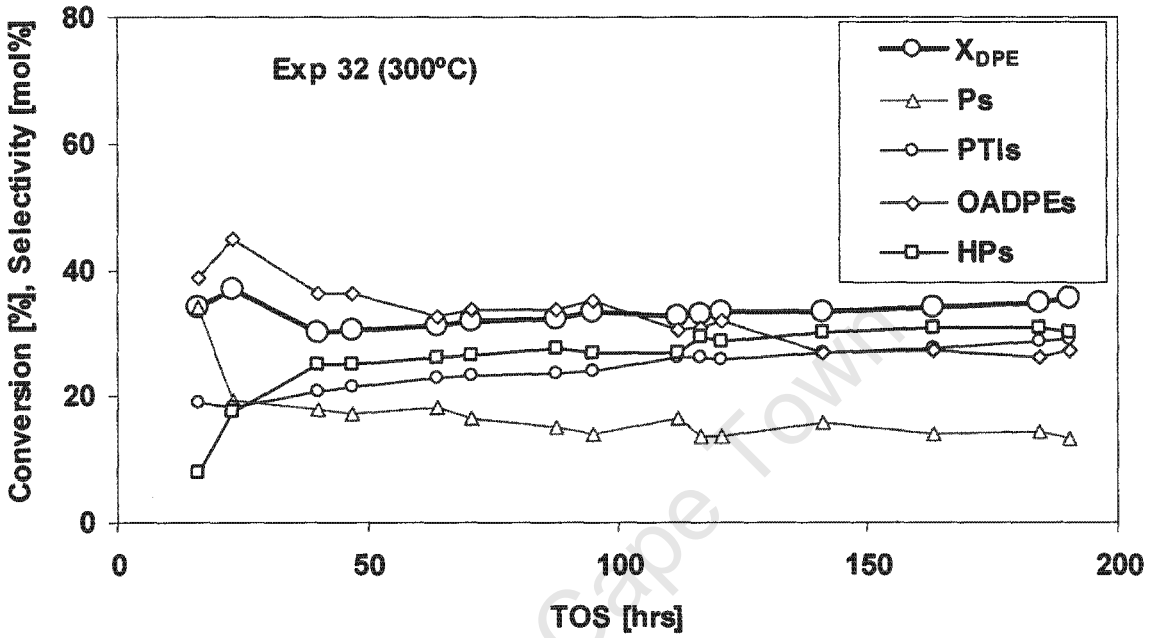

Figure 5-30: DPE conversion and selectivity of the product families from DPE methylation over CBV21A (L2), calcined at 400°C, tested at standard conditions of Table 5-2, except at higher reaction temperature of 300°C

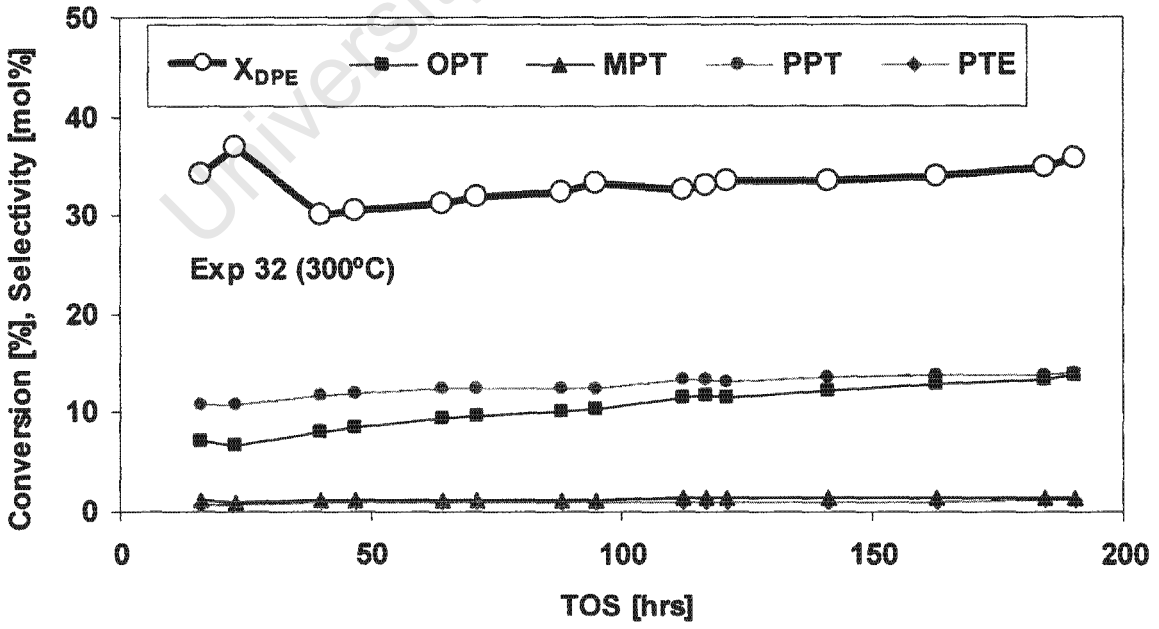

Figure 5-31: DPE conversion and selectivity of important products from DPE methylation over CBV21A (L2), calcined at 400°C, tested at 300°C

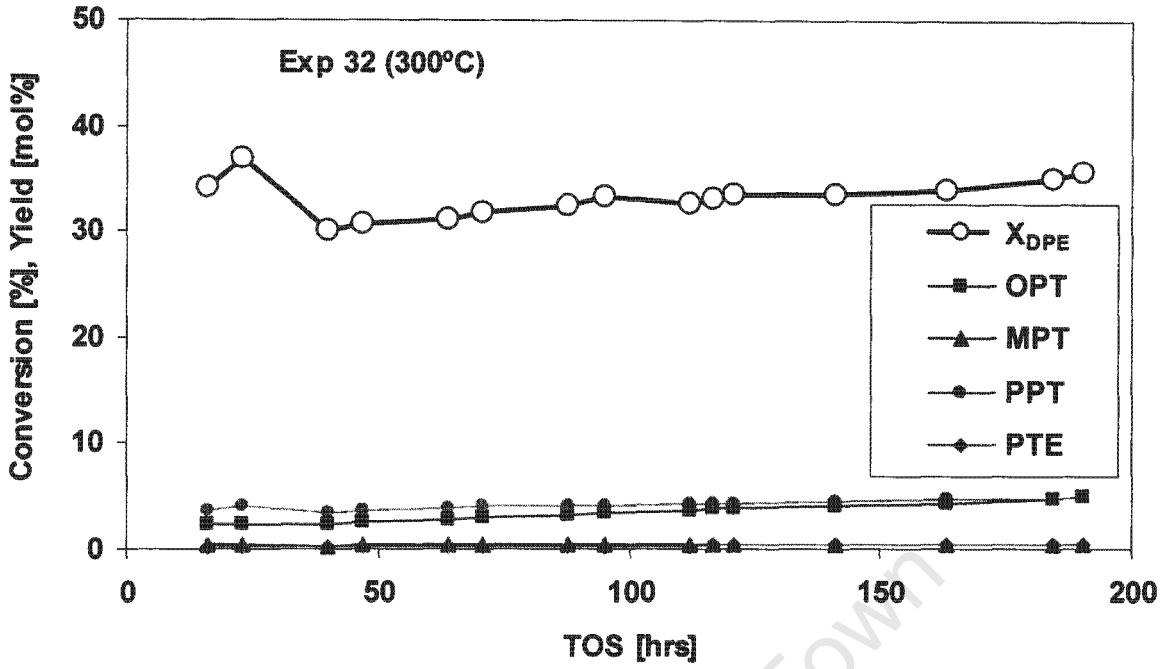

Figure 5-32: DPE conversion and yields of important products from DPE methylation over CBV21A (L1), calcined at 400°C, tested at standard conditions of Table 5-2 except at higher reaction temperature of 300°C

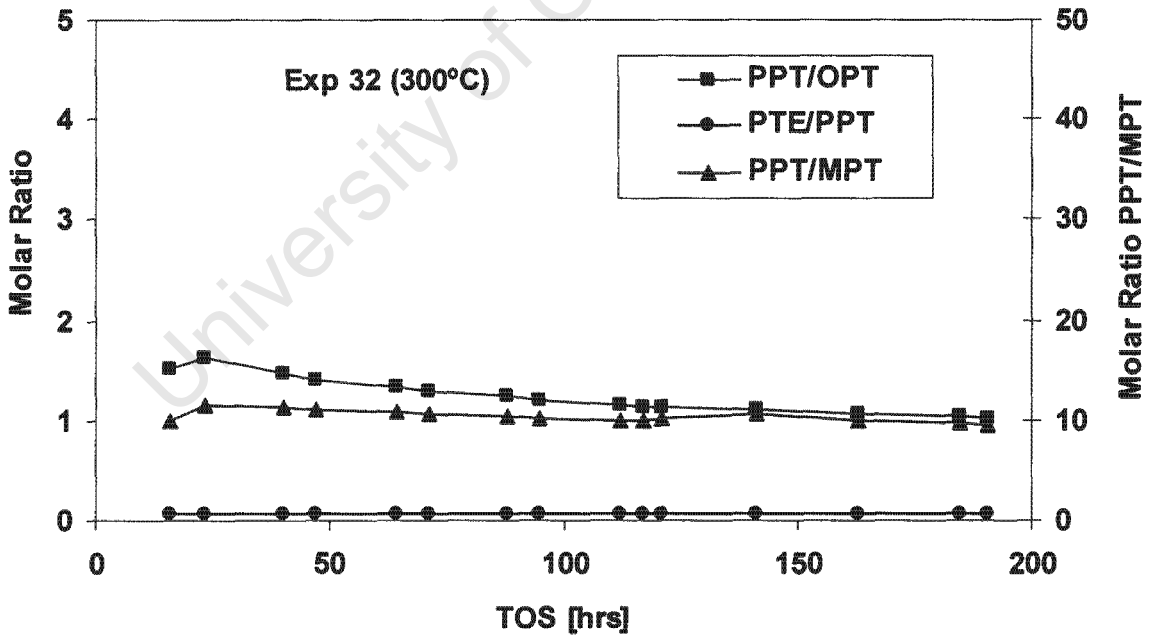

Figure 5-33: Ratios of the mono-methylated and the ratio of the di- to the mono-*para* methylated products from DPE methylation over CBV21A (L1), calcined at 400°C, tested at conditions of Table 5-2, except at higher temperature of 300°C

Conversion over CBV21A (calcined at 400°C) at 300°C was double as high as that obtained at standard screening conditions (250°C) over the same catalyst (see Figure 5-17 and Figure 5-30). At higher temperature, catalyst activity appears to be more stable, even slightly increasing with time-on-stream. However, the major products at higher temperature and conversion are heavier compounds, namely OADPEs and consequently, no befit is obtained in yields of the desired products, PTIs, PPT in particular (see Figure 5-19 and Figure 5-32). Selectivity to the *para*-isomer is initially higher than that for the *ortho*-isomer, but as reaction approaches steady state, the *ortho*-isomer approaches the *para*-isomer in selectivity (see Figure 5-31). This is different from low temperature operation (see Figure 5-18), where *p*-selectivity was always significantly higher.

The *para* to *meta* ratio decreased at higher temperature, to less than half the ratio at 250°C (see Figure 5-27 and Figure 5-33).

Data reflecting reaction temperature effects is given in Table 5-3. The effects of increasing reaction temperature can be summarised as follows:

- A significant increase in conversion
- Decreasing selectivity to phenoxy toluenes, PTIs
- Decreasing selectivity to the heavy products, HPs
- Increasing selectivity to the other alkylated diphenyl ethers, OADPEs
- Selectivity for the light products, Ps, decreases for the 400°C calcination temperature, but increases on a low level for the 500°C calcination temperature.
- Ratios of PPT/OPT and PPT/MPT decline with increasing reaction temperature

The higher conversion may have contributed to reaction temperature effects on selectivity.

5.7 EFFECT OF CALCINATION TEMPERATURE (CBV21A)

Mordenite based CBV21A catalyst was delivered with the zeolite in ammonium form (NH_4-Mor). It was therefore necessary to activate the zeolite by calcination under nitrogen flow (see Section 4.3.2 and Table 4-3).

Calcination was carried out at two different temperatures, 400 and 500°C, prior to conversion experiments (see Table 4-3). The results of Figure 5-17 to Figure 5-19 and Figure 5-27, as well as Figure 5-30 to Figure 5-33 are from DPE methylation over CBV21A calcined at 400°C, whereas those of Figure 5-34 to Figure 5-37 are from DPE methylation over CBV21A calcined at 500°C.

Experiment 31 and Experiment 32 were conducted over CBV21A, which was calcined at 400°C, at reaction temperatures of 250°C and 300°C and all other variables the same as those in Table 5-2. Each of these experiments (31 and 32) was carried out over fresh catalyst loads of their own.

Temperature variation experiments from calcination temperature of 500°C were carried out at 300, 275 and 250°C, on the same load of catalyst, with all other variables at standard conditions of Table 5-2. See Table 5-3 for comparison of the reaction and calcination temperature effects.

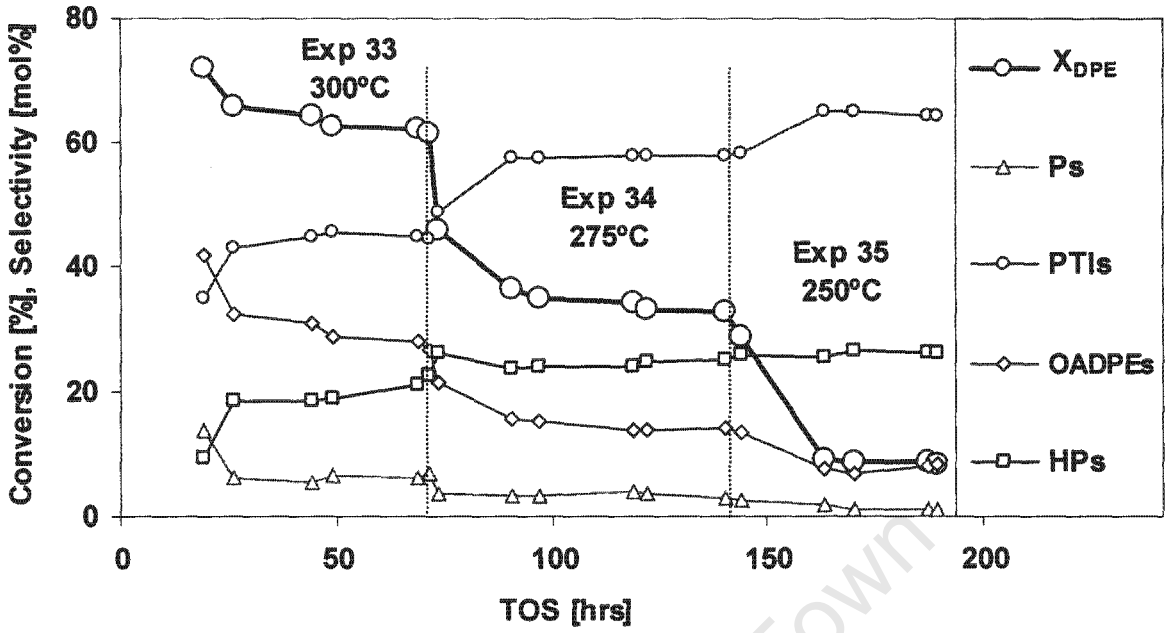

Figure 5-34: DPE conversion and selectivity of the product families from DPE methylation over CBV21A (L3), calcined at 500°C, tested at standard screening conditions of Table 5-2, except for reaction temperature

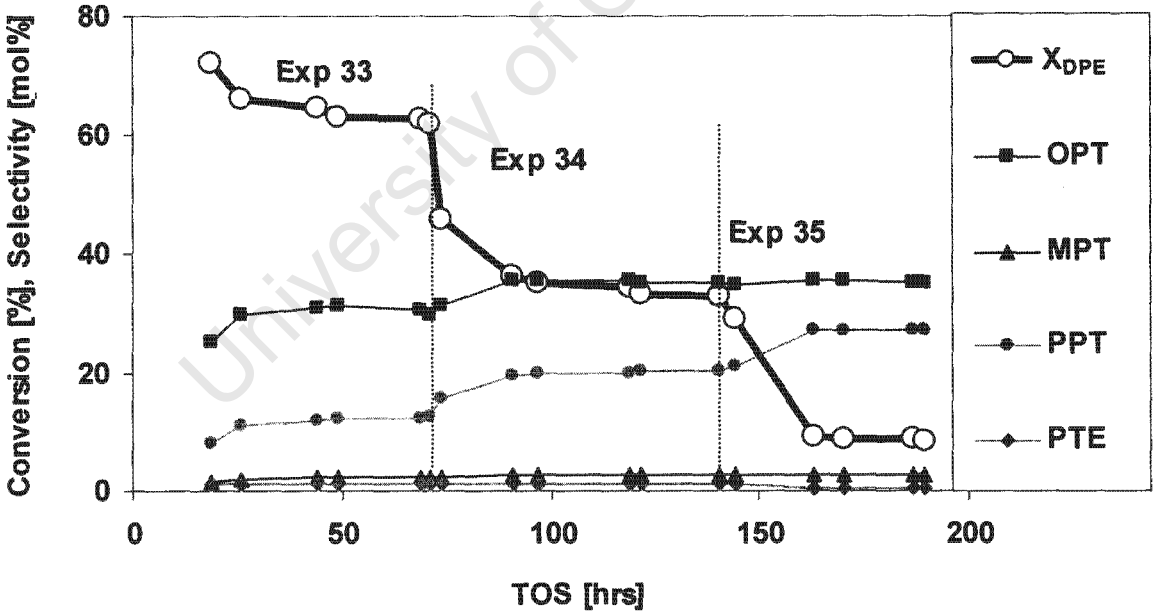

Figure 5-35: DPE conversion and selectivity of important products from DPE methylation over CBV21A (L3), calcined at 500°C, tested at standard screening conditions of Table 5-2, except for reaction temperature

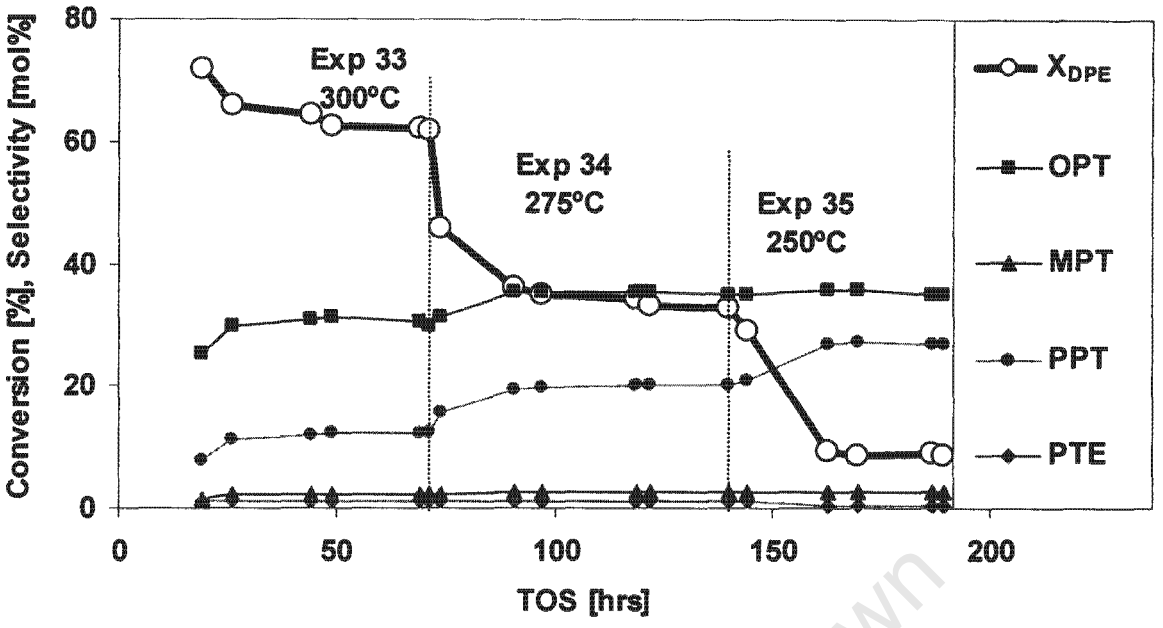

Figure 5-36: DPE conversion and yields of important products from DPE methylation over CBV21A (L3), calcined at 500°C, tested at standard screening conditions of Table 5-2, except for reaction temperature

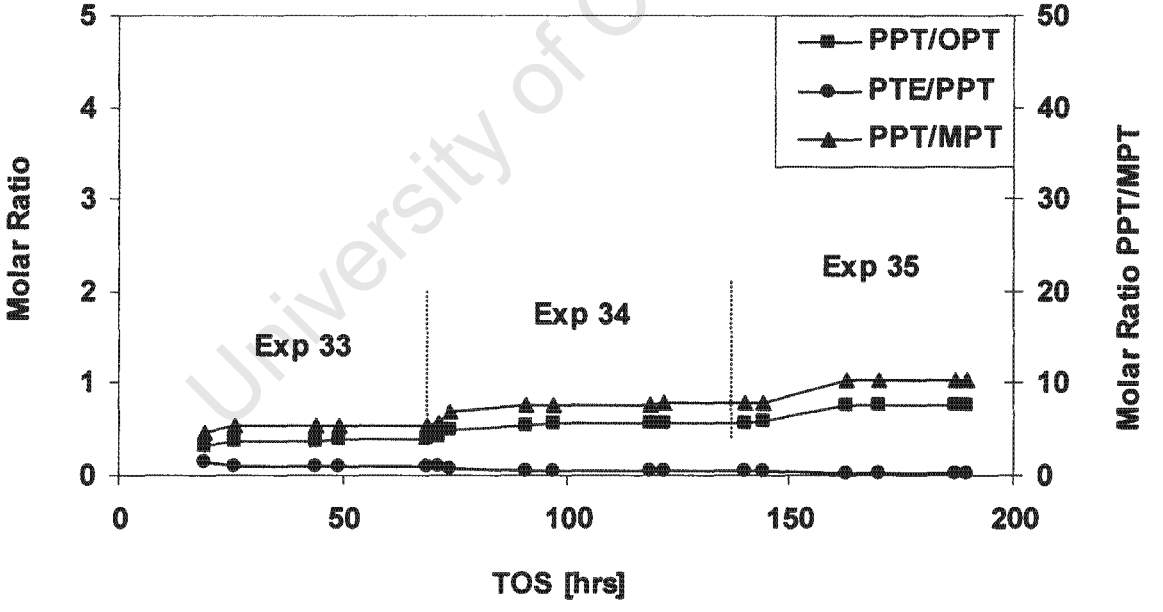

Figure 5-37: Ratios of the mono-methylated and ratio of the di- to the mono-*para*-methylated products from DPE methylation over CBV21A (L3), calcined at 500°C

The effects of calcination temperature of CBV21A, 400 and 500°C, each tested at two different temperatures, are summarised in Table 5-3.

Table 5-3: Summary of calcination and reaction temperature effects over CBV21A (steady state average data is given in Appendix IX.1,)

	$T_{calcination}$ = 400°C		$T_{calcination}$ = 500°C	
$T_{reaction}$	250°C	300°C	250°C	300°C
DPE conversion [%]	15	34	8	60
S_{Ps} [mol%]	20	14	1	6
S_{PTIs} [mol%]	23	27	65	45
S_{OADPEs} [mol%]	9	28	8	28
S_{HPs} [mol%]	47	30	26	20
S_{PPT} [mol%]	16	14	27	12.3
S_{MPT} [mol%]	0.5	1.4	2.6	2.2
S_{PTE} [mol%]	1.5	1	0.4	1.2
Y_{PPT} [mol%]	2.4	4.8	2.2	7.4
$\frac{PPT}{OPT}$	2	1	0.8	0.4
$\frac{PPT}{MPT}$	30	10	10	5

The effects of increased calcination temperature are as follows:

- Conversion increased, reaching 60% at the highest reaction temperature applied, but was lower for lower reaction temperature.
- Selectivity to PTIs, the mono-methylated products, increased significantly.
- Selectivity to the para-isomer, PPT, decreased while its yield was slightly higher due to the much higher conversion.
- Selectivity to the other alkylated diphenyl ethers, OADPEs, was not affected by calcination temperature.
- Selectivity to the phenols, Ps, dropped significantly.
- Selectivity to the heavy products, HPs, also declined.
- MPT selectivity was higher at all reaction temperatures, for the high calcination temperature case.

- Monomethylated isomer ratios changed significantly, with PPT/MPT ratio declining and PPT/OPT ratio even reversing to values <1.

It is also important to note that different conversion, particularly at the highest reaction temperature applied, may affect calcination temperature effects on selectivity.

5.8 SELECTION OF THE CATALYST OF CHOICE

Table 5-4 shows a summary of DPE conversion, as well as selectivities and molar ratios of phenoxy toluene isomers (PTIs), for the tested zeolites obtained at standard screening conditions of Table 5-2.

Based on Table 5-4 data, the following can be stated :

- Taking *p*-phenoxy toluene (PPT), the target product, selectivity as a criterion, the catalysts are ranked as follows:
  $CBV21A_{500°C}$ > H-beta-25 > H-USY > CBV90A > $CBV21A_{400°C}$ ≈ H-Mor-40 > H-MFI-50
  (subscripts next to CBV21A refer to the calcination temperature)

- Considering only the PTI fraction, the order of catalysts according to selectivity towards *para*-monoalkylation is the following:
  H-Mor-40 > CBV90A > $CBV21A_{400°C}$ > H-MFI-50 > $CBV21A_{500°C}$ > H-beta-25 > H-USY
  (subscripts next to CBV21A refer to the calcination temperature)

- With regard to the p-phenoxy toluene to m-phenoxy toluene ratio (PPT/MPT), the order is as follows:
  H-Mor-40 > CBV90A > $CBV21A_{400°C}$ >> $CBV21A_{500°C}$ > H-beta-25 ≈ H-MFI-50 > H-USY
  (subscripts next to CBV21A refer to the calcination temperature)

Table 5-4: Summary of steady state average conversions and selected steady state average selectivities and product ratios from DPE methylation reaction over the catalysts screened at standard conditions of Table 5-2 (based on Figure 5-5 to Figure 5-28, see data in Appendix IX.1)

Catalyst	Exp.	X_{DPE} [%]	S_{PTIs} [mol%]	S_{Ps} [mol%]	S_{OADPEs} [mol%]	S_{HPs} [mol%]	S_{PPT} [mol%]	S_{PTE} [mol%]	S_{OPT} [mol%]	S_{MPT} [mol%]	PPT/OPT	PTE/PPT	PPT/MPT
H-beta-25	27	35	75	8	16	1	24	1.2	48	2.5	0.5	0.1	9
H-MFI-50	28	4.5	18	67	4	11	11	0	5.4	1.2	2.1	0	9
H-USY	30	9	58	37	4	1	20	0.1	34	2.8	0.6	0.01	7
H-Mor-40	29	—[c]	18	32	9	41	16	2.2	2.2	0.2	7.4	0.05	94
$CBV21A^{a}_{400°C}$	31	15	23	21	9	47	16	1.5	7.1	0.5	2.2	0.1	29
$CBV21A^{b}_{500°C}$	35	9	65	1	8	26	27	0	35	3	0.8	0	10
CBV90A	38	13.4	22	19	22	37	18	2.3	3.9	0.3	4.5	0.1	53

[a] Calcined at 400°C

[b] Calcined at 500°C

[c] No steady state conversion achieved. Selectivities are averaged over data points at the end of the experiment.

- Conversion was low to moderate for all the catalysts tested except H-beta-25 that reached 35% at steady state. The order of catalysts according to activity, i.e. steady state conversion of diphenyl ether, X_{DPE}, is as follows:
  H-beta-25 >> CBV21A$_{400°C}$ ≈ CBV90A > CBV21A$_{500°C}$ ≈ H-USY > H-MFI-50 > H-Mor-40
  (subscripts next to CBV21A refer to the calcination temperature)

H-Mor-40 showed a constant rapid loss of activity. No steady state was achieved.

The highest *para*-to-*ortho* ratios (PPT/OPT) were obtained over the three mordenite-based catalysts, particularly over CBV90A. This catalyst also gave desired high *para*-to-*meta* ratio and had a high di-*para*-methylated-to-mono-*para*-methylated product ratio (PTE/PPT). Conversion and selectivity to the targeted product, PPT, were medium.

The other type of shape selective zeolite, H-MFI-50 also produced a high PPT/OPT ratio but at very low PPT/MPT ratio, low selectivity to PTIs as such and very low conversion (see Figure 5-8 and Figure 5-24).
Zeolite H-beta-25 had the highest conversion and high selectivity to *para*-methylated products (see Table 5-4), and also had the highest selectivity (75%) towards the total phenoxy toluene isomers (PTIs). However, the ratios of the *para*-to-*ortho* and *para*-to-*meta* methylated isomers, PPT/OPT and PPT/MPT, were comparably poor.

The above implies that CBV90A demonstrated shape selectivity and based on the screening criterion of conversion and *p*-selectivity, it was outstanding among the other three shape selective zeolites, which are CBV21A, H-Mor-40 and H-ZSM-50.

Therefore, Zeolyst mordenite CBV90A was selected as the preferred catalyst for DPE methylation.

5.9 OPTIMISATION OF PROCESS VARIABLES

Using the catalyst of choice, mordenite based CBV90A, a series of experiments were carried out in order to optimise reaction conditions. Results are shown from Figure 5-38 to Figure 5-41.

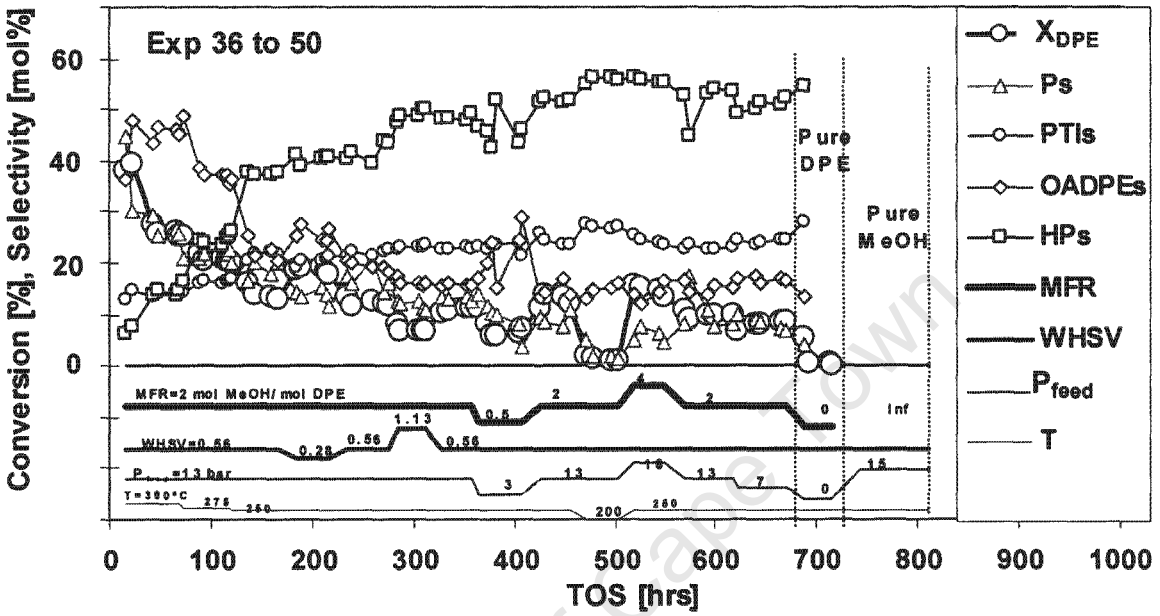

Figure 5-38: DPE conversion and selectivity of the product families from DPE methylation over CBV90 (L1) at various reaction conditions

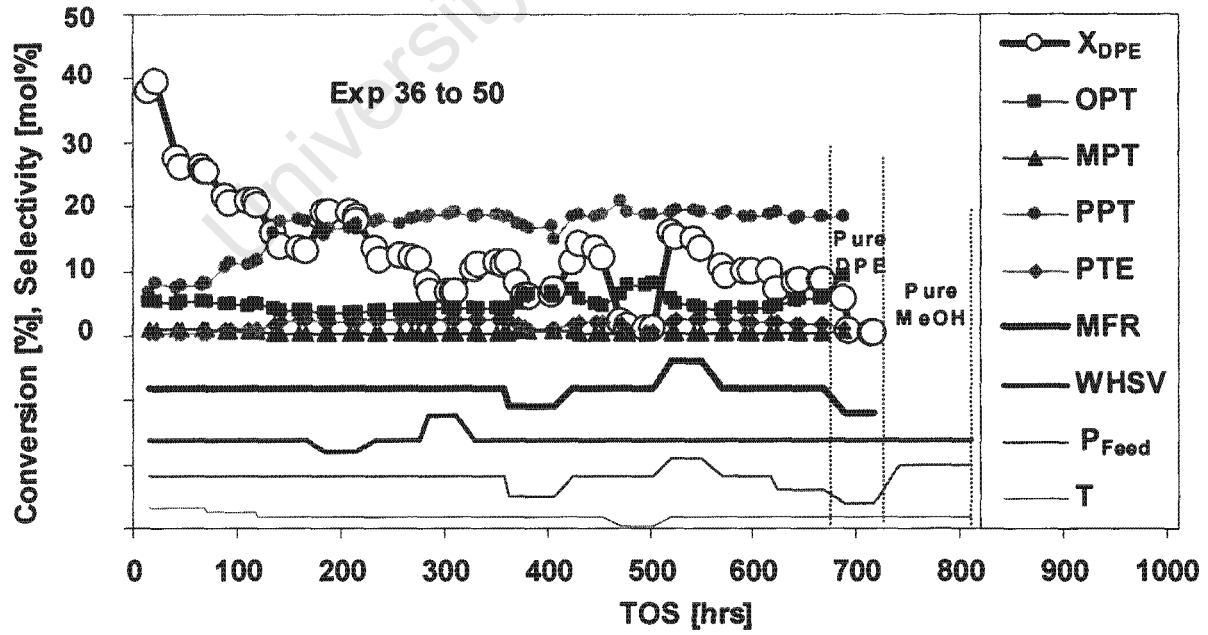

Figure 5-39: DPE conversion and selectivity of important products from DPE methylation over CBV90A (L1) at various reaction conditions

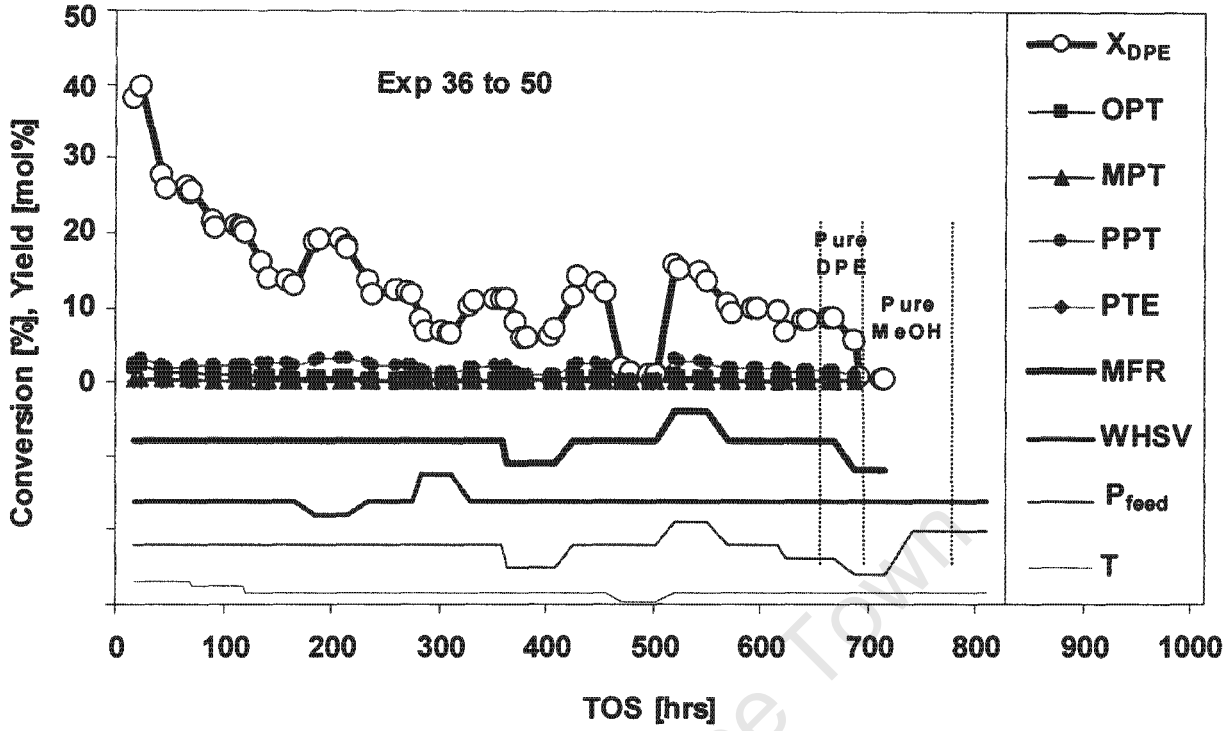

Figure 5-40: DPE conversion and yields of important products from DPE methylation over CBV90A (L1) at various reaction conditions

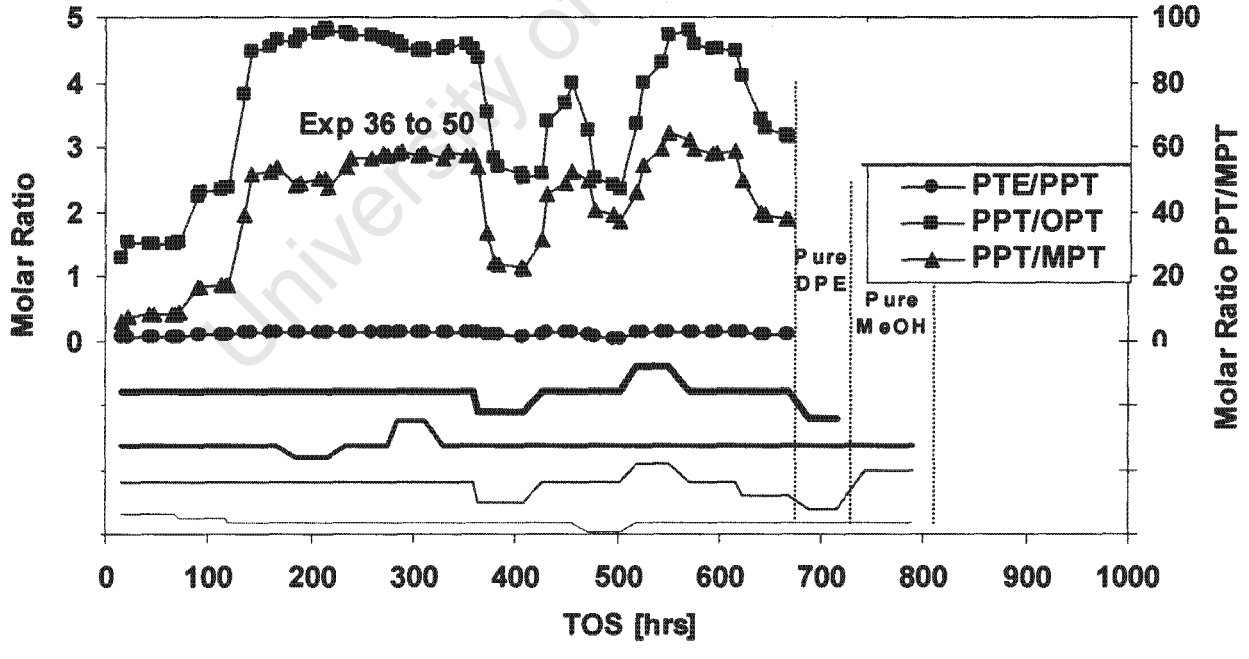

Figure 5-41: Ratios of the mono-methylated and the ratio of di- to the mono-*para*-methylated products from DPE methylation over CBV90A (L1) at various conditions

Note that the last experiments were carried out using pure DPE and pure methanol, respectively, as feeds.

The same criteria as in catalyst screening (see Section 5.8) were applied for reaction conditions optimisation.

Maximum PPT/OPT and PPT/MPT ratios of about 5 and 55, respectively, could be achieved through optimisation process over CBV90A, see Figure 5-41. This comes together with high selectivity to PPT over the entire range of conditions tested, except when the reaction temperature was >250°C, see Figure 5-39. The yields were more or less following conversions, see Figure 5-40.

Ratios of PTE/PPT were very low, <0.2, particularly at low conversion and high temperature (see Figure 5-41).

After a significant increase with declining reaction temperature (during the first 150 hours on stream), selectivity of total phenoxy toluene isomers (PTIs), like p-phenoxy toluene (PPT), remained almost constant and independent of other process variables (except temperature), see Figure 5-38 and Figure 5-39. The significant variations in product ratios (Figure 5-41) are mostly a result of changes in selectivities of ortho- and meta-phenoxy toluene, i.e. OPPT and MPT.

Other alkylated diphenyl ethers, OADPEs, on the other hand had the highest selectivity during the high initial temperature (300°C) and activity phase of the catalyst. Selectivity of the HPs settled out at a low value whereas that of the OADPEs increased at low space velocity and surprisingly, also at low MFR.

Selectivity to the heavy products (HPs) rose from low values at high temperature (300°C) and increased to its highest values at a temperature of 200°C. It was always the highest at temperatures ≤ 250°C and settled out at about 50%, after 400 hours of time-on-stream. This selectivity seemed to have increased slightly at high space velocity and decreased at low MFR. In the absence of either one of the feed components, i.e. methanol or DPE, selectivity of the HPs drops immediately.

Light products (Ps) declined from high selectivity at initially high reaction temperature and catalyst activity and then settled at low values, following the trend in the conversion of DPE.

Low temperature of 200°C resulted in low conversion, with significant change in the product selectivities.

At the end of the optimisation series of experiments, two other experiments were carried out, one with pure DPE as the feed (Experiment 49) and another one with pure MeOH as the feed (Experiment 50). With pure DPE, conversion dropped immediately to <0.5%, the only product (in traces) being phenol, probably due to DPE hydrolysis with moisture in the feed. With methanol as the feed, traces of light hydrocarbons were formed.

5.10 REPRODUCIBILITY

Reproducibility experiments were conducted only over H-beta-25 and CBV90A catalysts. Experiments 25 and 27 were both carried out at standard screening conditions, over the same load (L4) of H-beta-25 catalyst (see Figure 5-5 to Figure 5-7 and Figure 5-23).

Experiments repeated at standard screening conditions over the single load of CBV90A (L1) confirmed reproducibility as well (Figure 5-38 to Figure 5-41, Experiments 38, 40, 42, 44 and 47, at 140-160, 240-280, 330-350, 410-450 and 570-610 hours on stream, respectively). Selectivities and conversion changed slightly due to slow deactivation of the catalyst.

Data for experiments at standard conditions only are shown in Figure 5-42 and Figure 5-43, to illustrate the above.

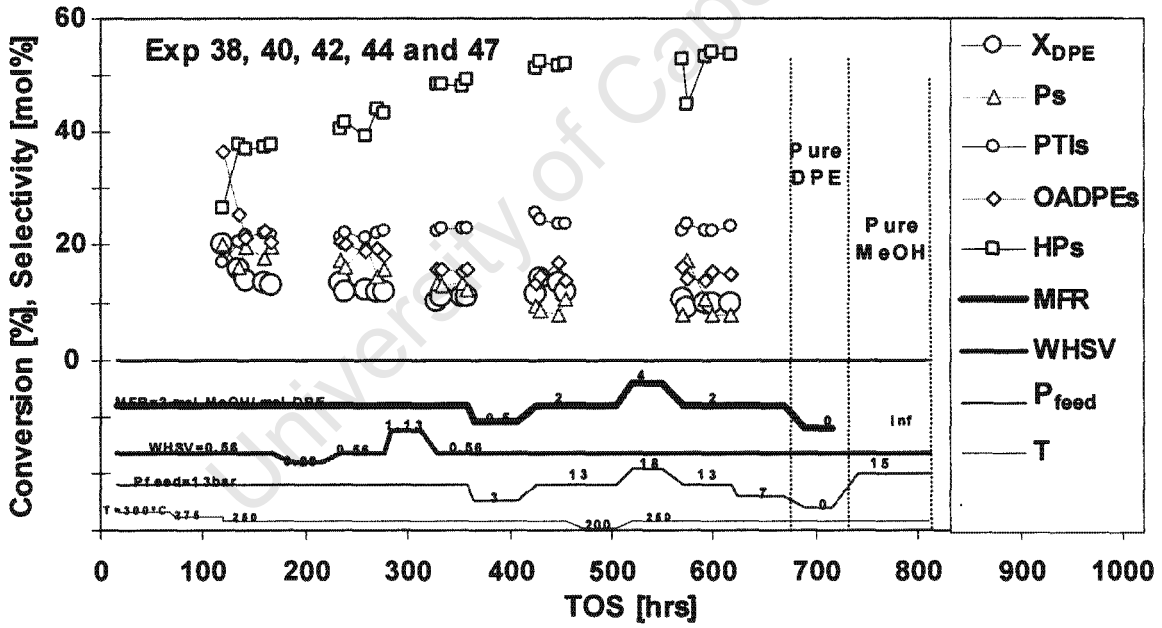

Figure 5-42: DPE conversion and selectivity of the product families from DPE methylation over CBV90 (L1). Selected data points obtained from repeat experiments at the standard screening conditions of Table 5-2

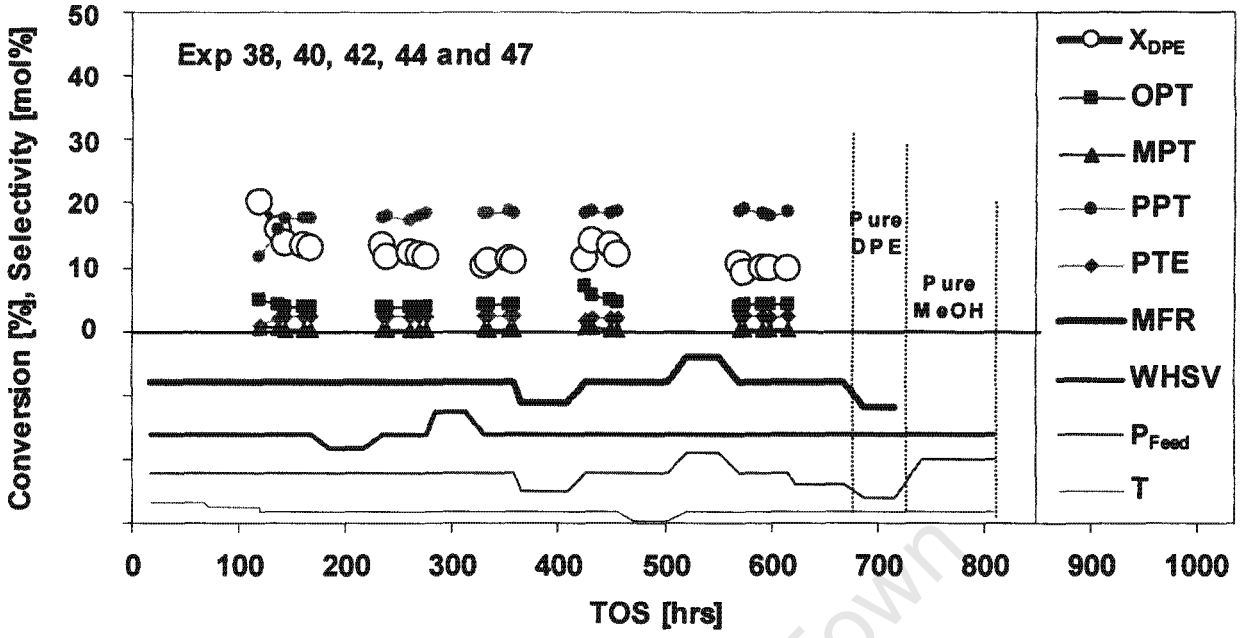

Figure 5-43: DPE conversion and selectivity of important products from DPE methylation over CBV90A (L1). Selected data points obtained from repeat experiments at the standard screening conditions of Table 5-2

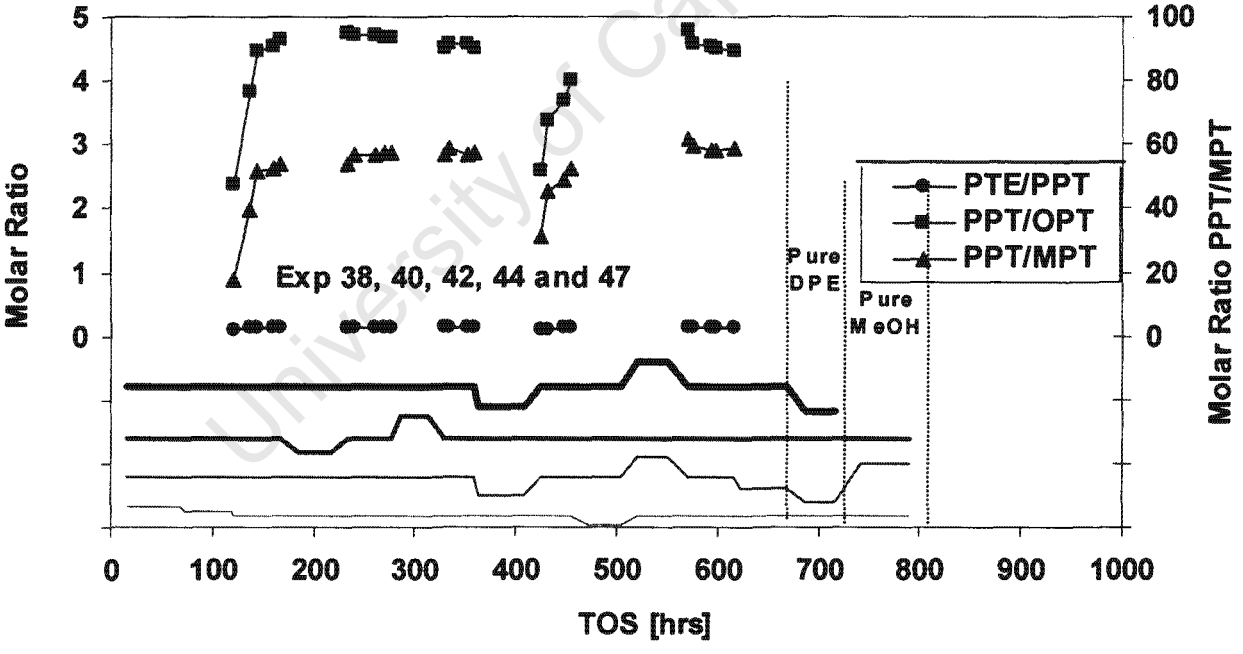

Figure 5-44: Ratios of the mono-methylated the ratio of di- and mono-*para*-methylated products from DPE methylation over CBV90A (L1). Selected data points obtained from repeat experiments at the standard screening conditions of Table 5-2

5.11 RESULTS FROM THERMODYNAMIC EQUILIBRIUM CALCULATIONS

Synthetic route to p-cresol from phenol, via DPE, is a three-stage process according to the following sequence of reactions (shown in Figure 1-3 and Figure 1-4) :

1. Phenol condensation to diphenyl ether (DPE)
2.a Methylation of DPE to p-phenoxy toluene (PPT)
2.b Methylation of PPT to p-tolyl ether (PTE)
3. Cleavage of p-tolyl ether to p-cresol

Estimation of thermodynamic properties was carried out using the various methods described in Section 2.3.1. Water was considered as described in Section 2.3.2, and the Gibbs free energy was calculated according to Equation 2-12, Section 2.3, as follows:

$$\Delta G_{rxn}(T) = \sum \nu_i \Delta G_i(T) \qquad \text{Equation 2-12}$$

Estimations obtained from quantum mechanics, using molecular modelling techniques, are given in Appendix VII, Figure A.6.

5.11.1 Phenol condensation

The gas phase equilibrium curves of phenol condensation to diphenyl ether and water

$$2\ PhOH \rightleftharpoons DPE + H_2O$$

are based on stoichiometry shown in Table 5-5.

Table 5-5: Compound table for phenol condensation to DPE and water

Compound	Initial moles	Moles at equilibrium	Mole fraction
Phenol	2	$2(1-X_{eq})$	$1-X_{eq}$
Water	0	X_{eq}	$X_{eq}/2$
DPE	0	X_{eq}	$X_{eq}/2$
Σ	2	2	1

The equilibrium constant for this condensation reaction based on compound Table 5-5, is given by Equation 2-9.

$$K_1 = \left(\frac{X_{eq}}{2(1-X_{eq})} \right)^2$$

Equation 5-1

$$K_1 = e^{-\frac{\Delta G_{rxn1}}{RT}}$$

Table 5-6 gives the calculated thermodynamic properties and the equilibrium conversion of phenol condensation to diphenyl ether and water, at normal conditions, calculated from literature data as well as using various estimate methods.

Table 5-6: Predicted gas phase equilibrium conversion for phenol condensation to diphenyl ether and water at normal conditions, 298 K, ΔG_f° and ΔH_f° in kJ/mol, see Appendix I.1

	2*PhOH[a]	⟶	DPE	+	H_2O[b]	ΔH°_{rxn}	ΔG°_{rxn}	K°_{rxn}	X°_{eq}
$\Delta Gf^\circ_{,Ideal\ gas}$	-65.82		175		-228.8		12.05	0.01	0.15
$\Delta Hf^\circ_{,Ideal\ gas}$	-193.94		49.99		-242.0	1.93			
$\Delta Gf^\circ_{,Joback}$	-65.88		169.98		-228.8		7.09	0.057	0.32
$\Delta Hf^\circ_{,Joback}$	-192.96		49.83		-242.0	0.79			
$\Delta Gf^\circ_{,vKV}$	-90.66		156.6		-228.6		18.65	0.001	0.04
$\Delta Gf^\circ_{,Ben}$	-59.18		165.00		-228.8		-4.59	6	0.83
$\Delta Hf^\circ_{,Ben}$	-186.7		42.32		-242.0	-12.98			

[a] Stoichiometric values (i.e. 2 PhOH)

[b] Literature data (experimental), except van Krevelen and Chermin

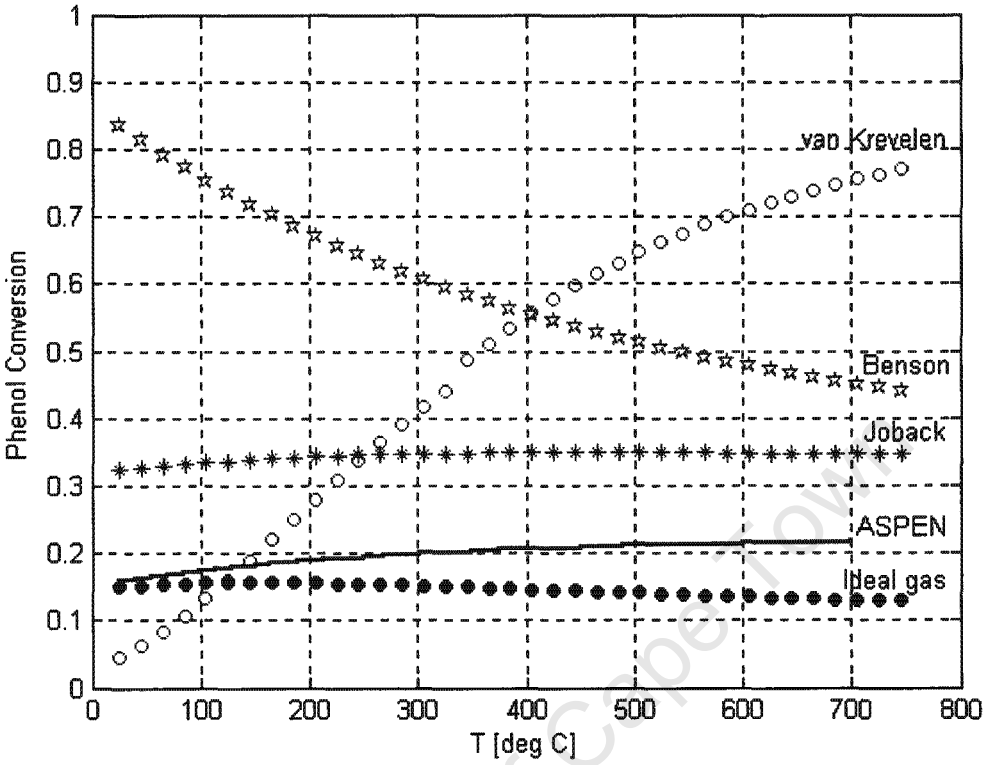

Figure 5-45: Predicted gas phase equilibrium conversion of phenol to diphenyl ether and water

Thermodynamic equilibrium curves vs temperature for reaction in which phenol is condensed to diphenyl ether is shown in Figure 5-45. The curve labelled "Ideal Gas" in Figure 5-45 is partially based on literature data (see Appendix I). This curve appears to go through a maximum, a very unusual phenomenon for equilibrium curves.

ASPEN curve and Ideal gas curve are both based on the same data, from literature (see Appendix I.1), except that the ASPEN calculation takes fugacity coefficients into account, which improves the curvature of the equilibrium curve. ASPEN suggests a slightly endothermic reaction and a slight increase in equilibrium conversion with increasing temperature.

Joback's method predicts a curve that rises slightly, flattening out as temperature increases. This curve, together with the ideal gas one, as well as the ASPEN curve suggests that the equilibrium

conversion is low and that the extent of the reaction is weakly affected by the reaction temperature.

Benson's method shows a steady drop of equilibrium conversion with increasing temperature, hence an exothermic reaction.

The method by van Krevelen and Chermin predicts the reaction to be endothermic, with equilibrium conversion rising with increasing temperature.

Generally, van Krevelen's is considered to be the most inaccurate of the above mentioned property methods whereas Benson's is generally considered to be the most accurate (see Section 2.3.1). Benson's method suggests that the condensation is exothermic, whereas van Krevelen and Chermin's method suggests an endothermic reaction whilst "Ideal Gas" and "ASPEN" curves together with the curve from Joback's method predict close to thermo-neutrality for this reaction.

It is not clear at this stage, as to which of these methods has the best accuracy in terms of equilibrium conversion and what the real trends are. However, all the methods suggest that phenol condensation in the temperature range of interest, 200 to 300°C, is possible but equilibrium limited, far below 100% conversion.

5.11.2 Methylation of diphenyl ether

Equilibrium conversion in the reaction, methylation of diphenyl ether to *p*-phenoxy toluene and water was calculated from various thermodynamic estimate methods.

The equilibrium conversion at normal conditions calculated from these methods is given in Table 5-8. Methanol side reaction to dimethyl ether was ignored. In a study conducted on phenol methylation using methanol (Landau et al., 1997), this side reaction was found to be negligible (see Section 2.1.14).

The compound table for methylation of diphenyl ether to *p*-phenoxy toluene and water is shown in Table 5-7.

Table 5-7: Compound table for methylation of DPE with methanol to *p*-phenoxy toluene and water

Compound	Initial moles	Moles at equilibrium	Mole fraction
DPE	1	$1- X_{eq}$	$(1- X_{eq})/2$
Methanol	1	$1- X_{eq}$	$(1- X_{eq})/2$
Water	0	X_{eq}	$X_{eq}/2$
PPT	0	X_{eq}	$X_{eq}/2$
Σ	2	2	1

The equilibrium constant for the first methylation step, based on compound Table 5-7, is given by Equatio 5-2.

$$K_2 = \frac{X_{eq}^2}{(1-X_{eq})^2}$$

Equation 5-2

$$K_2 = e^{-\frac{\Delta G_{rxn\,2}}{RT}}$$

Table 5-8: Predicted gas phase equilibrium for methylation of diphenyl ether (DPE) at normal conditions, 298 K, ΔG_f° and ΔH_f° in kJ/mol, see Appendix I.1

	DPE	+	MeOH	→	PPT	+	H_2O[a]	ΔH°_{rxn}	ΔG°_{rxn}	K°_{rxn}	X°_{eq}
$\Delta Gf^\circ_{,Joback}$	170.0		-179.3		168.8		-228.8		-51	8.E+08	1
$\Delta Hf^\circ_{,Joback}$	49.8		-216.2		17.7		-242.0	-57.91			
$\Delta Gf^\circ_{,vKV}$	156.6		-176.1		150.2		-228.6		-59	2.E+10	1
$\Delta Gf^\circ_{,Ben}$	165.0		-162.5		158.1		-228.8		-73	7.E+12	1
$\Delta Hf^\circ_{,Ben}$	42.3		-201.0		10.7		-242.0	-72.68			

[a] Literature data (experimental), except van Krevelen and Chermin

Equilibrium conversion as a function of temperature for DPE methylation to p-phenoxy toluene and water, using different thermodynamic estimate methods is shown in Figure 5-46.

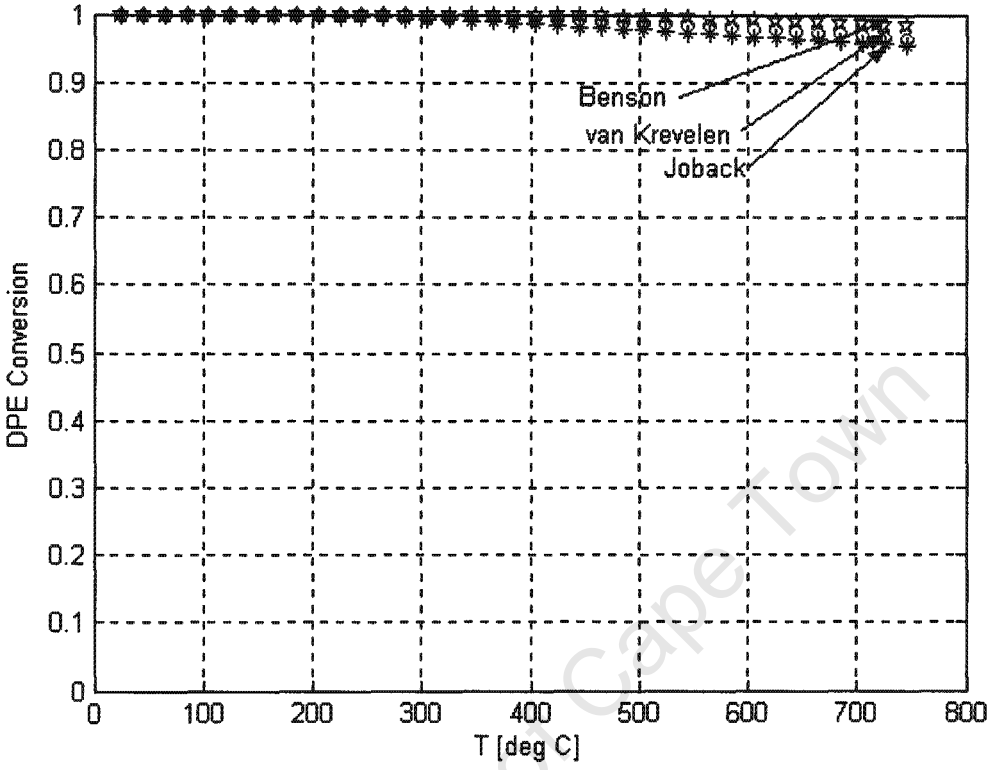

Figure 5-46: Equilibrium conversion for methylation of DPE with methanol to *p*-phenoxy toluene and water

All the estimate methods predict high equilibrium conversion for this reaction, over the temperature range of interest, which is 200 – 300°C.

5.11.3 Methylation of *p*-phenoxy toluene

Compound table for methylation of *p*-phenoxy toluene (PPT) with methanol to *p*-tolyl ether (PTE) and water (second methylation step of DPE) is given in Table 5-9.

Table 5-9: Compound table for methylation of *p*-phenoxy toluene with methanol to *p*-tolyl ether and water

Compound	Initial moles	Moles at equilibrium	Mole fraction
PPT	1	$1- X_{eq}$	$(1- X_{eq})/2$
Methanol	1	$1- X_{eq}$	$(1- X_{eq})/2$
Water	0	X_{eq}	$X_{eq}/2$
PTE	0	X_{eq}	$X_{eq}/2$
Σ	2	2	1

Equilibrium constant for the second methylation step is given by Equation 5-3.

$$K_3 = \frac{X_{eq}^2}{(1-X_{eq})^2}$$

Equation 5-3

$$K_3 = e^{-\frac{\Delta G_{rxn3}}{RT}}$$

Equilibrium conversion for methylation of *p*-phenoxy toluene (PPT) to *p*-tolyl ether (PTE) at normal conditions is tabulated for various thermodynamic estimate methods in Table 5-10.

Table 5-10: Predicted gas phase equilibrium for methylation of *p*-phenoxy toluene with methanol to *p*-tolyl ether and water at normal conditions, 298 K, ΔG_f° and ΔH_f° in kJ/mol, see Appendix I.1

	PPT	+	MeOH	⟶	PTE	+	H_2O[a]	ΔH°_{rxn}	ΔG°_{rxn}	K°_{rxn}	X°_{eq}
$\Delta Gf^\circ_{,Joback}$	168.77		-179.3		167.56		-228.8		-51	8.E+08	1
$\Delta Hf^\circ_{,Joback}$	17.72		-216.2		-14.39		-242.0	-57.91			
$\Delta Gf^\circ_{,vKV}$	150.2		-176.1		147.2		-228.6		-55	5.E+09	1
$\Delta Gf^\circ_{,Ben}$	158		-162.5		156.3		-228.8		-68	9.E+11	1
$\Delta Hf^\circ_{,Ben}$	10.67		-201.0		-22.3		-242.0	-73.98			

[a] Literature data (experimental), except van Krevelen and Chermin

Equilibrium conversion as a function of temperature for methylation of *p*-phenoxy toluene to *p*-tolyl ether and water is plotted in Figure 5-47, using different thermodynamic estimate methods.

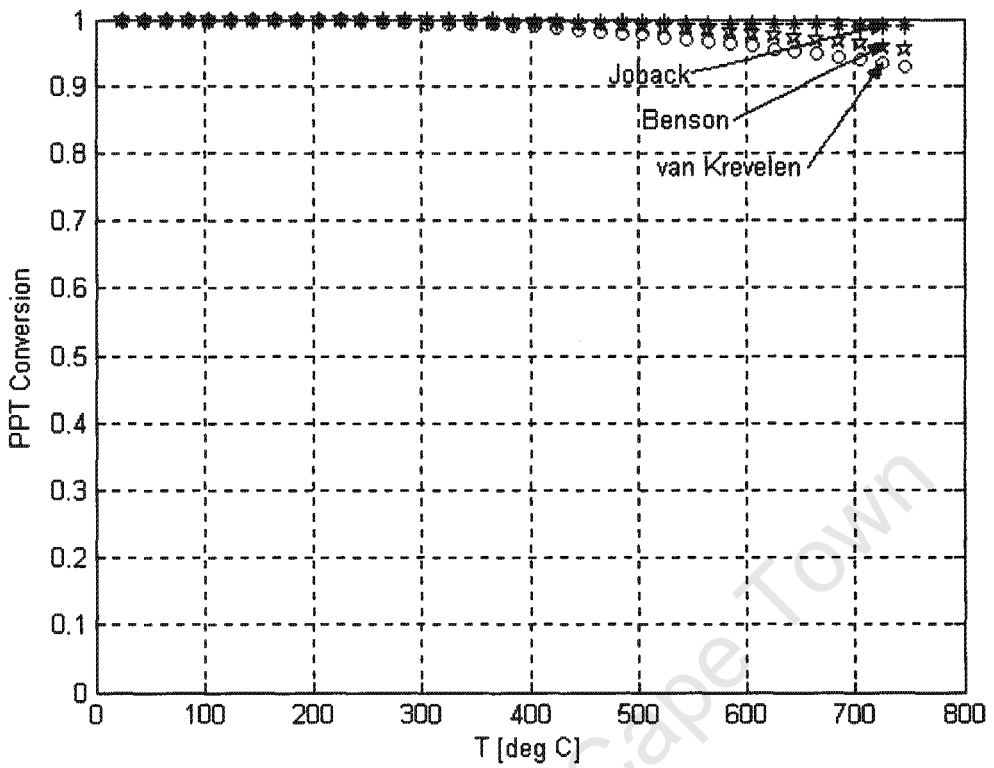

Figure 5-47: Equilibrium conversion plot for methylation of *p*-phenoxy toluene with methanol to *p*-tolyl ether and water

All the methods also predict high equilibrium conversion for the second methylation step, over the temperature range of interest, which is 200 – 300°C.

5.11.4 Cleavage of *p*-tolyl ether

Equilibrium conversion for *p*-tolyl ether cleavage with water to *p*-cresol at normal conditions was calculated from various thermodynamic estimate methods.

Compound table for *p*-tolyl ether cleavage reaction is given in Table 5-11.

Table 5-11: Compound table for *p*-tolyl ether cleavage with water to to *p*-cresol

Compound	Initial moles	Moles at equilibrium	Mole fraction
PTE	1	$1- X_{eq}$	$(1- X_{eq})/2$
Water	1	$1- X_{eq}$	$(1- X_{eq})/2$
p-Cresol	0	$2\ X_{eq}$	X_{eq}
Σ	2	2	1

The equilibrium constant for cleavage reaction, according to compound table (Table 5-11) is given by Equation 5-4.

$$K_4 = \frac{4 \cdot X_{eq}^2}{(1-X_{eq})^2} \qquad \textbf{Equation 5-4}$$

$$K_4 = e^{-\frac{\Delta G_{rxn4}}{RT}}$$

The equilibrium conversion at normal conditions calculated from various estimate methods is given in Table 5-11.

Table 5-12: Estimated equilibrium conversion for *p*-tolyl ether (PTE) cleavage with water to *p*-cresol at normal conditions, 298 K, ΔG_f° and ΔH_f° in kJ/mol, see Appendix I.1

	PTE	+	H_2O[b]	⟶	2*PC[a]	ΔH°_{rxn}	ΔG°_{rxn}	K°_{rxn}	X°_{eq}
$\Delta Gf^\circ_{,Joback}$	167.6		-228.8		-68.3		-7	17.5	0.68
$\Delta Hf^\circ_{,Joback}$	-14.4		-242.0		-257.2	-0.79			
$\Delta Gf^\circ_{,vKV}$	147.2		-228.6		-100.0		-19	1875	0.96
$\Delta Gf^\circ_{,Ben}$	156.3		-228.8		-66.3		6	0.08	0.13
$\Delta Hf^\circ_{,Ben}$	-22.3		-242.0		-252.6	11.7			

[a] Stoichiometric values (i.e. 2 PC)

[b] Literature data (experimental), except van Krevelen and Chermin

Equilibrium conversion as a function of temperature for *p*-tolyl ether cleavage with water to *p*-cresol is shown in Figure 5-48.

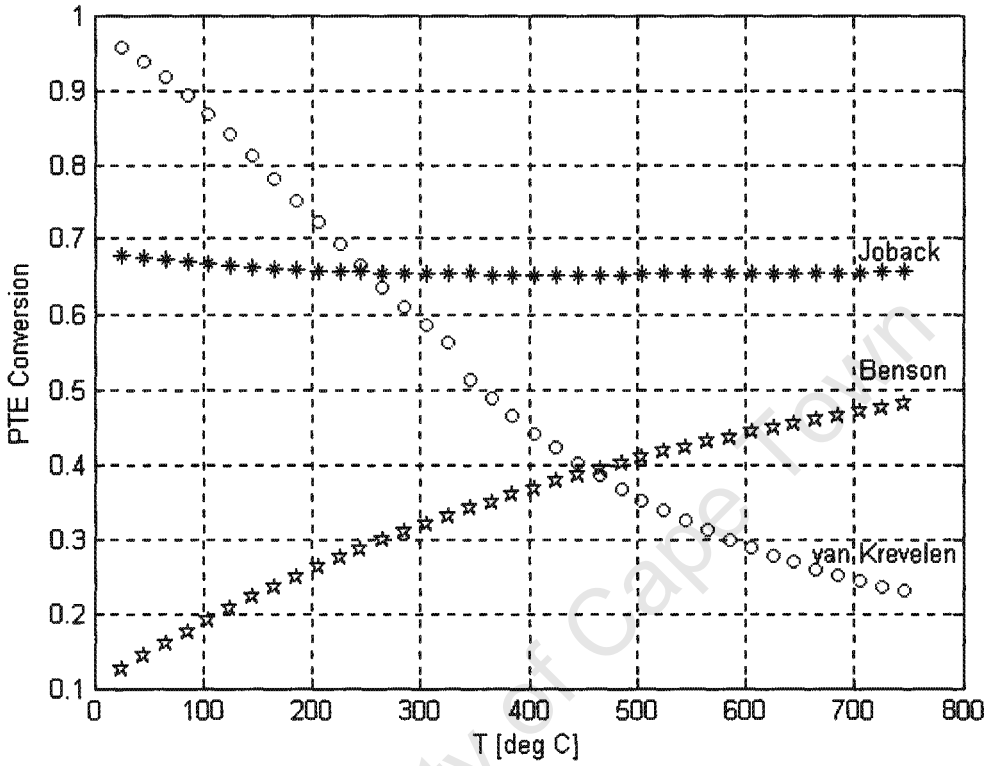

Figure 5-48: Equilibrium conversion plot for cleavage of *p*-tolyl ether with water, to p-cresol

The cleavage step is somewhat a reverse of the first step, which is condensation. This is reflected in the curves of Figure 5-48, curving in directions opposite to those of Figure 5-45, for each thermodynamic estimate method.

It appears that the reaction, p-tolyl ether cleavage with water to p-cresol is possible in the temperature range of interest, 200 – 300°C, but does not undergo total conversion due to equilibrium limitations.

5.12 RESULTS FROM MOLECULAR DYNAMICS

In Table 5-13, the drift speeds (average velocities) of various products diffusing through the pore system (wide pores) of zeolite mordenite are shown. Diffusivity of a species through the zeolite is related to the drift speed, by Equation 2-43 through to Equation 2-45. The diffusion constant of each species, calculated according to Equation 2-45, is also given in Table 5-13.

Table 5-13: Diffusion coefficients in the wide pores of zeolite mordenite, estimated from molecular dynamics

Compound	Drift speed, s [Å/ps]	N_{Atoms}	$t_{simulation}$ (ps)	$D_i \times 10^{-8}$ [cm/s]
PPT	5.31	26	40	19
MPT	1.42	26	40	1
OPT	2.1	26	40	3
PTE	3.55	29	40	8

The diffusion constants suggest configurational diffusion, according to Figure 2-16 and Figure 2-17.

6. DISCUSSION OF RESULTS

It could be shown that methylation of diphenyl ether with methanol over a shape selective zeolite, H-mordenite, indeed resulted in enhanced *p/o*-substitution ratios of about 5, Figure 5-41, which is significantly higher than what was achieved hitherto, via direct methylation of phenol with methanol over shape selective acid zeolites. The highest *p/o*-substitution ratio in direct phenol methylation reported to-date being 1.5, over H-MCM-22, (see Section 2.1.14.1).

The results were reproducible, as shown in Section 5.10.

6.1 PRODUCTS OF THE REACTION

The products of interest from DPE methylation reaction are shown on the chromatogram of Figure 4-9, namely *p*-phenoxy toluene (PPT) and *p*-tolyl ether (PTE) or the mono-*para* and the di-*para*-methylated DPE, respectively.

It appears that the light products recorded at the very beginning of the chromatogram were a result of the conversion of methanol to olefins and other hydrocarbons (Methanol-to-olefins and methanol-to-gasoline reactions, Chen et al. (1994)).

The majority of the light products appearing in the chromatogram prior to DPE, lumped as Ps, are phenolics (phenol, cresols, xylenols) and are thought of being due to cleavage of DPE and other alkylated diphenyl ethers (OADPEs). The cleavage is made possible by water that is produced from the methylation reactions, as well as from etherification of methanol to dimethyl ether (Chen et al., (1994)) and to some extent by further methylation of the resulting phenols.

It was expected, as discussed in Section 2.1.7, for the ether linkage of DPE to be stable over the temperature range tested. Very little cleavage was observed with H-beta zeolite for temperatures below 250°C, indicated by very little amounts of phenol and some methylated phenols, however this was not the case with other catalysts, wherein the ether cleavage selectivity closely followed catalyst activity.

However, no general or systematic trends pertaining to the reaction conditions could be identified for the formation of these phenolic compounds, when considering other results.

Selectivities range from 5 to 70% at the standard screening conditions (see Figure 5-5 Exp 25 and Exp 27, Figure 5-8, Figure 5-11, Figure 5-14, Figure 5-17, Figure –20 and Figure 5-38 at around 420 to 450 hours on stream). Selectivity of phenols, for instance, increased from 5 mol% to about 30 mol%, with increasing reaction temperature, from 200 to 300°C, over CBV90A but declined over the same temperature range from 80 mol% to 10 mol% over H-beta-25. Both catalysts were tested at feed partial pressure of 13 bar and same MeOH to DPE molar ratio of 2 (see Figure 5-38 and Figure 5-5).

The OADPEs (other alkylated diphenyl ethers) are thought to be unidentified tolyl ether isomers as well as other multialkylated derivatives of DPE either by methylation with methanol and/or possibly alkylation with olefins formed from methanol-to-olefins (Chen et al., 1994) reaction.

The heavy products (HPs), were, as shown in the second part of the chromatogram (Figure 4-10), thought to be the result of the reaction of DPE with the products of methanol conversion and not just dimers of DPE. This was postulated from an observation that the heavy products disappear in the absence of any of the two feed components, that is methanol or DPE (see Experiment 49 and Experiment 50, in Figure 5-38 and Section 5.9). However, the retention times of the HPs in the gas chromatograms (Figure 4-9 and Figure 4-10) are significantly higher than those of the OADPEs. It was therefore concluded that the HPs are not multialkylated derivatives of DPE but multicyclic compounds.

The high selectivity towards one to three specific HP compounds could also mean that the HPs are a family of polycyclic, probably tricyclic compounds. It can be speculated that tricyclics may have formed as a result of condensation of DPE with phenol from DPE cleavage reaction. This may be supported by an observation that the trends of Ps and HPs are always opposed regardless of the kind of zeolite, see Figure 5-5 (over H-beta-25), Figure 5-8 (over H-MFI-50) and Figure 5-14, Figure 5-20, Figure 5-30, Figure 5-34 and in particular Figure 5-38 (all these over mordenite based zeolites).

It is notable that selectivity to HPs was high only for the catalysts with a mono-dimensional channel system, namely the mordenites. Also different from other zeolites (see Section 5.2), the HPs fraction obtained from mordenites consisted essentially of a single compound (see chromatogram, Figure 4-10). It can be speculated that this reflects the shape selective

properties of this zeolite as well, also indicating long residence times in the non-interconnected pore systems.

6.2 CATALYST SCREENING CONDITIONS

Search for catalyst screening conditions was carried out over H-beta-25. The results are given in Section 5.3 (introductory experiments) and Section 5.4 (search for catalyst screening conditions) and the figures given in the respective sections, together with Figure 5-23.

Finding the suitable catalyst screening conditions was a crucial intermediate target in the early stages of the research program, and as a result, discussion of the results of the search process has been included in the results chapter (see Section 5.4).

The screening conditions derived were as follows (see Table 5-2):

T	= 250°C
P_{total}	= 20 bar
P_{feed}	= 13 bar[a]
P_{N2}	= 7 bar
$m_{dry\ zeolite}$	= 3 g
MFR	= 2 mol MeOH/mol DPE
WHSV	= 0.56 $g_{DPE}/(g_{dry\ zeolite} \cdot h)$

[a] At 250°C, the vapour pressure of methanol is 93 bar whereas that of DPE is 0.8 bar. It was on this basis that the feed partial pressure was considered to be solely due to methanol.

6.3 CATALYST SCREENING – THE CATALYST OF CHOICE

Steady state results from catalyst screening are given in Table 5-4, with the summary of the most important data in Table 6-1.

The different catalysts were ranked according to the following criteria, wherein high values were desired for each parameter.

- para-/ortho-phenoxy toluene ratio (PPT/OPT)
- para-/meta-phenoxy toluene ratio (PPT/MPT)
- selectivity to para-phenoxy toluene (S_{PPT})
- selectivity to total phenoxy toluenes (S_{PTIs})

- conversion and catalyst stability

Finding the best catalyst was a crucial intermediate target in the early stages of the research program, and as a result, ranking was done in Section 5.8, of the results chapter, based on the data of Table 5-4.

The multiple rankings carried out in Section 5.8 concluded mordenite based catalyst, CBV90A, as the catalyst of choice, based mainly on the first two criteria, but excluding H-Mor-40 on the basis of catalyst stability (see Figure 5-29 and Section 5.5.4).

Table 6-1: Steady state average DPE conversion as well as selectivities and isomer ratios for the PTIs from DPE methylation over various catalysts tested at standard screening conditions of Table 5-2

Catalyst	X_{DPE} [%]	S_{PTIs} [mol%]	S_{PPT} [mol%]	S_{OPT} [mol%]	S_{MPT} [mol%]	$\frac{PPT}{OPT}$	$\frac{PPT}{MPT}$
H-beta-25	35	75	23	48	3	0.5	9
H-MFI-50	5	18	11	5	1	2	9
H-USY	9	58	20	34	3	0.6	7
H-Mor-40	9	18	16	2	0.2	7	94
$CBV21A^{a}_{400°C}$	15	23	16	7	1	2.2	29
$CBV21A^{b}_{500°C}$	9	65	27	35	3	0.8	10
CBV90A	13	22	18	4	0.3	4.5	53

[a] Calcined at 400°C

[b] Calcined at 500°C

6.4 INFLUENCE OF PRETREATMENT AND REACTION CONDITIONS

6.4.1 Calcination temperature

Zeolite CBV21A was obtained in ammonium form and was therefore calcined for deammination to obtain the acid form. Two temperatures, 400°C and 500°C were chosen to determine the effect of calcination temperature on the performance of the catalyst. Indeed, calcination temperature was found to have a strong effect. Effects of higher calcination temperature on conversion, individual selectivities and isomer ratios are tabulated in Table 5-3, Section 5.7. An excerpt of Table 5-3 and Table 5-4, with major selectivities and isomer ratios, is given as Table 6-2 (see also Appendix IX.1).

Table 6-2: Effect of calcination temperature on DPE methylation over CBV21A at different reaction temperatures

CBV21A calcined at 400°C (see Figure 5-17 to Figure 5-18 and Figure 5-27)								
Exp.	T_{rxn} [°C]	X_{DPE} [%]	S_{PPT} [mol%]	S_{PTE} [mol%]	S_{OPT} [mol%]	S_{MPT} [mol%]	PPT/OPT	PPT/MPT
31	**250**	15	16	1.5	7	0.5	2.2	29
32	**300**	34	14	1	13	1.4	1.1	10
CBV21A calcined at 500°C (see Figure 5-30 to Figure 5-33)								
Exp	T_{rxn} [°C]	X_{DPE} [%]	S_{PPT} [mol%]	S_{PTE} [mol%]	S_{OPT} [mol%]	S_{MPT} [mol%]	PPT/OPT	PPT/MPT
35	**250**	9	27	0.4	35	2.6	0.8	10
34	**275**	33	20	1	35	2.6	0.6	8
33	**300**	63	12	1.2	31	2.2	0.4	6

Increase in calcination temperature has the following effects :

- Loss of activity at low reaction temperatures
- Loss of para-selectivity (in terms of PPT/OPT and PPT/MPT ratios)
- Decrease in selectivity of both light and heavy by-products

Considering that the calcination procedure was carried out at high pressure (20 bar) and very low flow rate of the purging gas (nitrogen at 20 ml/min, see Table 4-3), the build up of harmful levels of ammonia and steam partial pressures appears possible.

It can be speculated that this results in a partial collapse of the crystal structure and hence reduced acidity and formation of mesopores resulting in reduced shape selective properties and residence times of reactants and products in the zeolite channels.

6.4.2 Reaction temperature

The reaction temperature for DPE methylation over mordenite based catalysts, CBV21A and CBV90A, had significant effect on the conversion and product selectivities. This was summarised for CBV21A in Section 5.6 and is shown for CBV90A in Table 6-3. The values represent the steady state averages derived from Figure 5-35 and Figure 5-37.

Table 6-3: Effects of reaction temperature on DPE methylation over CBV90A, obtained at steady state with all other variables at standard screening conditions of Table 5-2

Exp.	T_{rxn} [°C]	X_{DPE} [%]	S_{PPT} [mol%]	S_{OPT} [mol%]	S_{MPT} [mol%]	S_{PTE} [mol%]	PPT/OPT	PPT/MPT
45	**200**	1.1	19	8	0.5	0.7	2.4	39
38	**250**	13.4	17.7	3.9	0.3	2.3	4.5	52.5
37	**275**	21	11	5	0.6	0.9	2.3	17
36	**300**	26	8	5	0.9	0.3	1.5	8

Selectivity to PPT and PTE, the para-methylated products, decreased with an increase in reaction temperature, whereas that of OPT remained almost constant. Though selectivity of MPT is small, an increase in selectivity was noticed, with increasing reaction temperature and conversion. Decreasing selectivity to PPT with increasing temperature could have been due to both the reduction in the extent of side reactions that are only significant at high temperature and increased conversion.

The high selectivity of other alkylated diphenyl ethers, OADPEs, at high temperature and conversion (see Figure 5-38 at low time on stream), suggests that the latter, i.e. mainly conversion, is the reason for this high selectivity. This is to an extent proved by the selectivity versus conversion plots of Section 6.6.

Overall, selectivity to phenoxy toluenes declined and *p*-selectivity also decreased with increasing reaction temperature. However, due to limited data, it cannot be ascertained whether this is a real temperature effect or a result of enhanced conversion.

Very low temperature of 200°C also appears to produce poor *p*-selectivity. However, these results may be erroneous due to very low conversion.

6.4.3 Pressure

Table 6-4 shows the effect of reaction pressure on conversion and selectivity over the catalyst of choice, CBV90A. Effects of pressure on the reaction under study were also conducted during the first phase (search for standard screening conditions, with zeolite H-beta-25), and respective data are included for comparison.

Table 6-4: Effect of pressure on DPE methylation over CBV90A and H-beta-25, obtained at steady state with all other variables at standard screening conditions of Table 5-2

CBV90A (see Figure 5-39)								
Exp.	**P_{Feed} [bar]**	X_{DPE} [%]	S_{PPT} [mol%]	S_{OPT} [mol%]	S_{MPT} [mol%]	S_{PTE} [mol%]	$\frac{PPT}{OPT}$	$\frac{PPT}{MPT}$
48	**7**	12	18	6	0.5	1.8	3.2	38
38	**13**	13.4	17.7	3.9	0.3	2.3	4.5	52.5
H-beta-25 (see Figure 5-1 and Figure 5-5)								
Exp.	**P_{Feed} [bar]**	X_{DPE} [%]	S_{PPT} [mol%]	S_{OPT} [mol%]	S_{MPT} [mol%]	S_{PTE} [mol%]	$\frac{PPT}{OPT}$	$\frac{PPT}{MPT}$
23	**0.75**	17	29	43	3.4	1.5	0.7	9
15	**4**	34	23	49	2.5	1.4	0.5	9
27	**13**	34	24	48	2.5	1.2	0.5	9

Except below 4 bar partial pressure of feed when the total reaction mixture was in the gas phase ($y_{DPE} = 0.25$, $T_{nbp,\ DPE} = 258°C$; $T_{reaction} = 250°C$), pressure effect on both conversion and selectivity is minor, as expected for liquid or dual phase reactions.

6.4.4 Weight hourly space velocity

Table 6-5: Effects of weight hourly space velocity on DPE methylation over CBV90A and H-beta-25, obtained at steady state with all other variables at standard screening conditions of Table 5-2

CBV90A (see Figure 5-38); MFR=2, P_{feed}=15 bar								
Exp. No.	**WHSV [h^{-1}][a]**	X_{DPE} [%]	S_{PPT} [mol%]	S_{OPT} [mol%]	S_{MPT} [mol%]	S_{PTE} [mol%]	PPT/OPT	PPT/MPT
39	**0.28**	19	16	3	0	2.1	4.7	49
38	**0.56**	14	17	4	0	2.3	4.5	53
41	**1.13**	7	19	4	0	2.4	4.5	58
H-beta-25 (see Figure 5-1); MFR=1, P_{feed}=0.7 bar								
Exp. No.	**WHSV [h^{-1}][a]**	X_{DPE} [%]	S_{PPT} [mol%]	S_{OPT} [mol%]	S_{MPT} [mol%]	S_{PTE} [mol%]	PPT/OPT	PPT/MPT
5	**0.41**	8.5	35	49	4	0.9	0.7	9
14	**0.41**	11	34	49	4	1.1	0.7	9
4	**1**	7	36	50	4	0.8	0.7	9

[a] g_{DPE} / ($g_{dry\ zeolite}$·h)

Varying space velocity influences conversion, as expected, but has no substantial effect on isomer selectivity except for the di-methylated product, PTE. Though on a low level, selectivity of PTE seemed to increase with increasing conversion for H-beta-25 and decrease with increasing conversion for CBV90A.

6.4.5 Molar feed ratio

Due to methanol being the major contributor to feed partial pressure, a change in molar feed ratio resulted in a change in feed partial pressure.

Table 6-6: Effects of molar feed ratio (MFR) on DPE methylation over CBV90A and H-beta-25, obtained at steady state with all other variables at standard screening conditions of Table 5-2

CBV90A (see Figure 5-38)									
Exp No.	**MFR**	P_{Feed} [bar]	X_{DPE} [%]	S_{OPT} [mol%]	S_{MPT} [mol%]	S_{PPT} [mol%]	S_{PTE} [mol%]	$\frac{PPT}{OPT}$	$\frac{PPT}{MPT}$
43	**0.5**	3	6	6	1	15	0.9	2.8	25
38	**2**	13	14	4	0	17	2.2	4.5	53
46	**4**	18	15	4	0	19	2.5	4.1	56
H-beta-25 (see Figure 5-1)									
Exp No.	**MFR**	P_{Feed} [bar]	X_{DPE} [%]	S_{OPT} [mol%]	S_{MPT} [mol%]	S_{PPT} [mol%]	S_{PTE} [mol%]	$\frac{PPT}{OPT}$	$\frac{PPT}{MPT}$
7	**0.1**	0.6	0.1	50	5	39	0.4	0.8	8
4	**1**	0.7	7	50	4	36	0.7	0.7	9

Varying the molar feed ratio (MFR) in both CBV90A and H-beta-25 zeolites influences conversion significantly, but has little effect on selectivities for OPT and MPT, over both catalysts. However, isomer ratios show a significant decline at low MFR (see Figure 5-41, data points around 400 hours on stream). The effect on PPT and PTE with CBV90A was a pronounced increase in selectivity with increasing MFR. In the case of H-beta-25, increase in conversion, following an increase in MFR, resulted in a decrease in PPT selectivity and a slight increase in PTE selectivity.

6.5 OPTIMUM CONDITIONS

Reaction conditions were optimised with the catalyst of choice, CBV90A. High *p*-/*o*-ratio is desired because p-cresol, the targeted final product, is to be obtained from cleavage of the methylated ethers. Low content of the meta-isomer is also desired because separation of meta- and para-cresol is cost intensive, due to their close boiling points (see Section 2.12.4).

Selectivities over the catalyst of choice, CBV90A, seemed not to vary much with the change of conditions except in the beginning when the catalyst was fresh and when the reaction

temperature was high (see Figure 5-38 and Figure 5-39). However, a more differentiating approach reveals the details and changes.

There are four major criteria for optimisation, and these are as follows :

1. para/ortho ratio (PPT/OPT)
2. para/meta ratio (PPT/MPT)
3. selectivity to para-phenoxy toluene (PPT)
4. conversion and catalyst stability

A combination of the last two in the criteria list gives another criterion, which is yield.

Figure 5-41 shows that criteria 1 and 2 were generally met at conditions of medium reaction temperature (250°C), high molar feed ratio (MFR≥2) and high feed partial pressure (13 bar). Note that feed partial pressures higher than the above could not be tried because of the technical limitations of the experimental equipment. Under the conditions mentioned above, PPT/OPT ratio of around 5 and maximum PPT/MPT ratio of around 55 were obtained.

Figure 5-39 and Figure 5-40 indicate that within the range of high PPT/OPT ratios, PPT selectivity was almost constant, slightly below 20%, and that the highest DPE conversion (ca. 25%) and thus the highest yield of PPT (ca. 5%) were achieved at low space velocity (minimum possible WHSV of 0.28 $g_{DPE}/ (g_{zeolite}.h)$) and high methanol to DPE molar feed ratio (i.e. MFR>2).

In can be concluded that the optimum reaction conditions for DPE methylation over CBV90A are as shown in Table 6-7.

Table 6-7: Optimum reaction conditions for DPE methylation with methanol over zeolite mordenite based Zeolyst catalyst, CBV90A

T	Temperature	250°C
P	Pressure[a]	>13 bar
MFR	Molar feed ratio (MeOH/DPE)	>2 mol/mol
WHSV	Weight hourly space velocity	0.3 – 0.5 $g_{DPE}/ (g_{dry\ zeolite}\cdot h)$

[a] Pressure must be high enough to keep as much of the feed in the liquid phase as possible. No carrier gas would be needed.

The effect of conversion on selectivity (i.e. indirect consequence of varying reaction conditions such as WHSV) is discussed in Section 6.6.

It is notable that the heavy products, HPs, account for about half of the total product (see Figure 5-38). Selectivities are lower at high catalyst activity and high reaction temperature but this change is combined with higher selectivity to products from ether cleavage and not beneficial to PTI selectivity.

The conversion and product composition obtained from diphenyl ether methylation over CBV90A catalyst under optimised conditions are the following (see steady state average results from Exp. 38 to Exp. 40, Appendix IX.1):

Diphenyl ether conversion : 12.5 – 18.6 %
p-/o-phenoxy toluene ratio : 4.6 – 4.7
p-/m-phenoxy toluene ratio : 49 – 54
Selectivity of *p*-phenoxy toluene : 16.6 – 17.8 mol%
Selectivity of phenoxy toluenes : 20.4 – 22 mol%

However, formation of heavy compounds, which may have been due to condensation of diphenyl ether with phenol from the side reaction of DPE cleavage, is high, resulting in heavy product selectivity of 40 mol % (of the converted DPE).

6.6 SELECTIVITY VS CONVERSION

Plots of selectivity vs conversion give access to information about stable and unstable products, primary and secondary products as well as the way reaction parameters influence selectivity, that is be it directly or indirectly via conversion, as shown Figure 6-1 to Figure 6-4. The figures show selected data from DPE methylation over CBV90A catalyst.

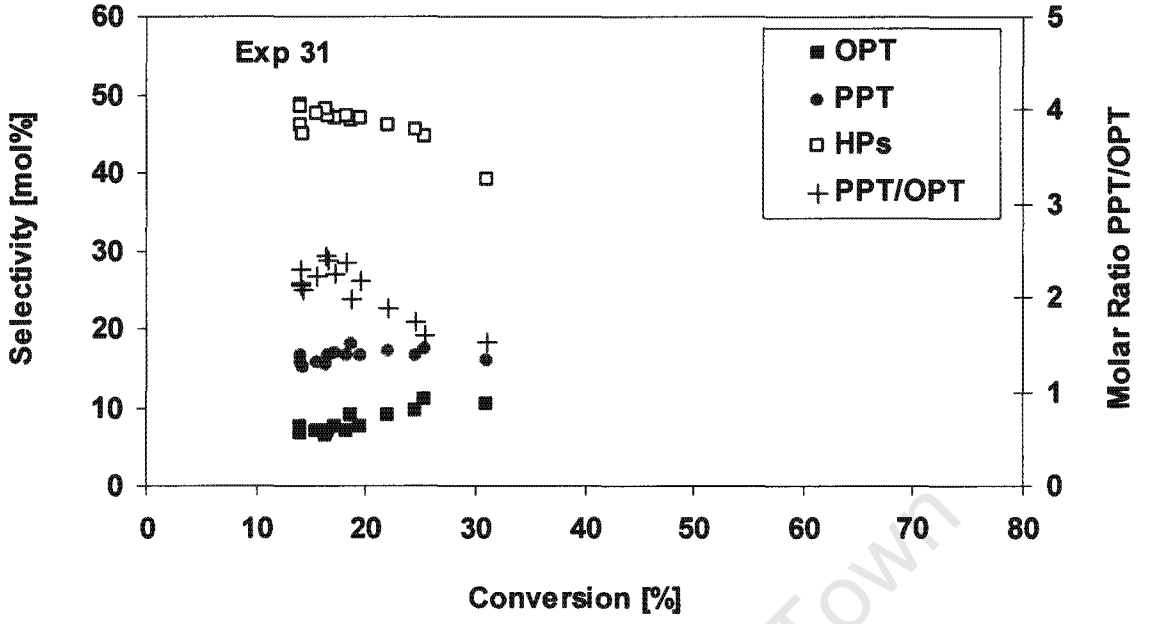

Figure 6-1: Selectivity plot as a function of conversion for mono-methylated products, their ratio and the heavy products, over CBV21A calcined at 400°C, at standard screening conditions

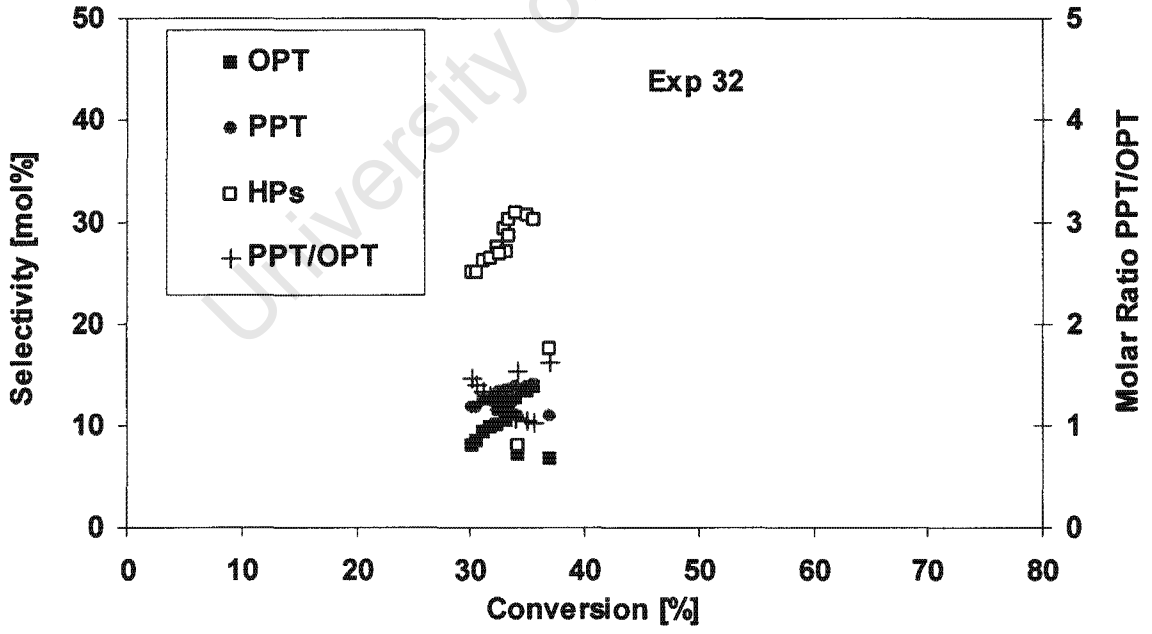

Figure 6-2: Selectivity plot as a function of conversion for mono-methylated products, their ratio and the heavy products, over CBV21A calcined at 400°C, at reaction temperature of 300°C

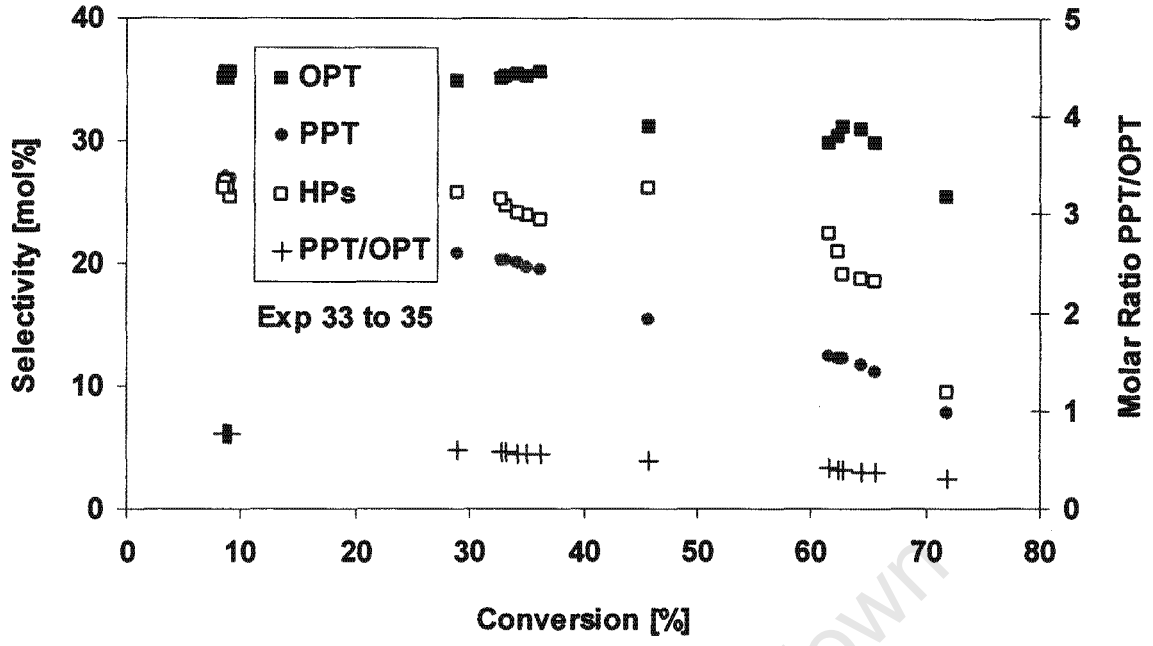

Figure 6-3: Selectivity plot as a function of conversion for mono-methylated products, their ratio and the heavy products, over CBV21A calcined at 500°C, at reaction temperatures of 300, 275 and 250°C

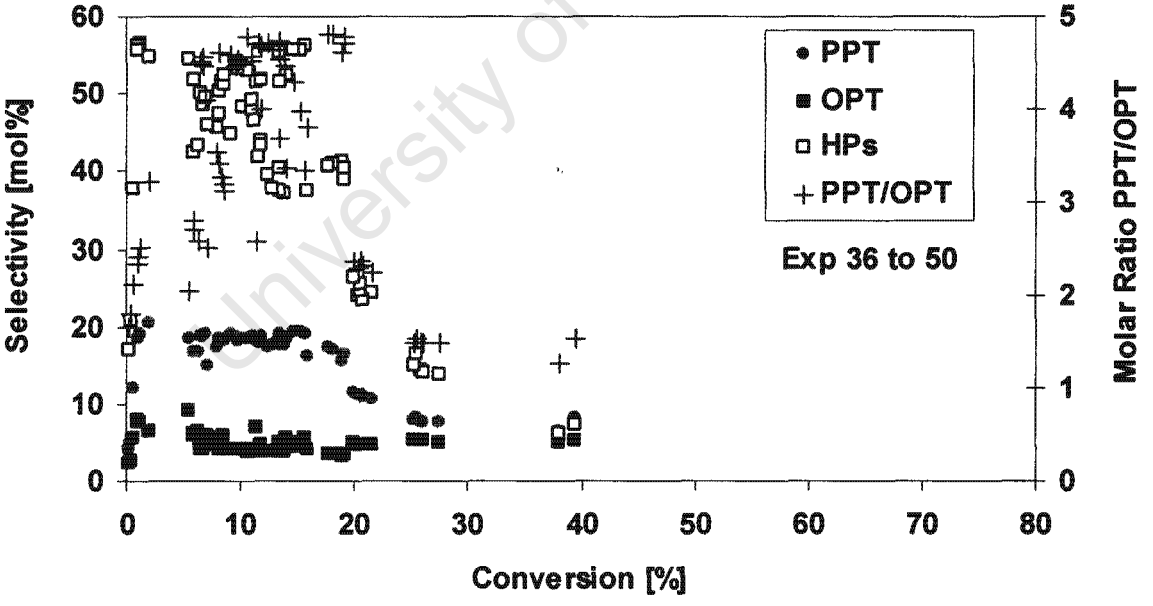

Figure 6-4: Selectivity plot as a function of conversion for mono-methylated products, their ratio and the heavy products, over CBV90A at various reaction conditions

Figure 6-1 shows selectivity versus conversion plots for $CBV21A_{400°C}$ at standard screening conditions. In this graph, selectivity to OPT increases with increasing conversion with a simultaneous drop in selectivity to HPs. Selectivity to PPT, the desired product, remained almost constant.

Examining selectivity data when arranged as a function of conversion, results appear not to be very consistent. However, para-selectivity, expressed as PPT/OPT ratio, appears to decline constantly and consistently with increasing conversion. Low PPT/OPT ratio at low conversion in Figure 6-4 is a result of unfavourable conditions, which are very low temperature (200°C) and low MFR (<1 mol MeOH/mol DPE). These effects can be seen from Table 6-3 and Figure 5-41 at ca. 500 hours on stream, as well as Table 6-6 and Figure 5-4 at ca. 400 hours on stream.

The rate constant is a function of temperature according to Arrhenius relation expressed as:

$$k = k_o \cdot e^{-\frac{E_a}{RT}} \qquad \textbf{Equation 6-1}$$

An increase in temperature increases the rate constant. From Equation 2-1, an increase in the rate constant increases the Thiele modulus, which implies that mass transport limitations also increase. Increased mass transport limitations will result in higher selectivity for the product with a higher diffusion constant and thus increase *p/o*-ratio. This would be the case if the reaction is product selectivity controlled.

A restricted transition state selectivity to an *ortho* methylated product corresponds to higher activation energy (E_a) for *ortho* methylated product relative to that for *para* product. High temperature favours the high activation energy reaction, which means that transition state restricted *o*-methylation would be accelerated. However, the observed decrease of the *p/o*-ratio with increasing temperature could also be due to secondary isomerisation and that the shape selective effects obtained over zeolite mordenite based catalysts could be by product selectivity.

Constant decline of the PPT/OPT ratio with increasing conversion may indicate isomerisation. However, since selectivity to meta substituted isomers is very low, isomerisation via 1,2-methyl shift on the ring can be excluded. Isomerisation would then have to occur via transalkylation, with unconverted DPE. However, in the straight non-interconnected channels

of zeolite mordenite, this may be suppressed as well as at high PPT/OPT ratios, even at medium conversion. This is however not so over wide pore zeolites with wide pore intersections (H-beta-25) of supercages (H-USY), see Table 5-4.

6.7 DEDUCTION FROM THERMODYNAMIC CALCULATIONS

Reaction equilibria calculated from estimated thermodynamic properties revealed that methylation would be able to proceed to almost completion but data was not sufficient to affirm equilibria for phenol condensation and methylated diphenyl ether cleavage, in the process route from phenol to *p*-cresol, via diphenyl ether (see Section 5.11 and Appendix VII, Figure A-6, for the results).

6.8 DEDUCTIONS FROM MOLECULAR MODELLING

An attempt was made calculating relative diffusion coefficients from molecular modelling data (see Section 5-12). Even though the relative diffusion constants have reasonable trends, the results were discarded on the basis of the force fields of the molecular dynamics software used at that time being inaccurate.

Molecular dynamics results on diffusion of OPT, MPT and PPT in zeolite mordenite pores are given in Section 5.12, Table 5.13. The diffusivities obtained are in the region of configurational diffusion (see Figure 2.16 and Figure 2-17). However, the results from molecular dynamics are not adequate to quantify relative diffusivities due to inaccuracy of the force fields, which were used.

7. CONCLUSIONS AND RECOMMENDATIONS

7.1 CONCLUSIONS

High *p/o*- and very high *p/m*-ratios of phenoxy toluenes from DPE methylation were obtained over mordenite based catalysts, which makes the process route interesting compared to the present and only commercial process selective to p-cresol manufacture, which is alkylation of toluene sulphonates.

Table 7-1: Comparison of phenoxy toluene isomer ratios for the commercial process, phenol methylation over zeolite H-MCM-22 and the process route investigated in this study

	Alkali fusion of toluene sulphonates[a]	Methylation of diphenyl ether	Phenol methylation over H-MCM-22[d]
p/o-ratio	8[b]	4.5[c]	1.3
p/m-ratio	8[b]	50[c]	high

[a] See Table 2-7, Section 2.1.11

[b] In the cresols

[c] In phenoxy toluenes

[d] See Section 2.1.14.1

Formation of the mono-para methylation product, PPT, is favoured at intermediate temperature of 250°C, high MeOH/DPE molar ratio, high pressures of 13 bars and more and at low space velocities of less than 0.5 $g_{DPE}/(g_{dry\ zeolite} \cdot h)$.

Since the above conditions result in low conversion, the di-para methylated product, PTE, which is formed by a series reaction, is formed with low selectivity.

In the case of product shape selectivity, it is required that the intrinsic kinetics allow for rapid isomerisation, reaching isomer equilibrium distribution inside the zeolite crystals (Haag and Olson, 1984). The less bulky isomers then diffuse rapidly out of the pores and the bulky ones isomerise back to re-establish equilibrium. Practically no *m*-isomer was obtained, even though it is the most thermodynamically stable isomer and comparable in bulkiness to the *o*-isomer, isomerisation is unlikely to occur via

1,2-methyl-shift so that a transalkylation mechanism of DPE with methylated DPEs must be considered.

However, in contrast to zeolite H-USY with its large supercages (see Section 2.2.7) and zeolite H-beta with its comparably wide pore crossings that are accessible from different directions, the pore spaces in mordenite are far more restricted to straight channels (of 6.7 x 7.0 Å diameter) and small side pockets wherein DPE molecules can be hardly accommodated such that *ortho*-to-*para* methyl group transalkylation appears possible.

Therefore it is concluded that the high selectivity to *para*-methylation of DPE over mordenite-based catalysts could be due to transition state selectivity, suppressing *o*-methylation, rather than product selectivity.

7.2 RECOMMENDATIONS

Product selectivity over mordenite based catalysts is still affected by significant amounts of heavy by-products, HPs, formed.

Optimisations of process variables with intent to minimise the heavy product still needs to be carried out, because this is a great potential for increasing selectivity to para-alkylated product. Studies should be undertaken to identify the HPs and the reactions through which they form, given the fact that neither of the two feed components alone forms the HPs. Given the suggested mechanism (see Section 6.1) of condensation of DPE with phenol from DPE cleavage reaction (with reaction water), converting DPE/water mixture may be the first step into this investigation.

There is therefore a need to clarify the effect of co-product water, from the reaction investigated.

Future work should include mordenite catalysts with deactivated external crystal surface area to passivate sites which may be contributing to non-*para*-alkylation and isomerisation by transalkylation, to see if this will improve selectivity to the *para* product.

Given the big differences observed between the three mordenite-based catalysts tested, it is still necessary to test other SiO_2/Al_2O_3 ratios, as well as mordenite based catalyst from other sources.

8. REFERENCES

- Accelrys Inc., "DMol – Introduction", [online], 2001. Available from http://www.msg.ucsf.edu/local/programs/insightII/doc/life/insight2000.1/dmol/1_Intro.html (Last visited on 16/11/2002).

- Accelrys Inc, "Density Functional Theory", [online], 2002. Available from http://www.accelrys.com/technology/qm/erich/dft.htm (Last visited on 16/11/02)

- Anderson L. L., "Coal Liquefaction", *In:* Bissio A. and Boots S.,*Encyclopedia of Energy Technology and the Environment*, Vol 2, page 792 – 808 (1995)

- Atkins P. W., *Physical Chemistry*, 5th Ed, Oxford University Press, Oxford, Chpt 11, 19, 26 and 28 (1994).

- Baerlocher Ch., Meier W. M. and Olson, D. H., *Atlas of Zeolite Framework Types*, 5th Ed, Elsevier, Amsterdam, (2001).

- Bhattacharya R. N., "Prospects of Coal Tar Aromatics as Monomers for Plastics and Polymer Industries", *Chemical Engineering World*, [online], 1997. Available from: http://www.exicom.org/cew/sep97/bhatta.htm (Last visited on 30/05/01).

- Bondi A., "van der Waals Volumes and Radii", *The Journal of Physical Chemistry*, Vol 68, No. 3, American Chemical Society, page 441-551 (1964).

- Brzozowski R. and Tecza W., "Shape Selective Reactions of Naphthalene over Zeolites", Applied Catalysis A: General, Vol 166, page 21 – 27 (1998).

- Cadogan J. I. G., Ley S. V. and Pattenden G., *Dictionary of Organic Compounds*, 6th Ed, Chapman & Hall, London (1996).

- Chantal P., Kaliaguine S., Grandmaison J. L. and Mahay A., "Reactions of Phenolic Compounds over H-ZSM-5", *Applied Catalysis*, Vol 18, page 133-145 (1985).

- Chen N. Y., Degnan T. F. Jr. and Smith C. M., *Molecular Transport and Reaction in Zeolites: Design and Application of Shape Selective Catalysts*, Wiley-VCH, New York, Chpt 6 (1994).

- Collin G. and Höke H., "Tar and Pitch", *In*: Gerhartz W. and Yamamoto Y. S., *Ullman's Encyclopedia of Industrial Chemistry*, Vol A26, VCH, Weinheim (1995).

- Csicsery S. M., "Shape-Selective Catalysis in Zeolites", Zeolites, Vol 4, page 202 – 213 (1984).

- Daubert T. E. and Danner R. P., *Physical and Thermodynamic Properties of Pure Compounds*, John Wiley, New York (1990)

- Engelhard Inc., "Do Manufacturing Techniques Affect Performance of Ultrastable Zeolite FCC Octane Catalysts?" USA, [online], 2004, Available from http://www.refiningonline.com/EngelhardKB/crep/TCR4_34.htm (Last visited on 08/12/2004)

- EPA (Environmental Protection Agency), USA, [online], 1997, Available from http://www.epa.gov/fedrgstr/EPA-TOX/1997/December/Day-24/4645.pdf (Last visited on 10/04/2001)

- Fiege H., "Cresols and Xylenols", *In:* Gerhartz W. and Yamamoto Y. S., *Ullmann's Encyclopedia of Industrial Chemistry,* 5th Ed, Vol A8, VCH, Weinheim, page 25 –59 (1987).

- Fiege H., "Cresols and Xylenols", *In:* Gerhartz W. and Yamamoto Y. S., *Ullmann's Encyclopedia of Industrial Chemistry,* 6th Ed (Electronic Release), VCH, Weinheim (2000).

- Fiege H., Voges H., Hamamoto T., Umemura S., Iwata T., Miki H., Fujita Y., Buysch H. and Garbe D., "Phenol Derivatives", *In:* Gerhartz W. and Yamamoto Y. S., *Ullmann's Encyclopedia of Industrial Chemistry,* 6th Ed (Electronic Release), VCH, Weinheim (2000).

- Flanigen E. M., "Zeolites and Molecular Sieves: A Historical Perspective", *In:* van Bekkum H., Flanigen E. M., Jacobs P. A. and Jansen J. C., *Introduction to Zeolite Science and Practice*, 2nd Ed, Vol 137, Elsevier, Amsterdam, Chpt 2 (2001).

- Fogler H. S., *Elements of Chemical Reaction Engineering*, 3rd Ed, Prentice Hall, New Jersey, Chpt 3 and 10 (1999).

- Fritsch C., Cresol Isomerisation: Determination of the Thermodynamic Equilibrium, Chemical Technology Diploma Report, Department of Chemistry, University of Stuttgart, Germany / Department of Chemical Engineering, University of Cape Towm, Unpublished (2003).

- Fujita T., Kaneda M., Ono H. and Takahata K., "Preparation of 4-methyldiphenyl ethers and 4,4'-dimethyldiphenyl ethers", Japanese Patent No. JP 04,021,648 (1992).

- Gates B. C., "Catalysis", *In:* Kirk R. E. and Othmer D. F., *Encyclopedia of Chemical Technology*, 4th Ed, Vol 5, John Wiley, New York, page 321 (1993).

- Haag W. O. and Olson D. H., "Structure-Selectivity Relationship in Xylene Isomerisation and Selective Toluene Disproportionation", *In:* Whyte T. E., Dalla Betta R. A., Derouane E. G. and Baker R. T. K., *Catalytic Materials: Relationship Between Structure and Reactivity*, American Chemical Society Symposium Series, Vol 248, American Chemical Society, Washington D. C. page 275 – 307 (1984).

- Hammershaimb H. U., Imai T., Thompson G. J. and Vora B. V., "Alkylation", *In:* Kirk R. E., and Othmer D. F., *Encyclopedia of Chemical Technology*, 4th Ed., Vol 2, John Wiley, New York, page 106 – 108 (1993).

- Hölderich W. F. and van Bekkum H., "Zeolites and Related Materials in Organic Syntheses. Brönsted and Lewis Catalysis", *In:* van Bekkum H., Flanigen E. M., Jacobs P. A. and Jansen J. C., *Introduction to Zeolite Science and Practice*, 2nd Ed, Vol 137, Elsevier, Amsterdam, Chpt 18 (2001).

- Horniakova J., Mravec D., Joffre J. and Moreau P., "Selective Alkylation of Biphenyl over H-MOR and H-BEA Zeolites: Analysis of Experimental Results by Computational

Modelling", Journal of Molecular Catalysis A: Chemical, Vol 185, Elservier, page 249 – 257 (2002).

- Imbert F. E., Gnep N. and Guisnet M., "Comparison of Cresol Transformation on USHY and HZSM5", *Journal of Catalysis,* Vol 195, page 279 – 286 (2000).

- Intille G., "p-Cresol from p-Toluenesulfonic Acid", *PEP Review 83-1-2*, [online], 2001, Available from: http://process-economics.com/Reviews/83-1-2.htm (Last visited on 30/05/01).

- Jansen J. C., Creyghton E. J., Lan Njo S., van Koningsveld H. and van Bekkum H., "On the Remarkable Behaviour of Zeolite Beta in Acid Catalysis", *Catalysis Today*, Vol 38, page 205 – 212 (1997).

- Jordan W., van Barneveld H., Gerlich O., Kleine-Boymann M. and Ullrich J., "Phenol", *In:* Gerhartz W. and Yamamoto Y. S., *Ullmann's Encyclopedia of Industrial Chemistry,* 6th Ed, Vol A8, VCH, Weinheim, page 25 –59 (2002).

- Koennecke H. G., Kraenke K. and Langguth H., "p-Cresol from Aliphatic Compounds" DD 60047 (1968).

- Kopf P. W. and Little A. D., "Phenol Resins", In: Kirk R. E. and Othmer D. F., *Encyclopedia of Chemical Technology*, 4th Ed, Vol 18, John Wiley, New York, page 603 (1993).

- Kaiser R. E., *Chromatographie in der Gasphase*, BI-Hochschultaschenbücher, Mannheim (1960).

- Kühl G. H. and Kresge C. T., "Molecular Sieves", *In:* Kirk R. E. and Othmer D. F., *Encyclopedia of Chemical Technology*, 4th Ed, Vol 16, John Wiley, New York, page 888 (1993).

- Landau M. V., Kogan S. B., Tavor D., Herskowitz M. and Koresh J. E., "Selectivity in Heterogeneous Catalytic Processes", *Catalysis Today*, Vol 36, page 497-510 (1997).

- Lawton S. L., Leonowicz M. E., Partridge R. D., Chu, P. and Rubin M. K., "Twelve-Ring Pockets on the External Surface of MCM-22 Crystals", Microporous and Mesoporous Materials (1998), 23, 109 – 117.

- Leach A. R., *Molecular Modelling: Principles and Applications*, Long man, Singapore, Chpt 6 (1998).

- Leonowicz M. E., Lawton J. A., Lawton S. L. and Rubin M. K., "MCM-22: A Molecular Sieve with Two Independent Multidimensional Channel Systems", Science (1994), 264, 1910 - 13.

- Levenspiel O., *Chemical Reaction Engineering*, 2nd Ed, John Wiley, New York, Chpt 14 (1972).

- Lorence J. F., Lambeth G. and Scheffer W., "Alkylphenols", *In:* Kirk R. E. and Othmer D. F, *Encyclopedia Of Chemical Technology*, 4th Ed., Vol 2, John Wiley, New York, page 113 – 141 (1993).

- Martens J. A. and Jacobs P. A., "Introduction to Acid Catalysis with Zeolites in Hydrocarbon Reactions", *In:* van Bekkum H., Flanigen E. M., Jacobs P. A. and Jansen J. C., *Introduction to Zeolite Science and Practice*, 2nd Ed, Vol 137, Elsevier, Amsterdam, Chpt 14 (2001).

- Marx M. F., Caltex Report: Oil Refining, Cape Town (1995)

- Matsuda T., Urata T., Saito U. and Kikuchi E., "Effect of SiO_2/Al_2O_3 Ratio on the Catalytic Properties of Mordenite for Alkylation of Biphenyl with Propene", Applied Catalysis A: General, Vol 131, page 215 – 224 (1995).

- McCusker L. B. and Baerlocher C., "Zeolites Structures", *In:* van Bekkum H., Flanigen E. M., Jacobs P. A. and Jansen J. C., *Introduction to Zeolite Science and Practice*, 2nd Ed, Vol 137, Elsevier, Amsterdam, Chpt 3 (2001).

- McMurry J., *Organic Chemistry*, 3rd Ed, Prentice Hall, Upper Saddle River, Chpt 9, 16, 24 and 26 (1992).

- Mera H. and Takata T., "High Performance Fibres" *In:* Gerhartz W. and Yamamoto Y. S., *Ullmann's Encyclopedia of Industrial Chemistry,* 6th Ed, Vol 16, VCH, Weinheim, page 241 – 304 (2003).

- Merisol, "Company Overview", [online], 2001, Available from: http://merisol.hosting.redthistle.co.za (Last visited on 02/06/01)

- Meier W. M., Olson D. H. and Baerlocher C., *Atlas of Zeolite Structures*, 4th Ed., Elsevier, London (1996).

- Moon G., Möller K. P., Böhringer W. and O' Connor C. T., "The Influence of Pore Geometry on the Alkylation of Phenol with Methanol over Zeolites", Studies in Surface Science and Catalysis, Vol 135, page 15 (2001).

- Moon G., Moller K. P., Bohringer W. and O'Connor C. T., "Alkylation of Phenol with Methanol over Zeolite H-MCM-22 for the Formation of *p*-Cresol", Studies in Surface Science and Catalysis, Vol 142A, 635 – 642 (2002).

- Moon G., Alkylation of Phenol with Methanol over H-ZSM-5, H-Beta, H-Mordenite, H-USY and H-MCM-22, PhD Thesis, Department of Chemical Engineering, University of Cape Town, Cape Town (2003).

- Moon G., Bohringer W. and O'Connor C. T., "Pressure Induced Enhancement of Shape Selective Phenol Methylation", Proc. 14th International Zeolite Conference, Cape Town, (2004).

- Ndlovu S. and Gxavu S., Zeolite Catalysed Alkylation of Phenols, Final Year Research Project Report, Department of Chemical Engineering, Unpublished, University of Cape Town, Cape Town (2000).

- Nieuwoudt I., "Separation of Phenolic Compounds and Neutral Oils", ZA 974567 (1997).

- Nieuwoudt I., "Separation of Phenolic Compounds from Neutral Oils", ZA 98/111312 (1998).

- O'Connor C. T., Moon G.; Böhringer W. and Fletcher J. C. Q., "Alkylation of Phenol and *m*-Cresol over Zeolites." Collection of Czechoslovak Chemical Communications, 68, 1949 – 1968 (2003).
- Perry R. H. and Green D. W., *Perry's Chemical Engineers' Handbook*, 7th Ed, McGraw-Hill, New York (1997).
- Post M. F. M., "Diffusion in zeolite molecular sieves, in: Introduction to zeolite science and practice", *In:* van Bekkum H., Flanigen E. M., and Jansen J. C., *Studies in surface science and catalysis*, Vol. 58, pp. 391–443 (1991).
- Reid R. C., Prausnitz J. M. and Poling B. E., *The Properties of Gases and Liquids*, 4th Ed, McGraw-Hill, New York, Chpt 6 (1987).
- Reid R. C., Prausnitz J. M. and Sherwood T. K., *The Properties of Gases and Liquids*, 3rd Ed, McGraw-Hill, New York, Chpt 6 (1977).
- Rodkin M. A., Sobolev V. I., Dubkov K. A., Watkins N. H. and Panov G. I., "Room Temperature Oxidation of Hydrocarbons over FeZSM-5 Zeolite", Studies in Surface Science and Catalysis, Vol 130, page 875 – 880, (2000).
- Roland E. and Kleinschmit P., "Zeolites", *In:* Gerhartz W. and Yamamoto Y. S., *Ullmann's Encyclopedia of Industrial Chemistry,* 6th Ed, Vol 39, VCH, Weinheim, page 625 – 655 (2003).
- Rudent P., "Calibration Method and New Developments for High-Performance Mass Flow Controllers", QUALIFLOW SA, Montpellier, France. [online], 1998 Available from http://www.semiconductorfabtech.com/journals/edition.08/download/08.167.pdf (Last visited on 07/11/2003)
- Ruthven D. M. and Post M. F. M., "Zeolites Structures", *In:* van Bekkum H., Flanigen E. M., Jacobs P. A. and Jansen J. C., *Introduction to Zeolite Science and Practice*, 2nd Ed, Vol 137, Elsevier, Amsterdam, Chpt 12 (2001).

- Sage I., "Liquid Crystals", *In:* Gerhartz W. and Yamamoto Y. S., *Ullmann's Encyclopedia of Industrial Chemistry,* 6th Ed, Vol 19, VCH, Weinheim, page 241 – 304 (2003).
- Salzman W. R., "Notes on Statistical Thermodynamics – Partition Functions", [online], 2002, Available from http://www.chem.arizona.edu/~salzmanr/480b/statt01/statt01.html (Last visited on 07/03/2003)
- Sandra P. J. F., "Gas Chromatography", *In:* Gerhartz W. and Yamamoto Y. S., *Ullmann's Encyclopedia of Industrial Chemistry,* 6th Ed, Vol 15, VCH, Weinheim, page 241 – 304 (2003).
- Sasol Corporate Communications, Sasol Facts 2000, Sasol Ltd., Sasolburg (2001).
- Schuring D., Diffusion in Zeolites: Towards a Microscopic Understanding, PhD Thesis, Eindhoven University, The Netherland (2002).
- Shimuzu K., Miki K. and Saitou I., "Acid-Catalysed De-Polymerisation of Coal Model Compounds and Sub-Bituminous Coal in a Superacid-Isopentane Medium", *Fuel*, Vol 76, page 23-27 (1997).
- Shriver D. F., Atkins P. W. and Langford C. H., *Inorganic Chemistry*, 2nd Ed, Oxford University Press, Oxford, Chpt 17 (1994).
- Sinitsyna O. A. and Romanovskii B. V., "Correlation of Acidity and Catalytic Properties of Pentasils as Catalysts for the Alkylation of Phenol with Methanol", *Kinetics and Catalysis*, Vol 33, page 276-280 (1992).
- Sinitsyna O. A. and Romanovskii B. V., "Catalytic Properties of Pentasils in the Vapour Phase Alkylation of Phenol with Methanol", *Kinetics and Catalysis*, Vol 33, page 925-930 (1993).
- Sinnott T. K., *Chemical Engineering Volume 6: Chemical Engineering Design*, 3rd Ed, Butterworth-Heinemann, Swansea (1999).
- Smoot L. D., "Coal Combustion", *In:* Bissio A. and Boots S., *Encyclopedia of Energy Technology and the Environment*, Vol 1, page 731 (1995).

- Springborg M., *Density-Functional Methods in Chemistry and Materials Science*, John Wiley, Chichester, Chpt 1 (1997).

- Stull D. R., Westrum E. F. and Sinke G. C., *The Chemical Thermodynamics of Organic Compounds*, John Wiley, New York (1969).

- Sykes P., *A Guidebook to Mechanisms in Organic Chemistry*, 6th Ed., Longman, Harlow, England, Chpt. 6 (1986).

- Szostak R., "Secondary Synthesis Methods", *In:* van Bekkum H., Flanigen E. M., Jacobs P. A. and Jansen J. C., *Introduction to Zeolite Science and Practice*, 2nd Ed, Vol 137, Elsevier, Amsterdam, Chpt 6 (2001).

- Tepper H. L., Hoogenboom J. P., van der Vegt N. F. A. and Briels W. J., "Unidirectional Diffusion of Methane in $ALPO_4$-5", Journal of Chemical Physics, Vol 110, page 11511 – 11516 (1999).

- Van Santen R. A., van de Graaf B. and Smit B., "Zeolite Structures", *In:* van Bekkum H., Flanigen E. M., Jacobs P. A. and Jansen J. C., *Introduction to Zeolite Science and Practice*, 2nd Ed, Vol 137, Elsevier, Amsterdam, Chpt 10 (2001).

- Venter D. L. and Nieuwoudt I., "The Separation of Phenol from Neutral Oils with Liquid-Liquid Extraction", SAIChe R & D Conference, Cape Town (2001).

- Venter D. L., Separation of Phenolic Compounds from Neutral Oils, MSc Thesis, Department of Chemical Engineering, University of Stellenbosch, Stellenbosch (1997).

- Wallace J., "Phenol", *In:* Kirk R. E. and Othmer D. F., *Encyclopedia of Chemical Technology*, 4th Ed., Vol 18, John Wiley, New York, page 592 – 602 (1996).

- Welty J. R., Wicks C. E. and Wilson R. E., *Fundamentals of Momentum, Heat and Mass Transfer*, 3rd Ed, John Wiley, New York, Chpt 24 (1984).

- Xu J., Yan A.-Z. and Xu Q.-H., "Alkylation of Phenol with Methanol on H-Beta Zeolite", Reaction Kinetics and Catalysis Letters, Vol 62, page 71-74 (1997).

APPENDIX I

APPENDIX II

APPENDIX III

APPENDIX IV

APPENDIX V

V.1 Summary of catalyst loads.

APPENDIX VI

VI.1 Data for reactor temperature profiles

VI.2 Heating rate of the reactor

APPENDIX VII

VII.1 Thermodynamics from Quantum Mechanics

VII.2 Thermodynamic equilibria from Quantum Mechanics

APPENDIX VIII

VIII.1 Results from self-diffusion Molecular Dynamics Calculations

VIII.2 Diffusivities of various species molecules in H-ZSM-5

VIII.3 Other Molecular Dynamics Calculations results

APPENDIX IX

IX.1 Steady state average results

APPENDIX X

X.1 Chromatograms of products from H-MFI-50 screening

APPENDIX I

Thermodynamic Properties

APPENDIX I.1

Gas phase literature data for the reactants and products of the process route from phenol to p-cresol. used for "Ideal gas" calculations of Section 5.11.1 *(Sinnott, 1999)*

Compound	molar mass	ΔH_v^{nbp}	ΔH_f^o	ΔG_f^o	C_p [J/mol.K]			
	kg/kmol	kJ/mol	kJ/mol	kJ/mol	A	B	C	D
Water	18.0	40.68	-242	-228.77	32.24	1.92E-03	1.06E-05	-3.60E-09
Methanol	32.0	35.28	-201.3	-162.62	21.15	7.09E-02	2.59E-05	-2.85E-08
Phenol	94.1	45.64	-96.67	-32.91	-35.843	5.98E-01	-4.83E-04	1.53E-07
p-Cresol	108.1	47.48	-125.48	-30.9	-40.633	7.05E-01	-5.76E-04	1.97E-07
Diphenyl ether	170.2	47.14	49.99	*175*[a]	-60.73	9.28E-01	-5.87E-04	1.36E-07
p-Phenoxy toluene	184.2	-	-	-	-	-	-	-
p-Tolyl ether	198.2	-	-	-	-	-	-	-

[a] ***Source : Perry and Green (1997)***

ΔH_v^{nbp} = Change in the enthalpy of vapourisation

ΔH_f^o = Change in the enthalpy of formation at 298 K

ΔG_f^o = Change in the Gibbs Free Energy of formation at 298 K

APPENDIX I.2

Estimation of the Gibbs free energy using van Krevelen and Chermin's method (Reid et al., 1977)

R = 1.987 cal/gmol.K $\quad\quad$ **ΔG_f° ~ kcal/gmol**

$\Delta G = A + BT$ [T in K]

Compound	Groups	frequency	300 - 600 K A	300 - 600 K B	600 - 1500 K A	600 - 1500 K B
H_2O	H_2O	1	-58.076	1.154E-02	-59.138	1.316E-02
			-228.6 ΔG° [kJ/mol]			

Compound	Groups	frequency ($\sigma_{internal}$)	300 - 600 K A	300 - 600 K B	600 - 1500 K A	600 - 1500 K B
CH_3OH	H_3C—	1	-10.943	2.22E-02	-12.31	2.44E-02
	—OH	1	-41.56	1.28E-02	-41.56	1.28E-02
	+R Ln σ_{ext}	(1)	0	0.00E+00	0	0.00E+00
			-52.503	**3.495E-02**	**-5.387E+01**	**3.716E-02**
			-176.1 ΔG° [kJ/mol]			

Compound	Groups	frequency ($\sigma_{internal}$)	300 - 600 K A	300 - 600 K B	600 - 1500 K A	600 - 1500 K B
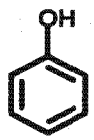	=C<	1	4.675	1.15E-02	5.01	9.88E-03
	—OH	1	-41.56	1.28E-02	-41.56	1.28E-02
	=CH—	5	3.047	6.15E-03	2.505	7.06E-03
	6-C ring	1	-1.128	-1.64E-02	-1.93	-1.50E-02
	+R Ln σ_{ext}	(2)	0	1.38E-03	0	1.38E-03
			-22.778	**4.008E-02**	**-25.955**	**4.432E-02**
			-45.33 ΔG° [kJ/mol]			

APPENDIX I.2

Compound	Groups	frequency ($\sigma_{internal}$)	300 - 600 K A	300 - 600 K B	600 - 1500 K A	600 - 1500 K B
	=C<	2	4.675	1.15E-02	5.01	9.88E-03
	—OH	1	-41.56	1.28E-02	-41.56	1.28E-02
	—CH_3	1	-10.943	2.22E-02	-12.31	2.44E-02
	=CH—	4	3.047	6.15E-03	2.505	7.06E-03
	6-C ring	1	-1.128	-1.64E-02	-1.93	-1.50E-02
	+R Ln σ_{ext}	(2)	0	1.38E-03	0	1.38E-03
			-32.093	**6.758E-02**	**-35.760**	**7.150E-02**

-50.0 ΔG° [kJ/mol]

Compound	Groups	frequency ($\sigma_{internal}$)	300 - 600 K A	300 - 600 K B	600 - 1500 K A	600 - 1500 K B
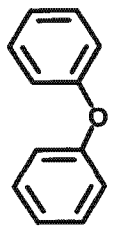	—O—	1	-18.37	8.00E-03	-16.07	4.00E-03
	=C<	2	4.675	1.15E-02	5.01	9.88E-03
	=CH—	10	3.047	6.15E-03	2.505	7.06E-03
	6-C ring	2	-1.128	-1.64E-02	-1.93	-1.50E-02
	+R Ln σ_{ext}	(2)	0	1.38E-03	0	1.38E-03
			19.194	**6.118E-02**	**15.140**	**6.566E-02**

156.6 ΔG° [kJ/mol]

Compound	Groups	frequency ($\sigma_{internal}$)	300 - 600 K A	300 - 600 K B	600 - 1500 K A	600 - 1500 K B
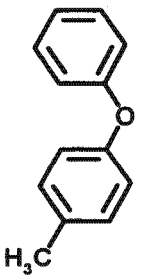	—O—	1	-18.37	8.00E-03	-16.07	4.00E-03
	—CH_3	1	-10.943	2.22E-02	-12.31	2.44E-02
	=C<	3	4.675	1.15E-02	5.01	9.88E-03
	=CH—	9	3.047	6.15E-03	2.505	7.06E-03
	6-C ring	2	-1.128	-1.64E-02	-1.93	-1.50E-02
	+R Ln σ_{ext}	(1)	0	0.00E+00	0	0.00E+00
			9.879	**8.730E-02**	**5.335**	**9.146E-02**

150.2 ΔG° [kJ/mol]

APPENDIX I.2

Compound	Groups	frequency ($\sigma_{internal}$)	300 - 600 K A	300 - 600 K B	600 - 1500 K A	600 - 1500 K B
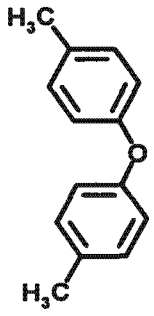	—O—	1	-18.37	8.00E-03	-16.07	4.00E-03
	—CH_3	2	-10.943	2.22E-02	-12.31	2.44E-02
	=C<	4	4.675	1.15E-02	5.01	9.88E-03
	=CH—	8	3.047	6.15E-03	2.505	7.06E-03
	6-C ring	2	-1.128	-1.64E-02	-1.93	-1.50E-02
	+R Ln σ_{ext}	(2)	0	1.38E-03	0	1.38E-03
			0.564	**1.162E-01**	**-4.470**	**1.200E-01**

147.2 ΔG° [kJ/mol]

APPENDIX I.3

Estimation of thermodynamic properties using Benson's method (Reid et al, 1987).

	Group	frequency / sigma	ΔH_f°/unit [kJ/gmol]	S_f°/unit [J/gmol.K]	Cp [J/gmol.K] 300	400	500	600	800	1000
CH_3OH (MeOH)	O-(C)(H)	1	-158.68	121.71	18.13	18.63	20.18	21.9	25.2	27.67
	$C-(O)(H)_3$	1	-42.29	127.32	25.92	32.82	39.36	45.18	54.55	61.84
	.+R Ln (σ)	3		-9.13						
				249.03						
	Σ =		-200.97	239.90	44.05	51.45	59.54	67.08	79.75	89.51
	ΔG°_f [kJ/mol]		-162.49	-129.12	-128.8	-114.0	-98.3	-82.2	-50.4	-20.8
					-200.9	-195.7	-188.9	-180.7	-160.9	-138.1
					-162.2	-150.1	-139.8	-131.4	-120.6	-117.4

249.90 - 9.13 =

$\Delta S_f = S^\circ_{MeOH} - \Sigma S^\circ_e$

← ΔS_f° [J/mol.K]
← ΔH_f° [kJ/mol]
← ΔG_f° [kJ/mol]

	Group	frequency / sigma	ΔH_f°/unit [kJ/gmol]	S_f°/unit [J/gmol.K]	Cp [J/gmol.K] 300	400	500	600	800	1000
 (Ph)	O-(C_B)(H)	1	-158.68	121.84	18.00	18.84	20.1	21.77	25.12	27.63
	C_B-(O)	1	-3.77	-42.71	16.33	22.19	25.96	27.63	28.89	28.89
	C_B-(H)	5	13.82	48.27	13.57	18.59	22.86	26.38	31.57	35.21
	.+R Ln (σ)	2		-5.76						
				320.48						
	Σ =		-93.35	314.72	102.1798	133.98	160.36	181.3	211.86	232.57
			-29.59	-213.96	-213.3	-174.5	-131.0	-87.1	-4.7	67.6
					-93.1	-79.7	-61.0	-38.6	13.0	69.9
					-29.2	-9.9	4.5	13.6	16.8	2.3

← ΔS_f° [J/mol.K]
← ΔH_f° [kJ/mol]
← ΔG_f° [kJ/mol]

APPENDIX I.3

(PC)

Group	frequency / sigma	ΔH_f°/unit [kJ/gmol]	S_f°/unit [J/gmol.K]	Cp [J/gmol.K] 300	400	500	600	800	1000
				guessed value					
O-(C_B)(H)	1	-158.68	121.84	18.00	18.84	20.1	21.77	25.12	27.63
C_B-(O)	1	-3.77	-42.71	16.33	22.19	25.96	27.63	28.89	28.89
C_B-(H)	4	13.82	48.27	13.57	18.59	22.86	26.38	31.57	35.21
C_B-(C)	1	23.07	-32.2	11.18	13.15	15.41	17.38	20.77	22.78
C-(C_B)$(H)_3$	1	-42.2	127.32	25.92	32.82	39.36	45.18	54.51	61.84
.-R Ln (σ)	6		-14.90						
			367.38						
Σ =		**-126.3**	**352.43**	**125.7098**	**161.36**	**192.27**	**217.48**	**255.57**	**281.98**
		-33.15	-312.58	-311.7	-265.1	-213.1	-160.4	-60.2	28.8 ← ΔS_f° [J/mol.K]
				-126.0	-109.8	-87.5	-60.6	2.0	71.6 ← ΔH_f° [kJ/mol]
				-32.5	-3.8	19.1	35.6	50.2	42.9 ← ΔG_f° [kJ/mol]

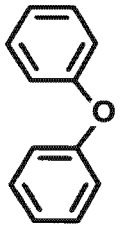

(DPE)

Group	frequency / sigma	ΔH_f°/unit [kJ/gmol]	S_f°/unit [J/gmol.K]	Cp [J/gmol.K] 300	400	500	600	800	1000
O-(C_B)$_2$	1	-88.34	30.7	4.56	5.11	6.28	8.33	11.93	14.7
C_B-(O)	2	-3.77	-42.71	16.33	22.19	25.96	27.63	28.89	28.89
C_B-(H)	10	13.82	48.27	13.57	18.59	22.86	26.38	31.57	35.21
Ether O	1	1.3	0	-0.42	-3.73	-4.61	-3.06	-2.51	-0.96
.-R Ln (σ)	4		-11.53						
			427.98						
Σ =		**43.62**	**416.45**	**172.5**	**231.66**	**282.19**	**324.33**	**382.9**	**423.62**
		165.00	-407.30	-406.1	-339.1	-261.3	-180.3	-29.2	105.6 ← ΔS_f° [J/mol.K]
				44.0	67.2	100.6	141.6	235.8	341.0 ← ΔH_f° [kJ/mol]
				165.8	202.9	231.3	249.8	259.2	235.4 ← ΔG_f° [kJ/mol]

APPENDIX I.3

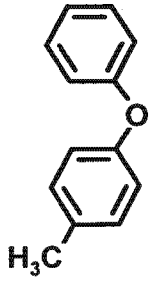

(PPT)

Group	frequency / sigma	ΔH_f°/unit [kJ/gmol]	S_f°/unit [J/gmol.K]	Cp [J/gmol.K] 300	400	500	600	800	1000
$O-(C_B)_2$	1	-88.34	30.7	4.56	5.11	6.28	8.33	11.93	14.7
$C_B-(O)$	2	-3.77	-42.71	16.33	22.19	25.96	27.63	28.89	28.89
$C_B-(H)$	9	13.82	48.27	13.57	18.59	22.86	26.38	31.57	35.21
$C_B-(C)$	1	23.07	-32.2	11.18	13.15	15.41	17.38	20.77	22.78
$C-(C_B)(H)_3$	1	-42.2	127.32	25.92	32.82	39.36	45.18	54.51	61.84
Ether O	1	1.3	0	-0.42	-3.73	-4.61	-3.06	-2.51	-0.96
-R Ln (σ)	3		-9.13						
			474.83						
Σ =		**10.67**	**465.70**	**196.03**	**259.04**	**314.1**	**360.51**	**426.61**	**473.03**
		158.12	-494.79	-493.5	-418.5	-332.2	-242.5	-73.5	77.9
				11.1	37.1	74.1	119.5	224.8	342.7
				159.1	204.5	240.2	265.0	283.6	264.9

← ΔS_f° [J/mol.K]
← ΔH_f° [kJ/mol]
← ΔG_f° [kJ/mol]

APPENDIX I.3

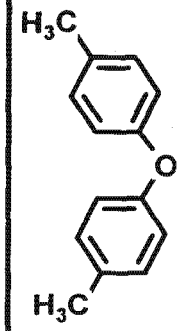

(PTE)

Group	frequency / sigma	ΔH_f°/unit [kJ/gmol]	S_f°/unit [J/gmol.K]	Cp [J/gmol.K] 300	400	500	600	800	1000
$O-(C_B)_2$	1	-88.34	30.7	4.56	5.11	6.28	8.33	11.93	14.7
$C_B-(O)$	2	-3.77	-42.71	16.33	22.19	25.96	27.63	28.89	28.89
$C_B-(H)$	8	13.82	48.27	13.57	18.59	22.86	26.38	31.57	35.21
$C_B-(C)$	2	23.07	-32.2	11.18	13.15	15.41	17.38	20.77	22.78
$C-(C_B)(H)_3$	2	-42.2	127.32	25.92	32.82	39.36	45.18	54.51	61.84
Ether O	1	1.3	0	-0.42	-3.73	-4.61	-3.06	-2.51	-0.96
			521.68						
.+R Ln (σ)	18		-24.03						
Σ =		**-22.28**	**497.65**	**219.56**	**286.42**	**346.01**	**396.69**	**470.32**	**522.44**
		156.28	-599.18	-597.7	-514.9	-420.1	-321.6	-134.7	33.3
				-21.8	6.9	47.6	97.5	213.8	344.5
				157.5	212.9	257.7	290.5	321.6	311.2

← ΔS_f° [J/mol.K]
← ΔH_f° [kJ/mol]
← ΔG_f° [kJ/mol]

APPENDIX I.4

Estimation of the thermodynamic properties using Joback's method (Reid et. al., 1987).

Compound	Group	frequency	Δ_H	Δ_G	Δ_a	Δ_b	Δ_c	Δ_d
			kJ/mol	kJ/mol	Cp [J/mol.K]			
CH_3OH	H_3C-	1	-76.45	-43.96	19.5	-8.08E-03	1.53E-04	-9.67E-08
	$-OH$	1	-208.04	-189.2	25.7	-6.91E-02	1.77E-04	-9.88E-08
			-216.2	**-179.28**	**7.27**	**1.33E-01**	**-6.10E-05**	**1.05E-08**
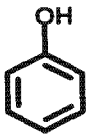	$=CH-$	5	2.09	11.3	-2.14	5.74E-02	-1.64E-06	-1.59E-08
	$=C<$	1	46.43	54.05	-8.25	0.101	-1.42E-04	6.78E-08
	$-OH$	1	-221.65	-197.37	-2.81	0.111	-1.16E-04	4.94E-08
			-96.48	**-32.94**	**-59.69**	**7.09E-01**	**-6.57E-04**	**2.44E-07**
	$-CH_3$	1	-76.45	-43.96	19.5	-8.08E-03	1.53E-04	-9.67E-08
	$=CH-$	4	2.09	11.3	-2.14	5.74E-02	-1.64E-06	-1.59E-08
	$=C<$	2	46.43	54.05	-8.25	0.101	-1.42E-04	6.78E-08
	$-OH$	1	-221.65	-197.37	-2.81	0.111	-1.16E-04	4.94E-08
			-128.59	**-34.15**	**-46.3**	**7.45E-01**	**-6.45E-04**	**2.31E-07**
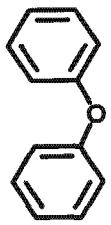	$=CH-$	10	2.09	11.3	-2.14	5.74E-02	-1.64E-06	-1.59E-08
	$=C<$	2	46.43	54.05	-8.25	0.101	-1.42E-04	6.78E-08
	$-O-$	1	-132.22	-105	2.55E+01	-6.32E-02	1.11E-04	-5.48E-08
			49.83	**169.98**	**-50.33**	**9.23E-01**	**-5.80E-04**	**1.28E-07**
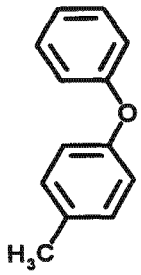	$=CH-$	9	2.09	11.3	-2.14	5.74E-02	-1.64E-06	-1.59E-08
	$=C<$	3	46.43	54.05	-8.25	0.101	-1.42E-04	6.78E-08
	$-O-$	1	-132.22	-105	2.55E+01	-6.32E-02	1.11E-04	-5.48E-08
	$-CH_3$	1	-76.45	-43.96	19.5	-8.08E-03	1.53E-04	-9.67E-08
			17.72	**168.77**	**-36.94**	**9.58E-01**	**-5.68E-04**	**1.15E-07**
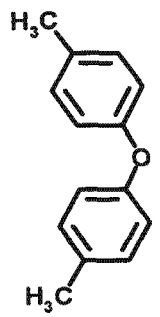	$=CH-$	8	2.09	11.3	-2.14	5.74E-02	-1.64E-06	-1.59E-08
	$=C<$	4	46.43	54.05	-8.25	0.101	-1.42E-04	6.78E-08
	$-O-$	1	-132.22	-105	2.55E+01	-6.32E-02	1.11E-04	-5.48E-08
	$-CH_3$	2	-76.45	-43.96	19.5	-8.08E-03	1.53E-04	-9.67E-08
			-14.39	**167.56**	**-23.55**	**9.94E-01**	**-5.55E-04**	**1.02E-07**

APPENDIX I.5

Estimation of the thermodynamic properties using Yoneda's method (Reid et. al., 1987).

Compound	Group	Operation	Δ_H	Δ_S	Δ_a	Δ_b	Δ_c
			kJ/mol	J/mol	Cp [J/mol.K]		
CH_3OH	CH_4	Base	-74.9	186.31	16.71	65.65	-9.96
	+ [—CH_3]	Primary methyl substitution	-9.84	43.33	-9.92	103.87	-43.54
	+ [—OH]	Replacing CH_3 group	-119.07	8.62	7.29	-65.73	24.45
		Correction for type-number and multiple substitution	-11.1	0.84	0.42	0	-0.42
			-214.91	239.1			
				-286.162			
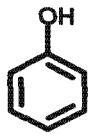			82.98	269.38	-22.52	402.81	-171.53
	+ [—CH_3]	Primary methyl substitution	-35.5	47.94	5.78	64.68	-19.51
	+ [—OH]	Replacing CH_3 group	-146.58	-1.26	12.02	-49.82	24.28
		Correction for type-number and multiple substitution	-11.1	0.84	0.42	0	-0.42
			-132.4	318.58			
				-227.337			
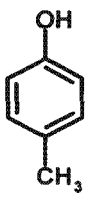			82.98	269.38	-22.52	402.81	-171.53
	+ [—CH_3]	Primary methyl substitution	-35.5	47.94	5.78	64.68	-19.51
	+ [—CH_3]	Secondary methyl substitution	-28.72	36.22	5.48	60.33	-16.16
	+ [—OH]	Replacing CH_3 group	-146.58	-1.26	12.02	-49.82	24.28
		Correction for type-number and multiple substitution	-11.1	0.84	0.42	0	-0.42
			-161.12	354.8			
				-266.85			

APPENDIX II

Thermo-Gravimetric Analysis

Thermo-Gravimetric Analysis

II.1 TGA for H-Beta-25 – Heating rate = 10 °C/min

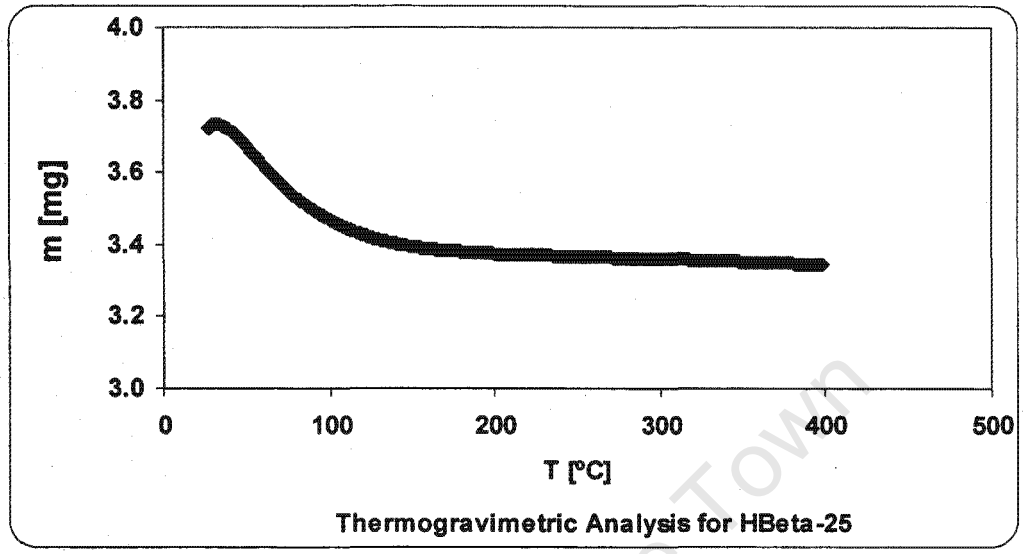

Thermogravimetric Analysis for HBeta-25

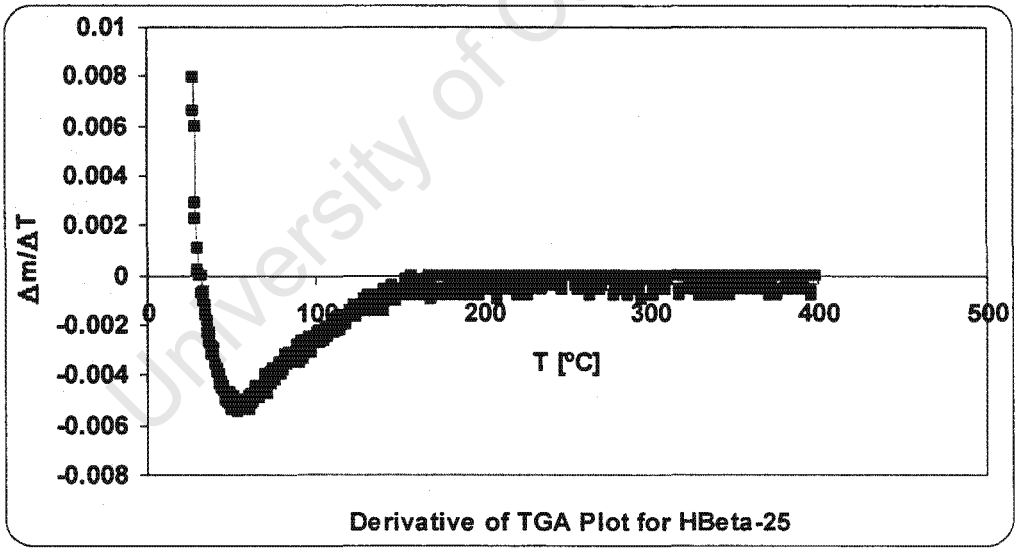

Derivative of TGA Plot for HBeta-25

Thermo-Gravimetric Analysis

II.3 TGA for H-USY – Heating rate = 10 °C/min

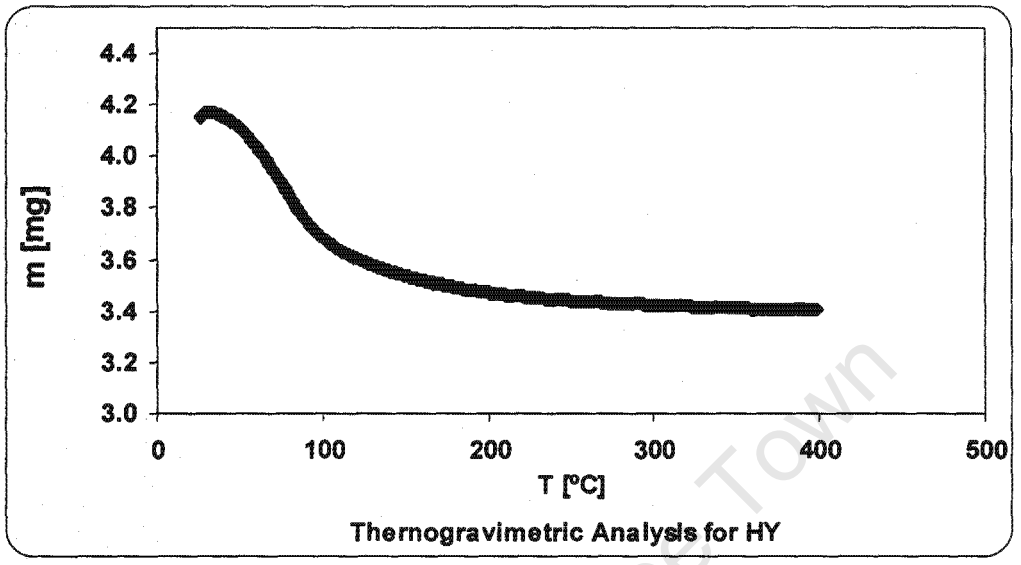

Thernogravimetric Analysis for HY

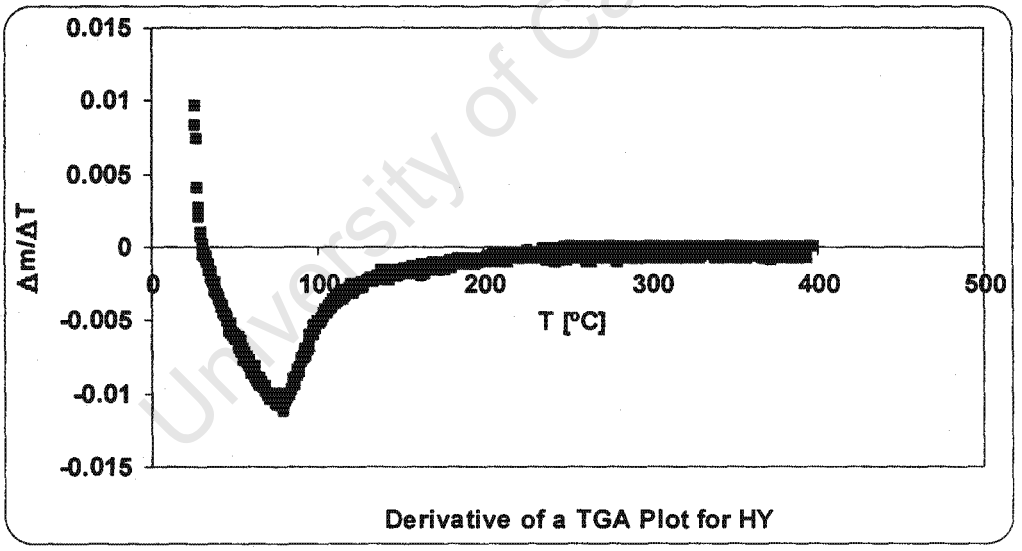

Derivative of a TGA Plot for HY

Thermo-Gravimetric Analysis

II.4 TGA for H-Mor-40 – Heating rate = 10 °C/min

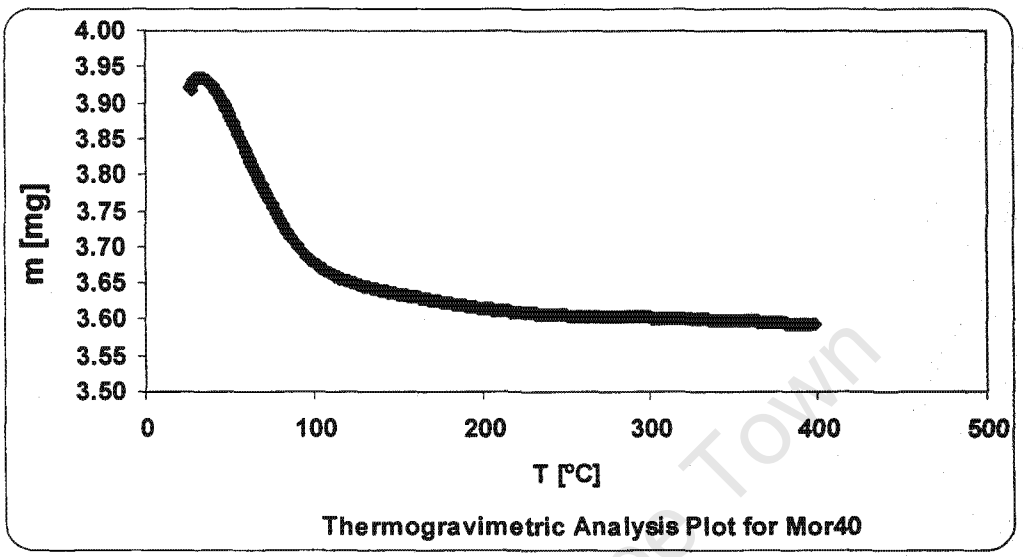

Thermogravimetric Analysis Plot for Mor40

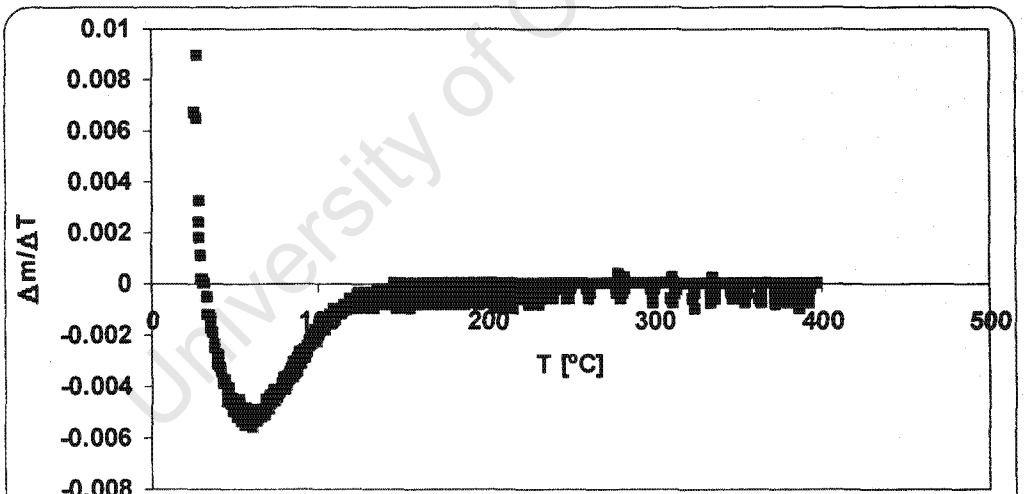

Derivative of a TGA Plot for Mor40

Thermo-Gravimetric Analysis

II.5 TGA for CBV21A – Heating rate = 2 °C/min

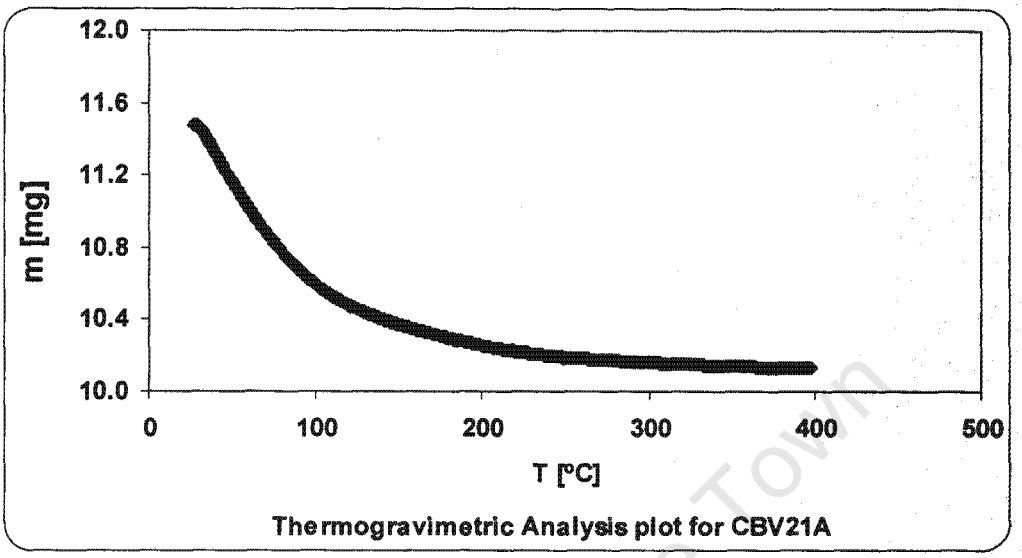

Thermogravimetric Analysis plot for CBV21A

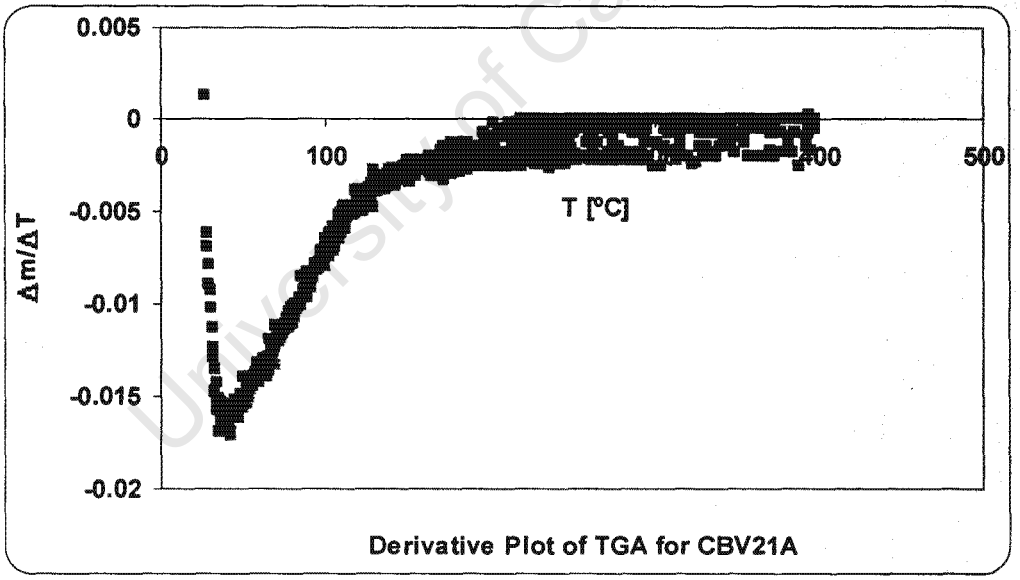

Derivative Plot of TGA for CBV21A

Thermo-Gravimetric Analysis

II.6 TGA for CBV21A – Heating rate = 40 °C/min

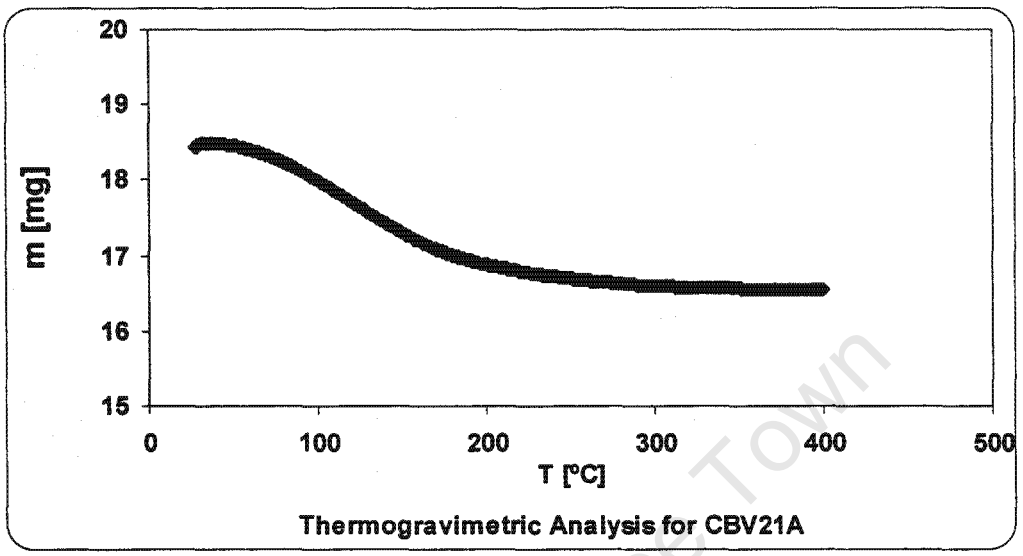

Thermogravimetric Analysis for CBV21A

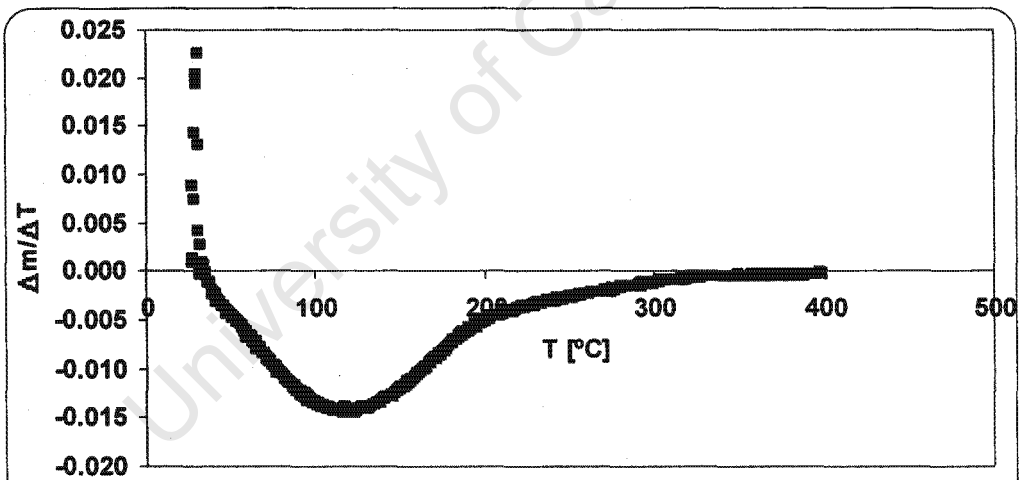

Derivative of TGA Plot for CBV21A

APPENDIX III

Calibration Data for the Pump and the Mass Flow Controllers

APPENDIX III.1

Carrier Gas Flow Rate

Set Flow	Avg |dV/dt|
4	0.87
9	2.04
17	3.94
29	6.92
43	10.30
57	13.72
70	17.13
91	23.33

Liquid Feed Rate

Pump Setting	F [ml/min]
0.50	0.52
1.00	1.03
1.50	1.53
2.00	2.03
3.50	3.58
4.00	4.10
4.50	4.61
5.00	5.09

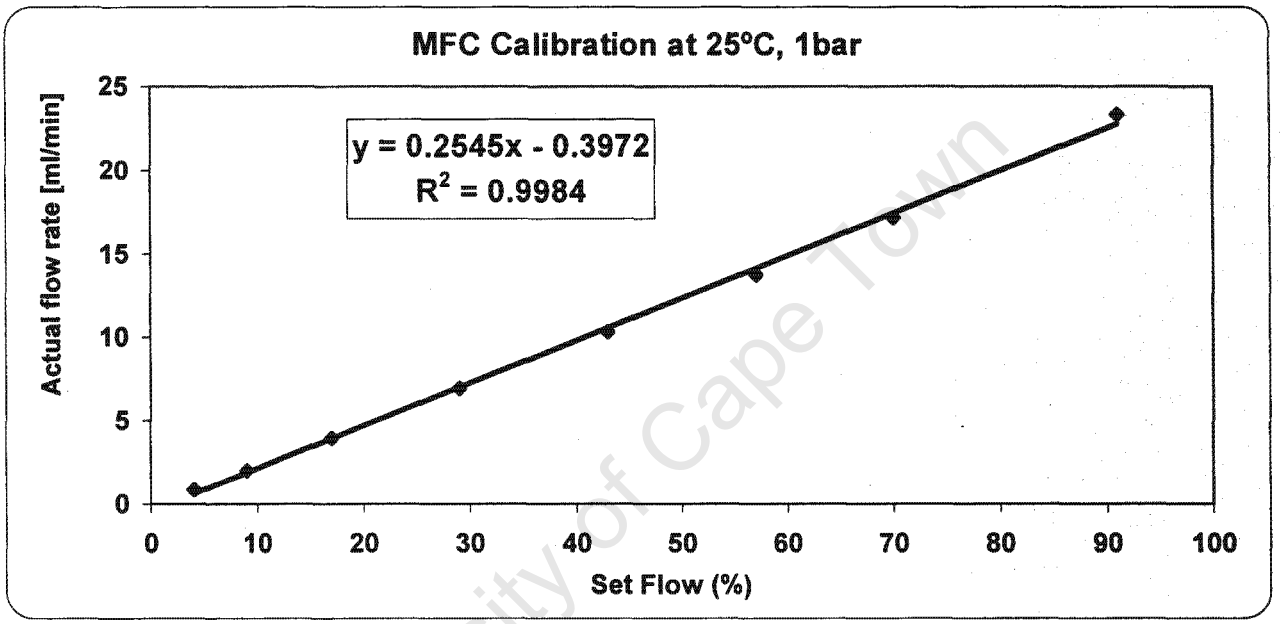

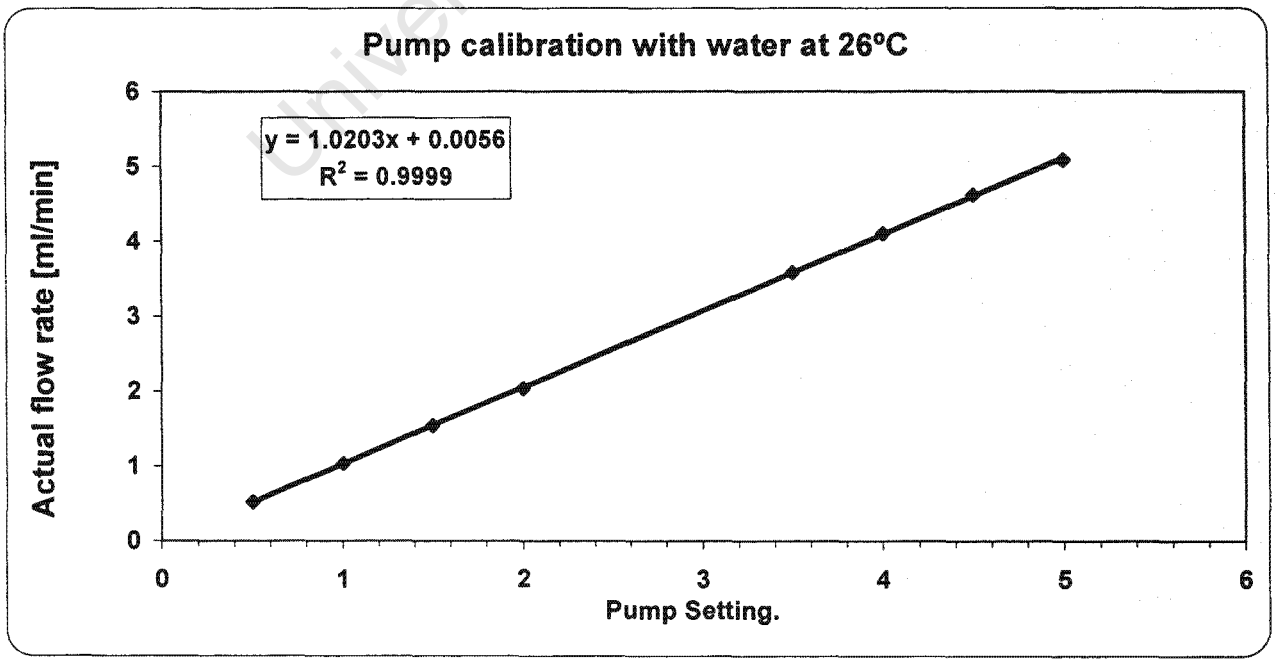

APPENDIX IV

Experimental Calculations

Pure Component Vapour Pressure Variation with Temperature

APPENDIX IV.1

Experimental Calculations

Density constants

	MM	A	B	C	D
MeOH	32.042	2.308	0.27192	5.13E+02	0.2331
DPE	170.211	0.5564	0.276	7.63E+02	0.2666

T_{Room} [°C] = 25

ρ_{MeOH} [mol/dm^3] = 24.6

ρ_{DPE} [mol/dm^3] = 6.23

m_{Cat} [g] = 3

$$\rho = \frac{A}{B^{\left[1+\left(1-\frac{T}{C}\right)^{D}\right]}}$$

ρ in $\frac{mols}{L}$

T in K

Base Case.

V_{pump} =	0.04	mL mix / min	
MFR =	2	Mols MeOH / Mols DPE	
x_{DPE} =	0.333	mol DPE / mol mix	
$V_{mixture}$ =	0.08	L mix / mol mix	
Φ_{DPE} =	0.664	L DPE / L mixture	
Φ_{MeOH} =	0.336	L MeOH / L mixture	
V_{DPE} =	0.03	mL/min	
V_{MeOH} =	0.013	mL/min	
n_{DPE} =	0.165	mmol/min	
n_{MeOH} =	0.33	mmol/min	
P_{DPE} =	1.5	bar	
P_{MeOH} =	3	bar	
P_T =	6	bar	0.667
P_{N2} =	1.5	bar	0.496
n_{N2} =	0.165	mmol/min	0.238056
V_{N2} =	4.043	mL/min	
m_{DPE} =	0.03	g/min	
WHSV =	0.56	g DPE/g Zeo/hr	
MFC =	17.5	% Old	
22/05/02	17.3	% New	

Case 1

V_{pump} =	0.05	mL mix / min	
MFR =	4	Mols MeOH / Mols DPE	
x_{DPE} =	0.200	mol DPE / mol mix	
$V_{mixture}$ =	0.06	L mix / mol mix	
Φ_{DPE} =	0.497	L DPE / L mixture	
Φ_{MeOH} =	0.503	L MeOH / L mixture	
V_{DPE} =	0.02	mL/min	
V_{MeOH} =	0.025	mL/min	
n_{DPE} =	0.155	mmol/min	
n_{MeOH} =	0.62	mmol/min	
P_{DPE} =	5	bar	
P_{MeOH} =	13.4	bar	
P_T =	20	bar	
P_{N2} =	1.6	bar	0.08
n_{N2} =	0.049	mmol/min	
V_{N2} =	1.210	mL/min	
m_{DPE} =	0.03	g/min	
WHSV =	0.53	g DPE/g Zeo/hr	
MFC =	6.4	% Old	
22/05/02	5.0	% New	

Case 2

V_{pump} =	0.03	mL mix / min	
MFR =	0.5	Mols MeOH / Mols DPE	
x_{DPE} =	0.667	mol DPE / mol mix	
$V_{mixture}$ =	0.12	L mix / mol mix	
Φ_{DPE} =	0.888	L DPE / L mixture	
Φ_{MeOH} =	0.112	L MeOH / L mixture	
V_{DPE} =	0.03	mL/min	
V_{MeOH} =	0.003	mL/min	
n_{DPE} =	0.166	mmol/min	
n_{MeOH} =	0.08	mmol/min	
P_{DPE} =	1.5	bar	
P_{MeOH} =	0.75	bar	
P_T =	6	bar	
P_{N2} =	3.75	bar	
n_{N2} =	0.415	mmol/min	
V_{N2} =	10.140	mL/min	
m_{DPE} =	0.03	g/min	
WHSV =	0.56	g DPE/g Zeo/hr	
MFC =	41.4	% Old	
22/05/02	43.8	% New	

APPENDIX IV.2

Pure component vapour pressure variation with temperature.

Antoine's constants (Sinnot, 1999)

	PhOH	MeOH	DPE	p-Cresol	Water
A	16.4279	18.5875	16.3459	16.1989	18.3036
B	3490.89	3626.55	4310.25	3479.39	3816.44
C	-96.59	-34.29	-87.31	-111.3	-46.13

T [°C]	T [K]	P_{Ph} [atm]	P_{MeOH} [atm]	P_{DPE} [atm]	P_{PC} [atm]	P_{Water} [atm]
150	423	0.41	13.80	0.04	0.20	4.68
160	433	0.56	17.43	0.06	0.29	6.08
170	443	0.75	21.78	0.09	0.40	7.80
180	453	1.00	26.92	0.13	0.54	9.88
190	463	1.31	32.95	0.17	0.72	12.37
200	473	1.68	39.96	0.23	0.95	15.33
210	483	2.14	48.04	0.31	1.23	18.81
220	493	2.69	57.29	0.40	1.57	22.87
230	503	3.34	67.82	0.52	1.98	27.57
240	513	4.10	79.72	0.66	2.47	32.98
250	523	4.99	93.09	0.83	3.05	39.14
260	533	6.02	108.02	1.04	3.72	46.13
270	543	7.20	124.62	1.29	4.51	54.02
280	553	8.55	142.98	1.58	5.41	62.86
290	563	10.07	163.19	1.92	6.44	72.71
300	573	11.79	185.35	2.31	7.61	83.65
310	583	13.70	209.55	2.77	8.93	95.74
320	593	15.84	235.86	3.28	10.41	109.03
330	603	18.20	264.38	3.87	12.05	123.58
340	613	20.79	295.18	4.54	13.88	139.46
350	623	23.64	328.33	5.29	15.89	156.73
360	633	26.75	363.91	6.13	18.11	175.43
370	643	30.14	401.99	7.07	20.53	195.62
380	653	33.81	442.62	8.11	23.16	217.36
390	663	37.77	485.87	9.26	26.02	240.69
400	673	42.03	531.79	10.52	29.11	265.65
410	683	46.60	580.44	11.90	32.44	292.30
420	693	51.49	631.85	13.41	36.02	320.67
430	703	56.71	686.07	15.06	39.86	350.81
440	713	62.26	743.14	16.84	43.95	382.74
450	723	68.15	803.09	18.77	48.30	416.51
460	733	74.39	865.95	20.85	52.93	452.15
470	743	80.98	931.75	23.08	57.84	489.67
480	753	87.92	1000.51	25.48	63.02	529.12
490	763	95.22	1072.25	28.04	68.49	570.51
500	773	102.89	1146.97	30.77	74.24	613.86
510	783	110.93	1224.70	33.68	80.29	659.20

$$\ln(P^{vap}) = A - \frac{B}{T + C}$$

P^{vap} in mm Hg

T in K

APPENDIX V

Summary of Catalyst Loads

APPENDIX V.1 **Summary of catalyst loads**

Catalyst (Load No.)	Number of Experiments	Form	m_{Total} [g]	$m_{wet\_zeolite}$ [g]	w_{H2O} [d]	$m_{dry\_zeolite}$ [c] [g]	V_{SiC_Top} [ml]	V_{SiC_Bottom} [ml]	$V_{SiC\_Diluent}$ [ml]	$V_{SiC,Total}$ [ml]
H-beta (L1)	15	Powder	3.31	3.31	0.10	2.99	15.0	8.0	20.0	43
H-beta (L2)[d]										
H-beta (L3)[d]										
H-beta (L4)	5	Powder	3.32	3.32	0.10	3.00	2.5	11.0	10.0	24
MFI 50 (L1)	1	Powder	3.31	3.31	0.04	3.19	6.2	10.0	10.2	26
Mor 40 (L1)	1	Powder	3.26	3.26	0.08	2.99	7.0	7.0	10.5	25
CBV21A (L1)	1	Extrudates	4.39[a]	3.51	0.10	3.16	6.0	8.0	10.0	24
CBV21A (L2)	1	Extrudates	4.17[a]	3.34	0.10	3.00	7.0	12.0	10.5	30
CBV21A (L3)	3	Extrudates	4.18[a]	3.34	0.10	3.01	8.5	11.5	9.5	30
CBV90A (L1)	15	Extrudates	4.05[a]	3.24	0.07	3.01	5.5	14.0	10.5	30
HUSY (L1)	1	Powder	3.31	3.31	0.18	2.72	7.0	5.0	10.0	22

a) Based on assumption that extrudates have 20% by mass binder

b) $m_{wet\_zeolite} = m_{Total} * 0.8$

c) $m_{dry\_zeolite} = m_{wet\_zeolite} * (1 - w_{H2O})$ w_{H2O} was obtained from TGA data

d) Mass fraction of water in the wet zeolite sample

d) Abandoned due to experimental difficulties

APPENDIX VI

Data for Reactor Temperature Profiles and the Heating Rate of the Reactor

APPENDIX VI.2

Heating rate of the reactor

ΔT/Δt @ L=90mm		ΔT/Δt @ L=50mm		ΔT/Δt @ L=110mm		ΔT/Δt @ L=70mm	
t [min]	T1	t [min]	T2	t [min]	T3	t [min]	T4
0	69	0.0	45	0.0	22	0.0	30
1.6	75	0.2	50	1.5	25	1.7	35
2.1	80	0.4	55	3.1	30	2.2	40
2.5	85	0.5	60	4.1	35	2.9	50
2.8	90	0.7	65	5.0	40	3.5	60
3.1	95	0.8	70	5.7	45	4.0	70
3.3	100	0.9	75	6.4	50	4.5	80
3.5	105	1.1	80	7.1	55	4.9	90
3.7	110	1.2	85	7.7	60	5.4	100
3.9	115	1.4	90	8.2	65	5.8	110
4.1	120	1.6	100	8.7	70	6.3	120
4.3	125	1.7	105	9.2	75	6.7	130
4.5	130	1.8	110	9.6	80	7.2	140
4.7	135	2.0	120	10.0	85	7.7	150
4.8	140	2.0	125	10.5	90	8.2	160
5.0	145	2.2	130	11.3	100	8.8	170
5.2	150	2.3	135	12.1	110	9.3	180
5.3	155	2.4	140	12.8	120	9.9	190
5.5	160	2.5	145	13.4	130	10.5	200
5.7	165	2.6	150	14.1	140	11.2	210
5.9	170	2.7	155	14.7	150	11.9	220
6.0	175	2.8	160	15.4	160	12.7	230
6.2	180	3.0	170	15.9	170	13.6	240
6.3	185	3.3	180	16.5	180	14.6	250
6.5	190	3.5	190	17.1	190	15.9	260
6.7	195	3.7	200	17.7	200	17.6	270
6.9	200	4.0	210	18.3	210	19.9	280
7.0	205	4.1	215	18.9	220	24.7	290
7.2	210	4.2	220	19.5	230		
7.4	215	4.4	230	20.3	240		
7.6	220	4.7	240	21.2	250		
8.0	230	4.9	250	22.3	260		
8.2	235	5.2	260	24.0	270		
8.5	240	5.5	270	26.9	280		
8.7	245	5.8	280	30.3	285		
8.9	250	6.1	290				
9.1	255	6.5	300				
9.3	260	6.8	310				
9.6	265	7.2	320				
9.8	270	7.6	330				
10.0	275	8.0	340				
10.3	280	8.4	350				
10.5	285	8.9	360				
10.7	290	9.4	370				
11.0	295	9.9	380				
11.2	300	10.6	390				
11.4	305	11.2	400				
11.7	310	12.0	410				
11.9	315	12.9	420				
12.1	320	13.9	430				
12.3	325	15.2	440				
12.4	330	16.6	450				
12.8	335	17.5	455				
13.1	340	18.5	460				
13.4	345	19.5	465				
13.7	350	20.5	470				
14.0	355	21.6	475				
14.3	360	22.7	480				
14.6	365	24.3	485				
15.0	370	27.2	490				
15.4	375	35.0	495				
15.7	380	40.1	499				
16.1	385						
16.5	390						
16.9	395						
17.4	400						
17.9	405						
18.4	410						
19.0	415						
19.6	420						
20.2	425						
20.9	430						
21.7	435						
22.6	440						
23.5	445						
24.5	450						
25.6	455						
26.7	460						
27.9	465						
29.2	470						
30.3	475						
31.5	480						
32.7	485						
34.6	490						
36.9	495						
40.0	500						

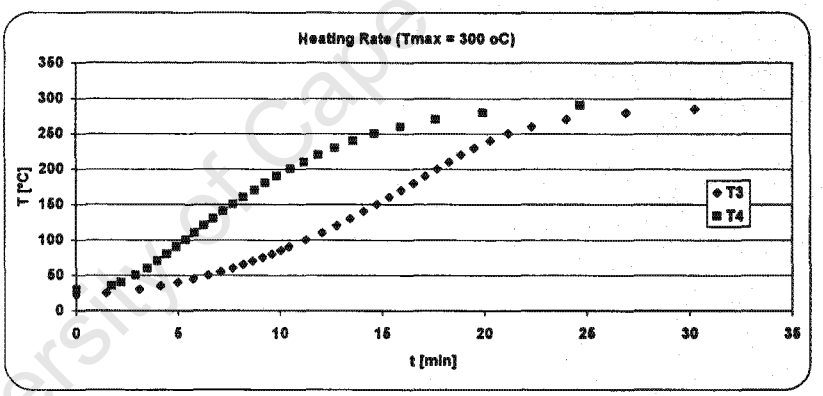

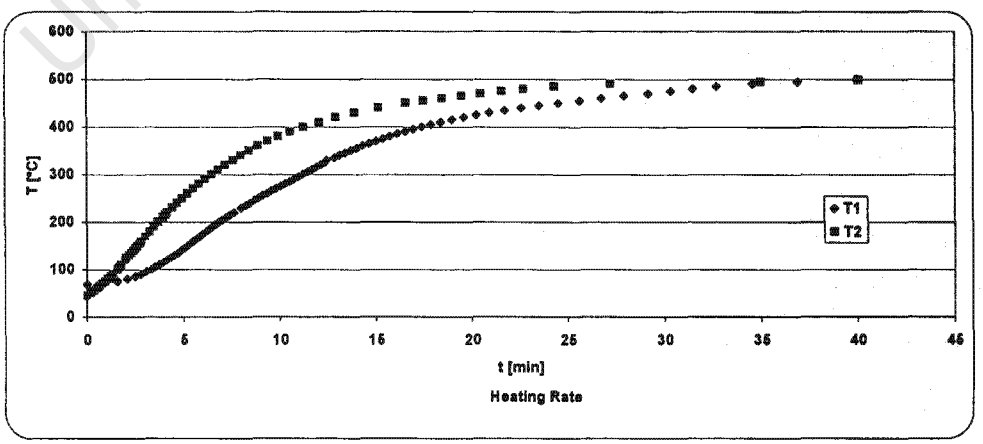

APPENDIX VI.1 **Data for reactor temperature profile**

Exp 1	13/02/02	Exp 1	13/02/02	Exp 2	19/02/02	Exp4	26/02/02	Exp X	18/04/02
L [mm]	Ta	L [mm]	Tb	L [mm]	T [°C]	L [mm]	T [°C]	L [mm]	T [°C]
0	299	0	300	0	255	0	253	0	255
10	299	20	300	20	253	10	251	20	253
20	299	40	300	40	252	20	251	40	251
30	300	60	300	60	252	40	251	60	251
40	301	80	300	80	253	60	251	80	250
50	301	90	300	100	253	80	251	100	250
60	302	100	301	120	251	100	251	110	249
70	302	110	301	130	249	110	251	120	248
80	302	120	301	140	248	120	250	130	247
90	302	130	301	150	244	130	249	140	245
100	302	140	300	160	241	140	248	150	243
110	301	150	299	170	237	150	245	160	239
120	300	160	297	180	231	160	242	170	233
130	297	170	293	190	225	170	238	180	225
140	295	180	287	200	217	180	232		
150	292	190	279			190	226		
160	287	200	270			200	220		
170	283	210	264			210	216		
180	276	220	261			220	213		
190	268	230	256			230	210		
200	258	240	253			240	207		
210	252	250	248			250	205		
220	248	260	244			260	202		
230	243	270	235			270	197		
240	238	280	223			280	194		

Exp X	28/04/02	Exp X	2002/03/06	Exp X	14/06/02	Exp4	26/06/02	Exp4	27/06/02
L [mm]	T [°C]	L [mm]	Td	L [mm]	Te	L [mm]	Tf [°C]	L [mm]	Tg [°C]
0	255	0	251	0	202	0	250	0	249
20	253	10	250	10	201	10	250	10	249
40	252	20	249	20	200	20	250	20	249
60	252	30	249	30	200	30	249	30	249
80	252	40	249	40	200	40	249	40	249
100	253	50	249	50	200	50	249	50	249
120	253	60	250	60	200	60	250	60	249
130	252	70	251	70	200	70	250	70	249
140	251	80	251	80	200	80	251	80	249
150	249	90	251	90	201	90	251	90	250
160	247	100	253	100	201	100	251	100	250
170	243	110	252	110	201	110	251	110	250
180	236	120	252	120	201	120	251	120	251
190	226	130	251	130	201	130	251	130	251
200	215	140	250	140	200	140	249	140	251
210	207	150	248	150	199	150	248	150	249
220	201	160	245	160	197	160	245	160	247
230	195	170	241	170	193	170	239	170	242
240	191	180	233	180	187	180	232	180	235
		190	223	190	180	190	224	190	225
		200	213	200	173	200	213	200	215
		210	206	210	166	210	205		
		220	201	220	161	220	198		
		230	196	230	157				
		240	192	240	154				
		250	187	250	150				

Calcining	########	Calcining	24/7/2002	Calcining	25/7/2002	Exp Y	29/7/2002	Calcining	########
L [mm]	T [°C]	L [mm]	T [°C]	L [mm]	T [°C]	L [mm]	T [°C]	L [mm]	Tc
0	397	0	484	0	479	0	275	0	297
10	400	10	489	10	484	20	275	20	298
20	403	20	494	20	491	40	275	40	300
30	404	30	497	30	496	60	275	60	302
40	404	40	500	40	498	80	275	80	302
50	402	50	501	50	499	100	275	100	302
60	401	60	501	60	500	120	275	120	301
70	400	70	502	70	501	130	276	130	301
80	399	80	502	80	501	140	276	140	299
90	399	90	502	90	501	150	275	150	298
100	399	100	502	100	502	160	272	160	294
110	399	110	502	110	502	180	260	180	281
120	399	120	500	120	502	200	240	200	257
130	400	130	497	130	501				
140	399	140	493	140	499				
150	396	150	487	150	496				
160	388	160	478	160	489				
170	373	170	465	170	478				
180	355			180	464				
190	332			190	443				
200	305			200	420				

APPENDIX VII

Thermodynamic and Dynamic Properties from Molecular Modelling

APPENDIX VII.1

PhOH DMol Estimates

STANDARD THERMODYNAMIC QUANTITIES
computed from 25.00 to 1000.00 in steps of 25.00

	Temperature T (K)	Entropy S (cal/mol.K) (ZPVE is included)	Heat_Capacity Cp	Enthalpy H (kcal/mol)	Free_Energy G
1	25	46.772	7.949	64.329	63.16
2	50	52.304	8.079	64.529	61.914
3	75	55.67	8.639	64.737	60.562
4	100	58.284	9.652	64.965	59.136
5	125	60.579	11.021	65.223	57.65
6	150	62.728	12.637	65.518	56.109
7	175	64.808	14.425	65.856	54.514
8	200	66.859	16.341	66.24	52.869
9	225	68.898	18.345	66.674	51.172
10	250	70.937	20.403	67.158	49.424
11	275	72.979	22.48	67.694	47.625
12	298.15	74.873	24.394	68.237	45.913
13	300	75.024	24.546	68.282	45.775
14	325	77.069	26.574	68.921	43.873
15	350	79.111	28.544	69.61	41.921
16	375	81.145	30.439	70.347	39.918
17	400	83.168	32.252	71.131	37.864
18	425	85.176	33.975	71.959	35.76
19	450	87.164	35.608	72.829	33.605
20	475	89.131	37.15	73.739	31.402
21	500	91.074	38.605	74.686	29.149
22	525	92.991	39.976	75.669	26.848
23	550	94.881	41.268	76.684	24.5
24	575	96.743	42.486	77.731	22.104
25	600	98.575	43.635	78.808	19.663
26	625	100.379	44.721	79.913	17.176
27	650	102.153	45.747	81.043	14.644
28	675	103.898	46.72	82.199	12.068
29	700	105.614	47.642	83.379	9.449
30	725	107.301	48.518	84.581	6.788
31	750	108.96	49.351	85.805	4.085
32	775	110.591	50.144	87.048	1.34
33	800	112.195	50.901	88.311	-1.445
34	825	113.773	51.623	89.593	-4.269
35	850	115.324	52.314	90.892	-7.133
36	875	116.85	52.974	92.209	-10.035
37	900	118.351	53.607	93.541	-12.975
38	925	119.829	54.213	94.889	-15.953
39	950	121.282	54.795	96.251	-18.967
40	975	122.713	55.353	97.628	-22.017
41	1000	124.121	55.889	99.019	-25.102

APPENDIX VII.1

DPE DMol Estimates

STANDARD THERMODYNAMIC QUANTITIES
computed from 25.00 to 1000.00 in steps of 25.00

	Temperature T (K)	Entropy S (cal/mol.K) (ZPVE is included)	Heat_Capacity Cp	Enthalpy H (kcal/mol)	Free_Energy G
1	25	53.707	10.257	113.539	112.197
2	50	61.633	12.646	113.828	110.747
3	75	67.11	14.509	114.168	109.135
4	100	71.562	16.597	114.556	107.4
5	125	75.52	19.023	115	105.56
6	150	79.229	21.807	115.51	103.626
7	175	82.821	24.934	116.094	101.6
8	200	86.371	28.358	116.759	99.485
9	225	89.92	32.011	117.513	97.281
10	250	93.488	35.815	118.361	94.989
11	275	97.083	39.69	119.305	92.607
12	298.15	100.435	43.282	120.265	90.321
13	300	100.703	43.568	120.346	90.135
14	325	104.342	47.387	121.483	87.571
15	350	107.991	51.105	122.714	84.917
16	375	111.639	54.686	124.037	82.172
17	400	115.279	58.112	125.447	79.335
18	425	118.901	61.369	126.941	76.408
19	450	122.497	64.454	128.514	73.391
20	475	126.06	67.366	130.162	70.284
21	500	129.586	70.111	131.881	67.088
22	525	133.07	72.696	133.666	63.805
23	550	136.509	75.13	135.515	60.435
24	575	139.899	77.422	137.422	56.98
25	600	143.241	79.583	139.385	53.44
26	625	146.531	81.621	141.4	49.818
27	650	149.77	83.545	143.465	46.114
28	675	152.957	85.366	145.576	42.33
29	700	156.093	87.089	147.732	38.467
30	725	159.178	88.724	149.93	34.526
31	750	162.213	90.276	152.168	30.508
32	775	165.197	91.751	154.443	26.415
33	800	168.132	93.155	156.755	22.249
34	825	171.019	94.493	159.1	18.009
35	850	173.859	95.769	161.479	13.698
36	875	176.653	96.988	163.888	9.317
37	900	179.402	98.152	166.328	4.866
38	925	182.107	99.266	168.795	0.347
39	950	184.768	100.332	171.291	-4.239
40	975	187.388	101.353	173.812	-8.891
41	1000	189.966	102.332	176.358	-13.608

APPENDIX VII.1

MPT DMol Estimates

STANDARD THERMODYNAMIC QUANTITIES
computed from 25.00 to 1000.00 in steps of 25.00

	Temperature T (K)	Entropy S (cal/mol.K) (ZPVE is included)	Heat_Capacity Cp	Enthalpy H (kcal/mol)	Free_Energy G
1	25	55.766	10.799	121.995	120.601
2	50	64.091	13.528	122.299	119.095
3	75	70.133	16.512	122.674	117.414
4	100	75.305	19.606	123.126	115.595
5	125	80.021	22.804	123.655	113.653
6	150	84.474	26.174	124.267	111.596
7	175	88.774	29.746	124.966	109.43
8	200	92.99	33.509	125.756	107.158
9	225	97.162	37.427	126.643	104.781
10	250	101.312	41.447	127.628	102.3
11	275	105.453	45.51	128.715	99.716
12	298.15	109.281	49.261	129.812	97.23
13	300	109.587	49.559	129.904	97.028
14	325	113.712	53.544	131.193	94.236
15	350	117.823	57.423	132.58	91.342
16	375	121.913	61.165	134.063	88.345
17	400	125.976	64.75	135.637	85.247
18	425	130.004	68.166	137.299	82.047
19	450	133.993	71.407	139.044	78.747
20	475	137.937	74.474	140.868	75.348
21	500	141.831	77.371	142.766	71.85
22	525	145.673	80.105	144.735	68.257
23	550	149.46	82.685	146.77	64.567
24	575	153.189	85.119	148.868	60.784
25	600	156.861	87.417	151.025	56.908
26	625	160.474	89.588	153.238	52.941
27	650	164.028	91.643	155.503	48.885
28	675	167.524	93.589	157.819	44.741
29	700	170.961	95.434	160.182	40.509
30	725	174.341	97.186	162.59	36.193
31	750	177.664	98.851	165.04	31.793
32	775	180.931	100.436	167.532	27.31
33	800	184.144	101.946	170.062	22.747
34	825	187.303	103.386	172.628	18.103
35	850	190.41	104.761	175.23	13.382
36	875	193.466	106.074	177.866	8.583
37	900	196.472	107.33	180.534	3.709
38	925	199.429	108.532	183.232	-1.24
39	950	202.339	109.683	185.96	-6.262
40	975	205.202	110.785	188.716	-11.356
41	1000	208.02	111.842	191.499	-16.522

APPENDIX VII.1

OPT DMol Estimates

STANDARD THERMODYNAMIC QUANTITIES
computed from 25.00 to 1000.00 in steps of 25.00

	Temperature T (K)	Entropy S (cal/mol.K) (ZPVE is included)	Heat_Capacity Cp	Enthalpy H (kcal/mol)	Free_Energy G
1	25	53.854	7.975	117.014	115.668
2	50	59.583	8.926	117.222	114.243
3	75	63.607	11.262	117.472	112.701
4	100	67.273	14.504	117.792	111.065
5	125	70.92	18.439	118.203	109.338
6	150	74.67	22.911	118.719	107.518
7	175	78.562	27.759	119.352	105.603
8	200	82.599	32.837	120.109	103.589
9	225	86.765	38.014	120.994	101.472
10	250	91.038	43.184	122.009	99.25
11	275	95.393	48.26	123.153	96.92
12	298.15	99.477	52.82	124.323	94.664
13	300	99.805	53.178	124.421	94.48
14	325	104.249	57.892	125.81	91.929
15	350	108.704	62.375	127.314	89.267
16	375	113.154	66.614	128.927	86.494
17	400	117.582	70.606	130.642	83.61
18	425	121.976	74.356	132.455	80.615
19	450	126.327	77.874	134.358	77.511
20	475	130.626	81.173	136.347	74.299
21	500	134.87	84.267	138.415	70.98
22	525	139.052	87.171	140.558	67.556
23	550	143.171	89.901	142.772	64.028
24	575	147.224	92.469	145.052	60.398
25	600	151.211	94.889	147.394	56.668
26	625	155.132	97.171	149.795	52.838
27	650	158.985	99.328	152.252	48.912
28	675	162.773	101.368	154.761	44.889
29	700	166.494	103.301	157.319	40.773
30	725	170.151	105.133	159.925	36.565
31	750	173.745	106.871	162.575	32.266
32	775	177.277	108.523	165.268	27.879
33	800	180.747	110.094	168.001	23.403
34	825	184.158	111.588	170.772	18.842
35	850	187.51	113.011	173.58	14.196
36	875	190.806	114.366	176.422	9.467
37	900	194.046	115.658	179.297	4.656
38	925	197.232	116.891	182.204	-0.235
39	950	200.365	118.067	185.141	-5.205
40	975	203.446	119.19	188.107	-10.253
41	1000	206.478	120.262	191.101	-15.377

APPENDIX VII.1

PPT DMol Estimates

STANDARD THERMODYNAMIC QUANTITIES
computed from 25.00 to 1000.00 in steps of 25.00

	Temperature T (K)	Entropy S (cal/mol.K) (ZPVE is included)	Heat_Capacity Cp	Enthalpy H (kcal/mol)	Free_Energy G
1	25	55.387	11.079	130.535	129.15
2	50	63.976	13.912	130.849	127.65
3	75	70.124	16.619	131.23	125.971
4	100	75.297	19.524	131.681	124.151
5	125	79.985	22.648	132.208	122.21
6	150	84.407	25.999	132.815	120.154
7	175	88.681	29.582	133.51	117.991
8	200	92.877	33.383	134.296	115.721
9	225	97.037	37.362	135.18	113.347
10	250	101.185	41.464	136.166	110.869
11	275	105.332	45.626	137.254	108.288
12	298.15	109.174	49.481	138.355	105.805
13	300	109.481	49.788	138.447	105.603
14	325	113.629	53.894	139.743	102.814
15	350	117.77	57.902	141.141	99.921
16	375	121.898	61.778	142.637	96.925
17	400	126.005	65.499	144.228	93.826
18	425	130.083	69.052	145.911	90.625
19	450	134.126	72.43	147.679	87.323
20	475	138.129	75.633	149.531	83.919
21	500	142.086	78.664	151.46	80.416
22	525	145.994	81.529	153.462	76.815
23	550	149.85	84.236	155.535	73.117
24	575	153.652	86.794	157.673	69.323
25	600	157.397	89.213	159.873	65.435
26	625	161.086	91.503	162.133	61.454
27	650	164.717	93.672	164.447	57.381
28	675	168.291	95.729	166.815	53.219
29	700	171.808	97.682	169.233	48.967
30	725	175.269	99.539	171.698	44.629
31	750	178.673	101.306	174.209	40.204
32	775	182.023	102.989	176.763	35.695
33	800	185.318	104.594	179.358	31.103
34	825	188.56	106.127	181.992	26.43
35	850	191.75	107.591	184.664	21.676
36	875	194.89	108.992	187.371	16.843
37	900	197.979	110.332	190.113	11.932
38	925	201.02	111.615	192.887	6.944
39	950	204.013	112.845	195.693	1.881
40	975	206.959	114.024	198.529	-3.256
41	1000	209.86	115.155	201.394	-8.466

APPENDIX VII.1

MeOH DMol Estimates

STANDARD THERMODYNAMIC QUANTITIES
computed from 25.00 to 1000.00 in steps of 25.00

	Temperature T (K)	Entropy S (cal/mol.K) (ZPVE is included)	Heat_Capacity Cp	Enthalpy H (kcal/mol)	Free_Energy G
1	25	35.681	7.949	31.604	30.712
2	50	41.195	7.979	31.803	29.743
3	75	44.461	8.174	32.004	28.67
4	100	46.853	8.48	32.212	27.527
5	125	48.778	8.779	32.428	26.331
6	150	50.402	9.041	32.651	25.09
7	175	51.814	9.286	32.88	23.812
8	200	53.071	9.544	33.115	22.501
9	225	54.211	9.838	33.357	21.16
10	250	55.265	10.181	33.607	19.791
11	275	56.254	10.573	33.867	18.397
12	298.15	57.124	10.977	34.116	17.085
13	300	57.192	11.01	34.137	16.979
14	325	58.092	11.483	34.418	15.538
15	350	58.961	11.981	34.711	14.075
16	375	59.805	12.494	35.017	12.59
17	400	60.628	13.014	35.336	11.085
18	425	61.432	13.535	35.668	9.559
19	450	62.221	14.05	36.012	8.013
20	475	62.994	14.556	36.37	6.448
21	500	63.753	15.05	36.74	4.863
22	525	64.499	15.531	37.122	3.26
23	550	65.232	15.997	37.516	1.639
24	575	65.954	16.449	37.922	-0.001
25	600	66.663	16.887	38.339	-1.659
26	625	67.361	17.31	38.766	-3.334
27	650	68.048	17.719	39.204	-5.027
28	675	68.724	18.115	39.652	-6.737
29	700	69.39	18.497	40.11	-8.463
30	725	70.045	18.868	40.577	-10.206
31	750	70.691	19.226	41.053	-11.965
32	775	71.327	19.573	41.538	-13.74
33	800	71.954	19.909	42.032	-15.531
34	825	72.572	20.234	42.533	-17.338
35	850	73.18	20.55	43.043	-19.16
36	875	73.78	20.855	43.561	-20.997
37	900	74.372	21.151	44.086	-22.849
38	925	74.956	21.438	44.618	-24.716
39	950	75.531	21.716	45.158	-26.597
40	975	76.099	21.985	45.704	-28.492
41	1000	76.659	22.247	46.257	-30.402

APPENDIX VII.1

H_2O DMol Estimates

STANDARD THERMODYNAMIC QUANTITIES
computed from 25.00 to 1000.00 in steps of 25.00

	Temperature T (K)	Entropy S (cal/mol.K) (ZPVE is included)	Heat_Capacity Cp	Enthalpy H (kcal/mol)	Free_Energy G
1	25	26.831	7.949	13.114	12.443
2	50	32.341	7.949	13.313	11.696
3	75	35.564	7.949	13.511	10.844
4	100	37.851	7.949	13.71	9.925
5	125	39.624	7.949	13.909	8.956
6	150	41.073	7.949	14.107	7.946
7	175	42.299	7.949	14.306	6.904
8	200	43.36	7.951	14.505	5.833
9	225	44.297	7.956	14.704	4.737
10	250	45.136	7.965	14.903	3.619
11	275	45.896	7.98	15.102	2.481
12	298.15	46.541	8	15.287	1.411
13	300	46.591	8.002	15.302	1.325
14	325	47.233	8.031	15.502	0.152
15	350	47.829	8.067	15.703	-1.037
16	375	48.387	8.109	15.906	-2.239
17	400	48.912	8.157	16.109	-3.456
18	425	49.408	8.209	16.314	-4.685
19	450	49.879	8.265	16.52	-5.926
20	475	50.327	8.324	16.727	-7.179
21	500	50.756	8.386	16.936	-8.442
22	525	51.166	8.449	17.146	-9.716
23	550	51.561	8.514	17.358	-11
24	575	51.941	8.58	17.572	-12.294
25	600	52.307	8.646	17.787	-13.597
26	625	52.662	8.714	18.004	-14.909
27	650	53.005	8.783	18.223	-16.23
28	675	53.338	8.852	18.443	-17.56
29	700	53.661	8.922	18.666	-18.897
30	725	53.975	8.993	18.889	-20.243
31	750	54.281	9.064	19.115	-21.596
32	775	54.58	9.136	19.343	-22.957
33	800	54.871	9.208	19.572	-24.325
34	825	55.155	9.281	19.803	-25.7
35	850	55.433	9.354	20.036	-27.082
36	875	55.706	9.427	20.271	-28.472
37	900	55.972	9.501	20.507	-29.868
38	925	56.233	9.574	20.746	-31.27
39	950	56.49	9.648	20.986	-32.679
40	975	56.741	9.721	21.228	-34.095
41	1000	56.988	9.794	21.472	-35.516

APPENDIX VII.1

PTE DMol Estimates

STANDARD THERMODYNAMIC QUANTITIES
computed from 25.00 to 1000.00 in steps of 25.00

	Temperature T (K)	Entropy S (cal/mol.K) (ZPVE is included)	Heat_Capacity Cp	Enthalpy H (kcal/mol)	Free_Energy G
1	25	54.864	8.062	133.516	132.145
2	50	60.834	9.659	133.734	130.692
3	75	65.284	12.648	134.011	129.114
4	100	69.423	16.427	134.373	127.43
5	125	73.557	20.899	134.838	125.643
6	150	77.803	25.91	135.422	123.752
7	175	82.197	31.267	136.136	121.752
8	200	86.732	36.807	136.987	119.641
9	225	91.39	42.406	137.977	117.414
10	250	96.147	47.968	139.107	115.07
11	275	100.976	53.422	140.375	112.606
12	298.15	105.49	58.324	141.668	110.217
13	300	105.852	58.708	141.777	110.021
14	325	110.753	63.788	143.308	107.314
15	350	115.659	68.636	144.964	104.483
16	375	120.553	73.237	146.738	101.531
17	400	125.42	77.587	148.624	98.456
18	425	130.248	81.691	150.615	95.26
19	450	135.028	85.557	152.706	91.944
20	475	139.752	89.196	154.891	88.509
21	500	144.415	92.623	157.165	84.957
22	525	149.013	95.851	159.521	81.289
23	550	153.543	98.895	161.956	77.507
24	575	158.003	101.768	164.464	73.612
25	600	162.392	104.483	167.043	69.607
26	625	166.71	107.051	169.687	65.493
27	650	170.957	109.483	172.394	61.272
28	675	175.132	111.789	175.16	56.946
29	700	179.237	113.978	177.983	52.516
30	725	183.274	116.057	180.858	47.985
31	750	187.242	118.033	183.785	43.353
32	775	191.143	119.913	186.759	38.623
33	800	194.979	121.704	189.779	33.797
34	825	198.75	123.409	192.843	28.875
35	850	202.458	125.035	195.949	23.86
36	875	206.105	126.586	199.095	18.752
37	900	209.692	128.066	202.278	13.555
38	925	213.221	129.478	205.497	8.268
39	950	216.692	130.827	208.751	2.894
40	975	220.107	132.117	212.038	-2.566
41	1000	223.467	133.349	215.357	-8.111

APPENDIX VII.1

PC DMol Estimates

STANDARD THERMODYNAMIC QUANTITIES
computed from 25.00 to 1000.00 in steps of 25.00

	Temperature T (K)	Entropy S (cal/mol.K) (ZPVE is included)	Heat_Capacity Cp	Enthalpy H (kcal/mol)	Free_Energy G
1	25	48.281	8.218	81.214	80.007
2	50	54.408	9.681	81.437	78.717
3	75	58.618	11.215	81.698	77.302
4	100	62.082	13.001	82	75.792
5	125	65.196	15.005	82.35	74.201
6	150	68.117	17.12	82.751	72.534
7	175	70.919	19.302	83.207	70.796
8	200	73.642	21.542	83.717	68.989
9	225	76.312	23.832	84.284	67.114
10	250	78.943	26.158	84.909	65.173
11	275	81.546	28.5	85.592	63.167
12	298.15	83.935	30.662	86.277	61.252
13	300	84.126	30.834	86.334	61.096
14	325	86.685	33.138	87.134	58.961
15	350	89.224	35.39	87.99	56.762
16	375	91.74	37.575	88.903	54.5
17	400	94.233	39.679	89.868	52.175
18	425	96.699	41.695	90.886	49.789
19	450	99.137	43.619	91.952	47.341
20	475	101.545	45.45	93.066	44.832
21	500	103.921	47.189	94.224	42.264
22	525	106.264	48.839	95.425	39.636
23	550	108.572	50.403	96.665	36.951
24	575	110.846	51.887	97.944	34.208
25	600	113.084	53.295	99.259	31.409
26	625	115.287	54.631	100.608	28.554
27	650	117.455	55.901	101.99	25.645
28	675	119.587	57.11	103.403	22.682
29	700	121.685	58.261	104.845	19.666
30	725	123.749	59.359	106.316	16.598
31	750	125.779	60.406	107.813	13.478
32	775	127.776	61.407	109.335	10.309
33	800	129.741	62.365	110.883	7.09
34	825	131.674	63.281	112.453	3.822
35	850	133.576	64.159	114.046	0.506
36	875	135.448	65.001	115.661	-2.856
37	900	137.291	65.809	117.296	-6.266
38	925	139.105	66.585	118.951	-9.721
39	950	140.89	67.329	120.625	-13.221
40	975	142.649	68.045	122.317	-16.765
41	1000	144.38	68.734	124.027	-20.353

THERMODYNAMIC PROPERTIES FROM QUANTUM MECHANICS

VII.1 Optimised geometries from quantum mechanics

Geometry optimisation was carried out using Dmol package (see Section 2.4.1), for DPE and the three phenoxy toluene isomers. The structures are shown in Figure A-1 to Figure A-6. Geometry optimisation, as an energy minimisation calculation from which thermodynamic properties may be computed, was used to determine the molecular conformation of the lowest energy.

The idea of determining the lowest energy conformation was twofold. Firstly, it was intended to quantitatively determine the effect that the conformation would have on the effective molecular diameter and to then infer this to pore diffusion. Secondly, thermodynamic properties would be determined once the structure was optimised.

The calculated standard Gibbs free energies of formation estimated for DPE and phenoxy toluene isomers and a few other relevant compounds are given in the table.

Table A Comparison of the standard Gibbs free energy of formation calculated from quantum mechanics (QM) with data available in the literature (Sinnot, 1999; Perry and Green, 1997)

	Quantum mechanics	Literature
Compound	ΔG_f^o [kcal/mol]	ΔG_f^o [kJ/mol]
DPE	90.3	175
PPT	105.8	–
MPT	97.2	–
OPT	94.5	–
PTE	110.2	–
p-Cresol	61.3	-30.9
PhOH	45.9	-32.9
MeOH	17.1	-162.6
H_2O	1.4	-228.8

The deviation of DMol generated data from experimental data is too large to explain the two ideas mentioned above.

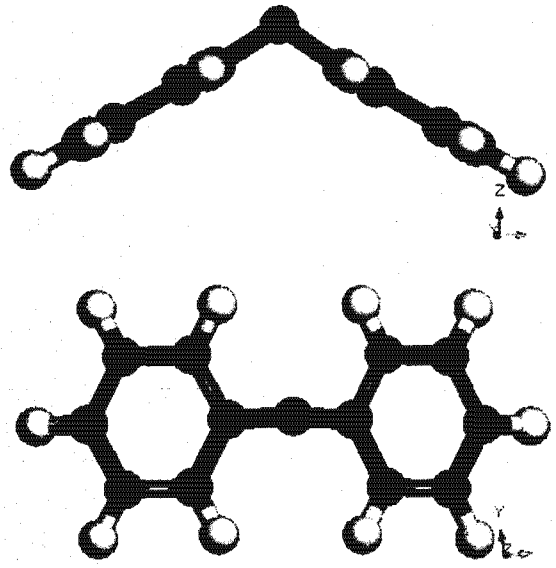

Figure A-1 : Geometry of the optimised structure of DPE

The optimised structure of DPE has a C_{2V} symmetry (two rings symmetrical about the oxygen).

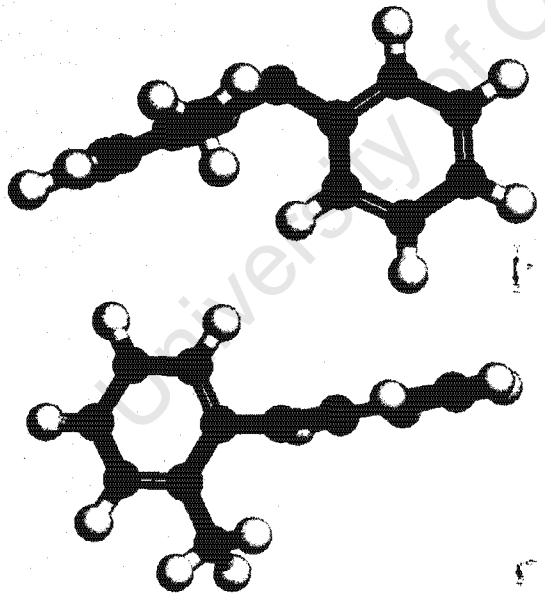

Figure A-2 : Geometry of an optimised structure for o-phenoxy toluene (OPT)

The optimised structure of OPT has twisted rings with a C_1 symmetry.

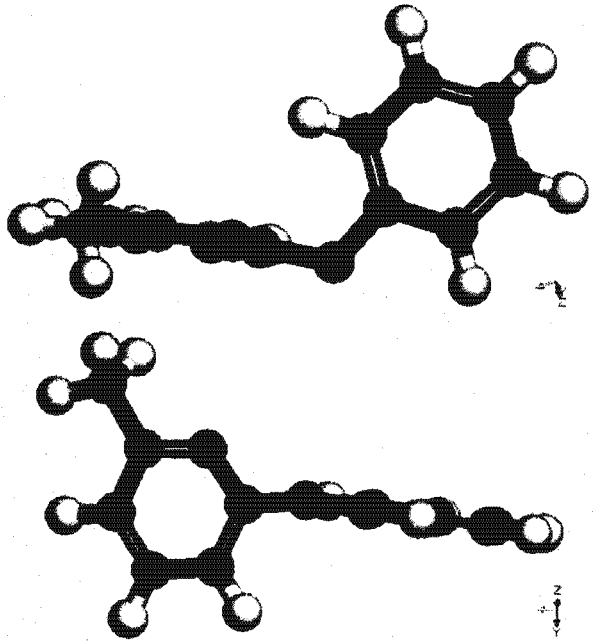

Figure A-3 : Geometry of an optimised structure of m-phenoxy toluene

The optimised structure of MPT has twisted rings with a C_1 symmetry.

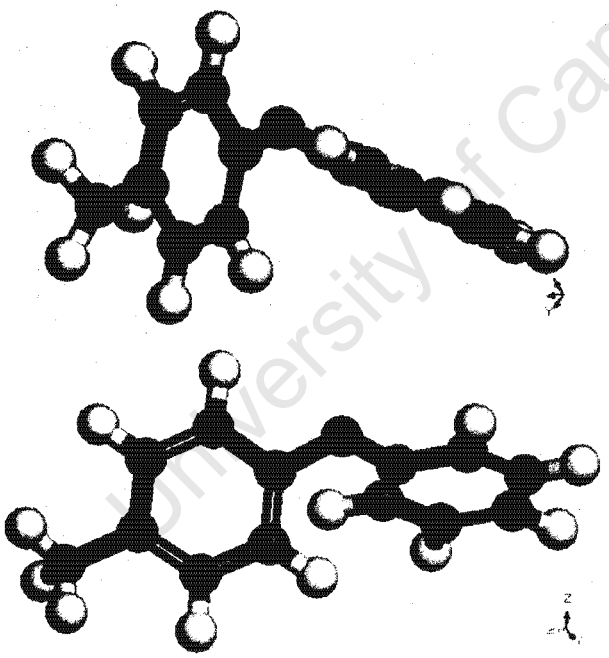

Figure A-4 : Geometry of an optimised structure of p-phenoxy toluene

The optimised structure of PPT, just like its two isomers, has twisted rings, meaning that the rings are not symmetrical about the oxygen atom. PPT also has a C_1 symmetry.

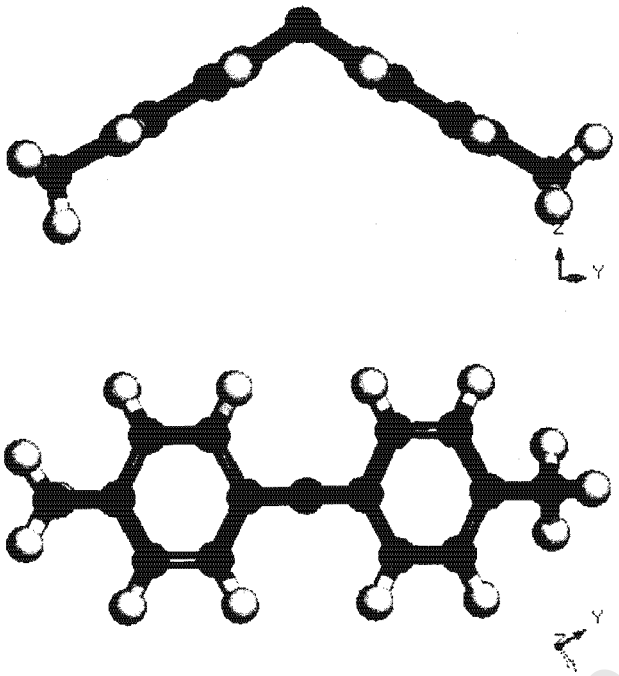

Figure A-5 : Geometry of an optimised structure of p-Tolyl Ether (PTE)

The optimised structure of PTE, just like DPE, has rings that are symmetrical about the oxygen atom. That is, PTE has C_{2V} symmetry.

VII.2 Thermodynamic equilibria from quantum mechanics

Geometry optimisation of each molecular structure by quantum mechanics allows for calculation of thermodynamic properties from statistical thermodynamics (see Section 2.4.1). The gas phase Gibbs free energies of all the species in the reactions of Figure 1-3 were estimated for each temperature in the range from 300 K to 1000 K, in steps of 25 K.

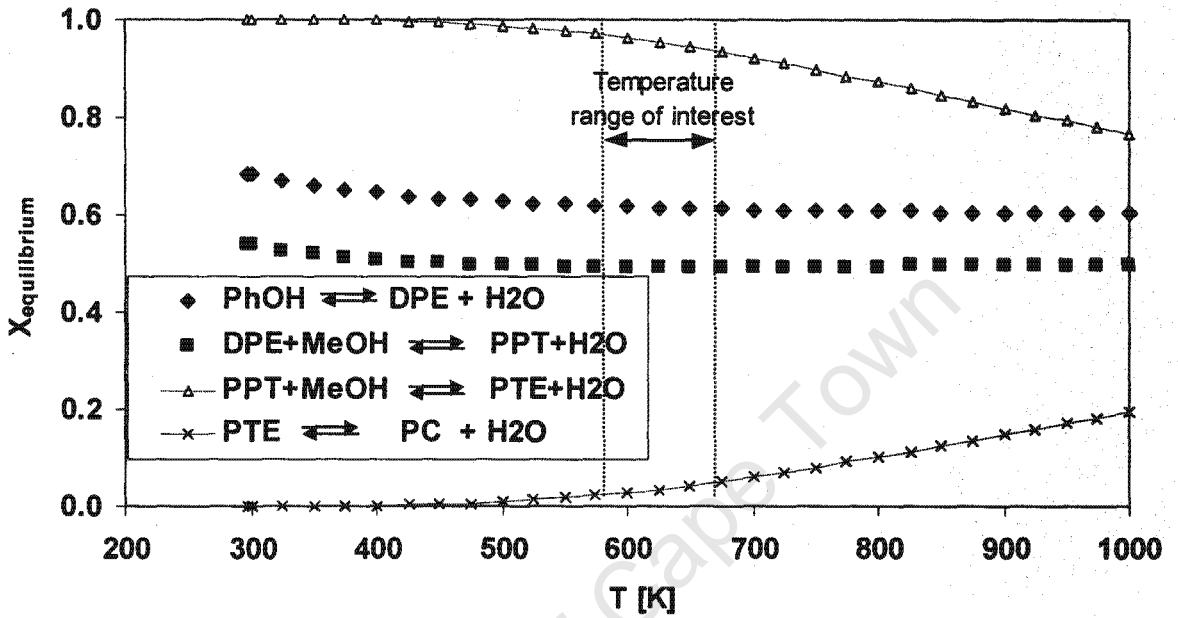

Figure A-6 : Equilibrium conversions from quantum mechanics

- The closed diamonds equilibrium curve is the condensation step, whereas the closed squares and the open triangles give the first and second methylation steps, respectively. The curve with cross marker is the cleavage step.
- The equilibrium curve for phenol condensation (obtained from quantum mechanics) in this case has a shape similar to that obtained from Benson method, except that it is 100°C to the left of that of Benson's (see Figure 5-45).
- The curve of the first methylation step is totally faulty. This is purely due to inaccurate thermodynamic data obtained.

Condensation and cleavage steps were expected to be mirror images of each other, based on the fact that the one is the reverse of the other. However, this was not the case as shown in Figure A.6.

APPENDIX VIII

Results from Molecular Dynamics Calculations

Appendix VIII.1

It was discussed in Section 2.4.2 that the slope of the plot of mean square displacement versus time travelled by a molecule is the diffusion coefficient of that molecule in that particular system.

Mean square displacement is a measure of the average distance that a molecule travels and since molecular dynamics simulations allow for following the path of individual molecules directly, the mean square is readily obtainable from these simulations (Tepper et al., 1999).

The first part of the mean square displacement plot versus time is usually non-linear due to relaxation or equilibration of the system. Therefore only the portion of this plot, after the system has equilibrated is used (Leach, 1998).

Molecular dynamics simulations for self diffusing molecules in mordenite pores are presented in this appendix. These were abondoned due to inconsistent non-reproducible results, as well as due to the fact that the simulations were very memory intensive and lasting long times of up to a week to converge.

Appendix VIII.1: Molecular Dynamics Results (H-beta)

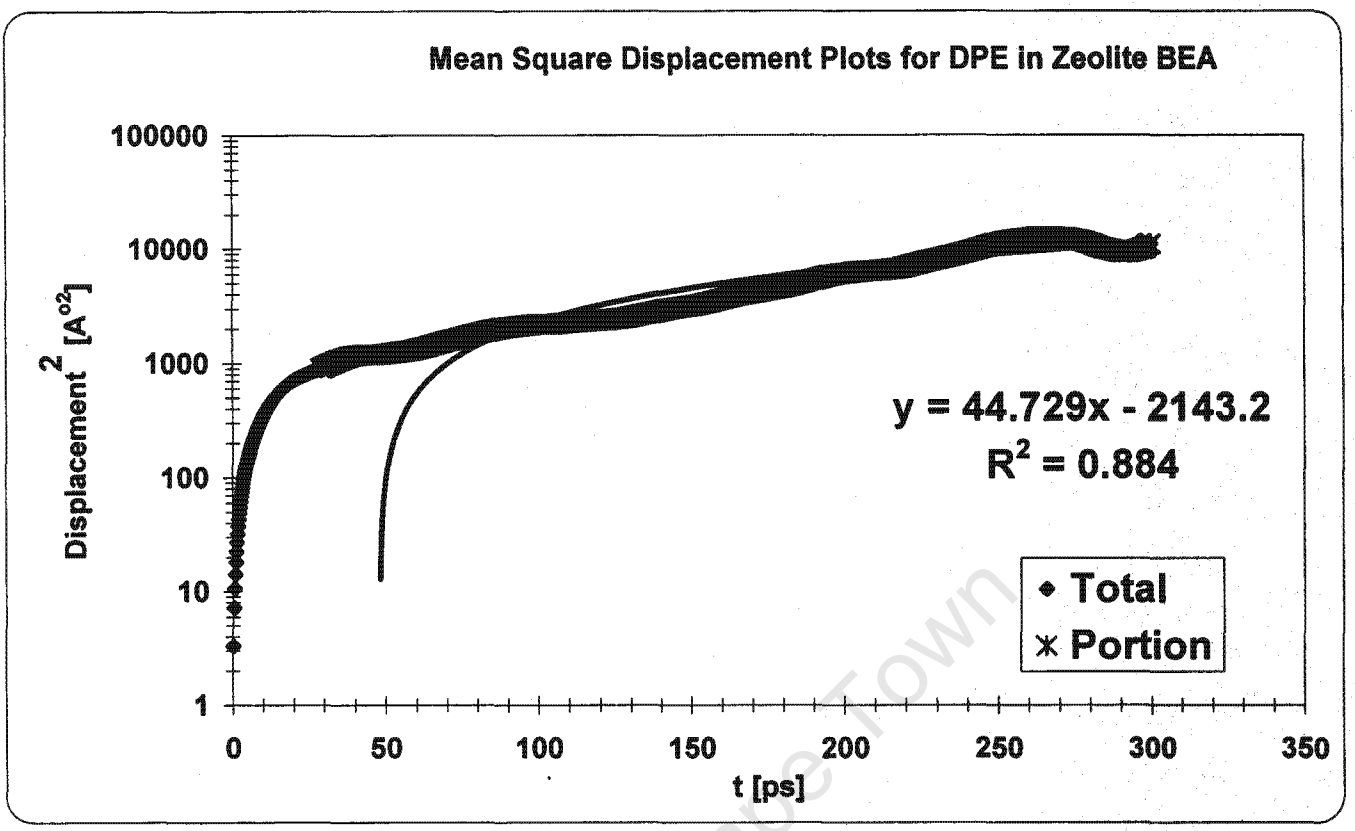

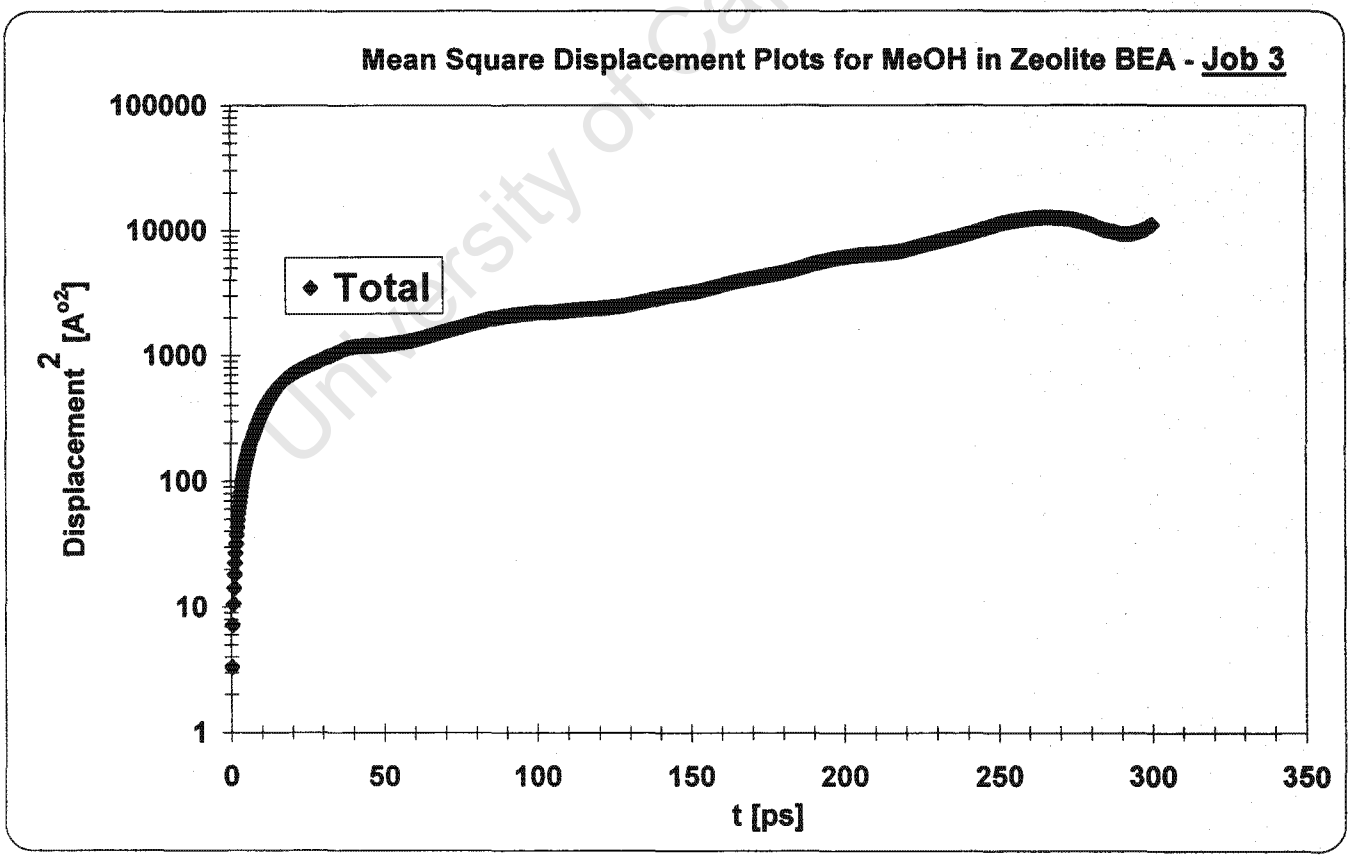

Appendix VIII.1: Molecular Dynamics Results (H-beta)

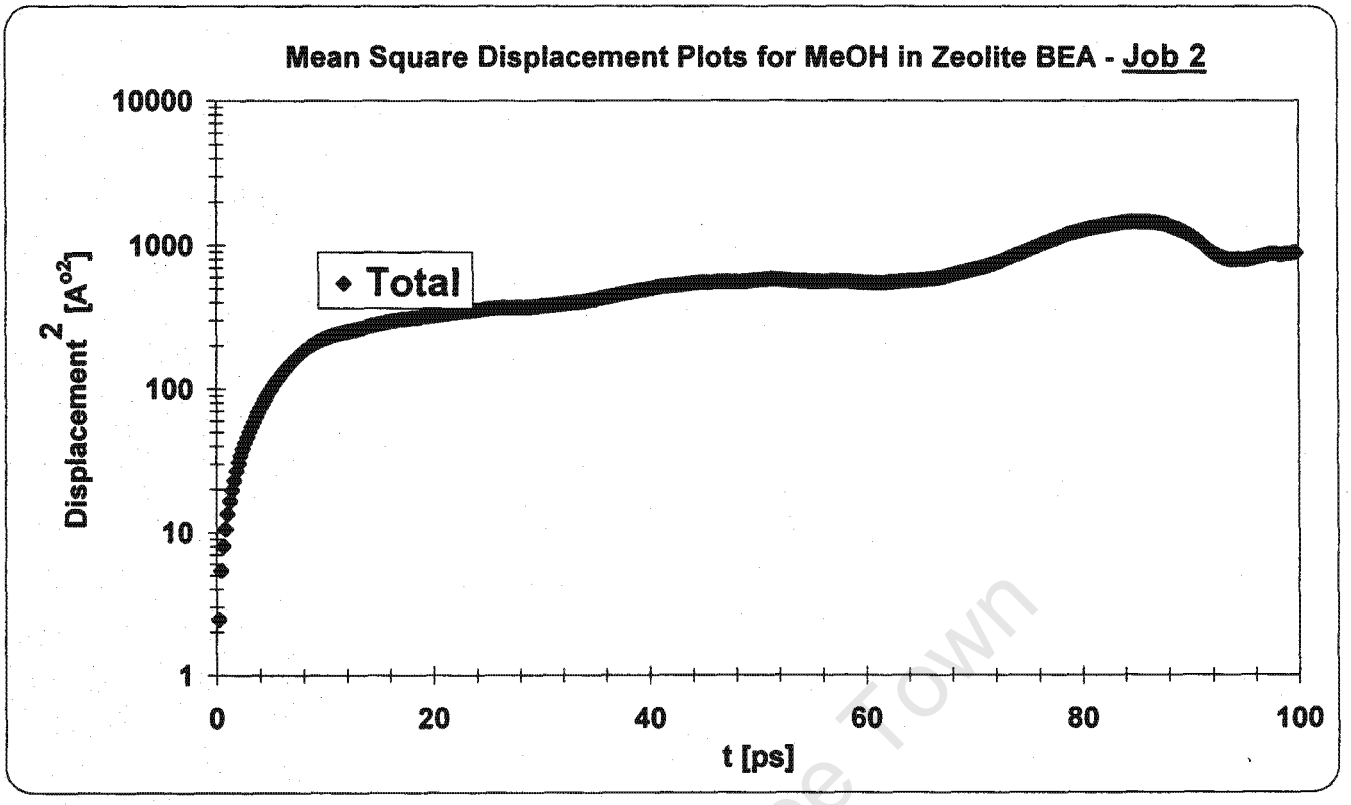

Appendix VIII.1: Molecular Dynamics Results (Mordenite)

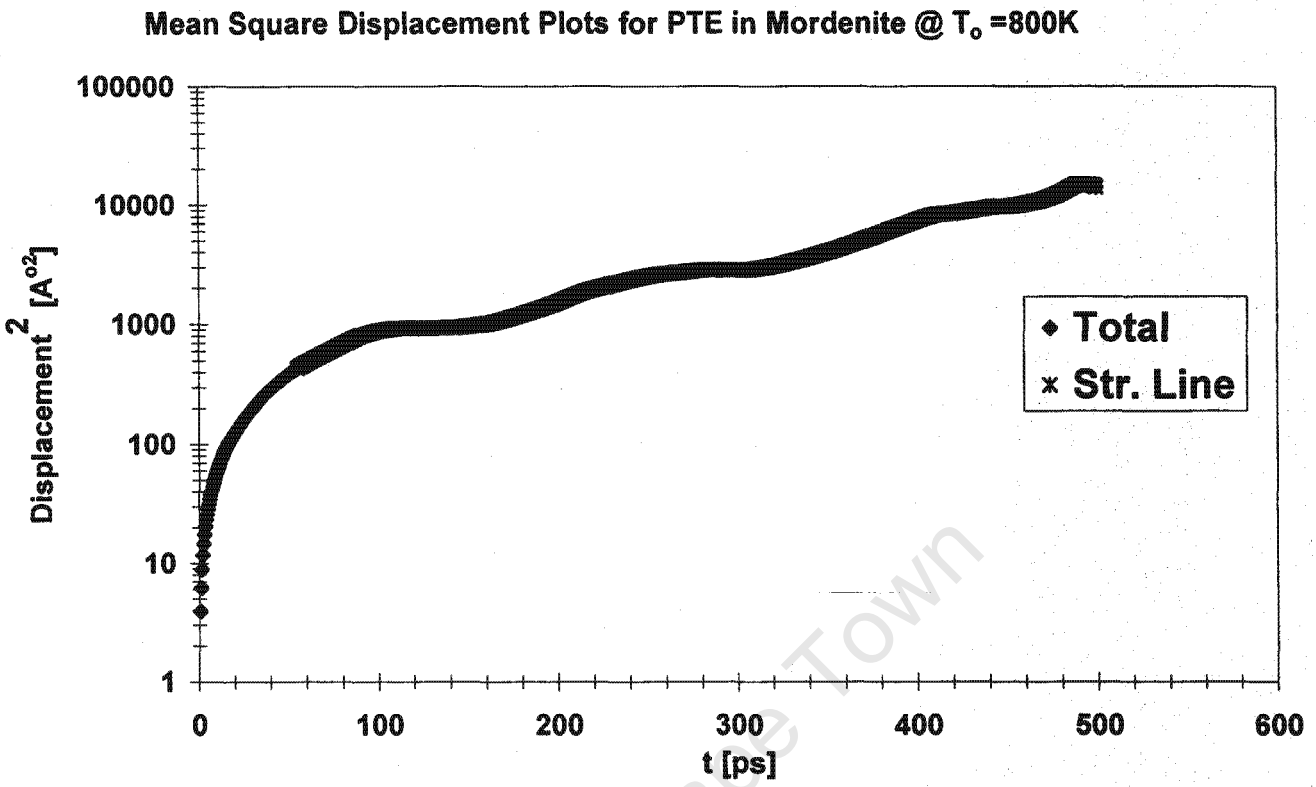

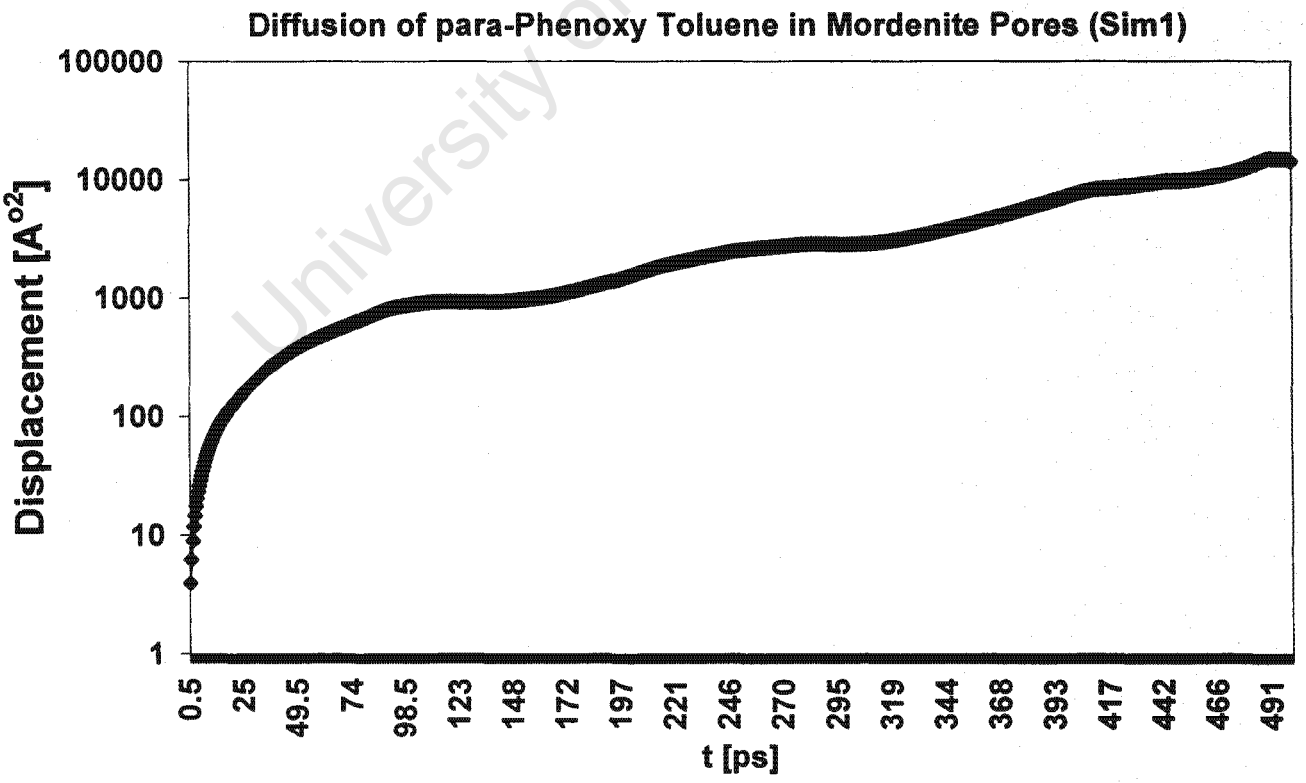

Appendix VIII.1: Molecular Dynamics Results (Mordenite)

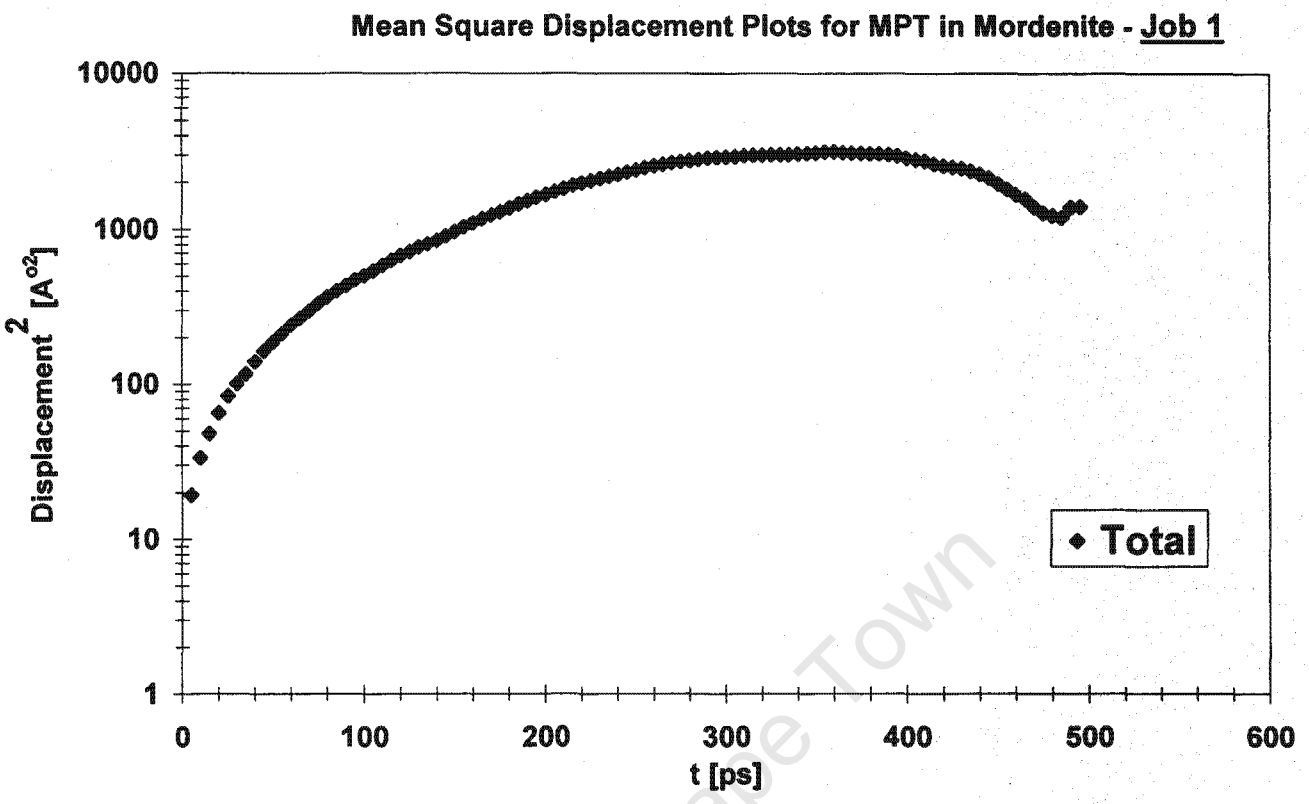

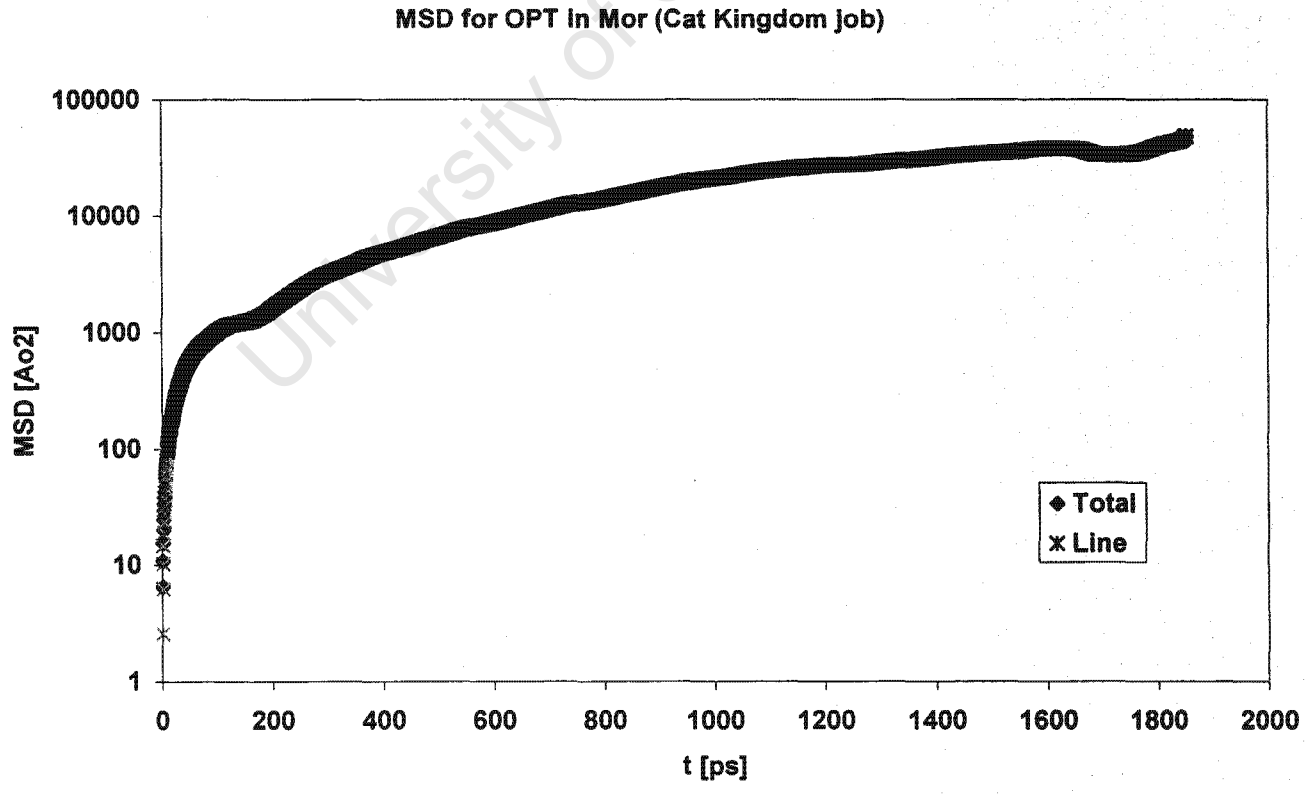

Appendix VIII.1: Molecular Dynamics Results (Mordenite)

Mean Square Displacement Plots for OPT in Mordenite - Job 3

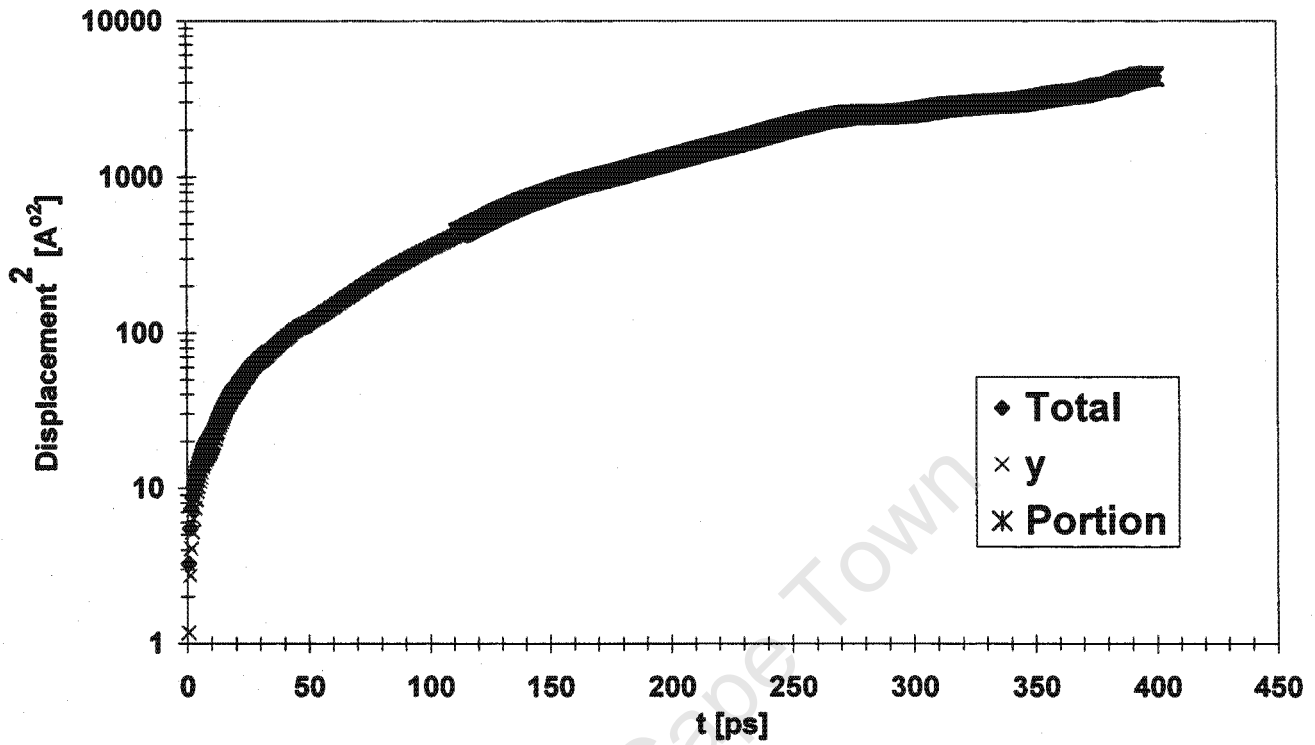

Mean Square Displacement Plots for OPT in Mordenite @ T_{av} =500K (Job 1)

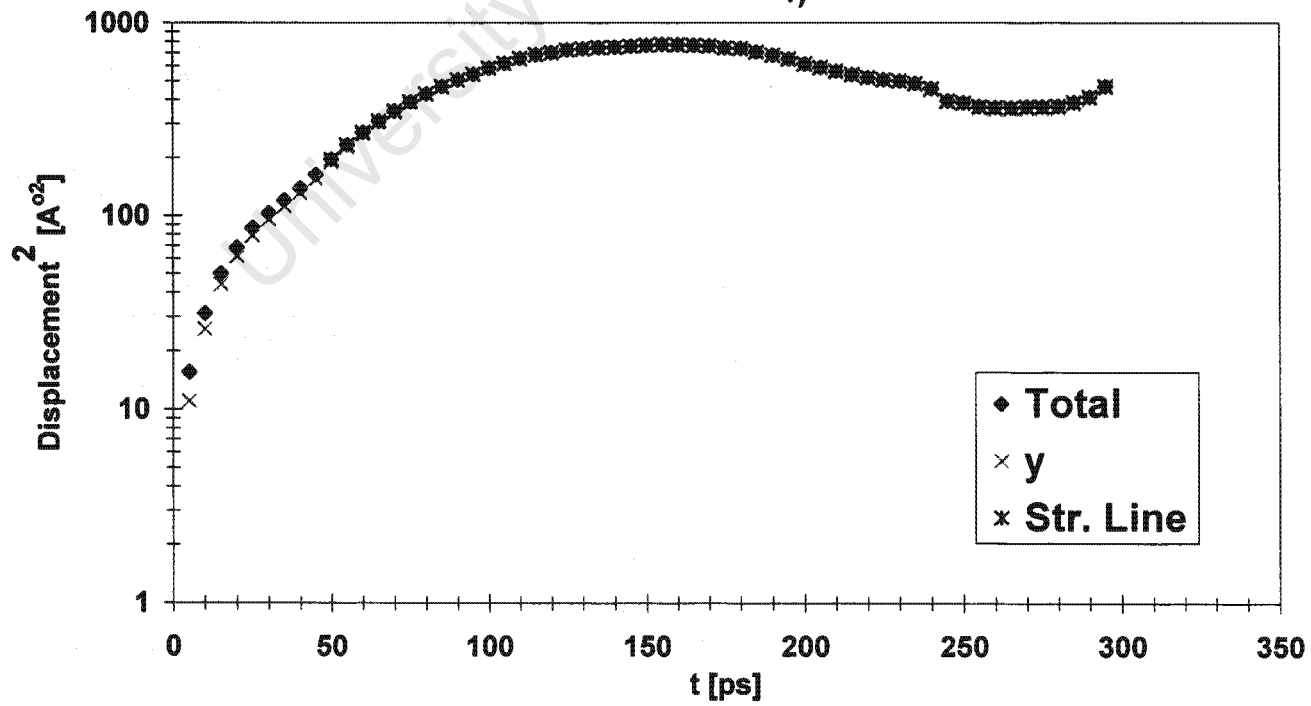

Appendix VIII.1: Molecular Dynamics Results (Mordenite)

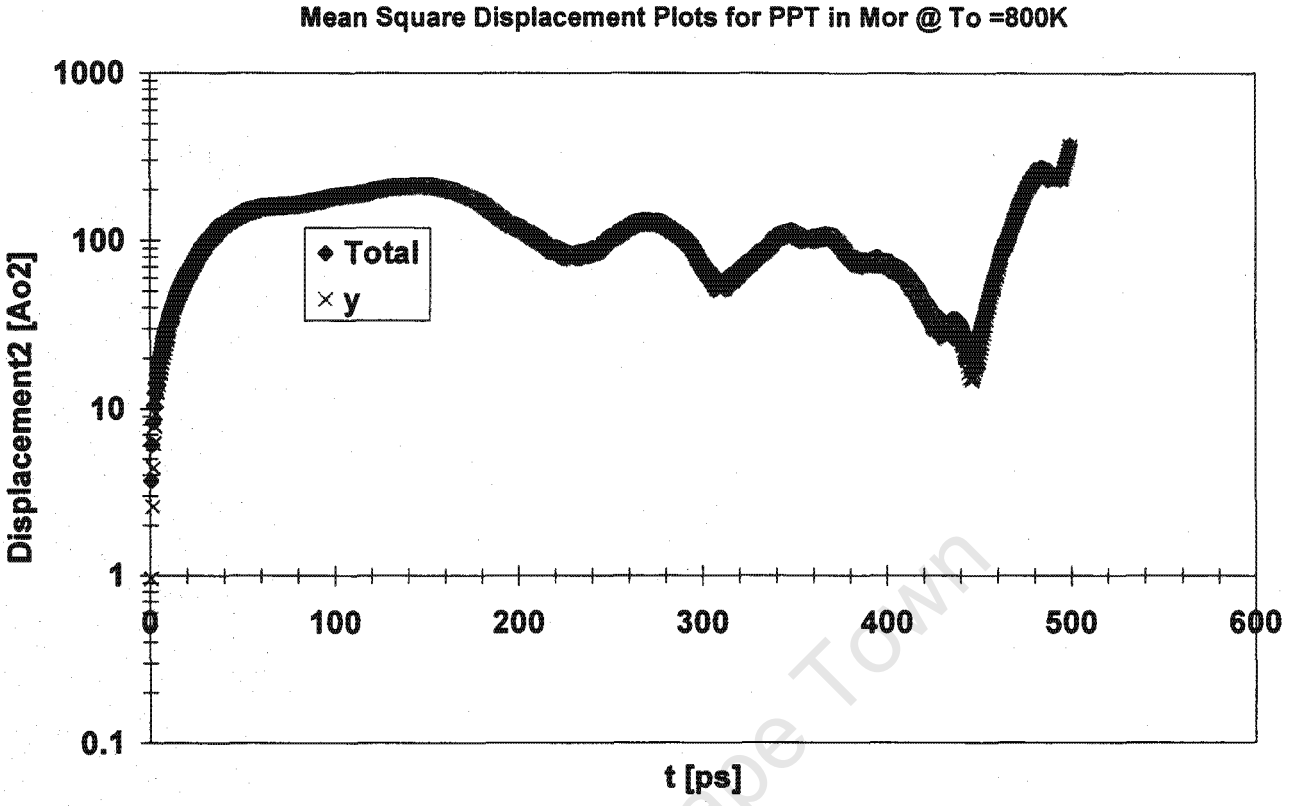

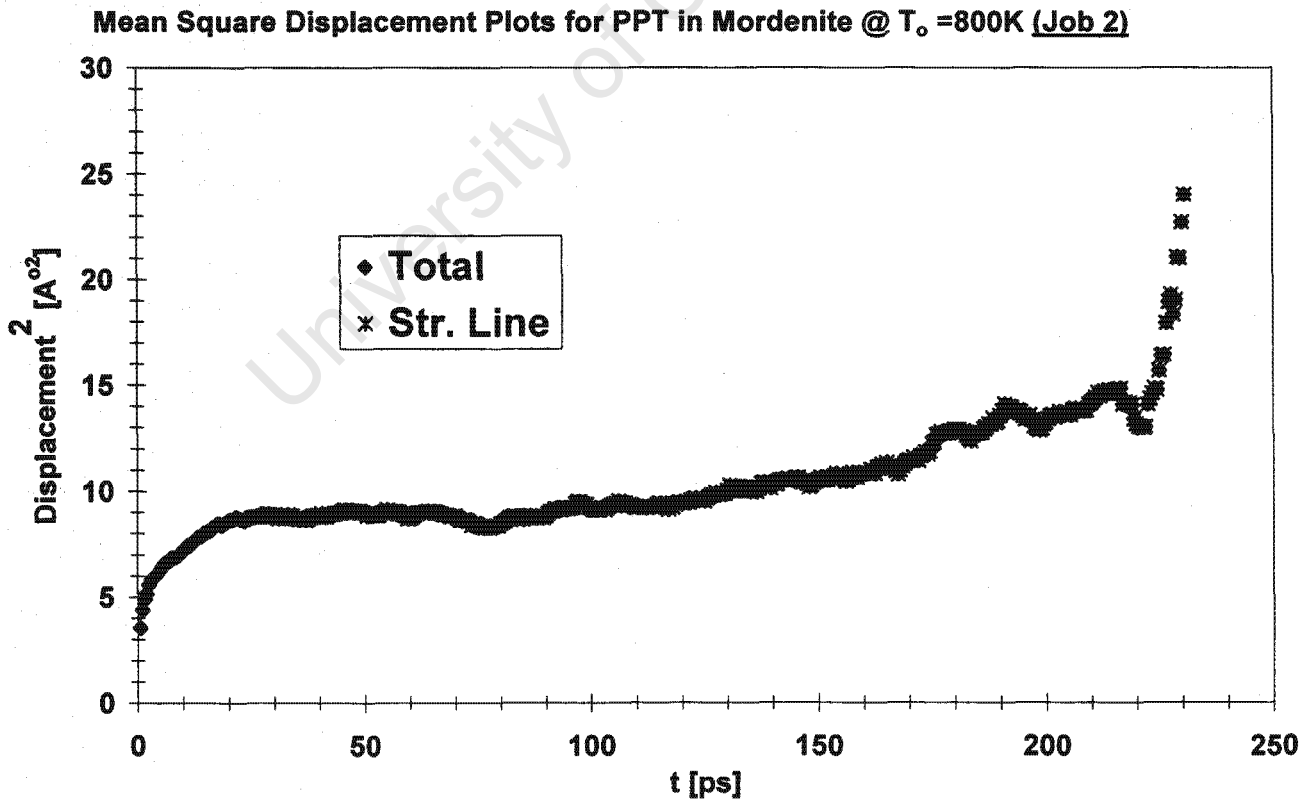

Diffusivity of various species in H-ZSM-5, at 300K

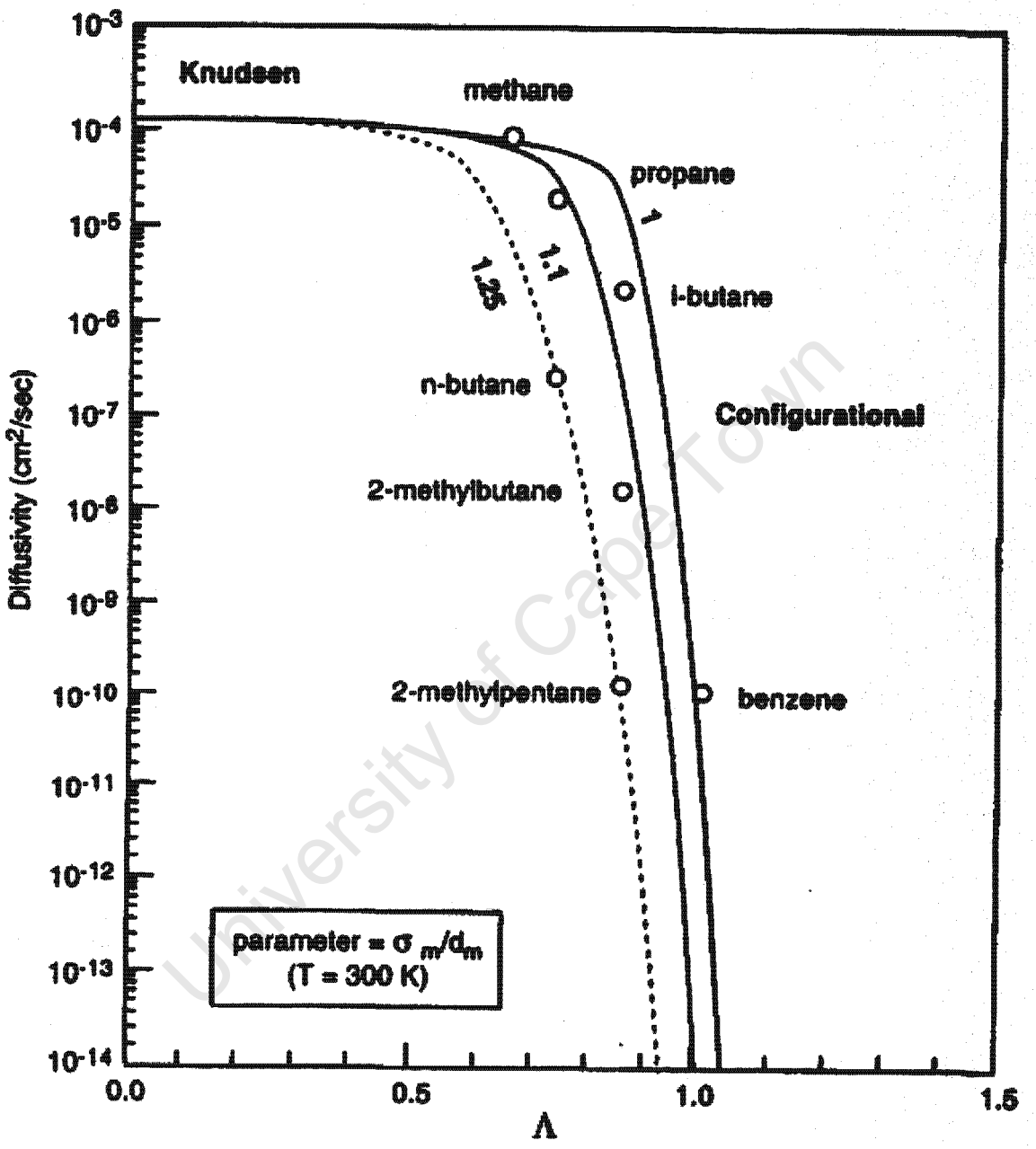

Diffusivity of various species in H-ZSM-5, at 300K

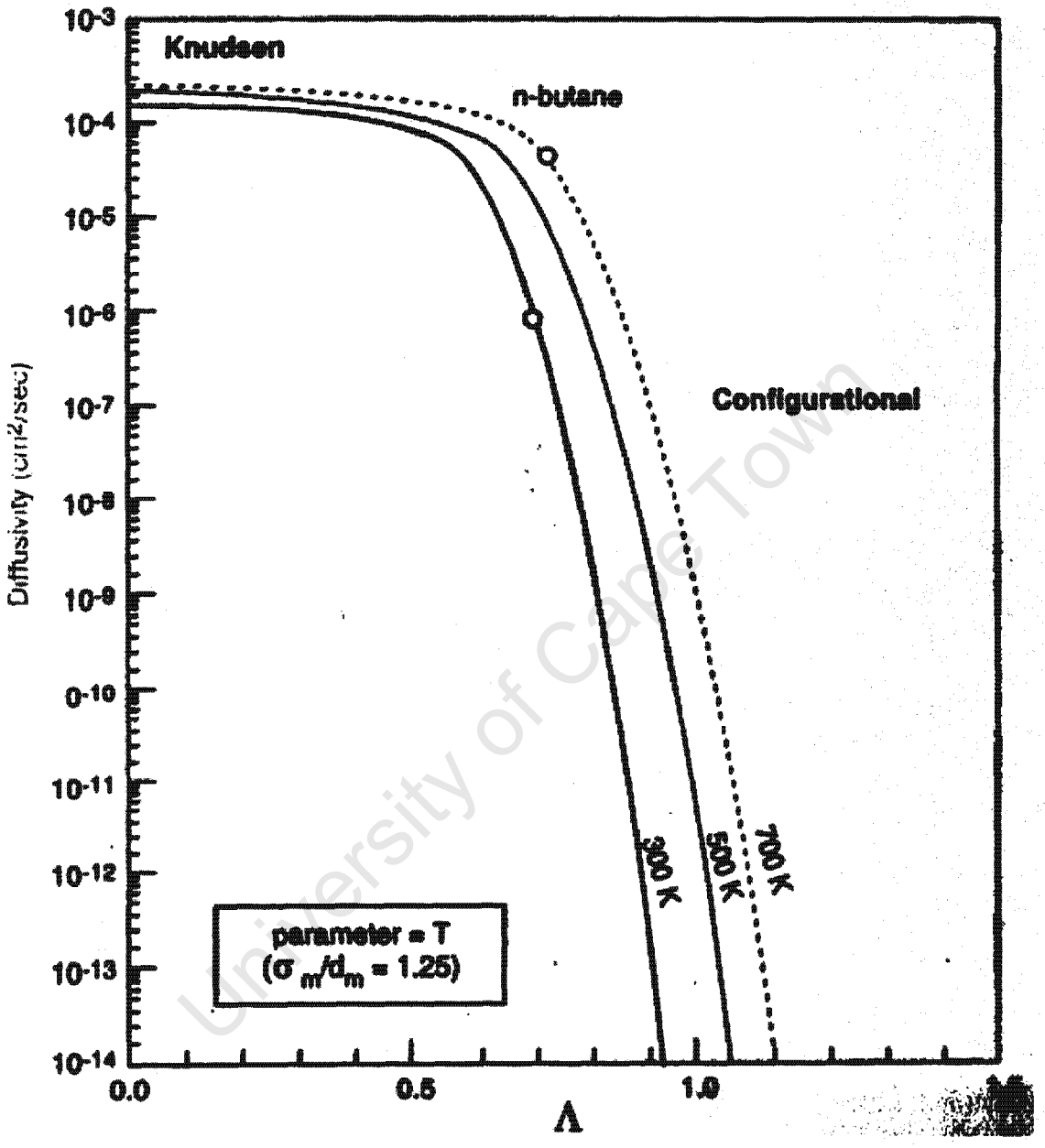

ESTIMATION OF SELECTIVITY FROM MOLECULAR DYNAMICS

Molecular mechanics calculations were used to estimate the molecular diameter of diphenyl ether. This is important to determine the degree of ease or difficulty of access of the bulk active sites, which are located inside the zeolite pores, by this guest molecule.

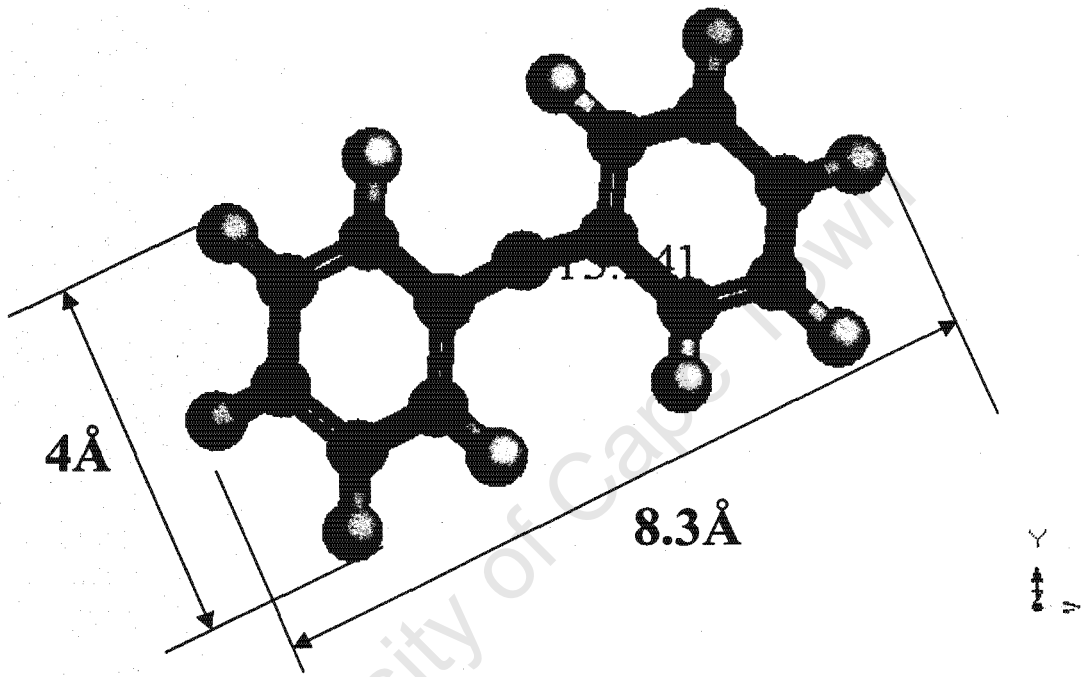

Figure B.1 : Estimate molecular diameter of diphenyl ether

In Figure B.1, the centre to centre distance between two hydrogen atoms in the meta positions of the molecule is 4 Å. An improvement is obtained on this estimate, by addition of the van der Waals radius of hydrogen, for both hydrogen atoms. Bondi (1964) gave the hydrogen radius as 1.06 Å. Accounting for the van der Waals radius, the molecular diameter of diphenyl ether is estimated to be 6.12 Å.

The pore dimensions of the major channels in mordenite are 6.7 x 7.0 Å, as shown in Table 2-14, which is just enough to allow diffusion of DPE through this zeolite along its longest axis.

In Table B.1, the drift speeds (average velocities) of various products diffusing through mordenite are shown. Diffusivity of a species through the zeolite is proportional to the drift speed, as shown in Equation 2-35 and Equation 2-39. The diffusion constant of each species, calculated according to Equation 2-39, is also given in Table B.1.

Table B.1 : Diffusion coefficients in zeolite mordenite, estimated from molecular dynamics

Compound	Terminal velocity [Å/ps]	N_{Atoms}	$t_{simulation}$ (ps)	D x 10^{-8} [cm/s]
PPT	5.31	26	40	19
MPT	1.42	26	40	1
OPT	2.1	26	40	3
PTE	3.55	29	40	8

Considering the methylation to be an electrophilic substitution whereby a protonated methanol molecule attacks the ring, deductions can be made, which are indicative of what happens inside the zeolite pores.

Deduction A

It was established from Sections 2.1.8 and 2.1.9 that reactivity per position in DPE is of the order:

ortho ≈ para » meta (reactivity per position on the ring).

There are two o-positions per ring which implies, from statistics, the following:

$k_{ortho} \approx 2 \cdot k_{para}$

Reactivity, in this case leads to similar trends in selectivity. This implies that the selectivity expected from electronic effects and statistics is: $S_{ortho} \approx 2 \cdot S_{para} \gg S_{meta}$.

This is the selectivity expected in the absence of both, steric hindrance and shape selectivity, like in large pore zeolites (e.g. Hbeta or HY) or amorphous acid catalysts (e.g. silica-alumina)

Considering the individual rings on DPE molecule, the other ring can be viewed as a bulky phenoxy substituent, which may introduce steric hindrance onto a methyl group in the ortho position, and on a protonated methanol species attacking the ortho position. This would result in the following selectivities: $2 \cdot S_{para} \geq S_{ortho} \gg S_{meta}$.

Deduction B

Di-methylation is undoubtedly sequential, as shown by Fujita et al. (1992) and this was also confirmed by the preliminary studies conducted by Ndlovu and Gxavu (2000). DPE is much more bulkier than MeOH which results in much lower diffusion rate for DPE and thus it can be assumed that the concentration of MeOH in the pores is much higher than that of DPE, such that the reaction is primarily dependent on DPE concentration in the pores. It is therefore reasonable to assume, for modelling purposes, a first order reaction in DPE.

Deduction C

In reaction kinetics a parameter called Thiele modulus is used to model intrapellet mass transport restrictions, which is simply the ratio of the intrinsic reaction rate to that of the diffusion rate (Fogler, 1999). This parameter, Thiele modulus, is mathematically defined as follows:

$$\phi = L\sqrt{\frac{k_i}{D_i}}$$

From Molecular Dynamics, using the data from Section 2.4.2 it follows that:

$\Psi_{PPT} = 2.5 * \Psi_{OPT}$ (drift speed)

Diffusivity is directly proportional to the drift speed (see Equation 2-1)

$\Rightarrow D_{PPT} = 2.5 * D_{OPT}$

Modelling of selectivity for MPT is not considered here because at low reaction temperature, as was the case in this study, reactivity of the meta-position is negligible and consequently selectivity negligible (see Section 0).

Calculated drift speeds of phenoxy toluene isomers (see Table B-1) and diffusion coefficients of phenoxy toluene isomers indicate that the diffusion rates of the isomers are in the order:

para >ortho > meta

Over the catalyst of choice, CBV90A, experimental results showed that isomer selectivities are of the order:

para >ortho >> meta

However, the relative diffusion coefficients from molecular dynamics do not adequately explain selectivities obtained with the catalyst of choice.

APPENDIX IX

Steady State Average Results

APPENDIX IX.1
SUMMARY OF EXPERIMENTAL RESULTS - Steady state averages

	Exp name	T [°C]	P_T [bar]	WHSV	MFR	y_{N2}	P_{Feed} [bar]	X [%]	S_{Ps} [%][a]	S_{PTTs} [%][a]	$S_{OADPE's}$ [%][a]	$S_{HP's}$ [%][a]	S_{OPT} [%][a]	S_{MPT} [%][a]	S_{PPT} [%][a]	S_{PTE} [%][a]	PPT/ OPT	PPT/ MPT	PTE/ PPT
MFI-50 L1																			
Exp 28	Z5OA	250	20	0.56	3.2	0.25	14	4.5	67.3	17.8	4.2	10.7	5.4	1.2	11.1	0.0	2.1	9.0	0.0
Mor-40 L1																			
Exp 29	M40A	250	20	0.56	3.2	0.25	14	8.9	31.7	18.2	8.7	41.4	2.2	0.2	15.9	2.2	7.4	93.5	0.1
HUSY L1																			
Exp 30	HUSY	250	20	0.56	2	0.25	13	9.0	37.2	57.6	4.1	1.2	34.4	2.8	20.4	0.1	0.6	7.2	0.0
CBV21A L1 ($T_{calcination}$ = 400°C)																			
Exp 31	CBV20A	250	20	0.56	2	0.25	13	14.7	20.8	23.2	8.8	47.2	7.1	0.5	15.6	1.5	2.2	29.4	0.1
CBV21A L2 ($T_{calcination}$ = 400°C)																			
Exp 32	M20B	300	20	0.56	2	0.25	13	34.0	14.2	27.4	28.4	30.0	12.5	1.4	13.5	1.0	1.1	10.0	0.1
CBV21A L3 ($T_{calcination}$ = 500°C)																			
Exp 33	M20D	300	20	0.56	2	0.25	13	62.5	6.4	45.3	28.4	20.0	30.7	2.2	12.3	1.2	0.4	5.5	0.1
Exp 34	M20E	275	20	0.56	2	0.25	13	33.4	3.6	57.8	14.0	24.6	35.1	2.6	20.1	1.0	0.6	7.8	0.1
Exp 35	M20F	250	20	0.56	2	0.25	13	8.8	1.3	64.8	7.8	26.1	35.3	2.6	26.9	0.4	0.8	10.4	0.0
CBV90A L1																			
Exp 36	CBV90A	300	20	0.56	2	0.25	13	26.1	26.7	13.8	45.2	14.3	5.2	0.9	7.7	0.3	1.5	8.2	0.0
Exp 37	CBV90B	275	20	0.56	2	0.25	13	20.6	22.4	16.4	36.8	24.4	4.7	0.6	11.1	0.9	2.3	17.1	0.1
Exp 38	CBV90C	250	20	0.56	2	0.25	13	13.4	19.2	21.9	21.5	37.4	3.9	0.3	17.7	2.3	4.5	52.5	0.1
Exp 39	WHSVA	250	20	0.28	2	0.25	13	18.6	13.5	20.4	25.7	40.4	3.5	0.3	16.6	2.1	4.7	48.9	0.1
Exp 40	WHSVB	250	20	0.56	2	0.25	13	11.9	16.7	22.0	19.2	42.1	3.8	0.3	17.9	2.4	4.7	57.0	0.1
Exp 41	WHSVC	250	20	1.13	2	0.25	13	6.7	11.5	23.3	15.9	49.3	4.2	0.3	18.8	2.4	4.5	58.0	0.1
Exp 42	WHSVD	250	20	0.56	2	0.25	13	11.0	12.9	22.9	15.7	48.5	4.1	0.3	18.5	2.3	4.5	57.6	0.1
Exp 43	MFRA	250	20	0.56	0.5	0.63	3	6.6	8.6	23.0	22.5	45.8	5.9	0.7	16.5	1.2	2.8	25.1	0.1
Exp 44	MFRB	250	20	0.56	2	0.25	13	12.6	9.0	24.5	14.7	51.8	5.6	0.4	18.5	1.9	3.4	44.4	0.1
Exp 45	T200	200	20	0.56	2	0.25	13	1.1	1.8	26.9	15.3	56.0	7.7	0.5	18.7	0.7	2.4	38.5	0.0
Exp 46	MFRC	250	20	0.53	4	0.08	18	14.8	5.9	24.3	14.1	55.6	4.8	0.3	19.2	2.3	4.1	55.8	0.1
Exp 47	MFRD	250	20	0.56	2	0.25	13	9.8	10.3	22.9	15.0	51.8	4.1	0.3	18.5	2.2	4.6	59.2	0.1
Exp 48	P10	250	10	0.56	2	0.25	7	8.4	7.8	24.1	16.7	51.3	5.6	0.5	18.1	1.8	3.2	38.4	0.1
Exp 49	DPE	250	20	0.64	0	1	0	0.5	40.1	11.0	23.8	25.2	3.6	0.4	7.0	0.2	1.9		0.0
Exp 50	MeOH	250	20	0	inf	0.25	15	0.0	51.4	25.8	21.6	1.3	7.3	0.5	17.9	3.7	2.4	34.0	0.2

[a]Selectivities in mole %

APPENDIX IX.1
SUMMARY OF EXPERIMENTAL RESULTS - Steady state averages

	Exp name	T [°C]	P_T [bar]	WHSV	MFR	y_{N2}	P_{Feed} [bar]	X [%]	S_{Ps} [%][a]	S_{PTTs} [%][a]	$S_{OADPE's}$ [%][a]	$S_{HP's}$ [%][a]	S_{OPT} [%][a]	S_{MPT} [%][a]	S_{PPT} [%][a]	S_{PTE} [%][a]	PPT/ OPT	PPT/ MPT	PTE/ PPT
MFI-50 L1																			
Exp 28	Z5OA	250	20	0.56	3.2	0.25	14	4.5	67.3	17.8	4.2	10.7	5.4	1.2	11.1	0.0	2.1	9.0	0.0
Mor-40 L1																			
Exp 29	M40A	250	20	0.56	3.2	0.25	14	8.9	31.7	18.2	8.7	41.4	2.2	0.2	15.9	2.2	7.4	93.5	0.1
HUSY L1																			
Exp 30	HUSY	250	20	0.56	2	0.25	13	9.0	37.2	57.6	4.1	1.2	34.4	2.8	20.4	0.1	0.6	7.2	0.0
CBV21A L1 ($T_{calcination}$ = 400°C)																			
Exp 31	CBV20A	250	20	0.56	2	0.25	13	14.7	20.8	23.2	8.8	47.2	7.1	0.5	15.6	1.5	2.2	29.4	0.1
CBV21A L2 ($T_{calcination}$ = 400°C)																			
Exp 32	M20B	300	20	0.56	2	0.25	13	34.0	14.2	27.4	28.4	30.0	12.5	1.4	13.5	1.0	1.1	10.0	0.1
CBV21A L3 ($T_{calcination}$ = 500°C)																			
Exp 33	M20D	300	20	0.56	2	0.25	13	62.5	6.4	45.3	28.4	20.0	30.7	2.2	12.3	1.2	0.4	5.5	0.1
Exp 34	M20E	275	20	0.56	2	0.25	13	33.4	3.6	57.8	14.0	24.6	35.1	2.6	20.1	1.0	0.6	7.8	0.1
Exp 35	M20F	250	20	0.56	2	0.25	13	8.8	1.3	64.8	7.8	26.1	35.3	2.6	26.9	0.4	0.8	10.4	0.0
CBV90A L1																			
Exp 36	CBV90A	300	20	0.56	2	0.25	13	26.1	26.7	13.8	45.2	14.3	5.2	0.9	7.7	0.3	1.5	8.2	0.0
Exp 37	CBV90B	275	20	0.56	2	0.25	13	20.6	22.4	16.4	36.8	24.4	4.7	0.6	11.1	0.9	2.3	17.1	0.1
Exp 38	CBV90C	250	20	0.56	2	0.25	13	13.4	19.2	21.9	21.5	37.4	3.9	0.3	17.7	2.3	4.5	52.5	0.1
Exp 39	WHSVA	250	20	0.28	2	0.25	13	18.6	13.5	20.4	25.7	40.4	3.5	0.3	16.6	2.1	4.7	48.9	0.1
Exp 40	WHSVB	250	20	0.56	2	0.25	13	11.9	16.7	22.0	19.2	42.1	3.8	0.3	17.9	2.4	4.7	57.0	0.1
Exp 41	WHSVC	250	20	1.13	2	0.25	13	6.7	11.5	23.3	15.9	49.3	4.2	0.3	18.8	2.4	4.5	58.0	0.1
Exp 42	WHSVD	250	20	0.56	2	0.25	13	11.0	12.9	22.9	15.7	48.5	4.1	0.3	18.5	2.3	4.5	57.6	0.1
Exp 43	MFRA	250	20	0.56	0.5	0.63	3	6.6	8.6	23.0	22.5	45.8	5.9	0.7	16.5	1.2	2.8	25.1	0.1
Exp 44	MFRB	250	20	0.56	2	0.25	13	12.6	9.0	24.5	14.7	51.8	5.6	0.4	18.5	1.9	3.4	44.4	0.1
Exp 45	T200	200	20	0.56	2	0.25	13	1.1	1.8	26.9	15.3	56.0	7.7	0.5	18.7	0.7	2.4	38.5	0.0
Exp 46	MFRC	250	20	0.53	4	0.08	18	14.8	5.9	24.3	14.1	55.6	4.8	0.3	19.2	2.3	4.1	55.8	0.1
Exp 47	MFRD	250	20	0.56	2	0.25	13	9.8	10.3	22.9	15.0	51.8	4.1	0.3	18.5	2.2	4.6	59.2	0.1
Exp 48	P10	250	10	0.56	2	0.25	7	8.4	7.8	24.1	16.7	51.3	5.6	0.5	18.1	1.8	3.2	38.4	0.1
Exp 49	DPE	250	20	0.64	0	1	0	0.5	40.1	11.0	23.8	25.2	3.6	0.4	7.0	0.2	1.9		0.0
Exp 50	MeOH	250	20	0	inf	0.25	15	0.0	51.4	25.8	21.6	1.3	7.3	0.5	17.9	3.7	2.4	34.0	0.2

[a]Selectivities in mole %

APPENDIX IX.1

SUMMARY OF EXPERIMENTAL RESULTS - Steady state averages

	Exp name	T [°C]	P_T [bar]	WHSV	MFR	y_{N2}	P_{Feed} [bar]	X [%]	S_{Ps} [%][a]	$S_{PTI's}$ [%][a]	$S_{OADPE's}$ [%][a]	$S_{HP's}$ [%][a]	S_{OPT} [%][a]	S_{MPT} [%][a]	S_{PPT} [%][a]	S_{PTE} [%][a]	PPT/ OPT	PPT/ MPT	PTE/ PPT
Hbeta L1																			
Exp 1	**R0**	300	1.5	1	2	0.34	1.0	26.6	14.9	71.2	13.9	0.0	40.5	3.5	27.1	1.7	0.7	7.7	0.1
Exp 2	**R1**	250	1.5	1	2	0.34	1.0	7.2	5.4	87.9	6.7	0.0	49.6	4.0	34.3	0.9	0.7	8.6	0.0
Exp 3	**R2**	300	1	1	1	0.34	0.7	22.2	14.7	73.0	12.2	0.0	40.1	3.8	29.2	1.6	0.7	7.7	0.1
Exp 4	**R2B**	250	1	1	1	0.34	0.7	7.0	3.6	90.0	6.4	0.0	50.4	4.1	35.5	0.8	0.7	8.7	0.0
Exp 5	**R3**	250	1	0.41	1	0.21	0.8	8.6	5.8	86.9	7.3	0.0	48.3	4.0	34.6	0.9	0.7	8.6	0.0
Exp 6	**R4**	300	1	1	0.1	0.45	0.6	7.7	13.5	81.1	5.4	0.0	42.1	4.9	34.1	0.8	0.8	7.0	0.0
Exp 7	**R4B**	250	1	1	0.1	0.45	0.6	2.7	3.4	93.6	3.0	0.0	49.9	4.8	38.8	0.4	0.8	8.1	0.0
Exp 8	**R4C**	250	7	1	0.1	0.45	0.7	5.7	7.2	89.4	3.3	0.0	48.4	4.1	36.9	0.5	0.8	9.1	0.0
Exp 9	**R4D**	300	7	1	0.1	0.45	0.7	10.0	16.8	79.0	4.3	0.0	42.8	5.8	30.3	0.5	0.7	5.3	0.0
Exp 10	**R4E**	300	7	0.21	0.1	0.8	0.2	10.0	33.0	64.0	3.0	0.0	32.8	6.5	24.7	0.3	0.8	3.8	0.0
Exp 11	**R5**	300	2	0.21	0.1	0.72	0.6	8.6	24.2	71.8	3.9	0.0	38.5	6.9	26.4	0.4	0.7	3.8	0.0
Exp 12	**R5B**	250	1	0.21	0.1	0.72	0.3	6.4	6.0	89.0	4.9	0.0	48.2	4.6	36.2	0.7	0.8	7.9	0.0
Exp 13	**R6**	250	1	0.21	1	0.58	0.4	16.4	8.0	80.5	11.5	0.0	45.9	3.7	30.9	1.5	0.7	8.4	0.0
Exp 14	**R3rpt**	250	1	0.41	1	0.25	0.8	11.0	4.9	86.7	8.4	0.0	48.5	4.0	34.2	1.1	0.7	8.6	0.0
Exp 15	**RA**	250	6	0.56	2	0.25	4.0	34.0	9.5	74.9	15.5	0.0	49.3	2.5	23.1	1.4	0.5	9.2	0.1
Hbeta L2																			
Exp 16	**RArpt**	250	6	0.56	2	0.25	4.0	**Abondoned due experimental difficulties**											
Exp 17	**RBC**	250	20	0.28	2	0.25	13.3												
Exp 18	**RCS1**	250	11	0.56	2	0.25	7.3												
Hbeta L3																			
Exp 19	**RCS1B**	250	20	0.56	2	0.25	13.3	**Abondoned due experimental difficulties**											
Exp 20	**RCS1C**	250	20	0.56	2	0.25	13.3												
Exp 21	**RCS1D**	300	20	0.56	2	0.25	13.3												
Exp 22	**RCS1rpt**	250	20	0.56	2	0.25	13.3												
Hbeta L4																			
Exp 23	**RLP**	250	1	0.56	2	0.25	1	16.5	7.1	75.3	17.6	0.0	42.5	3.4	29.4	1.5	0.7	8.7	0.1
Exp 24	**RCS1F**	300	20	0.56	2	0.25	13.3	64.4	11.6	51.5	32.3	6.5	35.7	1.9	11.7	0.9	0.3	6.1	0.1
Exp 25	**RCS1G**	250	20	0.56	2	0.25	13.3	35.5	8.2	74.0	16.6	1.2	48.3	2.5	23.1	1.2	0.5	9.3	0.1
Exp 26	**RCS1H**	200	20	0.56	2	0.25	13.3	3.6	83.7	15.0	1.3	0.0	8.6	0.5	5.9	0.0	0.7	13.0	0.0
Exp 27	**RCS1I**	250	20	0.56	2	0.25	13.3	34.1	8.1	74.7	16.0	1.3	48.4	2.5	23.7	1.2	0.5	9.3	0.1

[a]Selectivities in mole %

APPENDIX IX.1
SUMMARY OF EXPERIMENTAL RESULTS - Steady state averages

	Exp name	T [°C]	P_T [bar]	WHSV	MFR	y_{N2}	P_{Feed} [bar]	X [%]	S_{Ps} [%][a]	S_{PTTs} [%][a]	$S_{OADPE's}$ [%][a]	$S_{HP's}$ [%][a]	S_{OPT} [%][a]	S_{MPT} [%][a]	S_{PPT} [%][a]	S_{PTE} [%][a]	PPT/ OPT	PPT/ MPT	PTE/ PPT
MFI-50 L1																			
Exp 28	Z5OA	250	20	0.56	3.2	0.25	14	4.5	67.3	17.8	4.2	10.7	5.4	1.2	11.1	0.0	2.1	9.0	0.0
Mor-40 L1																			
Exp 29	M40A	250	20	0.56	3.2	0.25	14	8.9	31.7	18.2	8.7	41.4	2.2	0.2	15.9	2.2	7.4	93.5	0.1
HUSY L1																			
Exp 30	HUSY	250	20	0.56	2	0.25	13	9.0	37.2	57.6	4.1	1.2	34.4	2.8	20.4	0.1	0.6	7.2	0.0
CBV21A L1 ($T_{calcination}$ = 400°C)																			
Exp 31	CBV20A	250	20	0.56	2	0.25	13	14.7	20.8	23.2	8.8	47.2	7.1	0.5	15.6	1.5	2.2	29.4	0.1
CBV21A L2 ($T_{calcination}$ = 400°C)																			
Exp 32	M20B	300	20	0.56	2	0.25	13	34.0	14.2	27.4	28.4	30.0	12.5	1.4	13.5	1.0	1.1	10.0	0.1
CBV21A L3 ($T_{calcination}$ = 500°C)																			
Exp 33	M20D	300	20	0.56	2	0.25	13	62.5	6.4	45.3	28.4	20.0	30.7	2.2	12.3	1.2	0.4	5.5	0.1
Exp 34	M20E	275	20	0.56	2	0.25	13	33.4	3.6	57.8	14.0	24.6	35.1	2.6	20.1	1.0	0.6	7.8	0.1
Exp 35	M20F	250	20	0.56	2	0.25	13	8.8	1.3	64.8	7.8	26.1	35.3	2.6	26.9	0.4	0.8	10.4	0.0
CBV90A L1																			
Exp 36	CBV90A	300	20	0.56	2	0.25	13	26.1	26.7	13.8	45.2	14.3	5.2	0.9	7.7	0.3	1.5	8.2	0.0
Exp 37	CBV90B	275	20	0.56	2	0.25	13	20.6	22.4	16.4	36.8	24.4	4.7	0.6	11.1	0.9	2.3	17.1	0.1
Exp 38	CBV90C	250	20	0.56	2	0.25	13	13.4	19.2	21.9	21.5	37.4	3.9	0.3	17.7	2.3	4.5	52.5	0.1
Exp 39	WHSVA	250	20	0.28	2	0.25	13	18.6	13.5	20.4	25.7	40.4	3.5	0.3	16.6	2.1	4.7	48.9	0.1
Exp 40	WHSVB	250	20	0.56	2	0.25	13	11.9	16.7	22.0	19.2	42.1	3.8	0.3	17.9	2.4	4.7	57.0	0.1
Exp 41	WHSVC	250	20	1.13	2	0.25	13	6.7	11.5	23.3	15.9	49.3	4.2	0.3	18.8	2.4	4.5	58.0	0.1
Exp 42	WHSVD	250	20	0.56	2	0.25	13	11.0	12.9	22.9	15.7	48.5	4.1	0.3	18.5	2.3	4.5	57.6	0.1
Exp 43	MFRA	250	20	0.56	0.5	0.63	3	6.6	8.6	23.0	22.5	45.8	5.9	0.7	16.5	1.2	2.8	25.1	0.1
Exp 44	MFRB	250	20	0.56	2	0.25	13	12.6	9.0	24.5	14.7	51.8	5.6	0.4	18.5	1.9	3.4	44.4	0.1
Exp 45	T200	200	20	0.56	2	0.25	13	1.1	1.8	26.9	15.3	56.0	7.7	0.5	18.7	0.7	2.4	38.5	0.0
Exp 46	MFRC	250	20	0.53	4	0.08	18	14.8	5.9	24.3	14.1	55.6	4.8	0.3	19.2	2.3	4.1	55.8	0.1
Exp 47	MFRD	250	20	0.56	2	0.25	13	9.8	10.3	22.9	15.0	51.8	4.1	0.3	18.5	2.2	4.6	59.2	0.1
Exp 48	P10	250	10	0.56	2	0.25	7	8.4	7.8	24.1	16.7	51.3	5.6	0.5	18.1	1.8	3.2	38.4	0.1
Exp 49	DPE	250	20	0.64	0	1	0	0.5	40.1	11.0	23.8	25.2	3.6	0.4	7.0	0.2	1.9		0.0
Exp 50	MeOH	250	20	0	inf	0.25	15	0.0	51.4	25.8	21.6	1.3	7.3	0.5	17.9	3.7	2.4	34.0	0.2

[a]Selectivities in mole %

APPENDIX X

Chromatograms of Products

APPENDIX X.1

CHROMATOGRAMS

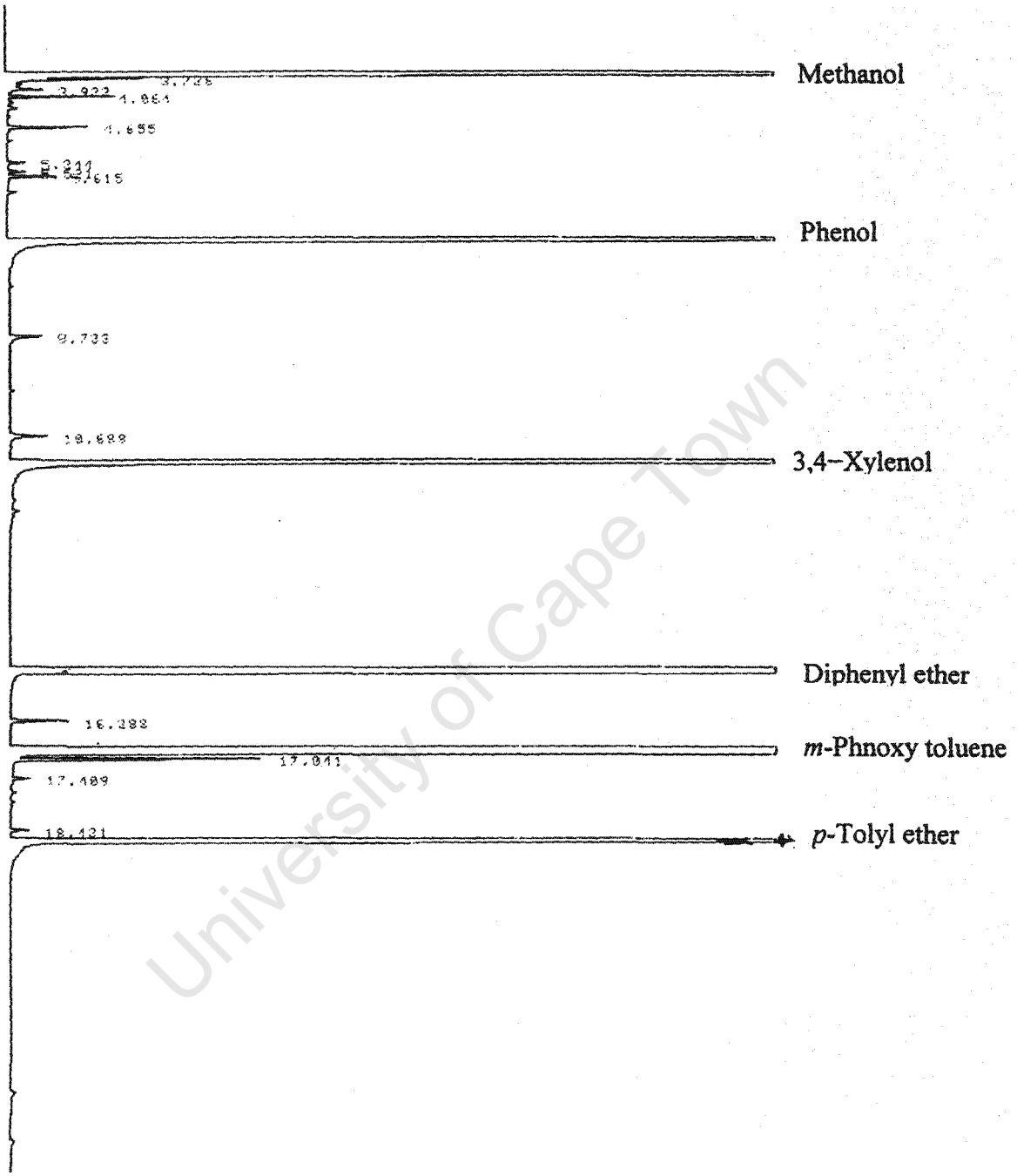

Figure XI-1 : Standard mixture

APPENDIX X.1

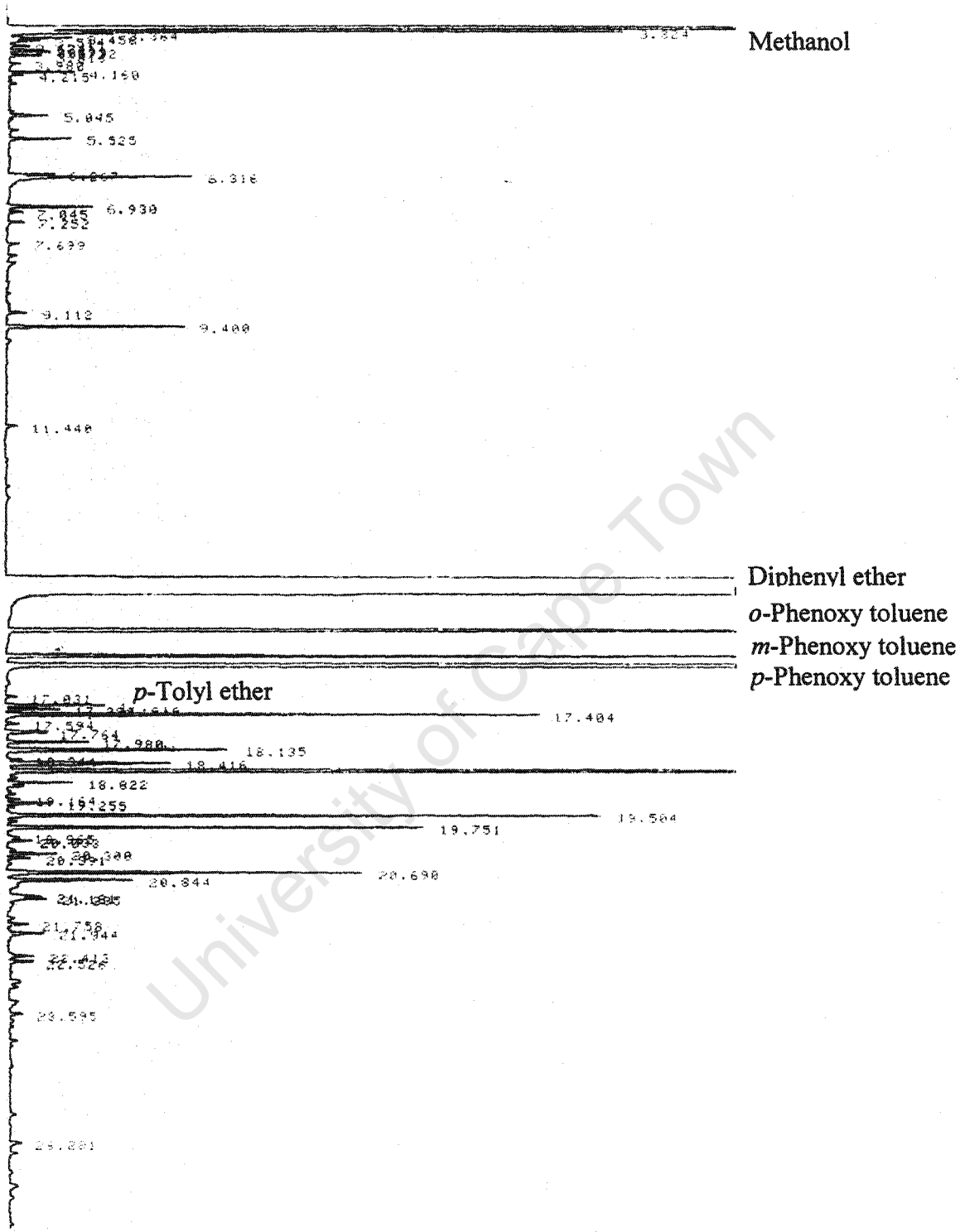

Figure XI-2 : Part A of the sample from Exp 28 (H-MFI-50 screening) after 5 hours on stream

APPENDIX X.1

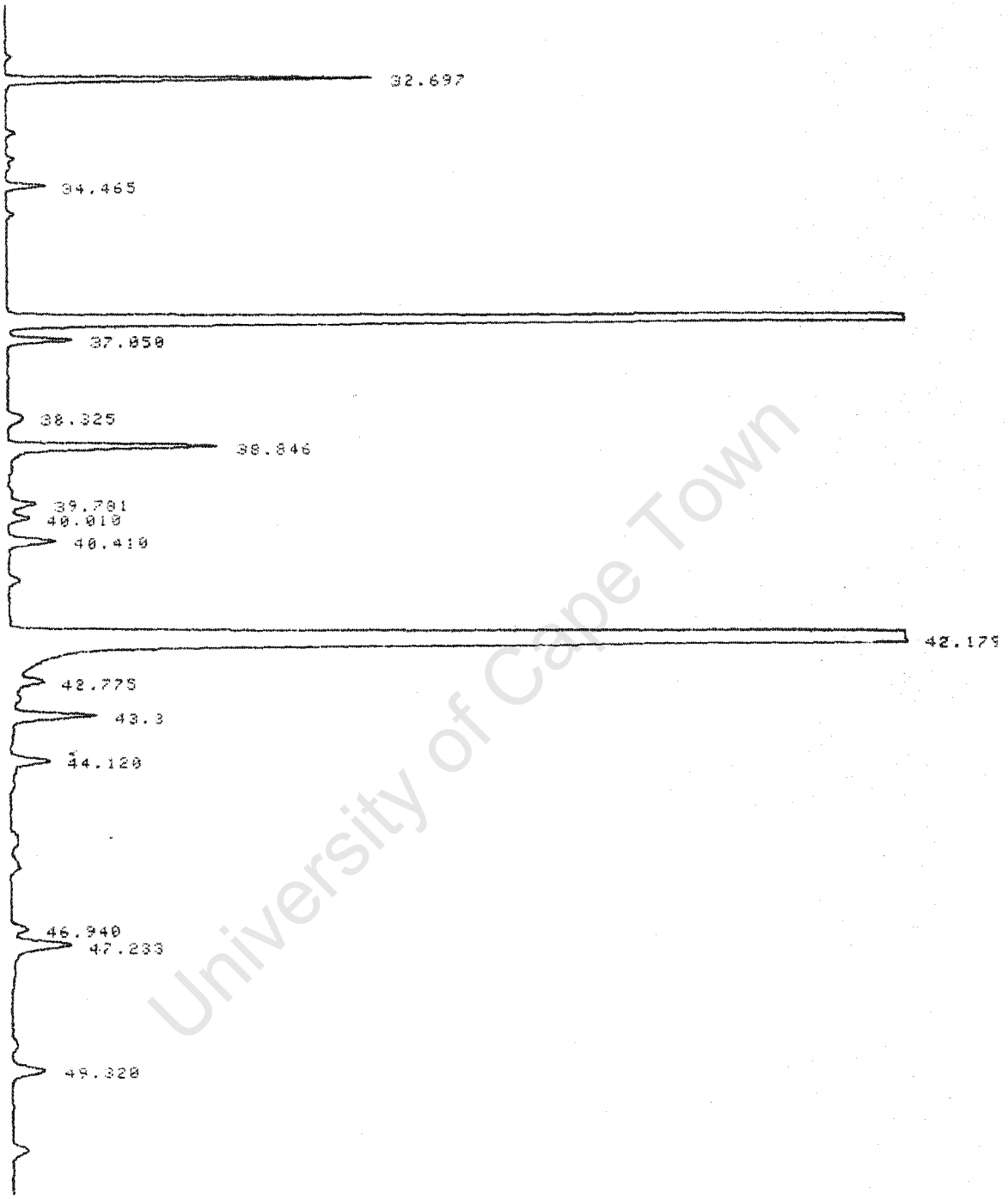

Figure XI-3 : Part B of the sample from Exp 28 (H-MFI-50 screening) after 5 hours on stream

APPENDIX X.1

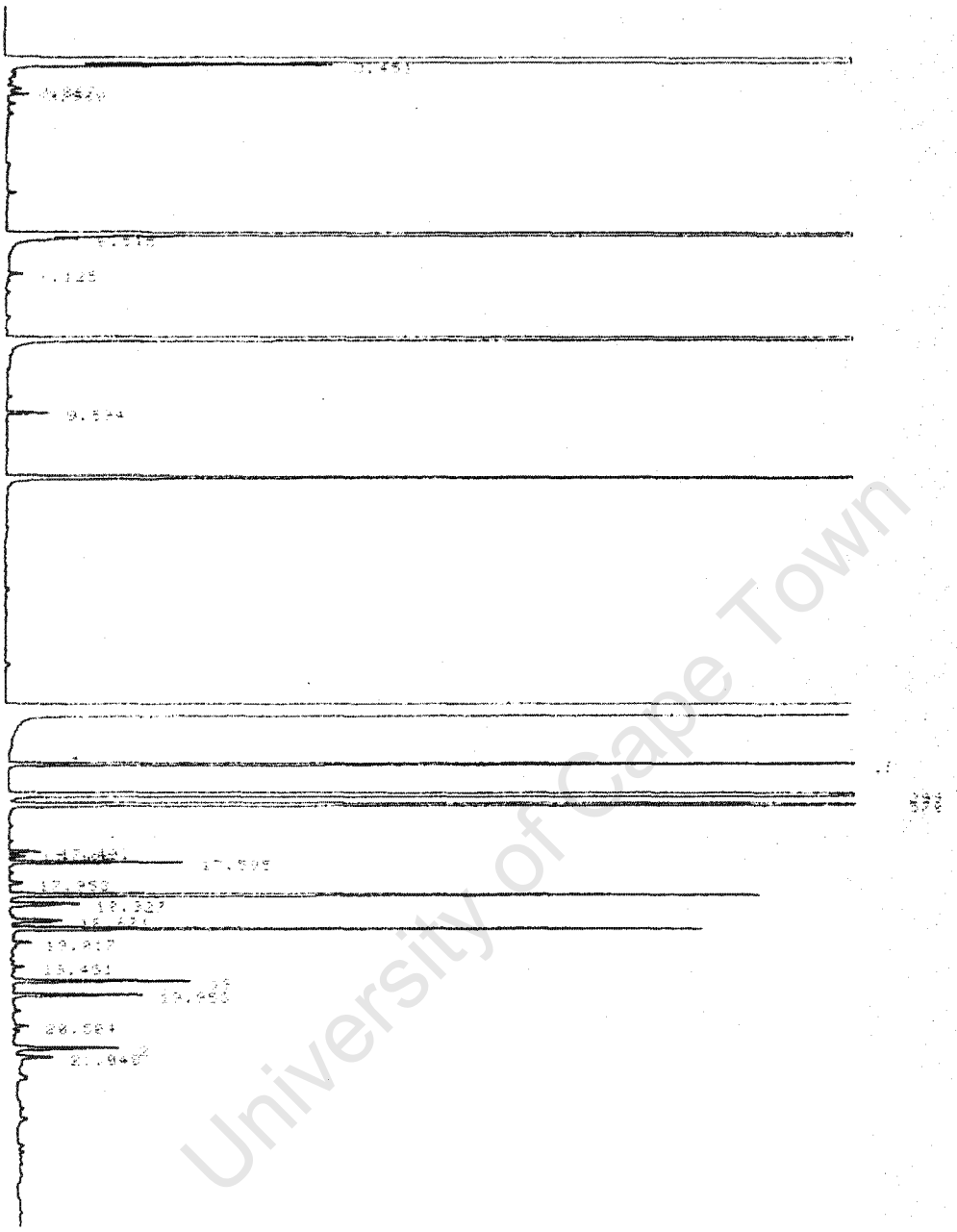

Figure XI-4 : Part A of a standard mixture mixed with the sample from Exp 28 (H-MFI-50 screening) after 5 hours on stream

APPENDIX X.1

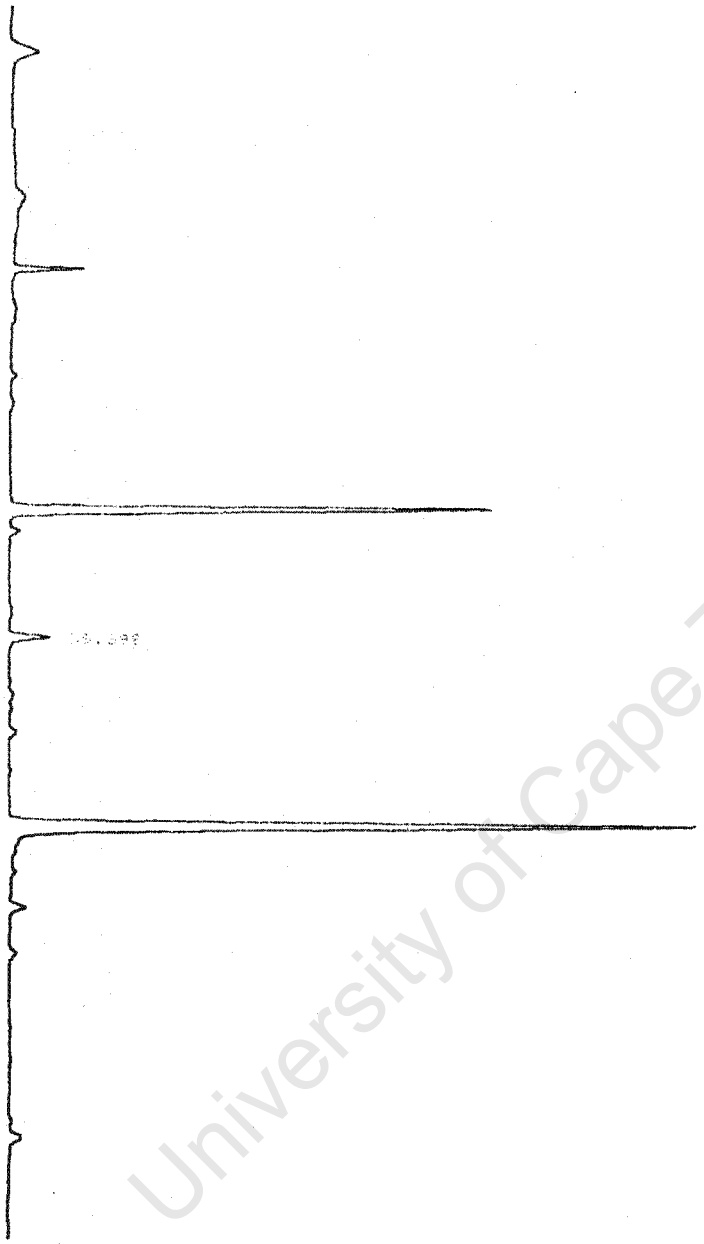

Figure XI-5 : Part B of a standard mixture mixed with the sample from Exp 28 (H-MFI-50 screening) after 5 hours on stream

APPENDIX X.2

ACTIVITY COEFFICIENTS FOR PHENOL-WATER SYSTEM

The ring balance focused only on the organic phase, as explained in Section 4.4 and Section 4.4.4, thus considering no significant quantities of phenols or aromatic in the aqueous phase.

An activity coefficient model, obtained from UNIFAC, considering the phenol-water binary system gave the results below:

T = 25°C									
x_{phenol}	0	0.1	0.2	0.3	0.5	0.7	0.8	0.9	1
γ_{phenol}	11.0	2.9	1.67	1.29	1.06	1.01	1.00	1.00	1
γ_{water}	1	1.06	1.17	1.27	1.43	1.53	1.56	1.58	1.60

A high activity coefficient indicates low solubility of a substance in the other, and this is usually a case for a substance that is present in low concentrations (Sandler, 1989). Analysis of the aqueous phase by GC showed that the aqueous phase had very small quantities of organic compounds. It can therefore be concluded that most of phenol produced from diphenyl ether cleavage was recovered in the organic phase.

It was discussed in Section 2.1.6 that phenol has limited solubility in water between 0 and 60°C, and the product was collected in this temperature range. It therefore seemed reasonable to ignore anyquantities of phenols that were lost via the aqueous phase.